GEOLOGICAL SURVEY OF CANADA
COMMISSION GÉOLOGIQUE DU CANADA

CURRENT RESEARCH 1997-E

RECHERCHES EN COURS 1997-E

Natural Resources Canada
Ressources naturelles Canada

Canada

GEOLOGICAL SURVEY OF CANADA
COMMISSION GÉOLOGIQUE DU CANADA

CURRENT RESEARCH 1997-E

RECHERCHES EN COURS 1997-E

1997

Includes/comprend:

Cordillera and Pacific Margin
Cordillère et marge du Pacifique

Interior Plains and Arctic Canada
Plaines intérieures et région arctique du Canada

Canadian Shield
Bouclier canadien

Eastern Canada and National and General Programs
Est du Canada et programmes nationaux et généraux

Catalogue number M44-1997/5E
ISBN 0-660-17065-5

Available in Canada from
Geological Survey of Canada offices:

601 Booth Street
Ottawa, Ontario K1A 0E8

3303-33rd Street N.W.
Calgary, Alberta T2L 2A7

101-605 Robson Street
Vancouver, B.C. V6B 5J3

or from

Canadian Government Publishing
Public Works and Government Services Canada
Ottawa, Ontario K1A 0S9

A deposit copy of this publication is also available for reference
in selected public libraries across Canada

Price subject to change without notice

Cover illustration

View to east of dipping Cambrian carbonates and clastics in thrust contact with flat-lying or gently dipping Cretaceous or Tertiary conglomerates, Franklin Pierce Bay, east-central Ellesmere Island. Relief of cliff in centre of photograph is about 800 m. See paper by de Freitas et al., this volume. GSC 1997-44A

Photo en page couverture

Roches carbonatées et clastiques du Cambrien en contact de chevauchement avec des conglomérats horizontaux ou légèrement inclinés du Crétacé ou du Tertiaire, baie Franklin Pierce, centre est de l'île d'Ellesmere. La falaise au centre de la photo a un relief d'environ 800 m. La photo, prise en regardant vers l'est, se rapporte à l'article de de Freitas et al. dans le présent volume. GSC 1997-44A

Separates

A limited number of separates of the papers that appear in this volume are available by direct request to the individual authors. The addresses of the Geological Survey of Canada offices follow:

Geological Survey of Canada
601 Booth Street
OTTAWA, Ontario
K1A 0E8
(FAX: 613-996-9990)

Geological Survey of Canada (Calgary)
3303-33rd Street N.W.
CALGARY, Alberta
T2L 2A7
(FAX: 403-292-5377)

Geological Survey of Canada (Pacific)
101-605 Robson Street
VANCOUVER, B.C.
V6B 5J3
(FAX: 604-666-1124)

Geological Survey of Canada (Pacific)
P.O. Box 6000
9860 Saanich Road
SIDNEY, B.C.
V8L 4B2
(FAX: 604-363-6565)

Geological Survey of Canada (Atlantic)
Bedford Institute of Oceanography
P.O. Box 1006
DARTMOUTH, N.S.
B2Y 4A2
(FAX: 902-426-2256)

Quebec Geoscience Centre/INRS
2535, boulevard Laurier
C.P. 7500
Sainte-Foy (Québec)
G1V 4C7
(FAX: 418-654-2615)

Tirés à part

On peut obtenir un nombre limité de «tirés à part» des articles qui paraissent dans cette publication en s'adressant directement à chaque auteur. Les adresses des différents bureaux de la Commission géologique du Canada sont les suivantes :

Commission géologique du Canada
601, rue Booth
OTTAWA, Ontario
K1A 0E8
(facsimilé : 613-996-9990)

Commission géologique du Canada (Calgary)
3303-33rd St. N.W.,
CALGARY, Alberta
T2L 2A7
(facsimilé : 403-292-5377)

Commission géologique du Canada (Pacifique)
101-605 Robson Street
VANCOUVER, British Columbia
V6B 5J3
(facsimilé : 604-666-1124)

Commission géologique du Canada (Pacifique)
P.O. Box 6000
9860 Saanich Road
SIDNEY, British Columbia
V8L 4B2
(facsimilé : 604-363-6565)

Commission géologique du Canada (Atlantique)
Institut océanographique Bedford
P.O. Box 1006
DARTMOUTH, Nova Scotia
B2Y 4A2
(facsimilé : 902-426-2256)

Centre géoscientifique de Québec/INRS
2535, boulevard Laurier
C.P. 7500
Sainte-Foy (Québec)
G1V 4C7
(facsimilé : 418-654-2615)

CONTENTS

CORDILLERA AND PACIFIC MARGIN
CORDILLÈRE ET MARGE DU PACIFIQUE

INTERIOR PLAINS AND ARCTIC CANADA
PLAINES INTÉRIEURES ET RÉGION ARCTIQUE DU CANADA

CANADIAN SHIELD
BOUCLIER CANADIEN

EASTERN CANADA AND NATIONAL AND GENERAL PROGRAMS
EST DU CANADA ET PROGRAMMES NATIONAUX ET GÉNÉRAUX

Cordillera and Pacific Margin

Cordillère et marge du Pacifique

Carte morphostructurale du secteur central du chaînon Ruby, Yukon

Mokili K. Mbuluyo[1] et Marie-Anne Geurts[2]
Division de la science des terrains, Ottawa

Mbuluyo, M.K. et Geurts, M.-A., 1997 : Carte morphostructurale du secteur central du chaînon Ruby, Yukon; dans Recherches en cours 1997-E; Commission géologique du Canada, p. 1-11.

Résumé : L'objectif de cette étude est de dégager par l'analyse des linéaments les structures tectoniques qui ont un effet sur la morphologie et l'organisation du réseau hydrographique dans le sud-ouest du Yukon. Selon le caractère de la déformation et l'observation des formes de relief apparentées, deux types de tectogenèse sont mis en évidence. La première tectonique est associée à la mise en place d'intrusions granitiques et est antérieure au Paléocène; elle est à l'origine du dôme occupant le secteur central de la région étudiée, d'où prennent naissance les principaux cours d'eau. La deuxième tectonique est de type cassant et est postérieure à la mise en place des granites; elle est responsable de la formation de failles radiales exploitées par des cours d'eau. Au Quaternaire, les glaciers ont élargi les vallées formées précédemment pour leur donner leur configuration actuelle. La tectonique cassante est encore active dans la région puisque ses effets peuvent être observés dans les dépôts quaternaires.

Abstract: Based on the study of lineaments, this paper clarifies the role of tectonic structures on the geomorphology and river system development in southwestern Yukon. From the kinds of deformation and the observation of related landforms, two types of tectonism are recognized. The first one is associated with the pre-Paleocene intrusion of granite bodies; the dome at the centre of the study area where the head of the major streams are located is related to it. The second one postdates the granites and consists of brittle fracturing that formed faults which are used by the streams. During the Quaternary, the glaciers enlarged these preexisting valleys. This neotectonism is still active in the region as evidenced by deformed Quaternary deposits.

[1] 181, rue Granville, app. 2, Vanier (Ontario) K1L 6Y3
[2] Université d'Ottawa, Département de géographie, Faculté des arts, 165, rue Waller, C.P. 450, Succ. A, Ottawa (Ontario) K1N 6N5

INTRODUCTION

La région considérée dans la présente étude est limitée à l'ouest par le lac Kluane et à l'est par le Sekulmun (fig. 1). Elle appartient à la partie du sud-ouest du Yukon comprise entre les latitudes 61°07' et 61°47' N et les longitudes 137°30' et 138°42' W.

Du point de vue physiographique, la région occupée par le chaînon Ruby fait partie des plateaux intérieurs de la Cordillère canadienne. Le chaînon s'élève à une altitude moyenne de 5 000 pieds (1 524 m). Son relief se caractérise par de longues crêtes profondément disséquées par un réseau hydrographique dense. Les traces de l'activité glaciaire du Quaternaire, telles que les cirques, les lacs glaciaires et les vallées larges et à fond plat sont omniprésentes et constituent les traits morphologiques dominants de la région.

Le réseau hydrographique présente de nombreuses perturbations dans son tracé. S'il est aisé d'associer ces perturbations à l'action des glaciers qui ont couvert la région durant le Quaternaire, il est par contre difficile d'admettre que toutes les vallées sont d'origine glaciaire. Il faut rechercher dans la morphologie et l'organisation du réseau hydrographique les traces estompées des autres facteurs morphodynamiques, en l'occurrence l'érosion fluviale et la tectonique, pour expliquer la formation et l'évolution des différents reliefs et bassins hydrographiques.

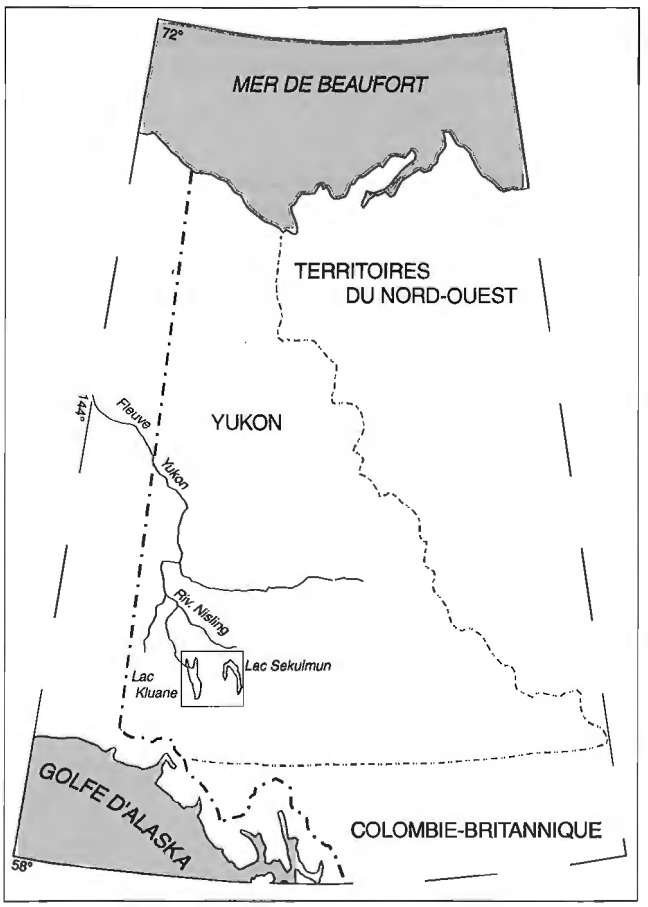

Figure 1. *Carte de localisation de la région d'étude.*

Le sud-ouest du Yukon est reconnu pour son instabilité tectonique. C'est, en effet, la région du pays qui connaît le taux de soulèvement le plus élevé, qui s'élèverait à 2,4 cm par an selon Vanicek et Nagy (1981). Si cette évaluation s'avère exacte, la réaction du socle à un tel soulèvement a donc dû se traduire, au cours du temps, par des perturbations du réseau hydrographique et l'accroissement local des pentes (escarpement de failles). Le levé des traces de l'extension glaciaire effectué par Hughes (1967) établit pour sa part que les glaciers ont utilisé les vallées et les cols préexistants comme «voie naturelle» pour couvrir la région. La morphologie et l'aspect actuel du réseau hydrographique de la région sont donc le résultat du jeu de plusieurs facteurs interreliés. Une étude qui vise à déterminer le poids de chacun des facteurs impliqués revêt donc un intérêt scientifique certain puisqu'elle nous permet d'obtenir une meilleure connaissance de la géomorphologie de cette partie du sud du Yukon.

Le but de la présente étude est de faire ressortir les structures tectoniques qui régissent la morphologie du sud-ouest du Yukon et qui ont guidé l'organisation des grands axes du réseau hydrographique dans cette région. Ces structures tectoniques sont peu visibles sur le terrain et peu présentes dans les documents cartographiques existants. Ce travail constitue un complément aux études géomorphologiques entreprises depuis longtemps dans cette région (Dewez, 1988; Kodybka, 1992; Geurts et Dewez, 1993; Dewez et Geurts, 1996), qui n'ont pas abordé cependant la question du rapport entre la morphologie et la tectonique. De nombreuses questions ont été posées dans les travaux précités au sujet de l'origine et de l'orientation de certains cols ou vallées du chaînon Ruby qui ont joué un rôle majeur dans l'avancée des langues glaciaires provenant du massif St. Elias.

Après un bref rappel du contexte géologique régional du sud-ouest du Yukon, l'article présentera tout d'abord le matériel et la méthodologie utilisés et abordera ensuite l'analyse et l'interprétation des résultats obtenus. Une carte morphostructurale permettra de satisfaire l'objectif visé et de founir une vue synoptique des interprétations proposées.

CADRE GÉOLOGIQUE

La lithologie

L'examen de la carte géologique 1398A de la Commission géologique du Canada (Gabrielse et al., 1977) nous montre que le sous-sol de la région est composé de trois grandes unités lithologiques qui appartiennent, selon Muller (1967), au Complexe du Yukon. D'après les roches qui les composent, ces trois grandes unités lithologiques peuvent être décrites de la manière suivante :

1. La première unité se compose de roches métamorphiques qui affleurent dans les zones marginales de la région et qui se présentent, par endroits, en enclaves dans les massifs granitiques. Leur âge va du Dévonien au début du

Mésozoïque. Ces roches groupent principalement des schistes à quartz-biotite et à quartz-séricite. On note toutefois dans certains endroits la présence d'amphibolite et de calcaire recristallisé (marbre). Les secteurs occupés par des schistes ou par d'autres types de roches métamorphiques se caractérisent par un relief moins accidenté et moins découpé que ceux associés à des massifs granitiques.

2. La deuxième unité est constituée de roches granitoïdes qui se présentent sous forme de massifs intrusifs. Ces roches affleurent dans la plus grande partie de la région étudiée et montrent une grande variété lithologique, allant des granites (*sensu stricto*) aux granodiorites, en passant par les granites monzonitiques. Muller (1967) distingue selon l'âge des intrusions deux grands corps intrusifs, les batholites de Ruby Range et de Nisling Range. Le premier, d'âge jurassique, est constitué de granodiorite. Le second, qui est partiellement circonscrit dans le précédent, a été mis en place au Paléogène et se compose à la fois de granodiorite et de monzogranite (alaskite). En examinant les relations qui existent, d'une part, entre les deux batholites et, d'autre part, entre ceux-ci et la topographie, il ressort que le secteur le plus élevé de la région, d'où prennent naissance les principaux cours d'eau (les ruisseaux Albert, Isaac, Gladstone et Alaskite), est un dôme structural qui coïncide avec le toit du batholite de Nisling Range. Le coeur du dôme est excentré vers le nord lorsqu'on se réfère à la répartition des faciès plus felsiques, comme le monzogranite (alaskite), alors que la périphérie du massif se compose des faciès plus mafiques, tels que la granodiorite. Les massifs intrusifs sont caractérisés par un relief vigoureux marqué par la présence de crêtes étroites. Le réseau hydrographique est encaissé et la présence de nombreux cirques glaciaires étagés confèrent aux massifs un aspect très différent de celui des secteurs occupés par d'autres lithologies tant sur les photographies aériennes que sur l'image satellitaire MSS (Multispectral Scanner).

3. Des coulées et des dykes de porphyre feldspathique de composition felsique qui occupent le centre nord de la région forment la troisième grande unité. La plus grande partie de ces roches se trouve au nord du chaînon Ruby. Les coulées sont du Tertiaire inférieur.

Selon Hughes (1967), la quasi-totalité du plateau aurait été couverte à deux reprises (Glaciation de Reid et Glaciation de McConnell) par les glaciers qui provenaient principalement de la calotte glaciaire du massif St. Elias. Ceux-ci auraient raboté les interfluves et les versants, mettant en évidence la moindre ligne de fracture. La déglaciation a laissé principalement dans les vallées, et par endroits sur les interfluves, d'épais dépôts de moraine et de till qui couvrent les unités du Complexe du Yukon (Dewez, 1988 et Kodybka, 1992).

La tectonique

Il y a peu de données relatives à la tectonique du secteur étudié qui apparaissent sur les cartes géologiques existantes en dehors de la faille de Shakwak et de celle qui s'étend de Jarvis au ruisseau Gladstone. Cependant, de nombreuses observations faites dans les régions voisines, principalement dans les secteurs du massif St. Elias et du ruisseau Cache (Loren, 1992), donnent des indications générales sur les mouvements du socle, qui peuvent être appliquées au secteur central du chaînon Ruby. D'après Clague (1979) et Gabrielse et al. (1991), la tectonique du sud-ouest du Yukon s'inscrit dans celle de la Cordillère canadienne où la déformation est associée à un système de failles de coulissage à faible composante de mouvement vertical. Les failles témoignent toutes d'une déformation de type cassant, ce qui nous indique que cette région est une zone de faiblesse de la croûte terrestre où des fractures anciennes pourraient être réactivées en réponse à de nouvelles contraintes. La direction principale des fractures est ouest-nord-ouest et correspond à celle des grandes cassures présentes le long de la côte du Pacifique (fig. 2).

Selon la nature des failles et des terrains qu'elles recoupent, on peut envisager la différentiation suivante quant à la tectonique de la région étudiée.

1. Une fragmentation postérieure à la mise en place des granites représentée par les dykes cartographiés au nord du ruisseau Talbot (Gabrielse et al., 1977). Ces failles anciennes sont caractérisées par une orientation subméridienne (nord-sud). Le réseau de dykes le plus important se trouve à l'extérieur de la région étudiée. Les dykes recoupent indifféremment les diverses unités lithologiques (schistes et granites), soulignant ainsi qu'ils sont plus récents que celles-ci. L'âge des dykes n'est pas encore déterminé.

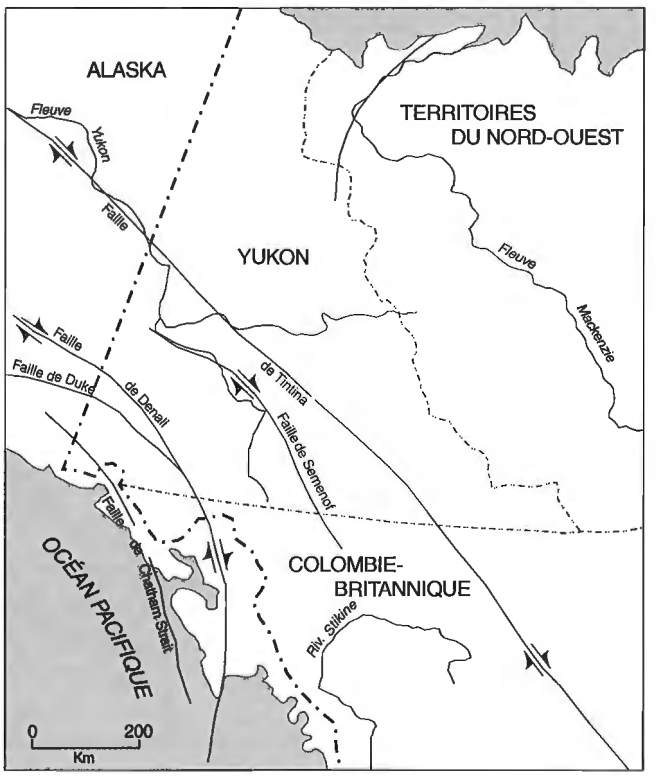

Figure 2. *Principales failles coulissantes de la Cordillère canadienne. Modifié d'après Gabrielse et al. (1991).*

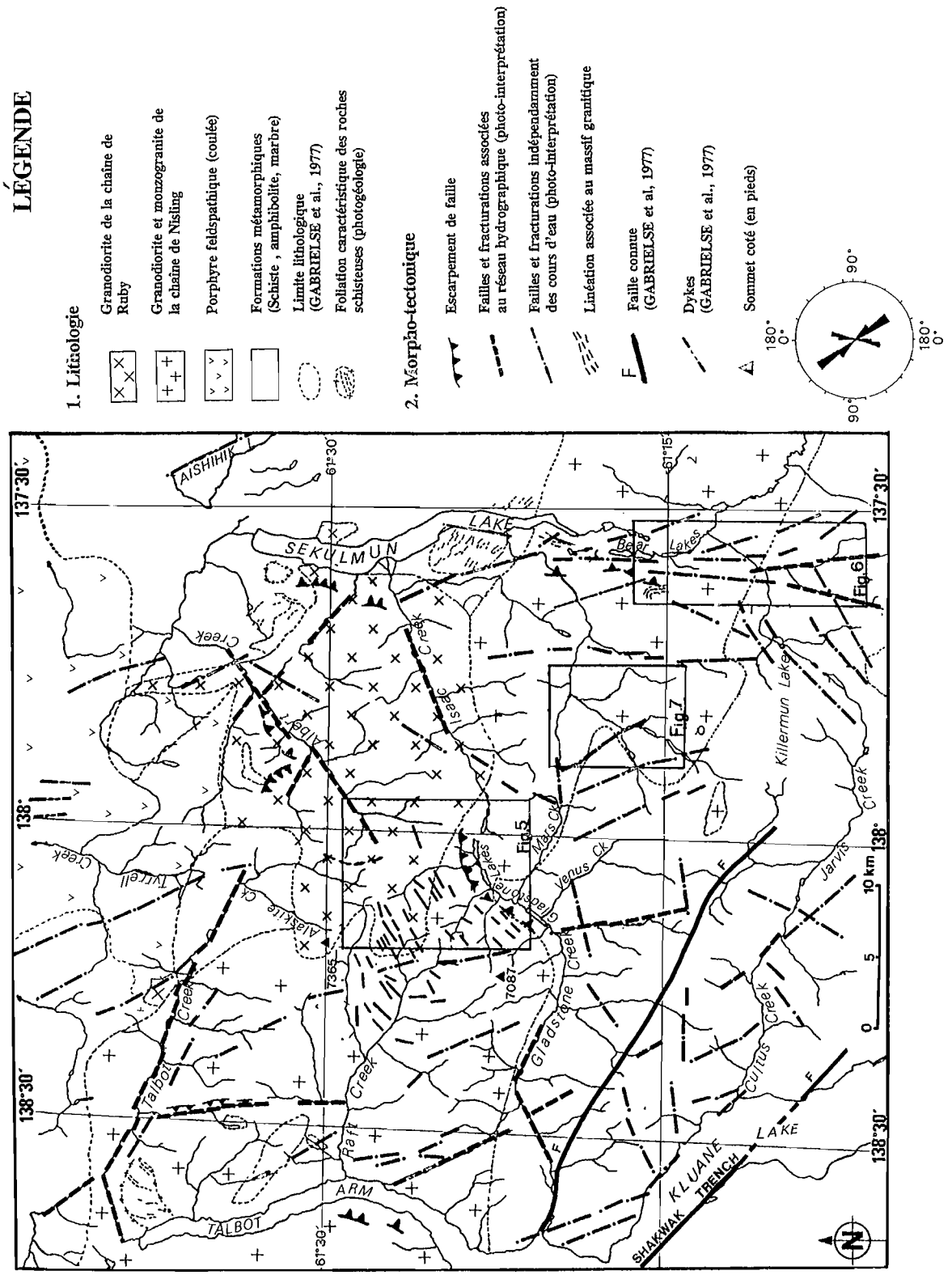

Figure 3. Carte morphostructurale du secteur central du chaînon Ruby.

2. Les chaînons Ruby et Nisling sont compris entre les failles de Tintina, au nord, et de Shakwak, au sud. Cette dernière appartient au système de failles coulissantes de Denali qui s'étend dans le sud-ouest du Yukon sur environ 300 km (fig. 2). La formation de cette fracture d'extension régionale, qui montre une direction ouest-nord-ouest, remonterait au Tertiaire (Clague, 1979).
3. Des failles récentes ainsi que des indices des mouvements auxquels elles ont donné lieu sont observés dans plusieurs endroits de la région. La plupart des mouvements survenus résultent de la réactivation de failles anciennes, comme l'ont montré des études géophysiques effectuées dans les dépôts quaternaires datant de 10 000 ans à l'embouchure du ruisseau Slims (Clague, 1979). L'activité tectonique actuelle dans la région se traduit par des secousses séismiques dont les magnitudes enregistrées sont souvent supérieures à 4 sur l'échelle de Richter (Clague, 1979).

MÉTHODOLOGIE

L'analyse de la fracturation ainsi que celle d'autres structures tectoniques dans le secteur considéré est basée sur l'approche classique des linéaments. En effet, le relevé détaillé de ces linéaments a été effectué à l'aide d'un stéréoscope et de photographies aériennes à l'échelle de 1/64 000.

Une carte résultant de l'assemblage des différentes planches a été numérisée par la suite à l'aide du logiciel Arc/Info afin d'être superposée aux autres fichiers d'information cartographique numériques de la région (géologie, hydrographie et topographie). À des fins de comparaison, les résultats de l'interprétation numérique ont été confrontés à ceux de l'interprétation analogique du tirage photographique de l'image satellitaire MSS. La rosace de direction des linéaments est obtenue à partir des coordonnées géographiques issues de la transformation des données chiffrées de la table numérique importée dans le logiciel DBase IV. Un pas de 10° a été retenu pour caractériser une direction structurale.

L'intérêt d'une telle approche consiste dans l'obtention d'une carte morphostructurale (fig. 3) à moindre coût, où la photo-interprétation classique constitue l'approche principale.

LES DONNÉES MORPHOSTRUCTURALES DU SECTEUR CENTRAL DU CHAÎNON RUBY

Le traitement statistique des linéaments a permis de déterminer deux directions structurales majeures (voir la rosace de direction des linéaments sur la figure 3). Les linéaments peuvent être attribués aux trois groupes suivants :

1. Le premier groupe, qui compte 58 % des linéaments, définit une direction prédominante N140°. Les linéaments de ce groupe sont caractérisés par leur longueur et leur continuité. L'orientation principale qu'ils définissent est parallèle à celle des accidents majeurs ouest-nord-ouest – est-sud-est identifiés dans la région, tels que les failles de Tintina et de Semenof, au nord, et de Shakwak et de Duke, au sud (fig. 2)
2. Le deuxième groupe, qui englobe 36 % des linéaments, définit une direction secondaire N10°. Les linéaments qui y sont rapportés sont localisés dans l'alignement de failles d'orientation subméridienne (nord-sud) de la Colombie-Britannique (faille de Chatham Strait) et des dykes nord-sud signalés précédemment.
3. Le troisième groupe comprend le reste des linéaments, soit 6% du total. Ces linéaments se distinguent par des directions nord-nord-est et est. Leur signification du point de vue tectonique reste à déterminer.

Une chronologie relative des structures linéamentaires peut toutefois être établie à partir des données géologiques régionales (Gabrielse et al., 1991) ainsi que du recoupement des nombreuses familles de failles connues. La formation des structures de direction subméridienne (N10°), associées aux dykes nord-sud, apparaît antérieure à celle des accidents ouest-nord-ouest (N140°), puisque les secondes recoupent les premières en y provoquant des décrochements latéraux. Cette interprétation reste toutefois hypothétique et délicate à généraliser avant que de nouvelles vérifications sur le terrain puissent être effectuées. Le sud-ouest du Yukon est donc situé sur un seuil tectonique où des failles de direction subméridienne et de direction ouest-nord-ouest se rejoignent. Ceci pourrait expliquer en partie l'ampleur des mouvements du socle et la fréquence des secousses séismiques.

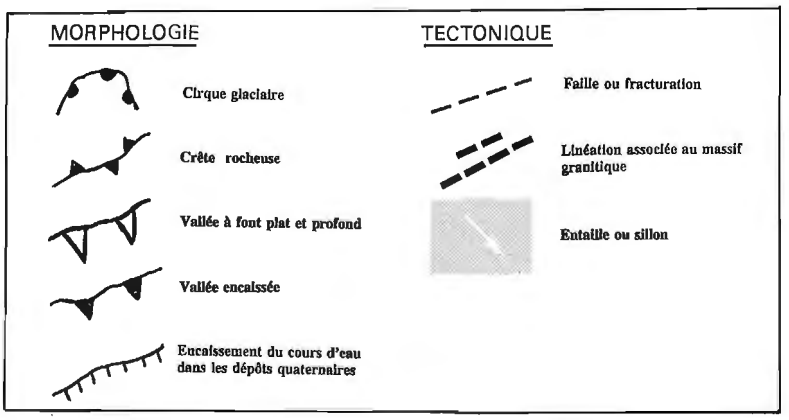

Figure 4.

Légende des symboles utilisés dans les mosaïques de photographies aériennes.

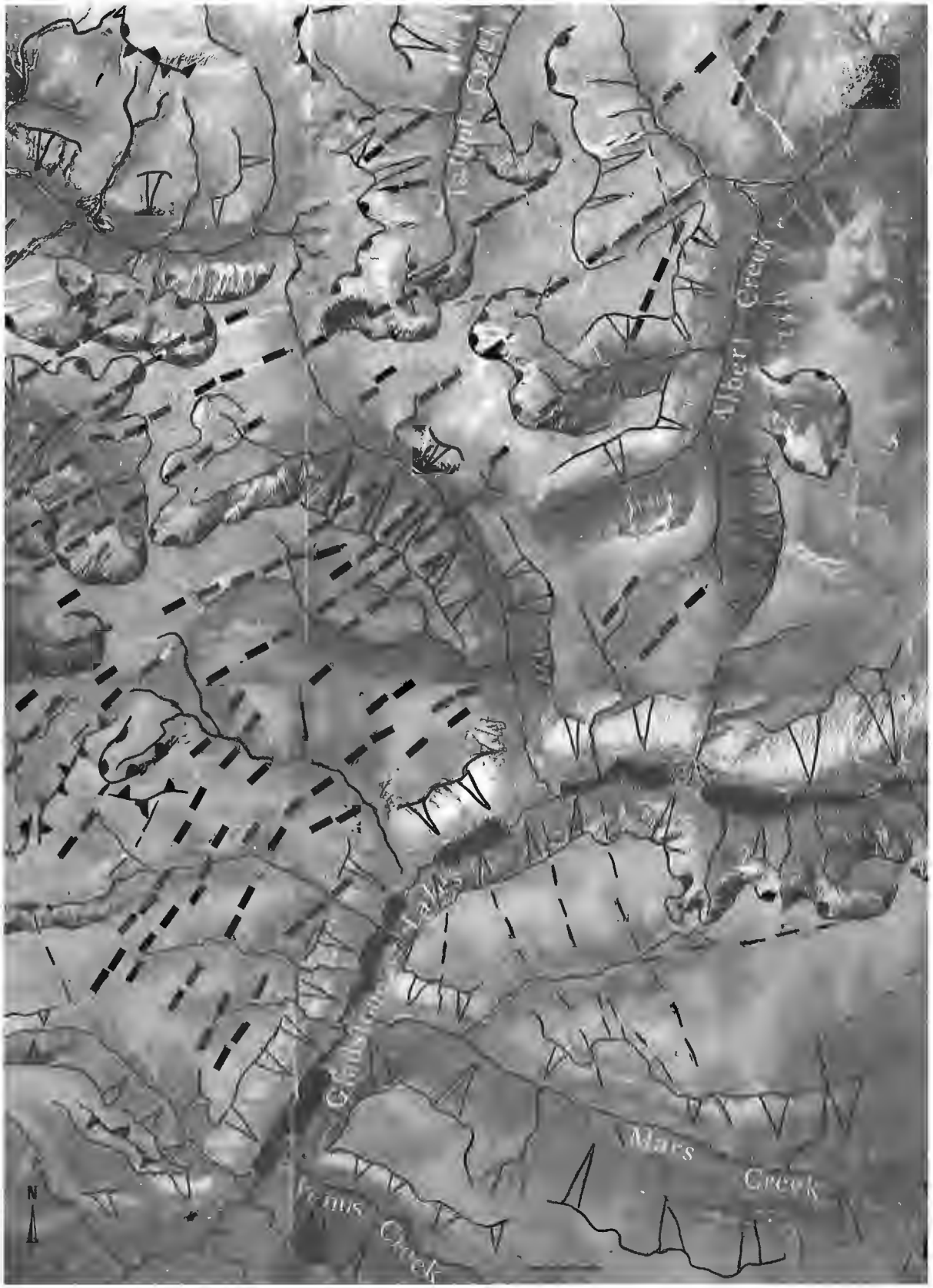

Figure 5. *Mosaïque de photographies aériennes du secteur des lacs Gladstone (Photothèque nationale de l'air, photographies n° A-25193-70 et A-25193-71).*

Les données morphostructurales regroupent ici les formes de relief et les tracés de cours d'eau pour lesquels la tectonique a joué un rôle prépondérant dans la formation et l'évolution. Ces deux aspects de l'étude sont analysés séparément.

Le système de fractures et le relief associé

L'interprétation des linéaments en termes de fracturation ou de traits morphologiques est représentée à la figure 3. Elle se fonde sur leur organisation, leur extension longitudinale et leur direction, ainsi que sur des liens établis avec les données géologiques connues. Des exemples de linéaments rapportés à des failles sont appuyés par des photographies aériennes (fig. 5 à 7; la légende des symboles utilisés est donnée à la figure 4). Ces exemples types n'ont pas d'équivalence sur les documents cartographiques antérieurs et constituent, par conséquent, des acquis nouveaux quant à la connaissance de la tectonique du secteur étudié. Les observations stéréoscopiques n'ont pas permis de retracer la faille qui va de Jarvis au ruisseau Gladstone sur la carte de Gabrielse et al. (1977).

Exemple n° 1 (fig. 5)

Des linéaments discontinus, par endroits parallèles et courbes, se concentrent à la limite des batholites de Ruby Range et de Nisling Range, au nord-ouest des lacs Gladstone. Ils présentent une direction générale nord-nord-est. De telles structures linéamentaires ne s'observent pas ailleurs dans le secteur étudié et constituent un aspect caractéristique de dislocation du substratum rocheux, qui se compose ici de granite.

La trame des segments linéaires peut révéler une expression locale de la fracturation à l'intérieur du massif granitique. Les microfissures formées à l'origine auraient été dégagées postérieurement par l'abrasion glaciaire. En l'absence de données de terrain, deux arguments sont en faveur d'une telle hypothèse.

1. Les segments linéaires à l'intérieur du massif granitique sont localisés sur le dôme, là où se serait produite la tension maximale lors de la mise en place de ce corps intrusif. On sait depuis plusieurs dizaines d'années, grâce aux travaux de Raguin (1969), de Lagasquie (1984) et de Blès (1984), que la fracturation observée dans un massif granitique correspond à un état final qui résulte de la superposition de plusieurs phases de déformation. La déformation a débuté par la mise en place du magma granitique (principe de diapirisme) et s'est poursuivie jusqu'à des périodes récentes. Les diverses phases de déformation sont matérialisées par des structures planaires ou linéaires qui traduisent la disposition des minéraux dans les roches granitiques. Dans une région d'instabilité tectonique comme celle dont il est question ici, la déformation peut être considérable lorsque les effets de la tectonique s'ajoutent à ceux créés par la montée diapirique des granitoïdes.
2. On ne saura pas attribuer l'origine des entailles linéaires observées à l'intérieur du massif intrusif à l'action de torrents juxtaglaciaires associés au processus de fusion des glaciers, comme il est en fait mention dans la littérature classique (Sudgen et John, 1976). La position de la plupart des structures observées est indépendante de la topographie. On les retrouve sur les versants comme sur les interfluves. Certaines sont perpendiculaires aux vallées alors que si ces entailles étaient d'origine glaciaire, elles seraient, comme les torrents qui les ont formées, parallèles à la direction des langues glaciaires.

Exemple n° 2 (fig. 6)

Des linéaments plurikilométriques d'orientation subméridienne limitent de part et d'autre l'extrémité méridionale du lac Sekulmun. Ils se poursuivent en faisceau vers le sud suivant

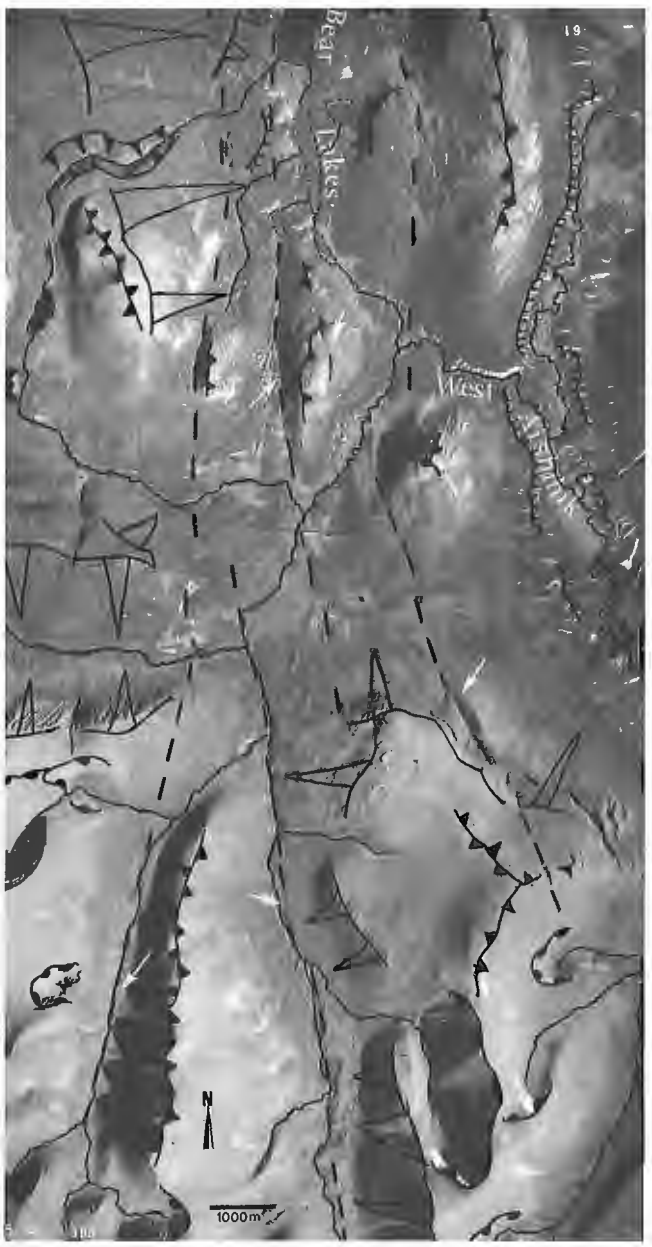

Figure 6. *Mosaïque de photographies aériennes du secteur sud du lac Sekulmun (Photothèque nationale de l'air, photographies n° A-25265-105 et A-25265-61).*

l'axe des lacs Bear, puis continuent en se ramifiant en dehors de la région selon la direction de la faille de Chatham Strait dans le nord de la Colombie-Britannique. Sur l'image satellitaire MSS, ces linéaments apparaissent avec netteté au nord du lac Sekulmun.

L'importance et la continuité de ces linéaments plurikilométriques permet d'assigner à ceux-ci une origine tectonique. L'interprétation s'appuie sur les éléments d'analyse suivants :

1. Les linéaments recoupent indifféremment toutes les unités lithologiques sur plusieurs centaines de kilomètres et ils sont localisés dans l'alignement d'accidents tectoniques connus.
2. La trace de ces linéaments plurikilométriques est matérialisée, sur les photographies aériennes de la région au sud du lac Sekulmun, par des gradins dans les formations lacustres du Quaternaire, ce qui nous indique une réactivation récente de fractures anciennes.

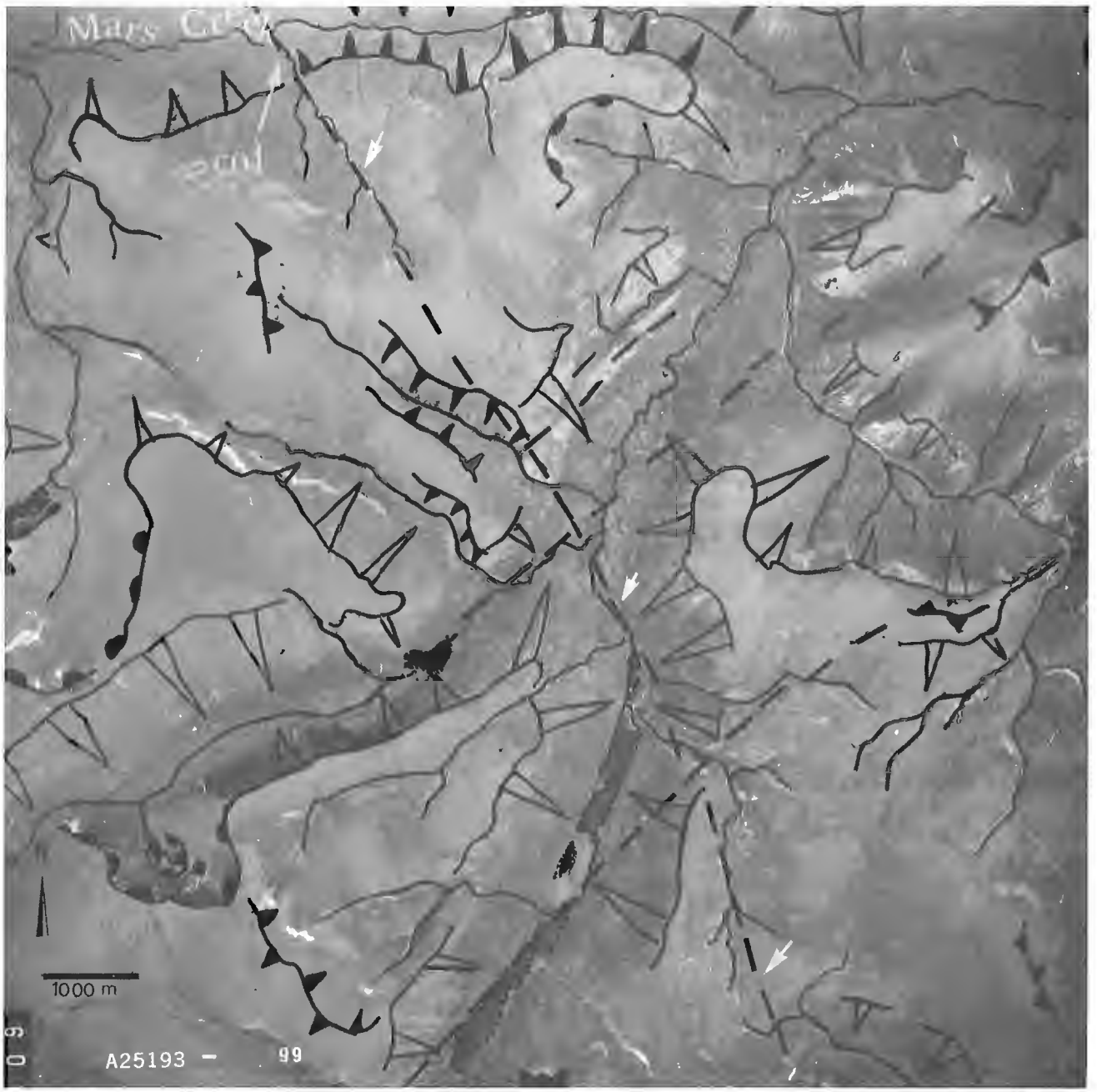

Figure 7. *Photographie aérienne du col de la vallée du ruisseau Mars (Photothèque nationale de l'air, photographie n° A-25193-99).*

3. Des exemples de failles similaires sont signalés dans la région voisine au sud du lac Aishihik (Gabrielse et al., 1977).

Le lac Sekulmun, à l'instar du lac Kluane, occupe un sillon tectonique. Les escarpements rectilignes qui le limitent sont des talus tectoniques, ce qui explique ainsi leur forme allongée caractéristique.

Exemple n° 3 (fig. 7)

Au sud-est des lacs Gladstone, apparaît un linéament plurikilométrique d'orientation nord-nord-ouest – sud-sud-est qui s'étend depuis le nord du lac Killermun jusqu'à la tête du ruisseau Albert, en passant par le col de la vallée du ruisseau Mars. Cette entaille rectiligne est une faille caractéristique. Le linéament est, en effet, localisé dans l'alignement de plusieurs vallées. Il forme un coude aigu, typique d'une fracture, au niveau du col de la vallée du ruisseau Mars.

Le réseau hydrographique

L'influence de la tectonique s'observe également dans l'organisation du réseau hydrographique. Les principaux cours d'eau prennent leur source sur le dôme structural formé par la montée diapirique de magma. C'est à partir de ce dôme que les rivières divergent et installent leurs vallées sur les lignes de faille.

La plupart des vallées affluentes des cours d'eau ont une orientation générale nord-sud, qui correspond à celle d'accidents majeurs comme les dykes. Les vallées principales sont caractérisées soit par une orientation ouest-nord-ouest – est-sud-est pour les cours d'eau se jetant dans le bras Talbot, soit par une orientation ouest-sud-ouest – est-nord-est pour les ruisseaux qui coulent vers le lac Sekulmun. La jonction entre les deux catégories de vallée (principale et affluente) se fait, dans la plupart des cas, selon un angle droit qui souligne ainsi l'existence d'une fracture. Le tracé des talwegs devient ainsi, à ce niveau d'analyse, l'expression de la fracturation du socle.

Au nord-ouest de la région étudiée, le tronçon supérieur du ruisseau Talbot constitue un exemple type d'une vallée-faille (fig. 8) : a) son orientation ouest-nord-ouest – est-sud-est est parallèle à celle d'importants accidents connus dans la région, tels que les failles de Shakwak et de Tintina; b) son tracé présente plusieurs déplacements horizontaux qui témoignent du jeu de failles conjuguées, dont l'emplacement et la direction devront être précisés par de nouvelles observations de terrain; c) la jonction de la vallée principale du ruisseau avec les vallées de ses affluents D^5 et D^9 se fait par un coude présumant l'existence d'une faille ou d'une fracture; d) son versant sud montre des talus étagés; e) et, enfin, le talus inférieur se caractérise par plusieurs sections décalées l'une par rapport à l'autre vers la droite, matérialisant ainsi les déplacements latéraux.

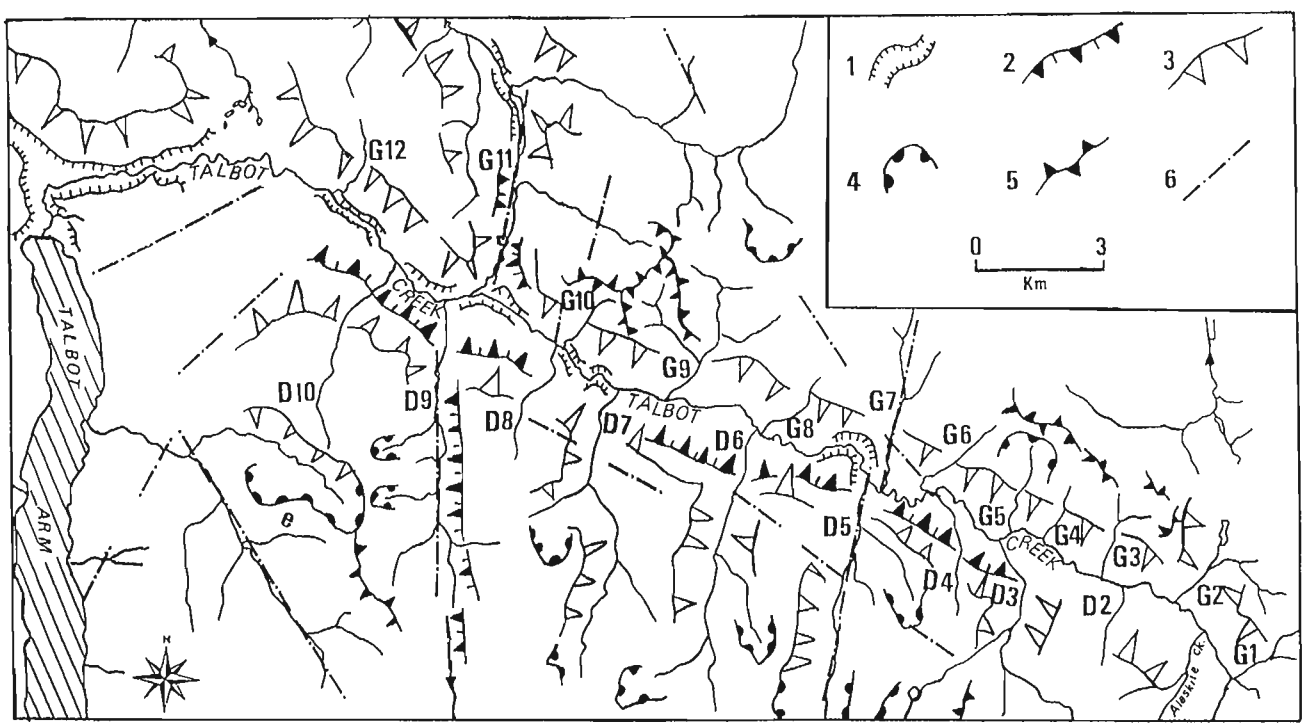

Figure 8. *Vallée du ruisseau Talbot et ses affluents. En l'absence des noms sur les cartes existantes, les rivières ont été désignées selon une numérotation utilisée par les premiers géologues belges en Afrique centrale (e.g. Cornet, 1894; Lepersonne, 1939)* ***D*** *= affluent de la rive droite et* ***G*** *= affluent de la rive gauche. Explications des symboles : 1. Encaissement du cours d'eau dans les dépôts quaternaires; 2. Talus associés à des failles; 3. Talus limitant une vallée glaciaire comme les vallées à fond plat des figures 5, 6 et 7; 4. Cirque glaciaire; 5. Crête rocheuse; 6. Fracture ou faille.*

Du fait que les failles ont permis un cheminement de l'eau dans la roche, elles ont guidé l'altération puis la dissection. Elles ont ainsi joué un rôle important dans la formation et l'évolution du réseau hydrographique. Les glaciers quaternaires ont retravaillé par la suite, les sillons initialement constitués par les failles, pour donner au réseau hydrographique sa configuration actuelle.

DISCUSSION DES RÉSULTATS

La mise en place d'un magma granitique par diapirisme demeure le facteur principal qui permet d'expliquer la position élevée de la partie centrale de la région. L'érosion différentielle ne peut expliquer à elle seule la présence du dôme qui constitue le point le plus élevé de la région étudiée. Une telle argumentation se justifie dans la mesure où le granite considéré ici comme roche de grande dureté affleure aussi bien dans les zones basses que dans les parties élevées dans la région.

Les exemples de linéaments-failles décrits plus haut sont les plus significatifs en termes de fracturation. Ils autorisent l'extrapolation de l'analyse à d'autres structures linéamentaires similaires. Toutefois, il convient de signaler que toutes les discontinuités observées ne sont pas des failles; leur signification nécessiterait une vérification sur le terrain. Des travaux antérieurs réalisés dans d'autres régions tectoniquement instables (Mbuluyo, 1993; Mbuluyo et al., 1994) ont montré que la signification définitive des linéaments devrait faire appel, en plus des critères précédemment définis, à d'autres facteurs tels que la composition pétrographique des roches, l'arrangement des minéraux au sein de celles-ci et l'étude microtectonique à l'échelle des affleurements. L'absence de ces observations constitue un facteur limitatif de nos interprétations.

En dehors des escarpements associés aux failles qui bordent les lacs Kluane et Sekulmun, le secteur étudié ne présente pas de talus de plus grande amplitude pouvant être l'expression en surface de failles. L'absence de grands escarpements de faille démontre la prépondérance des mouvements de coulissage de blocs sous l'influence de compressions horizontales sur les déplacements verticaux dont l'amplitude est relativement faible. Cette interprétation est en accord avec les données sur les failles majeures de la région qui témoignent de mouvements de coulissage dextre (Clague, 1979; Norris, 1987; Gabrielse et al., 1991). Par ailleurs, elle contredit l'idée du soulèvement général du sud-ouest du Yukon à une vitesse de 2,4 cm/an comme l'ont proposé Vanicek et Nagy (1981). En effet, dans l'hypothèse d'un soulèvement ininterrompu, la région aurait été située il y a 100 000 ans, 2 400 m plus bas que son niveau actuel. Elle se serait trouvée dans ce cas, au-dessous du niveau de la mer. Or, à notre connaissance, les observations de terrain ne signalent pas la présence de sédiments marins du Quaternaire dans la région.

CONCLUSION

L'étude du secteur central du chaînon Ruby a permis de dégager les éléments tectoniques qui expliquent la morphologie de la région et la configuration actuelle de son réseau hydrographique. L'influence de la tectonique s'observe notamment à grande échelle par la présence du dôme occupant la partie centrale de la région qui correspond au toit du batholite de Nisling. Les points les plus élevés de la région sont localisés sur ce dôme. C'est à partir de celui-ci que le réseau hydrographique s'organise.

Deux directions structurales majeures, l'une dominante et l'autre secondaire, peuvent être définies dans le secteur étudié. La direction dominante est révélée par des structures d'orientation ouest-nord-ouest – est-sud-est auxquelles appartiennent les principale failles connues (p. ex. faille de Shakwak). La direction secondaire est définie par des structures subméridiennes qui se situent dans le prolongement de fractures nord-sud, comme la faille de Chatam Strait dans le nord de la Colombie-Britannique. Le sud-ouest du Yukon apparaît donc comme une zone de jonction où les failles d'orientation nord-sud s'incurvent vers le nord-ouest. L'orientation des principaux talwegs est tributaire de cette direction tectonique. Le ruisseau Talbot est, à cet égard, assez démonstratif. Sa vallée montre une orientation ouest-nord-ouest – est-sud-est alors que ses affluents suivent une orientation méridienne (nord-sud).

REMERCIEMENTS

Nous tenons à remercier la Commission géologique du Canada et particulièrement la Division de la science des terrains pour avoir financé en partie les travaux de recherche associés à cette étude.

RÉFÉRENCES

Bles, J. L.
1984: Distribution de la fracturation en surface et en profondeur dans les granites; dans Journée sur le granite; Bureau de recherches géologiques et minières, Document n° 84, p. 69-80.

Clague, J. J.
1979: The Denali Fault System in southwest Yukon Territory: A geological hazard?; in Current Research, Part A; Geological Survey of Canada, Paper 79-1A, p. 169-178.

Cornet, J.
1894: Notes de terrain inédites; Dossiers d'archives n° 8, Musée royal d'Afrique centrale, Tervuren, Belgique.

Dewez, V.
1988: Sources, limites et fusion des glaciers au Wisconsinien supérieur dans la chaîne Ruby et le bassin d'Aishihik, Territoire du Yukon; Thèse de doctorat, Département de géographie, Université d'Ottawa, 320 p.

Dewez, V. et M.-A. Geurts
1996: Analyses minéralogiques multivariées de sédiments du Wisconsinien supérieur au sud-ouest du Yukon; Revue canadienne des sciences de la Terre, vol. 33, p. 42-51.

Gabrielse, H., Tempelman-Kluit, D. J., Bluisson, S.L., and Campbell, R.B.
1977: MacMillan River,Yukon – District of Mackenzie – Alaska; Geological Survey of Canada, 1:1 000 000 Geological Atlas, Sheet 105, 115, Map 1398A, scale 1:1 000 000.

Gabrielse, H., Monger, J.W.H., Yorath, C.S., and Dodds, C.J.
1991: Structural styles, Chapter 17 in Geology of the Cordilleran orogen in Canada, H. Gabrielse and C.J. Yorath (ed.); Geological Survey of Canada, Geology of Canada, no. 4, p.571-675 (also Geological Society of America, The Geology of North America, v. G-2).

Geurts, M.-A. et V. Dewez
1993: Le lac glaciaire Nisling et le Pléistocène dans le bassin supérieur de la Nisling River au Yukon; Géographie physique et Quaternaire, vol. 47, p. 81-92.

Hughes, O. L.
1967: Surficial geology studies, Aishihik Lake map-area; in Current Research, Part A; Geological Survey of Canada, Paper 67-1A, p. 48-49.

Kodybka, R. J.
1992: Aspects of the quaternary evolution of the plateau regions of the northern Ruby Range, Southwestern Yukon Territory; Ph.D. Thesis, Department of Geography, University of Ottawa, 219 p.

Lagasquie, J.-J.
1984: Géomorphologie des granites. Les massifs granitiques de la moitié orientale des Pyrénées françaises; Éditions du Centre national de la recherche scientifique, Centre régional de publication de Toulouse, 374 p.

Lepersonne, J.
1939: Série de la Kaïso, Lac Albert no 1, 9/10 au 1/12/1939; Dossiers d'archives n°116 et n°118, Musée royal d'Afrique centrale, Tervuren, Belgique.

Loren, J. J.
1992: Tectonic analysis of the Nisling, northern Stikine and northern Cache Ruisseau terranes, Yukon and British Columbia; Ph.D. Thesis, University of Arizona, 198 p.

Mbuluyo, M. K.
1993: Géomorphologie de l'Ituri oriental (nord-est du Zaïre). Analyse morphologique et structurale des effets d'une réactivation du Rift; Thèse de doctorat, Faculté des sciences, Université de Liège, Belgique, 303 p.

Mbuluyo, M. K., Ozer, A. et Lavreau, J.
1994: La carte morphostructurale de l'Ituri oriental (nord-est du Zaïre). Étude à partir de données satellitaires TM de Landsat; dans Dubois, J.M., Cavayas, F. et Lafrance P. (Eds), Télédétection appliquée à la cartographie thématique et topographique; Editions AUPELF-UREF et Presses de l'Université du Québec, p. 41-53.

Muller, J. E.
1967: Kluane Lake map-area, Yukon Territory; Geological Survey of Canada, Memoir 340, 137 p.

Norris, D. K.
1987: Évolution tectonique et décrochements dextres principaux; dans Pelletier, B. R. (Ed.) Atlas des sciences marines de la mer de Beaufort, Géologie et Géophysique, Commission géologique du Canada, Rapport divers 40, p. 2.

Raguin, E.
1969: Pétrographie des roches plutoniques dans leur cadre géologique; Masson, Paris, 239 p.

Sugden, D. E. and John, B.S.
1976: Glaciers and landscape; Edwart Arnold, London, 376 p.

Vanicek, P. and Nagy, D.
1981: On the compilation of the map of contempory vertical crustal movements in Canada; Tectonophysics, v. 71, p. 75-86.

Projet 930043 de la Commission géologique du Canada

Seismic reflection profiling in support of a deep borehole, Fraser River delta, British Columbia

J.B. Harris[1], R.A. Hillman[2], J.A. Hunter[3], and J.L. Luternauer
GSC Pacific, Vancouver

Harris, J.B., Hillman, R.A., Hunter, J.A., and Luternauer, J.L., 1997: Seismic reflection profiling in support of a deep borehole, Fraser River delta, British Columbia; in Current Research 1997-E; Geological Survey of Canada, p. 13-18.

Abstract: Approximately 3 km of seismic reflection data have been obtained in order to map the structure of the bedrock (Tertiary) surface in an area surrounding a deep borehole drilled as part of a continuing earthquake hazards assessment of the Fraser River delta. Seismic data quality was highly variable (even over relatively short distances) due primarily to the presence of gas in the shallow sediments. A map of two-way travel time suggests a northeast-trending bedrock channel beneath the area that is possibly fault controlled. The structure of the bedrock surface beneath the delta has been identified as an important boundary for controlling ground motion amplification from seismic shaking. It is anticipated that this new information will be combined with the existing bedrock data set to further assemble a geological and geophysical framework of the deep structure beneath the delta.

Résumé : Les chercheurs ont recueilli des données de sismique-réflexion sur environ 3 km, en vue de cartographier la structure de la surface du substratum rocheux (tertiaire) de la région entourant un sondage profond foré dans le cadre d'un programme d'évaluation continue des risques séismiques dans le delta du fleuve Fraser. La qualité des données sismiques est très variable (même sur des distances relativement courtes), en raison surtout de la présence de gaz dans les sédiments peu profonds. Une carte des temps de trajet aller-retour suggère la présence, dans le substratum rocheux, d'un chenal de direction nord-est qui pourrait être contrôlé par des failles. La structure de la surface du substratum rocheux sous le delta a été identifiée comme une limite importante susceptible d'influer sur l'amplification des mouvements du sol consécutifs aux secousses séismiques. On envisage de combiner ces données nouvelles à l'ensemble des données actuelles sur le substratum rocheux, afin d'affiner le cadre géologique et géophysique de la structure profonde sous le delta.

[1] Department of Geology, Millsaps College, Jackson, Mississippi U.S.A. 39210
[2] Frontier Geosciences Inc., 237 St. Georges Avenue, North Vancouver, British Columbia V7L 4T4
[3] Terrain Sciences Division, Ottawa

INTRODUCTION

In the spring of 1994, scientists from the Geological Survey of Canada (GSC) and several Canadian universities completed two 300 m deep geotechnical boreholes in the northern part of the Fraser River delta, British Columbia (Dallimore et al., 1995). The purpose of the work was to characterize the geology of the delta at two sites with contrasting geological settings, and provide in situ geological, geophysical, and geotechnical measurements of sediment properties at depths that had not previously been sampled. These data, in addition to a map of the bedrock (Tertiary) surface beneath the delta (Britton et al., 1995), have been used as part of a continuing effort to identify and help assess earthquake hazards associated with the thick Quaternary sediments in the region (e.g., Harris et al., 1995).

In borehole FD94-3, the Holocene delta sequence is anomalously thin (19 m) and is underlain by Pleistocene sands and clays. Surprisingly, Tertiary bedrock was not encountered in the borehole. To supplement the borehole data and provide a more detailed three-dimensional geological picture in the vicinity of FD94-3 (see Fig. 1 and 2 for location), a seismic reflection survey targeting the top of bedrock was conducted in March of 1995.

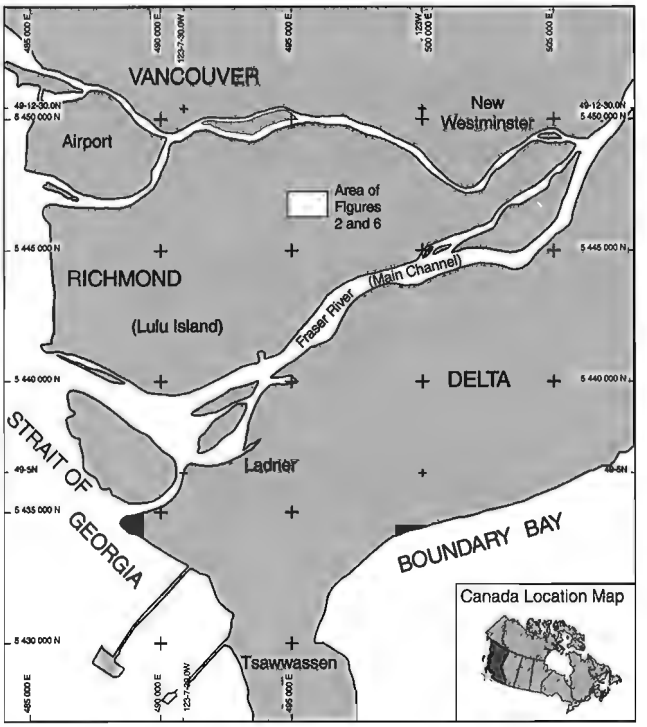

Figure 1. *Map of the Fraser River delta showing the location of the study area (white rectangle on inset map) in eastern Richmond.*

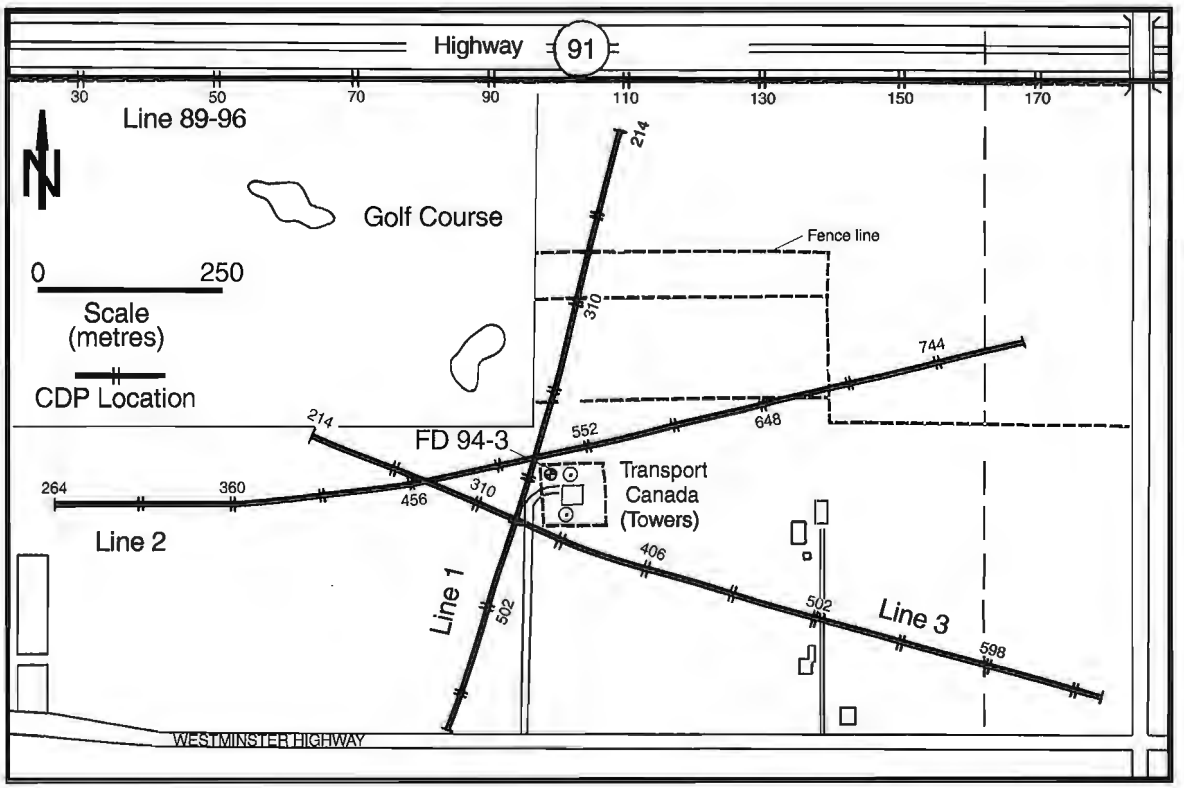

Figure 2. *Site map of the study area showing the locations of borehole FD 94-3, seismic lines 1, 2, and 3 (collected as part of this investigation), and seismic line 89-96 (Hunter et al., 1996).*

DATA ACQUISITION AND PROCESSING

Approximately three line-kilometres of common-depth-point (CDP) seismic reflection data were collected near borehole FD94-3 by Frontier Geosciences, Inc. Three lines were laid out to intersect near the borehole, with line 1 oriented approximately north-south and lines 2 and 3 oriented east-west and northwest-southeast, respectively (Fig. 2). The seismic energy source was an in-hole shotgun (Pullan and MacAulay, 1987) firing 8-gauge black powder blanks in 1 m deep, water-filled holes. The receivers were single 40 Hz geophones, in marsh casings, spaced at 5 m intervals. The lines were shot end-on using a source to first geophone offset of 30 m, and the data were recorded on a Geometrics (S-24) 24-channel seismograph.

The site of the borehole is a secured Transport Canada facility housing radio towers utilized by aircraft approaching and departing the Vancouver International Airport. Both aircraft noise and variable (strength and duration) radio frequency (RF) transmissions hindered the collection of high quality reflection profiles. Data collection proceeded, as much as possible, during intervals of low aircraft traffic and at times with minimal RF interference. In addition to noise problems, the RF transmissions caused numerous false triggers of the seismograph that were interpreted to be an "antenna effect" related to the amount of takeout cable and trigger line spread across the ground. In order to counteract this phenomenon, field equipment was changed to minimize the length of takeout cables/trigger line lying on the ground and first arrivals were constantly monitored to insure that accurate triggers were being recorded.

Processing was done with the WinSeis software package (Kansas Geological Survey) using a standard sequence for CDP reflection data that includes: data reformat, trace editing, CDP sort, velocity analysis, normal moveout correction, bandpass filtering (40 to 120 Hz), automatic gain control (200 ms window), and CDP stack. The most time consuming and difficult stage of processing involved trace editing; selective trace muting was applied to the data in order to remove undesirable seismic signals (i.e. aircraft and RF noise, refracted energy, and airwave and groundroll arrivals).

RESULTS

In many parts of the Fraser delta, the collection of high-quality seismic reflection data is hindered by the presence of gas in shallow sediments (S.E. Pullan, pers. comm., 1997). Even small amounts of gas can considerably reduce velocities and increase seismic attenuation. Upon viewing the processed seismic reflection sections (Fig. 3, 4, and 5), it is immediately apparent that abrupt changes in seismic amplitudes occur along the length of the lines. This variability in data quality clearly indicates the presence of near-surface gas in the study area.

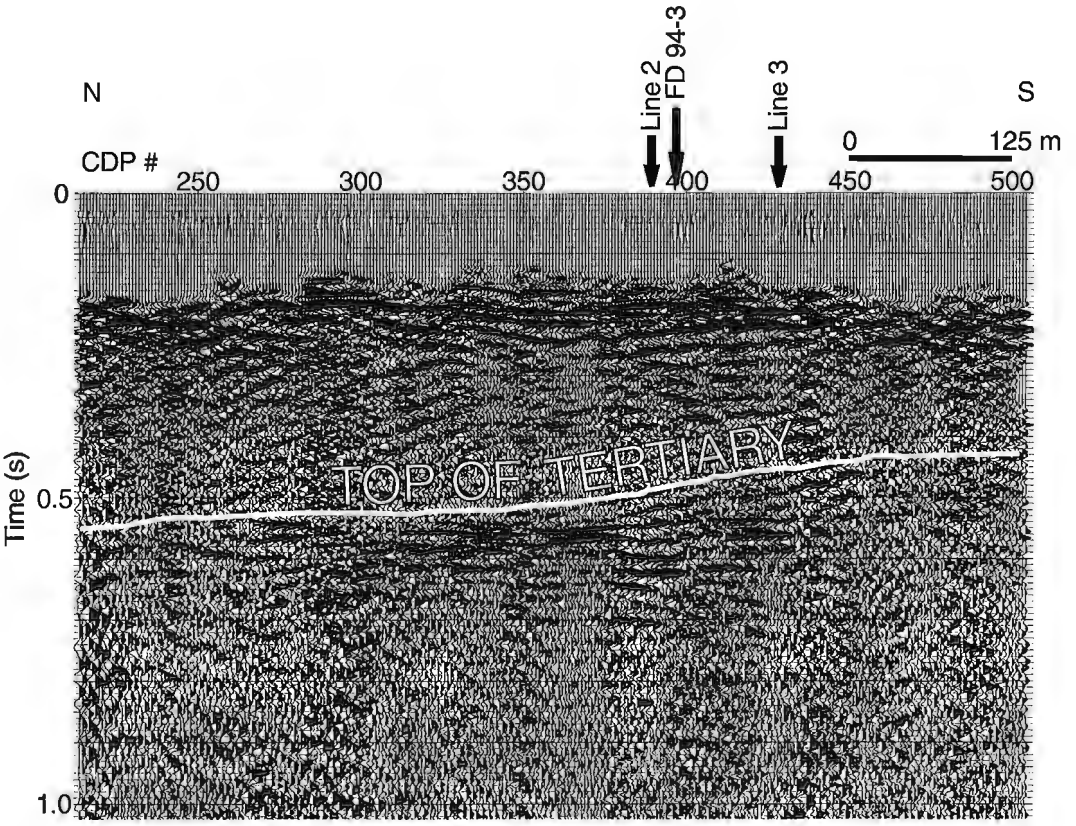

Figure 3. Interpreted seismic line 1.

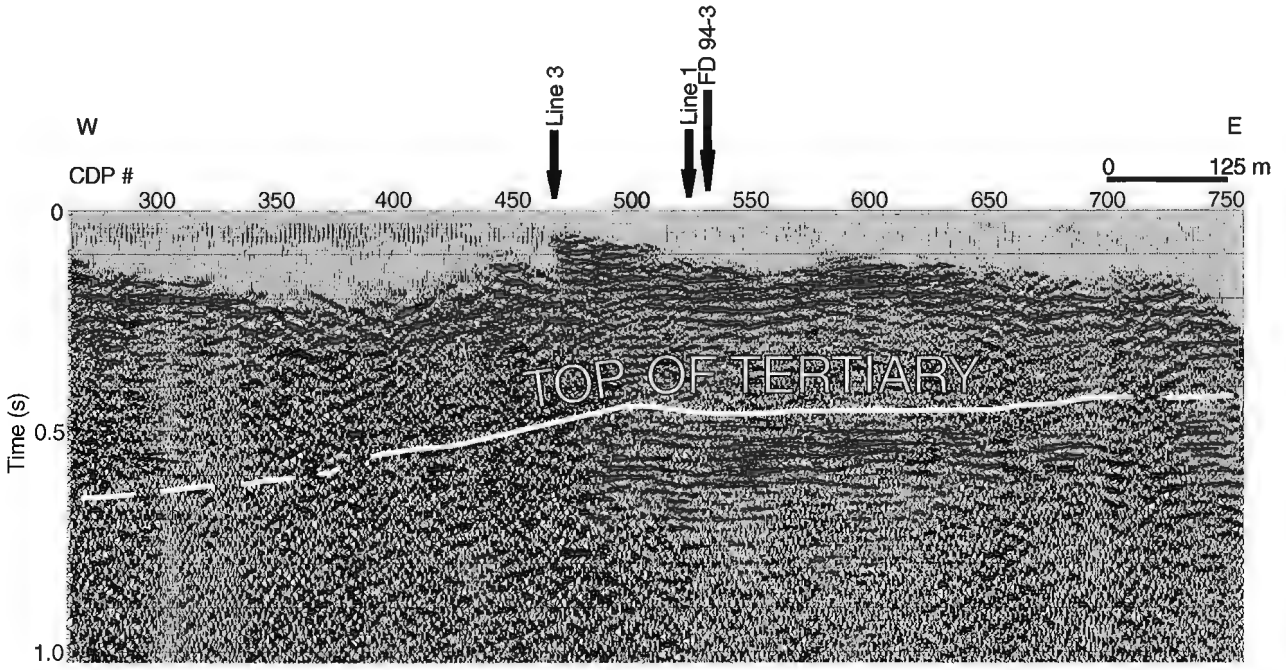

Figure 4. *Interpreted seismic line 2.*

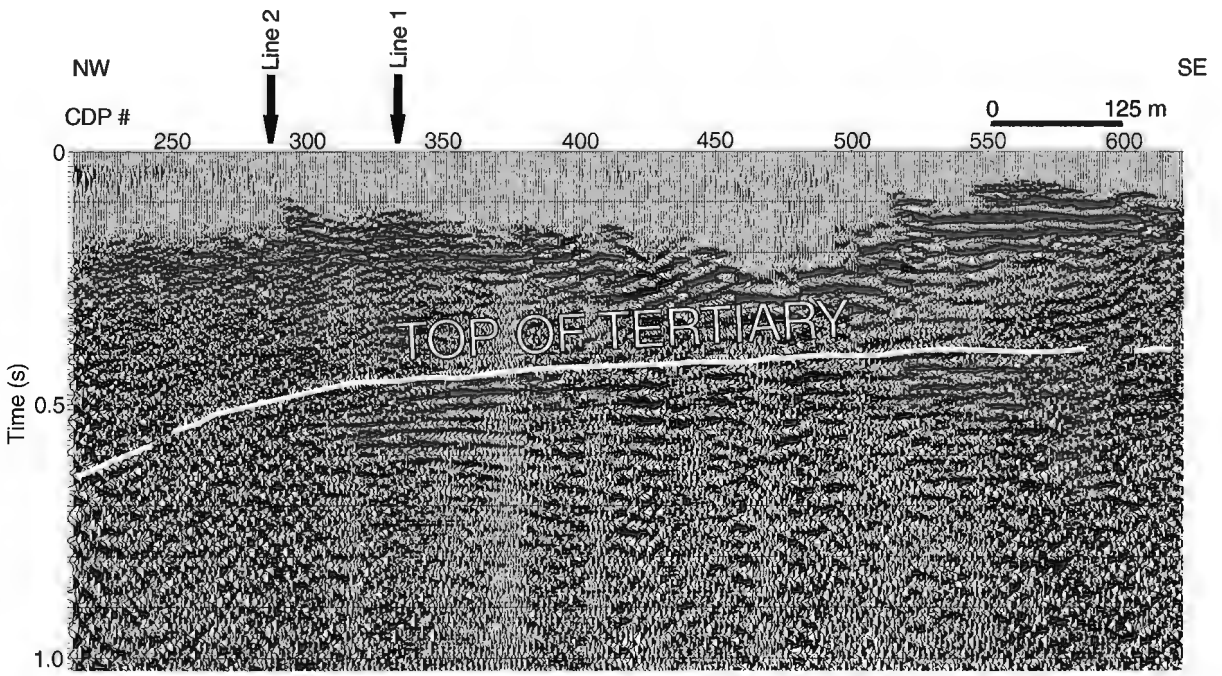

Figure 5. *Interpreted seismic line 3.*

Reflection profiles

In areas where gas in the sediments is not a problem or in seismic surveys utilizing more powerful seismic energy sources (i.e. Britton et al., 1995), the unconformity marking the top of Tertiary sediments beneath the Fraser delta is a strong reflecting horizon. Correlation of the reflection profiles from this study with a nearby seismic line (89-96) from the Britton et al. (1995) data set provided a starting point for our interpretation of the bedrock (Tertiary) surface.

Line 1 (Fig. 3) is approximately 0.75 km in length and its north end is less than 100 m south of CDP #110 (shotpoint #485) on line 89-96 (Hunter et al., 1996). The top of Tertiary has been interpreted at a two-way travel time of about 0.55 s on the north end of line 1. South of CDP #350, the Tertiary surface dips north and rises to less than 0.45 s near the south end of the line. This structure correlates with the east side of a channel-like bedrock feature imaged on line 89-96. A group of shallower (0.3 to 0.45 s) lens-shaped reflections in the middle of the section also correlate with a similar reflection pattern (channel-fill?) on line 89-96 (J. Britton, Dynamic Oil Ltd., pers. comm., 1995).

Line 2 (Fig. 4) is 1.3 km long and is oriented approximately east-west. On the east half of the line, the data quality is very good and the bedrock surface displays a subtle dip to the west. An abrupt change in data quality occurs at CDP #480, and data west of that point are undoubtedly attenuated by the presence of gas. Although the data are of lower quality on the west half of the line, the bedrock reflection is interpretable and shows a slightly steeper westward dip.

Line 3 (Fig. 5) has a northwest-southeast orientation and is 1.0 km in length. The top of Tertiary dips gently northwesterly from the southeast end of the line to near CDP #330. West of CDP #330, the data quality decreases markedly (gas) and the bedrock reflection suggests a steeper northwesterly dip of the Tertiary surface.

Bedrock structure

Interpretations of the two-way travel time to the bedrock surface were made every 24th CDP spacing (60 m) along each of the three seismic lines. The times were plotted on the site map and contoured as shown in Figure 6.

The map (Fig. 6) shows a northwest-dipping bedrock surface. Borehole FD 94-3 is situated near a break in slope on this surface that is believed to represent the southeast side of a northeast-trending bedrock channel. The northwest side of the channel is unconstrained based on the new data and is not included on the map, however correlation with line 89-96 suggests that the feature is a channel approximately 2 km wide. An interesting observation is that the onset of the

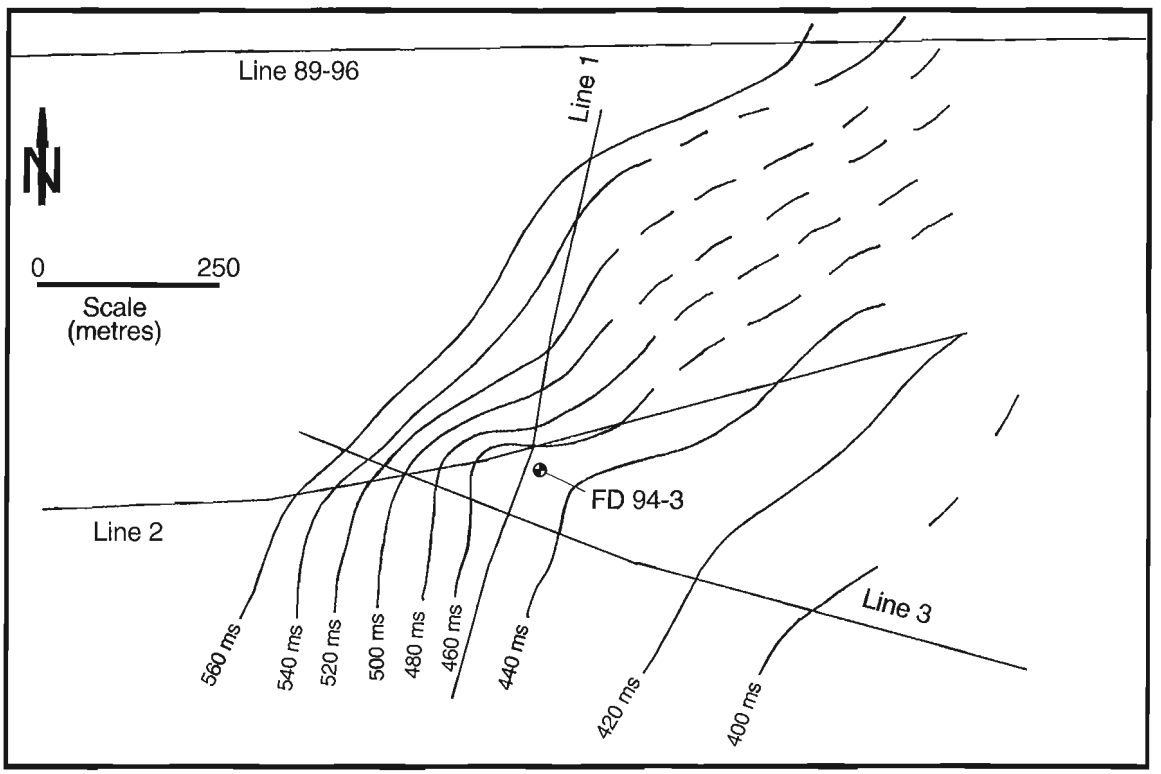

Figure 6. *Map of two-way travel time to the top of Tertiary bedrock from interpretation of the seismic reflection lines. The locations of borehole FD 94-3, lines 1, 2, and 3, and line 89-96 are shown.*

"gassed-out" parts of lines 2 and 3 correlates with the break in slope at the channel boundary, and suggests that the gas might be associated with the channel-fill sediments.

The trend of the bedrock channel (northeast) does not have the same northwest orientation as most of the large bedrock troughs mapped by Britton et al. (1995). However, northeast-trending Tertiary faults have been recognized to control the orientation of the Fraser lowland (Monger et al., 1995). Therefore, it is possible that the northeast-trending channel imaged in this survey is fault controlled and may represent a conjugate bedrock fabric that was previously unresolved on the scale of the Britton et al. (1995) map.

Although a detailed time-to-depth conversion has not been done, depths to bedrock are interpreted to range from approximately 325 m to 450 m using velocity information from the suite of geophysical logs collected in FD 94-3 (Dallimore et al., 1995).

CONCLUSIONS

This paper has presented new information on the local structure of the Tertiary bedrock surface in the area beneath borehole FD 94-3. Seismic data quality was highly variable (even over relatively short distances) due to aircraft and RF noise and the presence of gas in the shallow sediments. A two-way travel time map of the bedrock surface suggests a northeast-trending channel beneath the area and supports existing regional bedrock data (Britton et al., 1995) that presents the Tertiary surface as a structurally complex boundary. It has been suggested that the geometry and depth of the bedrock surface will influence ground shaking resulting from significant earthquakes in the region (Harris et al., 1995). Therefore, it is expected that the bedrock structure information generated in this study will be combined with the existing bedrock data set to improve interpretations of the deep structure beneath the Fraser delta.

ACKNOWLEDGMENTS

We thank Harold Christian (GSC, Atlantic), Dieter Weichert (GSC Pacific, Sidney), and Bev Vanlier (GSC Pacific, Vancouver) for their reviews of the manuscript. We also thank Jim Britton of Dynamic Oil Ltd. for providing access to seismic line 89-96.

REFERENCES

Britton, J.R., Harris, J.B., Hunter, J.A., and Luternauer, J.L.
1995: The bedrock surface beneath the Fraser River delta in British Columbia based on seismic measurements; in Current Research 1995-E; Geological Survey of Canada, p. 83-89.

Dallimore, S.R., Edwardson, K.A., Hunter, J.A., Clague, J.J., and Luternauer, J.L.
1995: Composite geotechnical logs for two deep boreholes in the Fraser River delta, British Columbia; Geological Survey of Canada, Open File 3018.

Harris, J.B., Hunter, J.A., Luternauer, J.L., and Finn, W.D.L.
1995: Site response modelling of the Fraser River delta, British Columbia: preliminary results from two deep boreholes; in Current Research 1995-E; Geological Survey of Canada, p. 69-75.

Hunter, J.A., Harris, J.B., and Britton, J.R.
1996: Compressional and shear wave interval velocity data for Quaternary sediments in the Fraser River delta from multichannel seismic reflection surveys; Geological Survey of Canada, Open File 3325, 228 p.

Monger, J.W.H., Journeay, J.M., Currie, L., and Hamilton, T.
1995: Neogene tectonics of southwestern British Columbia; Geological Association of Canada, Annual Meeting, Final Program and Abstracts, p. A-72.

Pullan, S.E. and MacAulay, H.A.
1987: An in-hole shotgun source for engineering seismic surveys; Geophysics, v. 52, p. 985-996.

Geological Survey of Canada Project 860022

Interior Plains and Arctic Canada

Plaines intérieures et région arctique du Canada

A problematic Early Cretaceous age for the conglomerates previously assigned to the Eureka Sound Group, east-central Ellesmere Island, Arctic Archipelago

T.A. de Freitas, A. Sweet, and R. Thorsteinsson
GSC Calgary, Calgary

de Freitas, T.A., Sweet, A., and Thorsteinsson, R., 1997: A problematic Early Cretaceous age for the conglomerates previously assigned to the Eureka Sound Group, east-central Ellesmere Island, Arctic Archipelago; in Current Research 1997-E; Geological Survey of Canada, p. 21-32.

Abstract: A conglomerate sequence more than 1 km thick was deposited in the footwall of the Parrish Glacier Thrust, in gravelly braided stream and alluvial fan settings. The conglomerate lithoclasts were derived from lower Paleozoic strata exposed in the hanging wall of the thrust. Internal disconformities in the conglomerates adjacent to the main regional thrust and the klippe of Ordovician carbonate resting on the conglomerates, indicate that thrusting was synchronous with, and postdated, sedimentation.

Fossils from the conglomerate outlier are Early Cretaceous in age. The apparent lack of exposed Cretaceous deposits in the hanging wall and the extent of fine grained deposits from which the fossils were collected suggest their deposition was in situ. However, alluvial deposits of this type and age are unknown in the Canadian Arctic, and conglomeratic outliers farther north have yielded Paleocene or younger fossils, thus placing the Cretaceous age assignment in question.

Résumé : Une séquence conglomératique de plus de 1 km d'épaisseur a été déposée dans le compartiment inférieur du chevauchement de Parrish Glacier, dans des milieux de cours d'eau anastomosés graveleux et de cônes alluviaux. Les lithoclastes conglomératiques sont dérivés de strates du Paléozoïque inférieur exposées dans le compartiment supérieur du chevauchement. La présence de disconformités internes dans les conglomérats jouxtant le chevauchement régional principal et d'un klippe de roches carbonatées ordoviciennes sur les conglomérats indique que le chevauchement a eu lieu pendant et après la sédimentation.

Les fossiles du lambeau d'érosion conglomératique datent du Crétacé précoce. L'absence apparente d'affleurements de dépôts crétacés dans le compartiment supérieur et l'étendue des dépôts à grain fin dans lesquels les fossiles ont été recueillis permettent de supposer que ceux-ci se sont accumulés sur place. Toutefois, les dépôts alluviaux de ce type et de cet âge sont inconnus dans l'Arctique canadien et les lambeaux d'érosion conglomératiques situés plus au nord renferment des fossiles paléocènes ou plus récents. L'attribution au Crétacé est donc problématique.

INTRODUCTION

The eastern Ellesmere Island Eureka Sound Group type beds have been visited sporadically for many years. Early explorers used Tertiary coals in Watercourse Valley as a source of energy during expeditions to the far north (Fig. 1; Nares, 1878; Greely, 1888). Members of the Nares expedition (Feilden and De Rance, 1878) also provided the first age and lithological information about these strata. Christie (1964) visited the Watercourse Valley and Pavy River outliers (Fig. 1) as part of a regional geological study, and assigned an Early Cretaceous or Early Tertiary age to the generally fine grained clastic deposits. In the early 1960s, J.W. Kerr examined the regions containing the three southern outliers (Fig. 1) during reconnaissance-scale bedrock mapping, but much of the work was based on air photo interpretation, and Kerr did not recognize the conglomeratic texture of the outliers and included them within the lower Paleozoic succession (Kerr, 1973a, b, c).

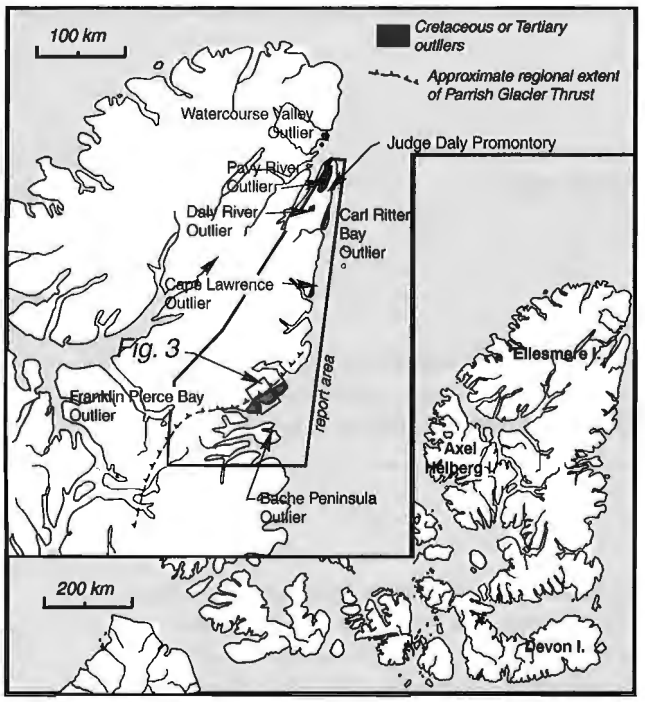

Figure 1. *Locality map, Canadian Arctic Islands.*

In 1972 and 1973, U. Mayr, then working for J.C. Sproule and Associates Ltd., prepared 1:250 000-scale bedrock geology maps of the area and recognized the syntectonic nature of the Cape Lawrence and Franklin Pierce Bay outliers. Mayr and de Vries (1982) later reinterpreted these strata, and assigned a Tertiary age to them based on a Paleocene macroflora collection from the Cape Lawrence Outlier in 1973 (Fig. 1). The Pavy River and Carl Ritter Bay outliers were visited by Miall (1982), who reported on the sedimentology of the thick syntectonic units, and concluded they were Paleocene (Fig. 2).

Ricketts (1994), in a comprehensive study of the upper Sverdrup Basin succession, equated the Franklin Pierce Bay conglomerates to the Buchanan Lake Formation and assigned an Eocene age to them. This age was not based on fossils but on the assumption that the Eurekan Orogeny was regionally synchronous and that Eocene fossils were associated with the

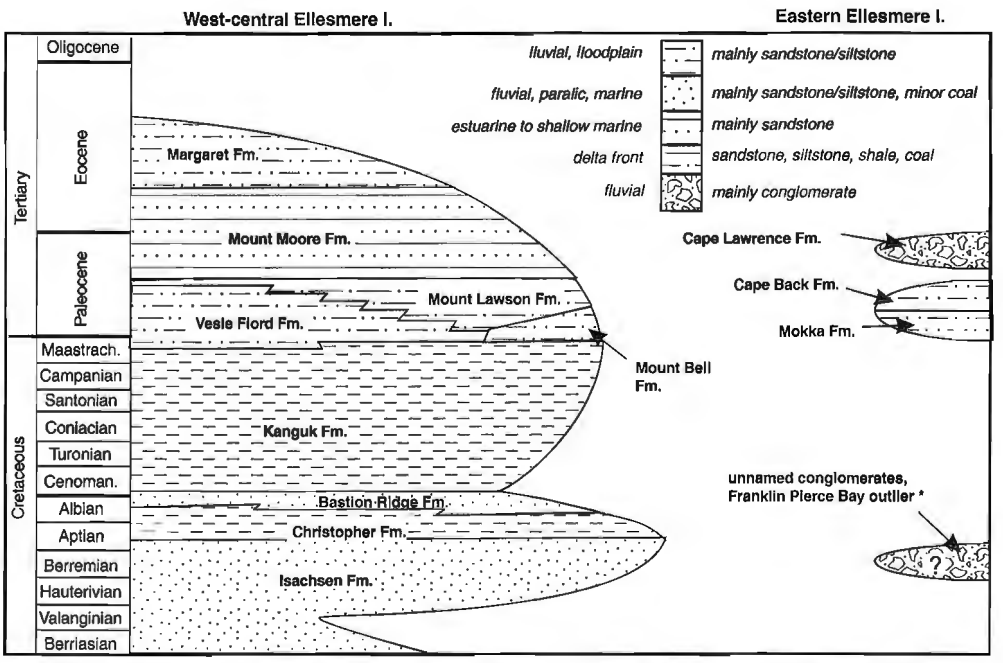

*conglomerates of the Franklin Pierce Bay Outlier contain Cretaceous and younger fossils, and thus its age is problematic (see text for discussion)

Figure 2. *Stratigraphic correlation of late Mesozoic-early Cenozoic strata, central and eastern Ellesmere Island. Modified from Miall (1991) and Embry (1991). For alternative stratigraphic nomenclature, see Ricketts (1994).*

syntectonic deposits on parts of Ellesmere and Axel Heiberg islands. While Ricketts (1994) acknowledged the Paleocene age reported earlier by Mayr and de Vries (1982) and Miall (1982), he did not explain this marked age discrepancy.

In 1984 and 1996, these deposits were revisited by R. Thorsteinsson and T. de Freitas, respectively, and additional organic-rich strata were sampled for age dating. The older sample set (*Eastern sample set*, C-61710, C-61716, C-61717; Fig. 3) was analyzed by D. McIntyre in 1985, and the second set (*Western sample set;* C-246243 – 246246; Fig. 3) by A. Sweet in 1996-1997. Both sets yielded Lower Cretaceous fossils notwithstanding the fact that they were collected by different field geologists at different times and dated by different paleontologists. This surprising age is reported and discussed herein, together with new reflectance data, map relationships, and lithological observations of the Franklin Pierce Bay and Cape Lawrence outliers and the nearby lower Paleozoic strata.

LITHOLOGY

The spectacular exposures of the Franklin Pierce Bay outlier were examined briefly during two days in early June, 1996 (T. De Freitas) and a single day of helicopter work in mid-July, 1984 (R. Thorsteinsson).

Franklin Pierce Bay Outlier

The Franklin Pierce Bay Outlier consists of vertical cliff facies up to 1 km high, composed of massive to vaguely stratified, oligomict carbonate, ortho- and paraconglomerates (Fig. 4B, C). Clasts appear to be mostly of cobble size, although many boulder sized clasts are visible. Clasts are abundantly imbricated and appear to show a southeastward transport direction, but this needs statistical verification. Many Ordovician and Silurian formations can be identified in the conglomerate lithoclasts.

Cliffs along the east coast of Franklin Pierce Bay show large-scale bed truncations (Fig. 4B). West of Cape Harrison, a well exposed synsedimentary normal fault features significant stratigraphic offset of Silurian strata and the lower part of the conglomerate sequence (Fig. 5). Conglomerates appear to everywhere rest on Silurian carbonates in the footwall of the Parrish Glacier Thrust (Fig. 3).

STRUCTURE

The hanging wall panel of the Parrish Glacier Thrust contains more than 3 km of Cambrian to Devonian carbonates and clastics. It has an exposed length of about 180 km and a variable orientation, from north-northeast near Bay Fiord to east-northeast near Dobbin Bay. The swing of the thrust is related to a regional cratonic promontory, centered south of Bache Peninsula (Fig. 1). The promontory consists of strongly deformed Precambrian crystalline basement and minor, flat-lying sedimentary rocks, unconformably overlain by a veneer of mildly deformed lower Paleozoic strata (Kerr, 1973a, b, c). The oldest units encountered in the hanging wall are interbedded sandstone and mudrock of the Lower Cambrian Kennedy Channel Formation (Fig. 3), which are overlain by a series of competent carbonate and clastic units. The generally northward-dipping panel contains several gentle, upright folds. Minor thrusts also occur, particularly where the Baumann Fiord Formation is exposed, but the full extent of these structures is presently unknown.

The Footwall structure is more complex. It contains several flat thrusts carrying Cambrian to Silurian strata, which locally form klippe on the Tertiary conglomerate, such as near Franklin Pierce Bay (Fig. 3) and at Cape Lawrence (Fig. 4A). These strata are generally gently dipping or contain upright folds and minor faults. The conglomerates are generally flat lying or gently folded.

PALEONTOLOGY

The nomenclature of the miospores shown in Table 1 and discussed below follows as closely as possible that of Hopkins (1971, 1973, 1974) for ease of comparison between the floras. Otherwise taxa conform to those of Singh (1971). All samples, except for C-61716, yielded prolific assemblages (Table 1; Plate 1).

Western sample set

Four paleontological samples (C-246243 – 246246), studied by A. Sweet in 1996, were collected by T. de Freitas from two sandstone and coal outcrops, each with an exposed area of less than 100 m^2 and thickness of about 2 m. The coal-bearing outcrops are badly weathered, poorly consolidated, and unstratified; they occur immediately south of a prominent, unnamed footwall thrust (Fig. 3) and appear to overlie conglomerate beds, but this contact is not exposed. Overlying strata are also not exposed, and thus the stratigraphic relationship of these beds with the conglomerates is uncertain: they could be interpreted as interbedded with the conglomerates, or they could represent tectonic slivers, transported there during development of the unnamed footwall thrust (Fig. 3).

As shown in Table 1 and Plate 1, the assemblages contain abundant gymnosperm pollen, mostly *Alisporites bilateralis*, *A. grandis*, and *Cerebropollenites mesozoicus* (*Tsugaepollenites mesozoicus* in Hopkins, 1971). These gymnosperms and the associated spore flora, in particular *Acanthotriletes varispinosus, Cicatricosisporites* spp., *Concavissimisporites variverrucatus*, and *C. verrucosus*, *Densoisporites* cf. *D. crassus*, *Gleicheniidites senonicus*, *Neoraistrickia* cf. *N. robusta*, *Perinopollenites elatoides*, *Pilosisporites trichopapillosus*, *Sestrosporites pseudoalveolatus* (*Hymenozonotriletes* cf. *H. pseudoalveolatus* in Hopkins, 1971), and *Trilobosporites* cf. *T. purverulentus,* are characteristic of Early Cretaceous floras such as those reported by Singh (1971), Burden and Hills (1989), and Hopkins (1971, 1973) from the Early Cretaceous Isachsen and Christopher

formations of the eastern Arctic Islands. This clearly establishes the dominant component of the assemblages as Early Cretaceous.

However, a secondary component of two of the samples (C-246245 and C-246246) is represented by triporate, betulaceous pollen and a single specimen of tricolpate pollen. Triporate pollen such as this first appears in the Maastrichtian and is characteristic of Tertiary assemblages.

To determine the source of the triporate pollen the two samples were split into three fractions: larger coal fragments, pieces of lithified mudstone, and a -150 μm fraction composed of clayey debris and fine mudstone and coal fragments. The triporate pollen and the single specimen of tricolpate pollen were found in the preparations of the fine fractions and not in the coal and mudstone fragments.

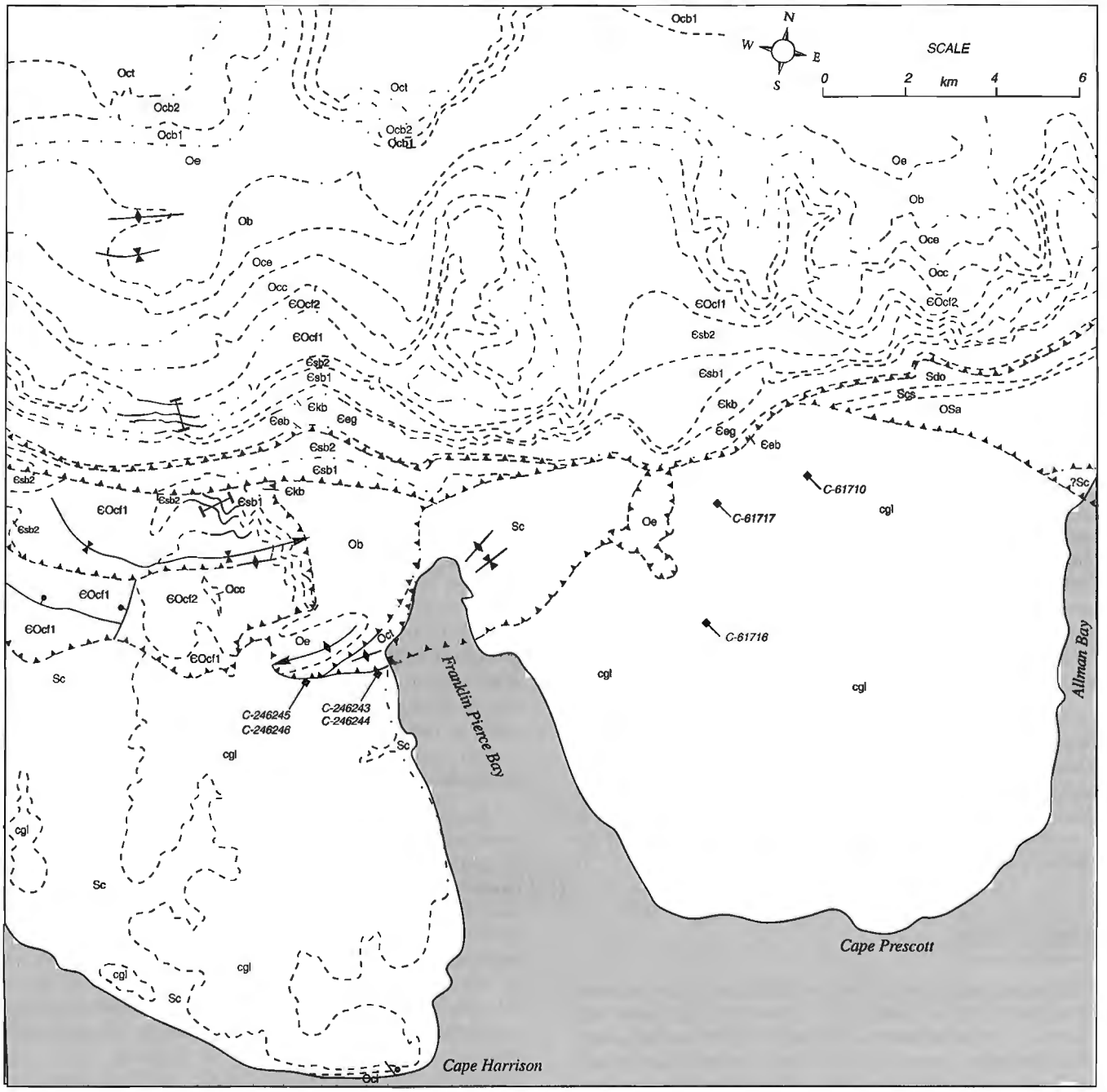

Figure 3. Bedrock geology map, southeastern part of the Dobbin Bay map area, eastern Ellesmere Island. For location see Figure 1.

The vitrinite reflectances of four samples were determined and are listed in Table 2.

Eastern sample set

These samples were collected by R. Thorsteinsson and studied by D. McIntyre in 1984. The slides were re-examined by A. Sweet in 1996 who confirmed the Early Cretaceous age of assemblages in samples C-61710 and C-61717 and their similarity to those of the Western Sample Set (Table 1). One difference between the two sample sets is the abundant occurrence of *Canningia* sp. specimens in sample C-61710 as reported by D. McIntyre. This dinoflagellate indicates a marine or marginal-marine depositional environment for the sampled stratum.

An abundance of a single species of dinoflagellate, *Canningia* sp. in the sample is significant, because it indicates a ecologically restricted marine or marginal-marine depositional environment, which excluded all other marine or marginal marine fossils. Such a low-diversity fossil assemblage is not significant by itself, because comparable monospecific assemblages do occur; however, if these fossils were derived from uplifted Cretaceous strata, one would expect representation of multiple ecological niches and hence more variety in the assemblage and associated paleoenvironmental interpretation. But this is not the case.

The third sample (C-61716) is very sparse and therefore its assemblage is more difficult to assess. A specimen of betulaceous triporate pollen, reported as *Triporopollenites mullensis* by D. McIntyre, was observed and, as for the Western sample set, indicates a younger, probably post-Cretaceous component.

LEGEND

CRETACEOUS OR TERTIARY AGE

cgl — *UNNAMED CONGLOMERATES: brown to reddish brown; granule to boulder grade; thick bedded; carbonate lithoclasts featuring lithologies of lower Paleozoic succession in hanging wall of the Parrish Glacier Thurst, common clast imbrication; <10% interbedded fine to medium grained sandstone*

SILURIAN

Sc — *UNDIVIDED SILURIAN CARBONATES: includes Allen Bay, Cape Storm, and Douro formations, as described below.*

Sdo — *DOURO FORMATION: Limestone and sandstone. Limestone: dolomitic, sandy and silty, greyish yellow green, medium and thin bedded, finely crystalline, bioturbated, highly fossiliferous. Sandstone: calcareous and dolomitic, greyish yellow green, fine grained, massive, bioturbated, fossiliferous*

Scs — *CAPE STORM FORMATION: Dolostone and sandstone. Dolostone: calcareous, sandy and silty, greyish yellow green and greyish yellow, medium and thin bedded, finely crystalline, laminated, stromatolitic. Sandstone: calcareous and dolomitic, greyish yellow green, fine grained, well sorted, massive, bioturbated*

SILURIAN AND UPPER ORDOVICIAN

OSa — *ALLEN BAY FORMATION: Limestone and dolostone. Limestone (in lower and upper part): dolomitic, greyish yellow, medium and thick bedded, finely crystalline, burrow-mottled in lower part; laminated, stromatolitic, conglomeratic in upper part; rare fossils including gastropods, stromatoporoids, brachiopods. Dolostone: light grey and greyish yellow, finely to medium crystalline, laminated, massive, <5% vuggy porosity*

UPPER ORDOVICIAN

Cornwallis Group

Oci — *IRENE BAY FORMATION: Limestone: dolomitic, argillaceous; greyish yellow green, medium bedded, rubbly weathering; finely crystalline, burrow-mottled, abudant fossil fragments, Arctic-Ordovician fossil fauna*

Oct — *THUMB MOUNTAIN FORMATION: Limestone: dolomitic, argillaceous intervals in upper part; yellowish grey, greenish in argillaceous upper part; thick bedded, resistant, finely crystalline, abundantly burrow-mottled, Arctic-Ordovician fossil fauna in upper part*

Ocb2 — *BAY FIORD FORMATION (upper member): limestone and dolostone; yellowish grey and medium grey, thin and medium bedded, finely crystalline, laminated, mudcracks; contains a basal 10-15 m thick resistant, burrow-mottled dolomitic limestone*

Ocb1 — *lower member: limestone, dolostone, minor gypsum. Limestone and dolostone: yellowish grey and medium grey, thin and medium bedded, finely crystalline, laminated, mudcracks; gypsum: calcareous, white, laminated*

MIDDLE ORDOVICIAN

Oe — *ELEANOR RIVER FORMATION: limestone and minor dolostone: yellowish grey and pale yellowish brown; thick bedded, resistant; finely crystalline, abundant burrow mottles, minor chert*

Ob — *BAUMANN FIORD FORMATION: gypsum, limestone, and dolostone. Gypsum: (mostly in lower 66% of formation) white, thin bedded, recessive, laminated, calcareous, common intraclast conglomerate. Limestone and dolostone: (mostly in upper 33%) gypsiferous; yellowish grey, medium and thin bedded; finely crystalline, intraclast conglomerates , laminated, locally abundant thrombolites*

Oce — *CHRISTIAN ELV FORMATION: limestone and dolostone: yellowish grey, medium and thick bedded; finely crystalline, intraclast conglomerates , laminated, locally abundant thrombolites in upper part; bedding planes feature numerous trace fossils*

LOWER ORDOVICIAN AND UPPER CAMBRIAN

Occ — *CAPE CLAY FORMATION: limestone and dolostone: yellowish grey, medium and thick bedded; finely crystalline, resistant, intraclast conglomerates; laminated, locally abundant thrombolites in upper part*

UPPER CAMBRIAN

€Ocf2 — *CASS FJORD FORMATION (upper member): limestone and dolostone: sandy in upper part, yellowish grey and light grey, medium and thick bedded; finely crystalline, intraclast conglomerates, laminated, thrombolites in lower part*

€Ocf1 — *lower member: limestone and dolostone: sandy in lower part, yellowish grey and light grey, local red weathering, medium and thick bedded; finely crystalline, intraclast conglomerates, laminated, mudcracks*

MIDDLE CAMBRIAN

€sb1 — *SCORESBY BAY FORMATION (upper member): limestone and dolostone: sandy; yellowish grey, locally red weathering; medium and thick bedded; finely crystalline, intraclast conglomerates, burrow mottles; laminated, rare thrombolites*

LOWER CAMBRIAN

€sb2 — *lower member: dolostone: calcareous and some limestone in lower part; yellowish grey, pale yellowish brown, and bright yellowish orange, thick bedded, resistant; medium and locally coarsely crystalline, bioturbated, trilobites*

€kb — *KANE BASIN FORMATION: Sandstone, siltstone, and mudrock: yellowish grey and dark grey; thin bedded recessive, laminated; some skolithos burrows in lower part*

€eg — *ELLESMERE GROUP: Sandstone and conglomerate: yellowish grey, moderate red, pale yellowish orange; thick bedded; medium grained, conglomeratic (pebble grade) in middle part; abundant trough cross-stratified*

€eb — *ELLA BAY FORMATION: Dolostone: bright yellowish orange and greyish yellow; thick bedded, coarsely crystalline; resistant, massive*

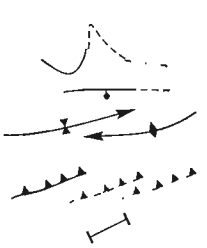

Geological boundary (defined, approximate, projected through ice or overburden)

Normal fault (defined, approximate)

Anticline, syncline (arrow indicates plunge)

Thrust fault (defined approximate, assumed or projected through overburden or ice; tieeth indicate upthrust side)

Measured stratigraphic section


A


B


C

Table 1. Fossil collections.

	Western sample set								Eastern set		
a=abundant, c=common, s=scarce, r=rare	C-246243 (mixed coal and mudstone)	C-246244 (coal and wood)	C-246245 (coal fragments)	C-246245 (mudstone clasts)	C-246245 (fine clay and rock fragments)	C-246246 (coal fragments)	C-246246 (mudstone clasts)	C-246246 (fine clay and rock fragments)	C-61710	C-61716	C-61717
MIOSPORES											
Alisporites spp.	C	A	A	A	A	A	A	A	A	R	A
Acanthotriletes varispinosus					R			R			
Cicatricosiporites spp.				R	R						
Classopollis sp.								R			
Concavissimisporites spp.					R			R			
Densoisporites cf. *D. crassus*				R					S		
Cycadopites sp.	R				R			R			R
Deltoidospora sp.	C		R	S		R	S		S		R
Eucommiidites troedssonii						R					
Gleicheniidites senonicus	C	S		S	S		C	C	S	R	C
Lycopodiumsporites austroclavatidites	C	S	C	S		S			S		
Neoraistrickia cf. *N. robusta*	S	C	R		S	S			R		
Osmundacidites wellmanii			R	C	R		R	R			R
Perinopollenites elatoides	R	S		R				R			R
Pilosisporites trichopapillosus				R			R	R			
Podocarpidites sp.	R				S	C	C	S	S		S
Sestrosporites pseudoalveolatus					R						
Stereisporites antiquasporites	C	S	C			S			C		
Cerebropollenites mesozoicus	C	C	S	C	R	S	C	S	C	S	
Trilobosporites cf. *T. purverulentus*						S					
triporate pollen (Betulaceous)					C			S		R	

Figure 4. *Conglomerates of the Franklin Pierce Bay and Cape Lawrence outliers.* ***A.*** *Cape Lawrence conglomerate succession. Line with teeth outlines a horizontal thrust and klippe of ?Ordovician carbonates. Height of hill is about 1000 m.* ***B.*** *East coast of Franklin Pierce Bay showing conglomerate units. Arrows indicate inclined conglomerate beds truncated by subhorizontal beds above. Height of hill is about 500 m.* ***C.*** *Typical outcrop expression of the conglomerates of the Franklin Pierce Bay Outlier, near Cape Hawks. Washington Irving Island in background (arrow) is indicated. Conglomerates also form cliffs on the southern part of this island. Height of near cliff is about 350 m.*

Figure 5. *Outcrop photograph, Cape Harrison, southeast of Franklin Pierce Bay. Normal fault (dash line) is indicated. The fault does not continue into overlying conglomerate beds. Dotted line indicates unconformable contact between Silurian carbonates and conglomerate unit. About 300 m of cliff is exposed.*

Table 2. Vitrinite reflectances of the western sample set.

Sample no.	Ro, %	St. dev.	Points	Remarks
C-246243	0.33	0.05	50	Humotelinite, densinite, abundant corpohumite
C-246244	0.32	0.03	50	Humotelinite, ulminite, abundant corpohumite
C-246245	0.34	0.03	50	Mudrock with coal lenses, gelinite, phlobaphite, corpohumite
C-246246	0.40	0.03	50	Humotelinite-ultimite, densinite (abundant terrestrial liptinites)
Vitrinite reflectance and maceral identification by M. Tomica (GSC, Calgary)				

PLATE 1

Selected Early Cretaceous taxa recovered from the indurated mudstone pieces and coal. Specimens will be stored permanently as part of the Geological Survey of Canada type collections, Ottawa but are at present in temporary storage at GSC (Calgary). All figures x750.

Gymnosperm pollen

1. *Alisporites bilateralis* Rouse; GSC 115241, P4261-3N, 132.9x7.4, GSC loc. C-246245. 2. *Podocarpidites* sp.; GSC 115242, P4261-3B, 127.3x11.8, GSC loc. C-246245. 3. *Classopollis* sp.; GSC 115243, P4261-3A, 129.7x21.8, GSC loc. C-246245. 4, 5. *Cerebropollenites mesozoicus* (Couper) Nilsson; GSC 115244, P4261-3A, 128.7x15.7, GSC loc. C-246245; GSC 115245, P4261-4K, 125.4x9.3, GSC loc. C-246246; respectively.

Spores

6. *Gleicheniidites senonicus* Ross; GSC 115246, P2726-1G, 130.2x18.6; GSC loc. C-61710. 7. *Densoisporites* cf. *D. crassus* Tralau, in Hopkins, 1971; GSC 115247, P2726-1G, 122.2x20.8; GSC loc. C-61710.

Dinoflagellates

8. *Canningia* sp.; GSC 115248, P2726-1K, 131.4x5.8, GSC loc. C-61710. 9. *Gardodinium* sp.; GSC 115249, P4261-4K, 126.2x10.7; GSC loc. C-246246.

Spores

10. *Acanthotriletes varispinosus* Pocock; GSC 115250, P4261-3A, 136.2x8.7, GSC loc. C-246245. 11. Indeterminate spore; GSC 115251, P2726-1K, 128.5x17.7; GSC loc. C-61710. 12. *Neoraistrickia* cf. *N. robusta* Brenner in Hopkins, 1974; GSC 115252, P4261-1C, 120.3x13.6; GSC loc. C-246243. 13. *Stereisporites antiquasporites* (Wilson and Webster) Dettmann; GSC 115253, P2726-1K, 132.9x10.7, GSC loc. C-61710. 14. *Concavissimisporites variverrucatus* (Couper) Singh; GSC 115254, P4261-3B, 125.4x16.5, GSC loc. C-246245. 15. *Trilobosporites* cf. *T. purverulentus* (Verbitskaya) Dettmann in Hopkins, 1971; GSC 115255, P4261-4B, 124.0x17.2; GSC loc. C-246246.

16, 17. *Cicatricosisporites* spp.; GSC 115256, P4261-3B, 126.7x11.7; GSC loc. C-246245; GSC 115257, P4261-3A, 132.6x18.8, GSC loc. C-246245. 18. *Concavissimisporites verrucosus* Delcourt and Sprumont; GSC 115258, P4261-3B, 121.7x13.8, GSC loc. C-246245. 19. *Pilosisporites trichopapillosus* (Thiergart) Delcourt and Sprumont; GSC 115259, P4261-3B, 134.3x9.8, GSC loc. C-246245. 20. *Perinopollenites elatoides* Couper; GSC 115260, P4261-4K, 112.6x21.5, GSC loc. C-246246.

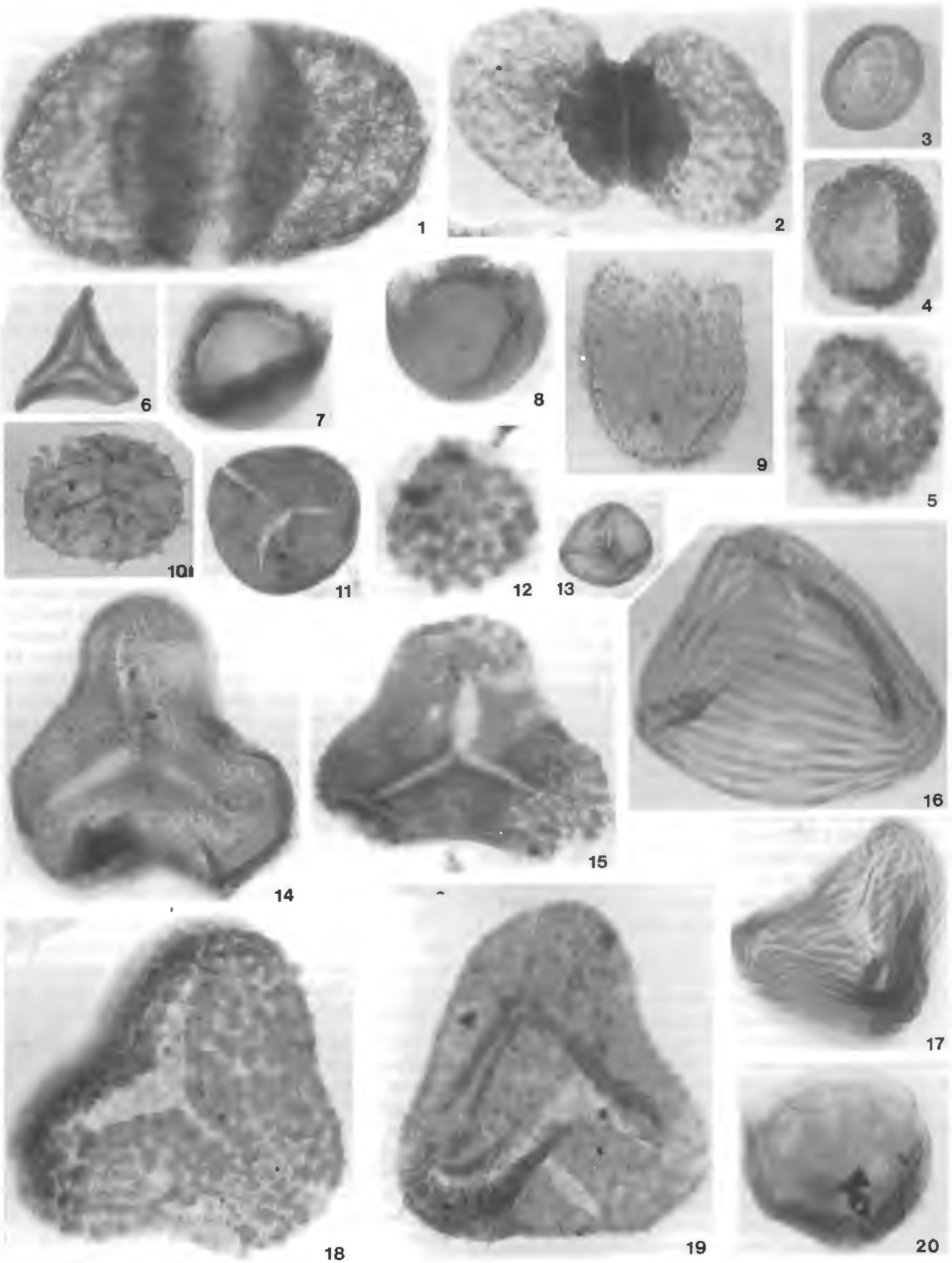
1
2
3
4
5
6
7
8
9
10
11
12
13
14
15
16
17
18
19
20

AGES AND COMPOSITION OF POSSIBLE CORRELATIVES ON NORTHEASTERN ELLESMERE ISLAND

The Pavy River Outlier (Christie, 1964; Miall, 1982) contains about 1000 m of sandstone, mudrock, and minor conglomerate. The latter tend to be confined to the northwestern and western part of the outlier. Two samples from the fine grained siliciclastics yielded Paleogene age microfossils, and a third contained ?Paleocene age palynomorphs, including *Sigmopollis, Osmunda, Sphagnum, Laeviegatosporites, Inaperturopollenites, Glyrptostrobus, Paraalnipollenites, Alnus, Triporopollenites, Typha,* cf. *Carpinis, Extratripropollenites, Tricolpites,* and *Pineaceae* (Miall, 1982).

Preparation from samples C-68673, C-68678, and C-68681 from outcrop stations 45 and 46 of Miall (1982, Fig. 9) were re-examined and no taxa specifically identifiable as Early Cretaceous were observed within prolific assemblages dominated by gymnosperm (T/C/T) and angiosperm pollen. In addition to the taxa listed in Miall, specimens of *Carya imparalis* and Ericaceae pollen were seen, and thus the fossil assemblages are similar to the Late Paleocene assemblages reported from Somerset Island (McIntyre, 1989).

The Daly River Outlier contains a thin sequence of limestone, sandstone and carbonaceous shale, and it too has yielded Lower Cretaceous spores and pollen (Christie, 1964, p. 57).

The Watercourse Valley Outlier was discovered by members of Nares Expedition (Nares, 1878; Christie, 1964). Plant remains collected during this expedition were identified as Miocene. However in a more recent publication, D.C. McGregor (in Christie, 1964) identified Paleocene or possibly Eocene plants, placing some question on the previous age interpretations. Macroflora listed by Christie (1964, p. 59) include *Corylus* sp. cf. *C. macquarrii, Feildenia rigida,* cf. *Arundo goeppertii,* cf. *Phragmites oeningensis,* and ?*Metasequoia occidentalis* (=*Taxodium distichum miocenicum*). Greely (1888) mined 9500 pounds of coal from this seam for his ill-fated expedition. The high volatile, bituminous coal (Ro=0.75; Miall, 1982) was extracted from a 6 m seam that forms the lower part of a 100 m thick sequence of fine grained, laminated, fossiliferous siliciclastics.

The Carl Ritter Bay Outlier contains about 2370 m of strata comprising four members: a cross-stratified sandstone member (member 1), sandstone-siltstone-mudrock member (member 2), siltstone and sideritic mudrock member (member 3), and a thick conglomerate member (member 4). The latter member unconformably overlies the other three members and contains spectacularly well developed internal angular unconformities (Miall, 1982). Paleocene macroflora were obtained from these strata (L.V. Hills, in Miall, 1982).

The Cape Lawrence Outlier is poorly known. It consists of thick bedded, red weathering, polymict to oligomict, poorly sorted conglomerate with pebble- to, locally, boulder-grade lithoclasts. Clasts appear to be composed mostly of Ordovician formations, although some quartzite lithoclasts suggests a Lower Cambrian source. A klippe composed of (?)Ordovician age carbonate strata is preserved in the highest part of the mountain (Fig. 4A). Mayr and de Vries (1982) found Tertiary leaf impressions (*Crednaria spectabilis*) in the upper part of the 1 km thick conglomerate sequence. Although Miall did not study the Cape Lawrence Outlier in detail, he did assign a new formation name to the sequence, and equated it with the conglomerates of the Carl Ritter Bay Outlier (Miall, 1991, Fig. 2).

The Bache Peninsula Outlier was examined by Christie (1964) and again by Kalkreuth et al. (1993, p. 280) who described 21 coal seams from a 300 m thick sequence of siliciclastics. The coals have yielded Early Paleocene palynomorphs (Kalkreuth, 1993). Petro-Canada geologists have assessed the economic potential of these coals and found them to be of good quality [22% ash, 1.5% sulphur, and a calorific value of 20 770 kJ/kg (8936 BTU/b); Gibbins, 1984, p. 122].

INTERPRETATION

The thick bedded, coarse, crudely stratified, clast supported conglomerates of the Franklin Pierce Bay Outlier contain features typical of gravelly braided streams (i.e. thick bedding, clast support framework, clast imbrication, lenticular bedding, and other attributes) (Blair and McPherson, 1994). Gravels were derived from the adjacent highlands, in the hanging wall panel of the Parrish Glacier Thrust, and transported to the adjacent floodplain in alluvial fans (rarely preserved). Abundant carbonate lithoclasts, some containing Ordovician and Silurian fossils, are clear evidence for a source in hanging wall. Sand and coaly sandstone represent accumulation and plant growth in abandoned channels (cf. Reinfelds and Nanson, 1993) or in vegetated, marginal marine settings, as evidenced by monospecific dinoflagellate assemblages. The lateral extent of some of the fine grained deposits appears to support the latter interpretation, while not the former, because channel fill sequences tend to be laterally discontinuous in other Phanerozoic, gravelly braided stream deposits. A similar syntectonic interpretation is advocated for the Cape Lawrence Outlier, but less is known of this sequence, and further fieldwork is required.

Coal samples from the western sample set contain abundant liptinite, suggesting deposition in a wet, subaquatic environment. R_o values (Table 1) indicate burial temperatures of about 50°C (Teichmüller, 1987) or about 2 km of burial, assuming a geothermal gradient of about 24°C/km.

Most of the conglomerates are gently folded or contain nappes of Ordovician carbonates. Nappes are clearly part of a regional footwall thrust splay with a flat fault geometry, developed within the Ordovician Baumann Fiord Formation. The flat fault geometry, carrying a hanging wall panel of Ordovician carbonates, is also developed with the conglomerate unit, suggesting that the thrust fault geometry did not alter significantly once it entered the conglomerate sequence. This fact may reflect poor lithification of conglomerates during regional shortening. It also indicates that some shortening significantly postdated syntectonic sedimentation.

The age of the fossils collected from the conglomerate are the most controversial aspect of this report, because comparable syntectonic deposits of the Arctic Islands are interpreted as being due to uplift during the Eurekan Orogeny, which was largely an Eocene event. If the lower Cretaceous age is concluded, the entire history of the Eurekan Orogeny and the Mesozoic-Cenozoic, circum-Arctic tectonic development needs substantial reevaluation. If the fossil ages, instead, reflect erosion of Cretaceous strata in the hinterland, then the sedimentological setting requires careful interpretation, because Cretaceous rocks are not exposed in the hanging wall, and lithoclasts in the conglomeratic sequence consist entirely of lower Paleozoic formations. These points are discussed more fully below.

The western sample set was collected from two, small, poorly lithified outcrops that may be interbedded with thick conglomerate beds, or they may represent thin panels of thrusted Cretaceous strata, as mentioned previously. Neither interpretation can be successfully argued considering only the data from the western exposures. However, the eastern sample set yielded lower Cretaceous fossils very similar to those in the western sample set, from fine grained strata clearly interstratified with thick conglomerate beds. These fossil-bearing strata were obviously not introduced during thrusting, and thus, two explanations for the Cretaceous age must be considered:

1. The coal and pieces of mudstone formed within the conglomeratic outlier; therefore, the conglomerates are Early Cretaceous age. The minor triporate and tricolpate angiosperm pollen would then have to be considered as having been introduced into the more weathered part of the sampled material relatively recently, perhaps during the Miocene or later.
2. The coal and pieces of mudstone were transported from a nearby, sizeable Early Cretaceous source and deposited as part of the conglomeratic unit, probably during the Tertiary. In this case, the long-ranging angiosperm pollen would be the indigenous component.

Solution 1 (the conglomerates are Cretaceous)

As stated above, the fine grained deposits are likely abandoned channel-fill or marginal-marine deposits. Fine grained alluvium is generally restricted to those alluvial environments characterized by low flow rates and lesser stream carrying capacity, as typically found in abandoned stream channels of gravelly stream systems (Blair and McPherson, 1994). This significant interpretation implies that the conglomerates and sandstone have a common source in the hanging wall panel of the Parrish Glacier Thrust, but reflect deposition under different hydraulic conditions in the floodplain. The trapped fine sediment promoted plant growth and the preservation of the palynomorphs, effectively dating the alluvium. If the fine grained deposits are products of marginal-marine settings, a common source in the hanging wall panel is also implied, and fine grained detritus again represents hydraulic sorting, but in a marginal-marine depositional environment. In this scenario, the Cretaceous fossils are in situ, and the long-ranging angiosperm pollen were introduced into the poorly consolidated strata during the Miocene or Holocene.

If the conglomerates are Cretaceous in age, the nature and composition of the Franklinian Pierce Bay Outlier is very different from Cretaceous deposits in other parts of the Canadian Arctic. Early Cretaceous sandstones are widely exposed and are assigned to the Isachsen and Christopher formations (Embry, 1991); these units generally consist of fine grained marine or continental sandstone and mudrock and are very different from the conglomerates at Franklin Pierce Bay. Further question is placed on the Cretaceous age assignment when dates from outliers farther north, as described above, are considered. The Cape Lawrence and Carl Ritter Bay outliers were clearly alluvial deposits associated with regional thrusting, probably under the same regional stress regimes that produced the Parrish Glacier Thrust, but these deposits have yielded samples indicating generally younger ages. In particular, Paleocene macroflora have been recovered from the highly conglomeratic Cape Lawrence and Carl Ritter Bay outliers, as mentioned above (Mayr and de Vries, 1982; Miall, 1982). Middle to Upper Eocene age thrusting is also widespread west of the report area, where it has been related to the Eurekan Orogeny (Thorsteinsson and Tozer, 1970).

Solution 2 (the conglomerates are younger, perhaps Tertiary)

If the Cretaceous fossils were derived from uplifted Cretaceous strata, a complex sedimentological solution may be advocated. For example, modern gravelly braided streams may contain numerous intersecting drainages from fold and thrust belts featuring a complex, interleaved stratigraphy. The provenance of the main stream reflects a multitude of sources in the hinterland, but smaller feeder channels may reflect more localized source areas. Using this reasoning, it is possible the Cretaceous strata were involved in thrusting during development of the Parrish Glacier Thrust and provided a source of sediment in an otherwise gravelly alluvium dominated by lower Paleozoic lithoclasts. As discussed above, the outcrops from which the western sample set was collected might represent tectonic slivers transported there during regional thrusting. However, these outcrops are less than 100 m^2 by 1 to 2 m thick and thus are clearly too small to have provided a significant source of sediment, particularly in contrast to the several kilometres of resistant, lower Paleozoic source rocks. Furthermore, the closest known large Cretaceous exposure is more than 150 km away, too far to have provided coal-bearing detritus to the succession.

CONCLUSIONS

Conglomerates in the vicinity of Franklin Pierce Bay were deposited in gravelly braided stream and less common alluvial fan environments. Lithoclasts appear to have been derived from lower Paleozoic sources, which are exposed to the west in the hanging wall of the Parrish Glacier Thrust. This thrust was probably activated in Cretaceous or later

times to produce the coarse conglomerate succession at Franklin Pierce Bay. Recent workers have concluded an Eocene age for these deposits, but the five samples reported herein provide a contradictory Early Cretaceous age. Two possible solutions are argued: 1) the conglomerates are Cretaceous age, or 2) Cretaceous strata were an important source of the syntectonic succession. Neither solution can be convincingly argued with the evidence available, but if the lower Cretaceous age is concluded, the entire history of the Eurekan Orogeny and Mesozoic-Cenozoic, circum-Arctic tectonic development needs substantial re-evaluation.

ACKNOWLEDGMENTS

Discussions with D. Leckie, D. Cant, U. Mayr, and V. Stasiuk improved the content of the manuscript. M. Tomica provided the data from coal analyses. P. Crowley provided cheerful field assistance.

REFERENCES

Blair, T.C. and McPherson, J.G.
1994: Alluvial fans and their natural distinction from rivers based on morphology, hydraulic processes, sediment processes, and facies assemblages; Journal of Sedimentary Research, v. A64, p. 450-489.

Burden, E.T. and Hills, L.V.
1989: Illustrated guide to genera of Lower Cretaceous terrestrial palynomorphs (excluding megaspores) of Western Canada; American Association of Stratigraphic Palynologists, Contribution Series Number 21, 147 p.

Christie, R.L.
1964: Geological reconnaissance of northeastern Ellesmere Island, District of Franklin; Geological Survey of Canada, Memoir 331, 79 p.

Embry, A.F.
1991: Mesozoic history of the Arctic Islands; Chapter 14; in Geology of the Innuitian Orogen and Arctic Platform of Canada and Greenland, (ed.) H.P. Trettin; Geological Survey of Canada, Geology of Canada, no. 3; (also Geological Society of America, The Geology of North America, v. E) p. 370-433.

Feilden, H.W. and De Rance, C.E.
1878: Geology of the coasts of the arctic lands visited by the late British Expedition under Captain Sir George Nares, R.N., K.C.B., F.R.S.; Quarterly Journal of the Geological Society, v. 34, p. 556-567.

Gibbins, W.A.
1984: Mineral Industry Report 1980/1981 Northwest Territories; Department of Indian and Northern Affairs and Northern Development.

Greely, A.
1888: Report on the proceedings of the United States expedition to Lady Franklin Bay, Grinnell Land; Volume I: Government Printing Office, 738 p.

Hopkins, W.S.
1971: Palynology of the Lower Cretaceous Isachsen Formation on Melville Island, District of Franklin; in Contributions to Canadian Paleontology; Geological Survey of Canada, Bulletin 1977, p. 109-132.

Hopkins, W.S. (cont.)
1973: Description, palynology and paleoecology of the Hassel Formation (Cretaceous) on eastern Ellef Ringes Island, District of Franklin; Geological Survey of Canada, Paper 72-37, 31 p.
1974: Some spores and pollen from the Christopher Formation (Albian) of Ellef and Amund Ringes islands, and northwestern Melville Island, Canadian Arctic Archipelago; Geological Survey of Canada, Paper 73-12, 39 p.

Kalkreuth, W.D., McCullough, K.M., and Richardson, R.J.H.
1993: Geological, archaeological, and historical occurrences of coal, east-central Ellesmere Island, Arctic Canada; Arctic and Alpine Research, v. 25, p. 277-307.

Kerr, J.W.
1973a: Geology, Kennedy Channel and Lady Franklin Bay, District of Franklin; Geological Survey of Canada, Map 1359A, scale 1:25 000.
1973b: Geology, Sawyer Bay, District of Franklin; Geological Survey of Canada, Map 1357A, scale 1:25 000.
1973c: Geology, Dobbin Bay, District of Franklin; Geological Survey of Canada, Map 1358A, scale 1:25 000.

Mayr, U. and de Vries, C.D.S.
1982: Reconnaissance of Tertiary structures along Nares Strait, Ellesmere Island, Canadian Arctic Archipelago; Meddelelser om Grønland Geoscience 8, p. 167-175.

McIntyre, D.J.
1989: Paleocene palynoflora from northern Somerset Island, District of Franklin, N.W.T.; in Current Research, Part G, Geological Survey of Canada, Paper 89-1G, p. 191-197.

Miall, A.D.
1982: Tertiary sedimentation and tectonics in the Judge Daly Basin, northeast Ellesmere Island, Arctic Canada; Geological Survey of Canada, Paper, 80-30, 17 p.
1991: Late Cretaceous and Tertiary basin development and sedimentation, Arctic Islands; Chapter 15; in Geology of the Innuitian Orogen and Arctic Platform of Canada and Greenland, (ed.) H.P. Trettin; Geological Survey of Canada, Geology of Canada, no. 3; (also Geological Society of America, The Geology of North America, v. E), p. 437-458

Nares, G.
1878: Narrative of a voyage to the polar sea during 1875-1876 in H.M. ship Alert and Discovery, with notes on the natural history; (ed.) H.M. Feilden London: Low Marston, Searle, and Tivington, Volume I, 395 p.; Volume II, 378 p.

Reinfelds, I. and Nanson, G.
1993: Formation of braided river floodplains, Waimakariri River, New Zealand; Sedimentology, v. 40, p. 1113-1128.

Ricketts, B.
1994: Basin Analysis, Eureka Sound Group, Axel Heiberg and Ellesmere islands, Canadian Arctic Archipelago; Geological Survey of Canada, Memoir 439.

Singh, C.
1971: Lower Cretaceous microfloras of the Peace River area, northwestern Alberta; Research Council of Alberta, v. 1, 296 p.

Teichmüller, M.
1987: Organic material and very low grade metamorphism, in Low Temperature Metamorphism, (ed.) M. Fret; Blackie and Son Ltd., p. 114-161.

Thorsteinsson, R. and E.T. Tozer
1970: Geology of the Arctic Archipelago, p. 547-590; in Geology and Economic Minerals of Canada, (ed.) R.J.W. Douglas; Geological Survey of Canada Economic Geology Report 1, 5th edition, p. 548-590.

Geological Survey of Canada Project 860006

Canadian Shield

Bouclier canadien

Metamorphism in the Weldon Bay-Syme Lake area, Manitoba[1]

Edgar Froese
Continental Geoscience Divison, Ottawa

Froese, E., 1997: Metamorphism in the Weldon Bay-Syme Lake area, Manitoba; in Current Research 1997-E; Geological Survey of Canada, p. 35-44.

Abstract: In the Weldon Bay-Syme Lake area, volcanic rocks of the Amisk Group (1.92-1.87 Ga) are overlain by greywacke of the Burntwood Group (1.85-1.84 Ga) and by lithic arenite and conglomerate of the Missi Group (1.85-1.83 Ga). These rocks were metamorphosed at 1.82-1.80 Ga.

At constant pressure, temperature, and H_2O activity, and in the presence of quartz, plagioclase of constant composition, magnetite, and ilmenite, mineral assemblages in pelitic, ferromagnesian, and mafic rocks can be represented in the system

$A = Al_2O_3 - (K_2O + Na_2O + CaO)$

$K = K_2O$

$F = FeO - (Fe_2O_3 + TiO_2)$

$M = MgO$

A reaction grid among minerals in this system restricts the stability of the observed association of mineral assemblages to about 5.5 kbar and 620°C for an H_2O activity of one, indicating a metamorphic grade somewhat greater than represented by the biotite-sillimanite-almandine isograd.

Résumé : Dans la région de la baie Weldon et du lac Syme, les roches volcaniques du Groupe d'Amisk (1,92-1,87 Ga) sont recouvertes par du grauwacke du Groupe de Burntwood (1,85--1,84 Ga) et par de l'arénite lithique et du conglomérat du Groupe de Missi (1,85-1,83 Ga). Ces roches ont été métamorphisées à 1,82-1,80 Ga.

À pression, température et activité d'H_2O constantes et en présence de quartz, de plagioclase de composition constante, de magnétite et d'ilménite, les associations de minéraux des roches pélitiques, ferromagnésiennes et mafiques peuvent être représentées par le système :

$A = Al_2O_3 - (K_2O + Na_2O + CaO)$

$K = K_2O$

$F = FeO - (Fe_2O_3 + TiO_2)$

$M = MgO$

La grille réactionnelle des minéraux de ce système limite les conditions de stabilité de la suite observée d'associations de minéraux à environ 5,5 kbar et 620 C avec une activité de H_2O de 1, ce qui indique un degré de métamorphisme quelque peu supérieur à celui de l'isograde biotite-sillimanite-almandin.

[1] Contribution to Canada-Manitoba Partnership Agreement on Mineral Development (1990-1995), a subsidiary agreement under the Canada-Manitoba Economic and Regional Development Agreement.

INTRODUCTION

The Weldon Bay-Syme Lake area forms part of the Flin Flon volcanic belt, a portion of which is shown in Figure 1 (modified from Zwanzig et al., 1995). Rocks have been assigned to three main units: the Amisk Group of mainly volcanic rocks (1.92-1.87 Ga), the Burntwood Group of greywacke (1.85-1.84 Ga), and the Missi Group of lithic arenite and conglomerate (1.85-1.83 Ga). These units were metamorphosed at 1.82-1.80 Ga. The age ranges have been taken from Lucas et al. (1997). In recent work (e.g. Lucas et al., 1997), the designation Amisk Group is not used and there is no collective term for rocks formed during the period 1.92-1.87 Ga.

West of Flin Flon, the biotite-sillimanite-almandine isograd has been mapped (Ashton, 1990; Ashton et al., 1992). This isograd is difficult to trace to the east, due to the rarity of rocks of appropriate composition. In the Duval Lake area, a melt isograd is shown (Jungwirth, 1995). The Weldon Bay-Syme Lake area was chosen for metamorphic studies because of the presence of metamorphosed felsic volcanic rocks and greywacke, immediately north of a large area of mafic volcanic rocks. This paper deals with metamorphism in the area which covers parts of four map sheets: Collins Point (Frarey, 1961), Sherridon (Bateman and Harrison, 1946), Weldon Bay (Kalliokoski, 1952), and Heming Lake (McGlynn, 1959). Brief notes on the geology were published by McRitchie (1980), Froese and Gall (1981), and Froese (1984).

Part of the Weldon Bay-Syme Lake area was included in a study of metamorphism by James (1983). The Collins Point and Sherridon map sheets, as well as an area around Lobstick Narrows, have recently been mapped by Zwanzig and Schledewitz (1992). Structural studies in the Lobstick Narrows area have been carried out by Norman et al. (1995). The Fay Lake area, east of Syme Lake, and a small area near Syme Lake have been investigated by Schledewitz (1993, 1994). Jungwirth (1995) studied metamorphism in the Duval Lake area. Isograds in the Flin Flon belt have been discussed by Bailes and McRitchie (1978), Gordon (1989), and Plint et al. (1995).

LITHOLOGY

A more detailed map of the study area is shown in Figure 2. Volcanic rocks of the Amisk Group, predominantly of mafic composition, have been recrystallized to amphibolite. Deformed pillow rims can be recognized in a few places. The greenish grey rocks contain hornblende crystals up to one millimetre long. Clinopyroxene is present in some layers. The amphibolite unit north of Lobstick Narrows includes rocks with a high garnet content. The thin layer of amphibolite along the south shore of Weldon Bay is coarser, having a grain size of several millimetres, and contains lenses of calc-silicate rock. In some rocks, the assemblage cummingtonite-hornblende is present, presumably indicating premetamorphic alteration. A narrow unit of grey, medium grained felsic gneiss, present south of Weldon Bay and extending to Syme Lake, commonly consists of quartz, plagioclase, biotite, almandine, and magnetite. Locally, poorly preserved fragments suggest a volcaniclastic origin. The east end of the Defender Lake gneiss dome (Froese and Gall, 1981), exposed southwest of Lobstick Narrows, is composed of medium grained felsic gneisses. Quartz lenses 5 mm in size are present. Similar rocks at the west end of Kisseynew Lake were regarded as volcaniclastic by Ashton (1989). In some places, premetamorphic alteration of the felsic rocks has produced a composition allowing the formation of sillimanite, staurolite, and orthoamphibole. Sulphide occurrences in mafic and felsic volcanic rocks have been described by Gale and Norquay (1996).

The Burntwood Group consists mainly of biotite-garnet gneiss, probably derived from greywacke. The rock is grey, has a relatively high biotite content of about 30% and is characterized by euhedral garnets several millimetres across. Sillimanite is common. Staurolite is stable in muscovite-free rocks and occurs as relics in muscovite-bearing rocks.

The dominant rock type of the Missi Group is a fine- to medium-grained quartzofeldspathic gneiss of variable composition, considered to be metamorphosed lithic arenite. Some rocks are quartz-rich and display quartz ridges on the weathered surface. Others contain hornblende and exhibit compositional layering on a scale of several centimetres, marked by biotite-rich and hornblende-rich layers. Clinopyroxene is present in some hornblende-bearing rocks. Quartz-sillimanite nodules occur in some localities. Norman et al. (1995) reported corundum-bearing gneisses from the Cleunion Lake area. Conglomerate consisting of volcanic and granitic fragments and characteristic grey, magnetite-bearing chert pebbles is common. Kyanite was noted in one sample. Particularly well preserved conglomerate in a hinge zone of a fold 3 km north of Lobstick Narrows was described by McRitchie (1980). This conglomerate was traced by Zwanzig (1983) as a thin and highly deformed unit along the contact with Amisk amphibolite to Lobstick Narrows. Pink leucocratic gneiss forms a unit from Lobstick Narrows to Syme Lake and some smaller bodies north of Weldon Bay. This is a fine grained rock consisting of quartz, microcline, plagioclase, and traces of muscovite, epidote, and biotite. A faint colour banding is typical. The presence of quartz eyes and feldspar phenocrysts, first noted by Zwanzig (1983), probably indicates a volcaniclastic origin. James (1983) suggested that the chemical composition supported derivation from felsic volcanic rocks.

A body of medium grained biotite granodiorite is present south of Weldon Bay. This is a light pink rock, with a foliation parallel to that of the adjacent volcanic rocks. In the northeast corner, a portion of the Gwillam Lake dome (Zwanzig and Schledewitz, 1992) is exposed. It consists of foliated pink granodiorite forming a shallow cylindrical structure plunging east.

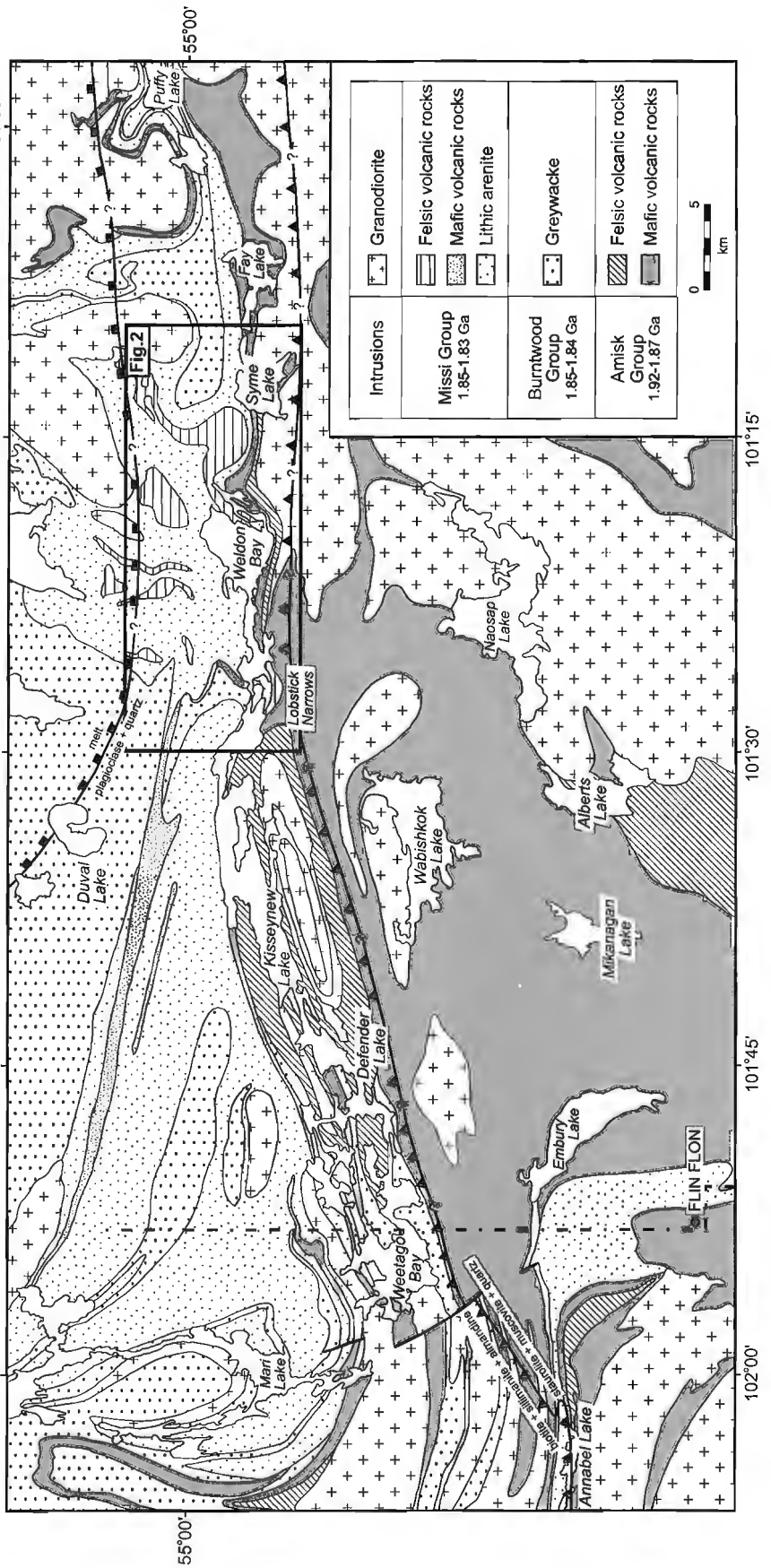

Figure 1. *Geology of the Flin Flon-Puffy Lake area.*

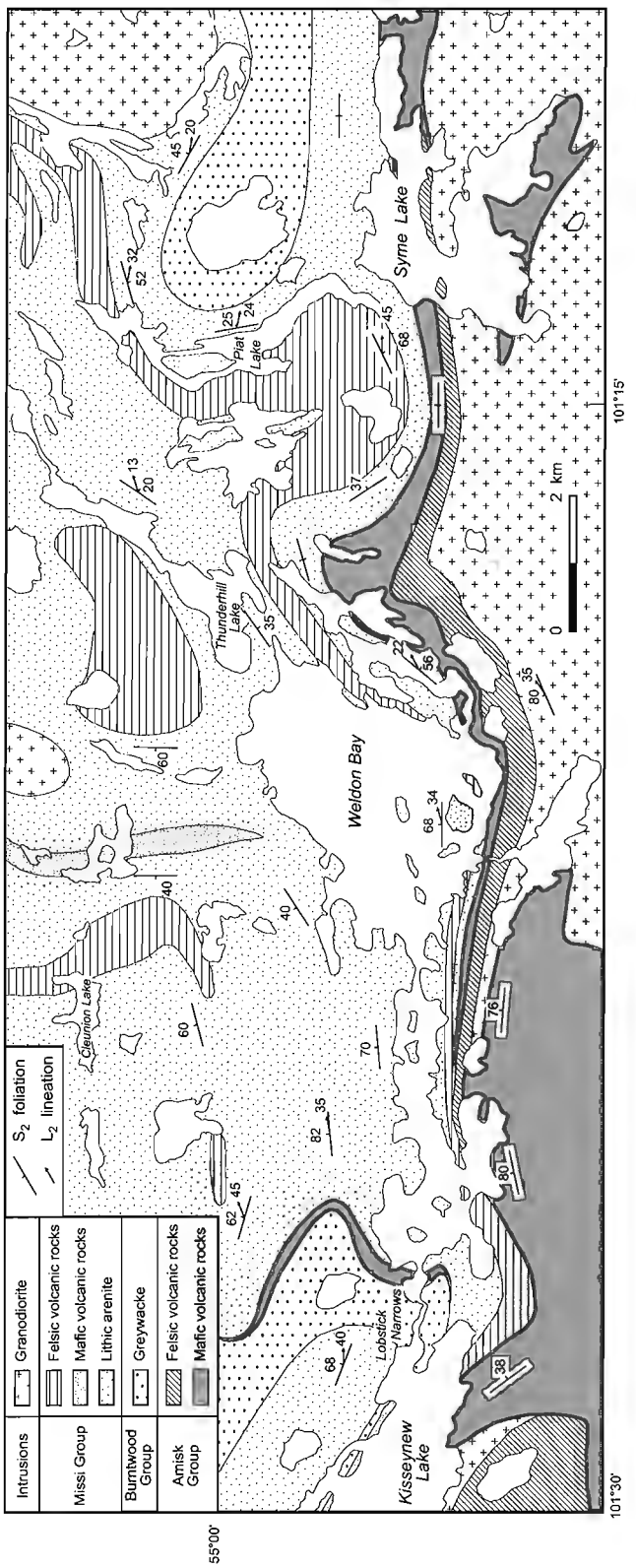

Figure 2. Geology of the Weldon Bay-Syme Lake area.

STRUCTURE

Three deformational events are reconized in the Weldon Bay-Syme Lake area affecting all rocks. The earliest foliation, S_1, is parallel to lithological contacts and probably was developed during a phase of isoclinal folding. This deformational event has been designated as D_1; it corresponds to F_1 folding described by Norman et al. (1995). Lithological layering and S_1 were deformed into folds ranging from open to isoclinal during the second phase of deformation D_2; it corresponds to F_2 folding described in Norman et al. (1995). A prominent S_2 foliation and L_2 stretching lineation were regionally developed; these are shown in Figure 2.

North of Lobstick Narrows, the regional foliation S_2 cuts across lithological layering; this fold is regarded as a D_2 structure. Elsewhere, the S_2 foliation is axial planar to small isoclinal folds 10 to 100 cm in size. The S_2 foliation is represented by compositional layering on a scale of 1 to 100 cm and by biotite aligned parallel to the compositional layering. An L_2 lineation is defined by stretched fragments, elongated mineral aggregates and oriented hornblende crystals. The S_2 foliation has been deformed into open folds with axes parallel to the L_2 stretching lineation.

In areas of extreme attenuation, along the south shore of Weldon Bay and north of Syme Lake, the S_2 foliation is marked by paper-thin layers of biotite spaced several millimetres apart; this imparts a platy character to the rock. The folding by F_3 of the S_2 foliation in the felsic gneisses of the Missi Group and adjacent Amisk volcanic rocks is disharmonic with respect to the volcanic rocks further south. The folds of the S_2 foliation are characterized by highly variable and commonly shallow dips. The first occurrence of shallow dips does not coincide with the Amisk-Missi contact; some of the Amisk rocks are affected as well.

METAMORPHISM

The formation of peak metamorphic assemblages probably coincided with the formation of the S_2 foliation and L_2 lineation. Recrystallization of the same assemblages during D_3 did not produce new fabrics. The mineral assemblages reflect metamorphic conditions that prevailed during D_2 and D_3.

Mineral assemblages in the Weldon Bay-Syme Lake area are listed in Table 1. At fixed values of pressure, temperature, and activity of H_2O, and in the presence of quartz, plagioclase of constant composition, magnetite, and ilmenite, many minerals (Fig. 3) can be represented in the system:

$A = Al_2O_3 - (K_2O + Na_2O + CaO)$

$K = K_2O$

$F = FeO - (Fe_2O_3 + TiO_2)$

$M = MgO$

In order to facilitate easier visualization, it is desirable to achieve a planar representation of mineral assemblages. Non-potassic minerals can be plotted in the AFM system (Fig. 4).

As noted by Albee (1965), the introduction of an additional component, in this case K_2O, will in general give rise to one additional phase, in this case either muscovite or biotite. Thus in Figure 4, fields of muscovite and biotite are shown. The biotite-muscovite boundary must lie in a two-phase field so that the number of coexisting phases in the system AKFM does not exceed four. Mineral assemblages from the Weldon Bay-Syme Lake area are shown in Figure 4.

Another method of showing phase relations makes use of a subdivision of the biotite composition surface according to coexisting minerals. Four-phase assemblages including biotite in the AKFM system are represented by subtetrahedra with one apex on the biotite composition surface. Similarly, three-phase assemblages subtend a line and two-phase assemblages an area on the biotite composition surface. Consequently, a subdivision of the biotite composition surface may be used to portray mineral assemblages in biotite-bearing rocks (Froese, 1978). Because the content of component K is nearly constant in biotite, the variation in composition is adequately represented by the relative amounts of components A, F, and M. Figure 5 shows mineral assemblages from the Weldon Bay-Syme Lake area on a diagrammatic biotite composition surface. Other assemblages have been inferred in order to complete the diagram.

Figure 6 shows a reaction grid; reactions are based on mineral compositions shown on the inset. Most compositions have been taken from Froese and Hall (1983). However, orthopyroxene is shown with a composition such that orthoamphibole falls on the Mg side of the cordierite-orthopyroxene tie line. Orthoamphibole and hornblende are shown with variable composition in order to allow a reversal

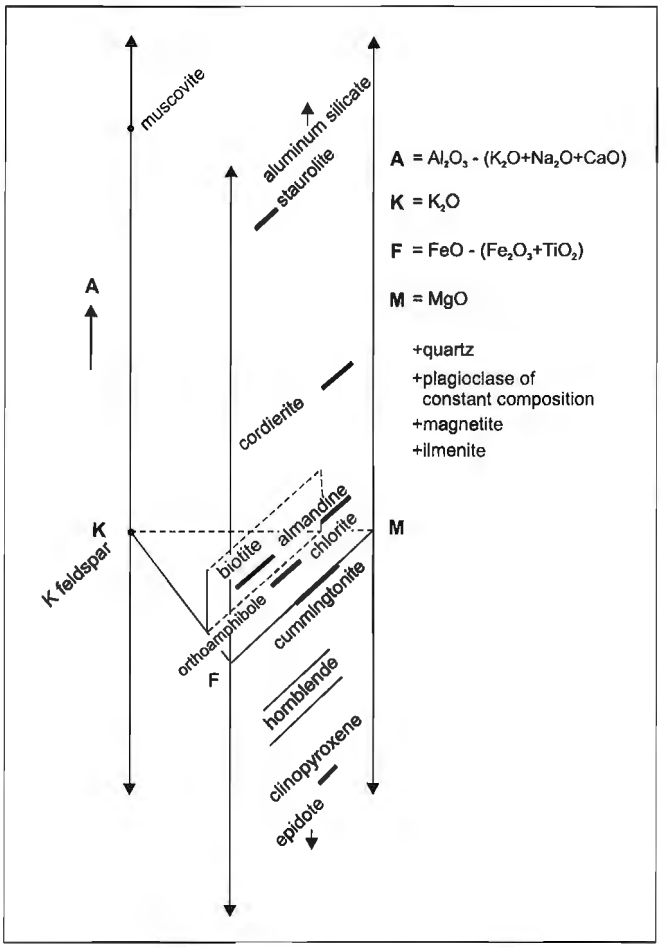

Figure 3. *Minerals represented in the system AKFM.*

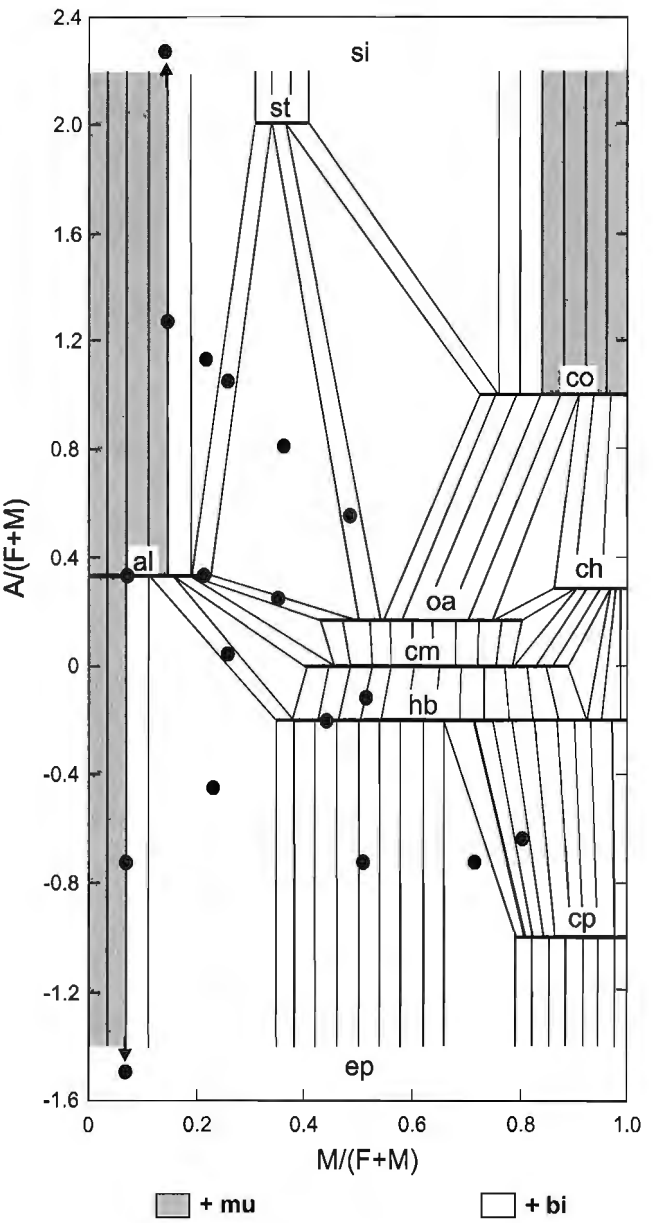

Figure 4. *Nonpotassic mineral assemblages shown in the AFM system. Coexisting potassic minerals are shown as additional phases; co = cordierite; ch = chlorite; see Table 1 for additional abbreviations.*

of the Fe-Mg partitioning in the pairs cummingtonite-orthoamphibole and cummingtonite-hornblende (Robinson et al., 1982). Such reversal leads to colinearity of some minerals in the system AFM, e.g. cordierite-orthoamphibole-cummingtonite and orthoamphibole-cummingtonite-hornblende. This feature produces a change of the stoichiometry of some reactions at singular points where one phase in a univariant reaction is absent. Singular points may be connected by degenerate univariant curves (Baker et al., 1991; Abart et al., 1992). Reactions among noncalcic minerals, except cummingtonite, have been taken from a grid prepared by D.M. Carmichael and published in Davidson et al. (1990). Most subsolidus reactions shown are also part of the grid presented by Xu et al. (1994). Reactions involving cummingtonite and calcic minerals, taken from Froese and Jen (1979), Froese (1980), Froese and Hall (1983), Spear and Rumble (1986), and Hollocher (1991) have been placed approximately with respect to the grid of Carmichael. At higher temperature, dehydration reactions terminate in an invariant point involving melt (marked by a dot). From this point, a reaction will emerge involving the same minerals and melt instead of vapour.

The field between the appearance of biotite + staurolite according to the reaction:

chlorite + almandine + muscovite =
biotite + staurolite + quartz + H_2O

and the decomposition of muscovite according to the reaction:

muscovite + plagioclase + quartz =
aluminum silicate + K feldspar + melt

was defined by Winkler (1979) as the range of medium grade metamorphism. In mafic rocks, the assemblage hornblende+calcic plagioclase is stabilized at a grade somewhat below the appearance of biotite+staurolite (Winkler, 1979). This change is present in mafic rocks about 4 km south of Weldon Bay (Kalliokoski, 1952).

In the field of medium grade metamorphism, the biotite-sillimanite-almandine isograd, based on the reaction:

staurolite + muscovite + quartz =
biotite + sillimanite + almandine + H_2O

separates the biotite-staurolite zone from the biotite-sillimanite-almandine zone.

The sequence of P-T conditions, approximately perpendicular to isograds on the erosion surface, has been called erosion surface P-T curve (Thompson, 1977) or metamorphic field gradient (Turner, 1981). A postulated metamorphic field gradient south of The Weldon Bay-Syme Lake area, similar to the one documented in the Snow Lake area (Froese and Moore, 1980), is shown in Figure 6, and reactions encountered along it are shown by changes on an AFM diagram and the biotite composition surface (Fig. 7). The metamorphic field gradient ends at peak metamorphic conditions of 5.5 kbar and 620°C, where mineral assemblages shown in Figures 4 and 5, indicating conditions of the biotite-sillimanite-almandine zone, are stable. The biotite-sillimanite-almandine isograd must be located somewhat south of Weldon Bay, at an estimated distance of about one kilometre. This study contributes to the documentation of isograds in the Flin Flon volcanic belt (Plint et al. 1995). It also illustrates the representation of pelitic, ferromagnesian, and mafic rocks in a common compositional system and provides a reaction grid in this system.

Table 1. Mineral assemblages.

qz	pl	bi	mu	ky	si	st	al	oa	cm	hb	cp	ep
x	x	x	x	x								
x	x	x	x		x							
x	x	x	x		x	(x)	x					
x	x	x	x				x					
x	x	x	x				x					x
x	x	x	x									x
x	x	x			x	x	x					
x	x	x				x	x					
x	x	x				x	x	x				
x	x	x				x		x				
x	x	x					x					
x	x	x					x	x				
x	x	x							x	x		
x	x	x					x			x		
x	x	x								x		
x	x	x					x			x		x
x	x	x								x		x
x	x	x								x	x	
x	x									x	x	x

Note: (x) indicates relict mineral

Abbreviations

qz	quartz	al	almandine
pl	plagioclase	oa	orthoamphibole
bi	biotite	cm	cummingtonite
mu	muscovite	hb	hornblende
ky	kyanite	cp	clinopyroxene
si	sillimanite	ep	epidote
st	staurolite		

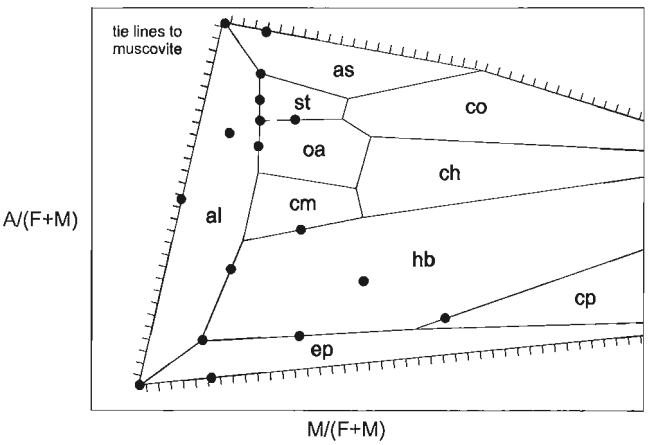

Figure 5. Mineral assemblages in the system AKFM shown on the biotite composition surface. Co = cordierite; ch = chlorite; as = aluminum silicate; see Table 1 for additional abbreviations.

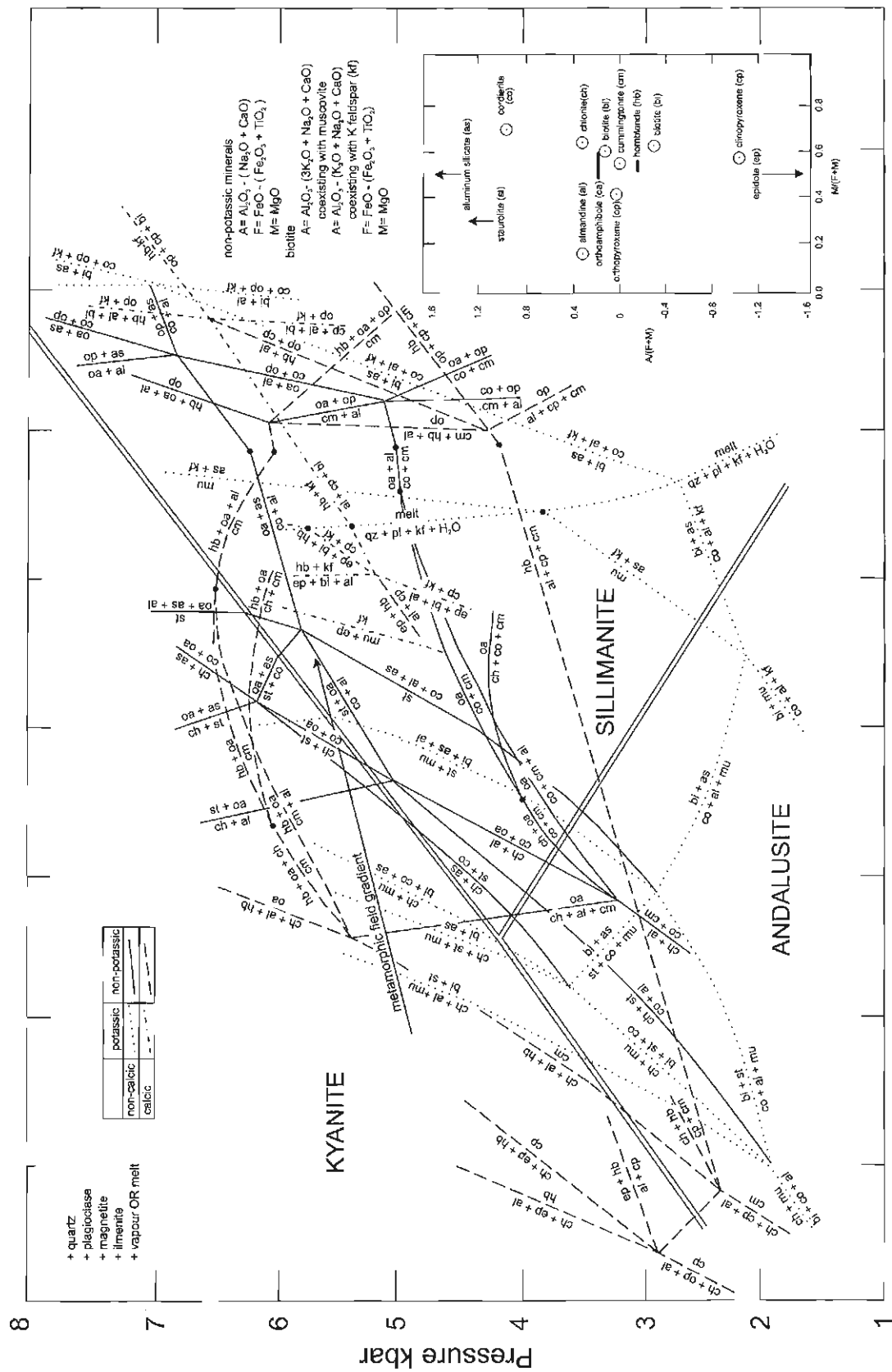

Figure 6. *Reaction grid for common minerals in the system AKFM; pl = plagioclase.*

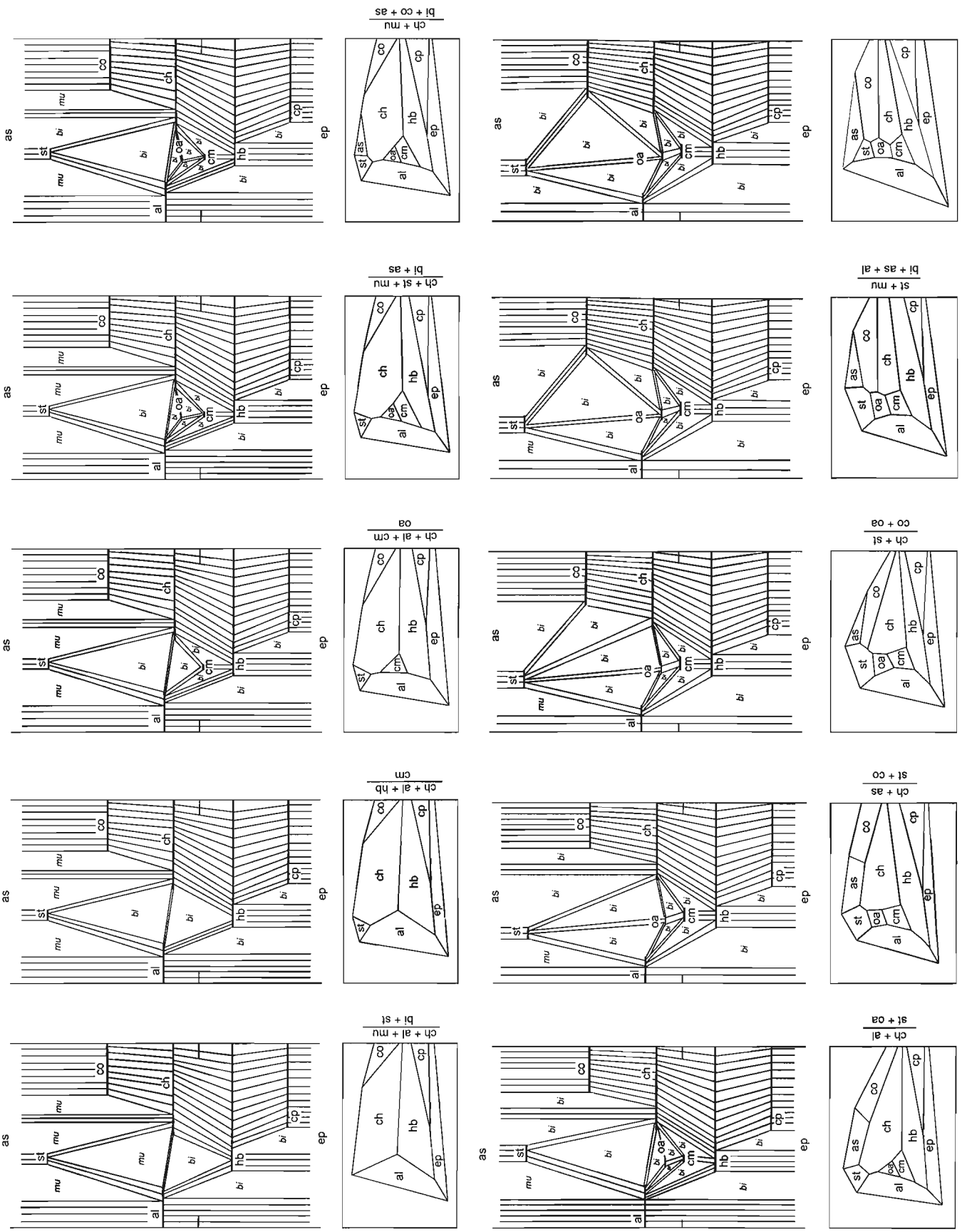

Figure 7. Reactions along the metamorphic field gradient shown in Figure 6. See abbreviation explanation Figure 6.

ACKNOWLEDGMENTS

I have benefitted greatly from discussions of various aspects of this study with a number of persons: K.E. Ashton, E.W. Brown, G.H. Gale, R. MacQuarrie, J.R. Pickell, D.P. Price, D.C.P. Schledewitz, and H.V. Zwanzig. Assistance in the field was provided by Q. Gall, T.D. Peterson, and L.B. McIntyre. The diagrams were drafted by D. Paul, D. Duquette, and D. Lemkow. The manuscript was critically read by K.L. Currie.

REFERENCES

Abart, R., Connolly, J.A.D., and Trommsdorff, V.
1992: Singular point analysis: construction of Schreinemakers projections for systems with a binary solution; American Journal of Science, v. 292, p. 778-805.

Albee, A.L.
1965: Phase equilibria in three assemblages of kyanite-zone pelitic schists, Lincoln Mountain quadrangle, central Vermont; Journal of Petrology, v. 6, p. 246-301.

Ashton, K.E.
1989: Kisseynew project: Kisseynew Lake - Florence Lake area; Manitoba Energy and Mines, Report of Field Activities 1989, p. 65-71.

1990: Geology of the Snake Rapids area, Flin Flon domain; Saskatchewan Geological Survey, Summary of Investigations 1990, p. 4-12.

Ashton, K.E., Hunt, P.A., and Froese, E.
1992: Age constraints on the evolution of the Flin Flon volcanic belt and Kisseynew gneiss belt, Saskatchewan and Manitoba; in Radiogenic Age and Isotopic Studies: Report 5; Geological Survey of Canada, Paper 91-2, p. 55-69.

Bailes, A.H. and McRitchie, W.D.
1978: The transition from low to high grade metamorphism in the Kisseynew sedimentary gneiss belt, Manitoba; Geological Survey of Canada, Paper 78-10, p. 155-178.

Baker, J., Holland, T., and Powell, R.
1991: Isograds in internally buffered systems without solid solutions: principles and examples; Contributions to Mineralogy and Petrology, v. 106, p. 170-182.

Bateman, J.D. and Harrison, J.M.
1946: Sherridon, Manitoba; Geological Survey of Canada, Map 862A, with desriptive notes.

Davidson, A., Carmichael, D.M., and Pattison, D.R.M.
1990: Metamorphism and geodynamics of the southwestern Grenville Province, Ontario; Field Trip Guidebook, IUGS/UNESCO International Geological Correlation Program Project 235-304, 123 p.

Frarey, M.J.
1961: Collins Point, Manitoba; Geological Survey of Canada, Map 1068A with descriptive notes.

Froese, E.
1878: The graphical representation of mineral assemblages in biotite-bearing granulites; in Current Research, Part A; Geological Survey of Canada, Paper 78-1A, p. 323-325.

1980: A reaction grid for medium grade mafic rocks; in Current Research, Part A; Geological Survey of Canada; Paper 80-1A, p. 53-55.

1984: Geology of the Weldon Bay-Fay Lake area, Manitoba; in Current Research, Part B; Gelogical Survey of Canada, Paper 84-1B, p. 355-358.

Froese, E. and Gall, Q.
1981: Geology of the eastern vicinity of Kisseynew Lake, Manitoba; in Current Research, Part A; Geological Survey of Canada, Paper 81-1A, p. 311-313.

Froese, E. and Hall, R.D.
1983: A reaction grid for potassium-poor pelitic and mafic rocks; in Current Research, Part A; Geological Survey of Canada, Paper 83-1A, p. 121-124.

Froese, E. and Jen, L.S.
1979: A reaction grid for biotite-bearing granulites; in Current Research, Part A; Geological Survey of Canada, Paper 79-1A, p. 83-85.

Froese E. and Moore, J.M.
1980: Metamorphism in the Snow Lake area, Manitoba; Geological Survey of Canada, Paper 78-27, 16 p.

Gale, G.H. and Norquay, L.I.
1996: Mineral deposits and occurrences in the Naosap Lake area; Manitoba Energy and Mines, Mineral Deposit Series, Report No. 20, 91 p.

Gordon, T.M.
1989: Thermal evolution of the Kisseynew sedimentary gneiss belt, Manitoba: metamorphism at an early Proterozoic accretionary margin; in Evolution of Metamorphic Belts, (ed.) J.S. Daly, R.A. Cliff, and B.W.D. Yardley; Geological Society, Special Publication No. 43, p. 233-243.

Hollocher, K.
1991: Prograde amphibole dehydration reactions during high-grade regional metamorphism, central Massachusetts, U.S.A.; American Mineralogist, v. 76, p. 956-970.

James, D.T.
1983: Origin and metamorphism of the Kisseynew gneisses, Kisseynew Lake-Cacholotte Lake area, Manitoba; M.Sc. thesis, Carleton University, Ottawa, 188 p.

Jungwirth, T.L.
1995: Metamorphism in the Duval Lake area, Kisseynew gneiss belt, Manitoba; M.Sc. thesis, University of Calgary, 165 p.

Kalliokoski, J.
1952: Weldon Bay map-area, Manitoba; Geological Survey of Canada, Memoir 270, 80 p.

Lucas, S.B., Stern, R.A., Syme, E.C., Zwanzig, H., Bailes, A.H., Ashton, K.E., Maxeiner, R.O., Ansdell, K.M., Lewry, J.F., Ryan, J.J., and Kraus, J.
1997: Tectonics of the southeastern Reindeer zone, Trans-Hudson Orogen (Manitoba and Saskatchewan); Geological Association of Canada, Abstract Volume 22, p. 93.

McGlynn, J.C.
1959: Elbow-Heming lakes area, Manitoba; Geological Survey of Canada, Memoir 305, 72 p.

McRitchie, W.D.
1980: Cacholotte Lake; Manitoba Mineral Resources Division, Report of Field Activities 1980, p. 65-69.

Norman, A.R., Williams, P.F., and Ansdell, K.M.
1995: Early Proterozoic deformation along the southern margin of the Kisseynew gneiss belt, Trans-Hudson Orogen: a 30 Maprogressive deformation cycle; Canadian Journal of Earth Sciences, v. 32, p. 875-894.

Plint, H.E., Gordon, T.M., Froese, E., and Berman, R.G.
1995: Metamorphic data, Flin Flon and Kisseynew belts, Saskatchewan-Manitoba; Geological Survey of Canada, Open File 3160, scale 1:400 000.

Robinson, P., Spear, F.S., Schumacher, J.C., Laird, J., Klein, C., Evans, B.W., and Doolan, B.L.
1982: Phase relations of metamorphic amphiboles: natural occurrence and theory; Reviews in Mineralogy, v. 9B, p. 1-227.

Schledewitz, D.C.P.
1993: Geology of the Webb Lake-Fay Lake area; Manitoba Energy and Mines, Report of Activities 1993, p. 29-32.

1994: Geology of the Webb Lake-Fay Lake area; Manitoba Energy and Mines, Report of Activities 1994, p. 42-46.

Spear, F.S. and Rumble, D.
1986: Pressure, temperature, and structural evolution of the Orfordville belt, west-central New Hampshire; Journal of Petrology, v. 27, p. 1071-1093.

Thompson, P.H.
1977: Metamorphic P-T distribution and the geothermal gradients calculated from geophysical data; Geology, v. 5, p. 520-522.

Turner, F.J.
1981: Metamorphic Petrology; second edition, McGraw-Hill Book Company, New York, 524 p.

Winkler, H.G.F.
1979: Petrogenesis of Metamorphic Rocks; fifth edition, Springer-Verlag, New York, 348 p.

Xu, G., Will, T.M., and Powell, R.
1994: A calculated petrogenetic grid for the system K_2O-FeO-MgO-Al_2O_3-SiO_2-H_2O, with particular reference to contact-metamorphosed pelites; Journal of Metamorphic Geology, v. 12, p. 99-119.

Zwanzig, H.V.
1983: Kisseynew project: Lobstick Narrows; Manitoba Mineral Resources Division Mines, Report of Field Activities 1983, p. 15-22.

Zwanzig, H.V. and Schledewitz, D.C.P.
1992: Geology of the Kississing-Batty lakes area: interim report; Manitoba Energy and Mines, Open File Report OF92-2.

Zwanzig, H.V., Ashton, K.E., and Schledewitz, D.C.P.
1995: Geology, Flin Flon belt-Kisseynew belt transition zone, Manitoba-Saskatchewan; Geological Survey of Canada, Open File 3054, scale 1:100 000.

Geological Survey of Canada Project 800007

Petrophysical characteristics of limestone xenoliths in kimberlites from Kirkland Lake, Ontario[1]

T.J. Katsube, S. Connell, M.B. McClenaghan, and D.K. Armstrong[2]
Mineral Resources Division, Ottawa

Katsube, T.J., Connell, S., McClenaghan, M.B.,and Armstrong, D.K., 1997: Petrophysical characteristics of limestone xenoliths in kimberlites from Kirkland Lake, Ontario; in Current Research 1997-E; Geological Survey of Canada, p. 45-57.

Abstract: Pore-size distribution has been determined by mercury porosimetry for six surface limestones, six diatreme-facies kimberlites, and six limestone xenoliths (from within the kimberlites) sampled from the Kirkland Lake (Ontario) area. The purpose was to investigate how the petrophysical characteristics of limestone fragments change as a result of their mixing with kimberlite magma.

Results indicate that while porosities of the xenolith core-material samples are higher than those of the parent limestones, the pore-size distribution patterns are similar, suggesting that these distribution patterns may reflect textural features that are related to the source rock. In contrast, the rim-material samples of the limestone xenoliths show lower porosities than their cores, and display pore-size distribution patterns which are similar to those of the kimberlite that hosted them. These distribution patterns most likely reflect alteration of the limestone xenoliths by the kimberlite magma.

Résumé : La distribution du diamètre des pores a été déterminée par porosimétrie au mercure pour six échantillons de calcaires de surface, six de kimberlites à faciès de diatrème et six de xénolites de calcaire (provenant des kimberlites) prélevés dans la région de Kirkland Lake (Ontario). L'objectif visé consiste à étudier les modifications des caractéristiques pétrophysiques des fragments de calcaire consécutives à leur incorporation à un magma kimberlitique.

Les résultats indiquent que, bien que les porosités des xénolites de noyau soient supérieures à celles des calcaires parentaux, la distribution du diamètre des pores est semblable. Cela laisse supposer que cette distribution pourrait refléter des caractéristiques texturales liées à la roche mère. Par opposition, les xénolites calcaires de bordure ont des porosités inférieures à celles des xénolites de noyau, et la distribution du diamètre des pores est semblable à celle des kimberlites encaissantes, ce qui est fort probablement le fait de l'altération des xénolites de calcaire par le magma kimberlitique.

[1] Contribution to Canada-Ontario Subsidiary Agreement on Northern Ontario Development (1991-1995), under the Canada-Ontario Economic and Regional Development Agreement.
[2] Ontario Geological Survey, 933 Ramsey Lake Road, Sudbury, Ontario P3E 6B5

INTRODUCTION

Pore-size distribution has been determined by mercury porosimetry for a set of samples consisting of six surface limestones (Ordovician and Silurian), six diatreme-facies kimberlites, and six limestone xenoliths, from the Kirkland Lake (Ontario) area. The Kirkland Lake kimberlites generally contain considerable numbers of limestone xenoliths. Some limestone xenoliths are encircled by a coloured rim, while an adjacent xenolith may not have a rim (Fig. 1). The two prominent rim types are brownish and purple, and of varying thickness.

The purpose of this study was to investigate how the petrophysical characteristics of surface limestone fragments change as a result of their incorporation into, and reaction with, kimberlite magma. A previous study (Katsube et al., 1996b), which included one limestone xenolith from the same area, showed an indication of a porosity increase as a result of the mixing process. The results presented here are part of a larger study (e.g. Katsube et al., 1992; Katsube and Scromeda, 1994; Scromeda et al., 1994; Richardson et al., 1995) to characterize the physical properties of Canadian kimberlites in order to assist the interpretation of surface and airborne geophysical survey data.

Another purpose of this study was to investigate whether the two types of xenoliths showed any difference in their physical characteristics. This includes the investigation of the physical characteristics of the rim material as well. This paper provides a description of the samples used, a description of the methods used in the investigation, and the results of the physical property characterization.

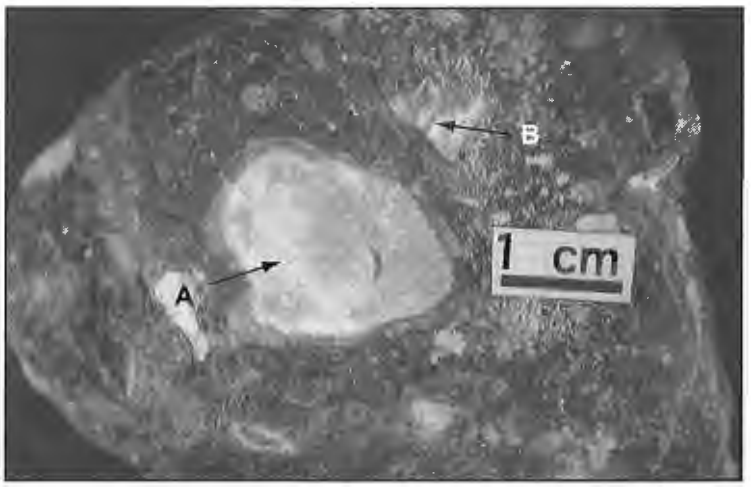

Figure 1.

*Photograph of a kimberlite sample containing limestone xenoliths, some which are encircled by a coloured rim (**A**) while others (**B**) have no rims. GSC: 1997-018C*

Table 1a. Kimberlite and limestone sample information (from Katsube et al., 1996b).

Sample number	Sample I.D.	Pipe	Drillhole	Depth (m)		Rock type
				DFS	DTKS	
KLM-2		C14	C14-05	38.9	34.0	KB
KLH-2		DL	DDH FL91-14	191	53.3	KB
KLH-5		DL	DDH FL92-23	124	53.3	KB
KLH-6		DL	DDH FL92-23	135	53.3	KB
KLD-1	DKA-94-28B			0		LS
KLD-2	DKA-94-32E			0		LS
KLD-3	DKA-94-34D			0		LS
KLD-4	DKA-94-36H			0		LS
KLD-5	DKA-94-39B			0		LS
KLD-6	DKA-94-43			0		LS

DL = Diamond Lake pipe (Fig. 1)
KB = Kimberlite
LS = Limestone
DFS = Depth of sample from earth surface
DTKS = Depth to kimberlite subcrop surface from earth surface

Table 1b. Sample/Specimens used in this study for mercury porosimetry testing

Surface limestones	Limestone xenoliths	Kimberlites
KLD-1	KLH-2a	KLH-2ka
KLD-2	KLH-2b	KLH-2kb
KLD-3	KLH-2bx	KLH-5ka
KLD-4	KLM-2a (rim & core)	KLH-6k
KLD-5	KLM-2b	KLM-2ka
KLD-6	KLM-2e (rim & core)	KLM-2kb

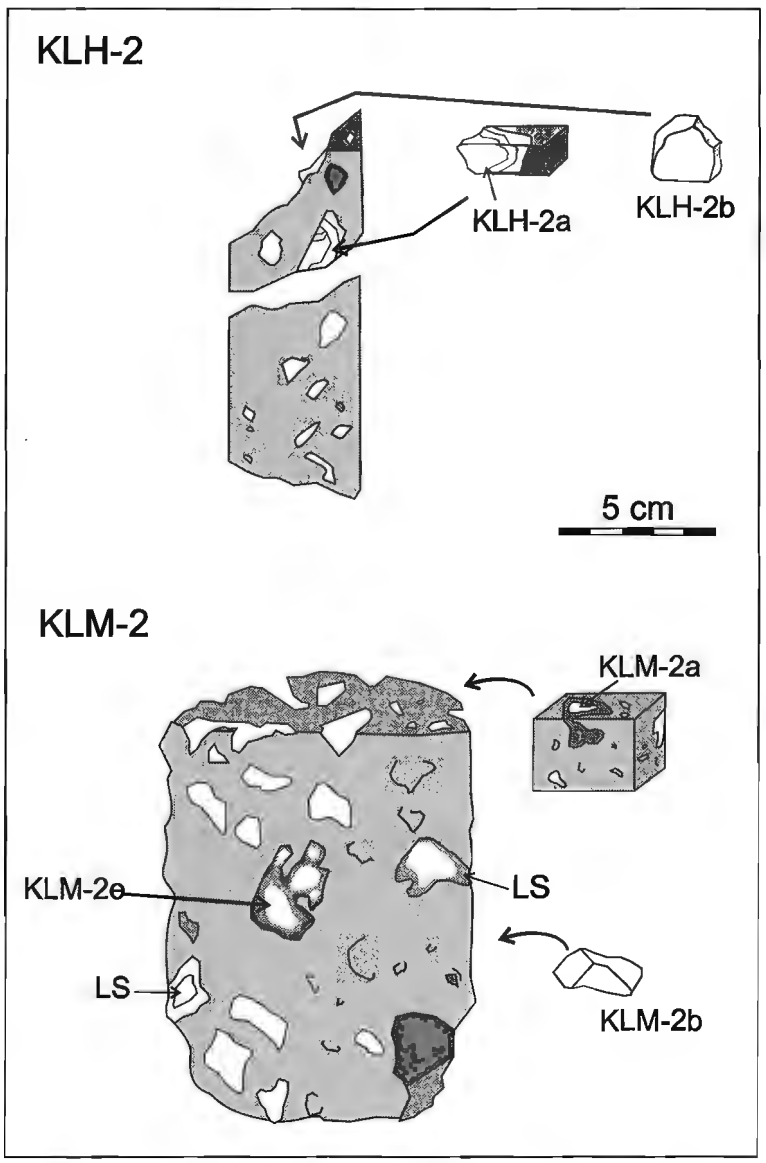

Figure 2.

Descriptions of two kimberlite samples (KLH-2k and KLM-2k), and the locations from which five of the xenolith specimens (KLH-2a, KLH-2b, KLM-2a, KLM-2b and KLM-2e) were extracted.

The Kirkland Lake kimberlite field is in the western part of the Abitibi Greenstone Belt, in the Superior Province of the Canadian Shield, approximately 10 km north and east of Kirkland Lake and 100 km southeast of Timmins (McClenaghan, 1993, 1996). Kimberlites intruded Archean metavolcanic and metasedimentary rocks and Paleozoic carbonate rocks during the Late Jurassic (155 to 160 Ma) (Brummer et al., 1992), and consist of blue-grey to grey-brown diatreme-facies heterolithic, tuffaceous, kimberlite breccia. The groundmass contains serpentine, phlogopite, chlorite, and calcite, and varies from light to medium greenish grey. Wall-rock fragments of greenish-grey to white Paleozoic carbonate are common, ranging in size from 1 cm to 1 m. Today, the nearest Paleozoic carbonate rocks are 40 km south of Kirkland Lake near New Liskeard. Most of the known kimberlite pipes have distinct circular magnetic signatures (Ontario Geological Survey, 1979; Brummer et al., 1992; Geological Survey of Canada, 1993; Keating, 1995).

Table 2a. Pore-size distribution data for different pore-size ranges, d_a, obtained by mercury porosimetry for the surface limestone samples from the Kirkland Lake area (Katsube et al., 1996b).

	KLD-1	KLD-2	KLD-3	KLD-4	KLD-5	KLD-6
d_a(nm)	ϕ_a (%)					
3.2	0.05	0.05	0.00	0.22	0.03	0.00
5.0	0.05	0.13	0.00	0.67	0.10	0.03
7.9	0.11	0.16	0.08	0.76	0.20	0.05
12.6	0.11	0.21	0.18	1.03	0.36	0.13
20.0	0.11	0.30	0.71	1.12	0.51	0.21
31.6	0.11	0.24	0.76	1.05	0.43	0.16
50.1	0.21	0.48	0.81	3.58	0.76	0.53
79.4	0.21	0.27	0.24	4.92	0.91	0.37
126	0.27	0.24	0.10	0.67	1.80	0.24
200	0.37	0.24	0.08	0.17	1.85	0.19
316	0.32	0.30	0.05	0.07	1.90	0.13
501	0.21	0.30	0.00	0.05	0.84	0.11
794	0.13	0.32	0.00	0.00	0.33	0.13
1259	0.11	0.30	0.00	0.00	0.13	0.13
1995	0.03	0.08	0.00	0.00	0.08	0.16
3162	0.05	0.03	0.00	0.00	0.05	0.16
5012	0.03	0.00	0.00	0.00	0.05	0.19
7943	0.00	0.00	0.00	0.00	0.00	0.08
ϕ_{Hg1}	2.5	3.7	3.0	14.3	10.3	3.0
ϕ_{Hg2}	3.0	3.8	3.4	14.5	10.4	4.8
d_{hg}	360	130.6	81.9	46.1	145.8	1403.1
δ_{BD}	2.66	2.68	2.62	2.39	2.54	2.66
δ_{SD}	2.75	2.79	2.71	2.79	2.83	2.80
A	0.85	1.60	1.42	8.91	2.44	0.75
ϕ_s	2.0	2.0	2.8	7.8	8.6	2.6
ϕ_{rr}	0.826	0.559	0.912	0.545	0.832	0.857*
h	0	0	0	0	0	0

d_a = Geometric mean pore-sizes for the different pore-size ranges (nm)
d_{hg} = Geometric mean of the entire pore-size distribution (nm)
ϕ_a = Partial porosity (%)
ϕ_{Hg1} = Total porosity measured by mercury porosimetry for pore sizes up to 10 μm (%)
ϕ_{Hg2} = Total porosity measured by mercury porosimetry for pore sizes up to 250 μm (%)
δ_{BD} = Bulk density (g/mL)
δ_{SD} = Skeletal density (g/mL)
A = Surface Area (m^2/g)
ϕ_s = Residual or isolated porosity (%)
ϕ_{rr} = ϕ_s / ϕ_{Hgl}
h = Depth (m) from which the sample was obtained
* = ϕ_{Hg2} used instead of ϕ_{Hg1}

METHOD OF INVESTIGATION

Samples and geological logging

Information on the kimberlite pipes, and on locations in the Kirkland Lake (Ontario) area from which the kimberlite and limestone samples used in this study were obtained, has previously been published (Katsube et al., 1996b). Some of that information is repeated in Table 1a.

The kimberlite samples were split drill cores, of 4-9 cm in diameter and 5-20 cm in length, recovered from holes drilled by the Geological Survey of Canada (McClenaghan, 1996) and Sudbury Contact Mines Limited. The six (two Ordovician and four Silurian) limestone samples were collected from outcrops near New Liskeard, Ontario. Geological logging was carried out for all of the samples. Detailed logging was performed on the kimberlites, specifically, for the purpose of locating limestone xenoliths large enough to extract and use for tests. Sketches were made of the samples received before and after cutting to indicate the approximate location of each xenolith. Sketches and some photographs were also taken of selected specimens. Descriptions of the samples/specimens are compiled in the Appendix. They include colour, hardness, homogeneity, size, and thickness of alteration rims where applicable.

Table 2b. Pore-size distribution data for different pore-size ranges, d_a, obtained by mercury porosimetry for the limestone xenolith samples from the Kirkland Lake Kimberlites.

	KLH-2a	KLH-2b	KLH-2bx	KLM-2a (core)	KLM-2a (rim)	KLM-2b	KLM-2e (core)	KLM-2e (rim)
d_a(nm)	ϕ_a (%)							
3.2	0.10	1.21	0.32	0.17	0.38	0.50	0.00	0.63
5.0	0.98	1.29	0.47	0.15	1.40	2.76	0.02	1.07
7.9	1.04	0.81	0.60	0.29	1.50	2.13	0.12	0.70
12.6	1.29	1.11	1.10	0.29	1.33	1.89	0.12	0.63
20.0	1.17	2.56	1.97	0.46	1.40	2.48	0.31	0.51
31.6	0.73	2.36	1.60	0.48	0.83	1.93	0.47	0.35
50.1	0.36	1.14	1.47	1.72	1.14	3.18	2.33	0.61
79.4	0.36	0.85	0.42	4.05	0.95	2.61	6.23	0.72
126	0.13	0.64	0.20	5.45	0.36	2.37	2.40	0.47
200	0.00	0.70	0.10	8.11	0.12	2.46	0.09	0.26
316	0.13	1.13	0.00	6.99	0.10	3.22	0.00	0.00
501	0.03	1.27	0.00	2.05	0.02	4.28	0.00	0.00
794	0.16	2.17	0.00	0.55	0.00	7.13	0.05	0.00
1259	0.05	3.52	0.00	0.04	0.05	0.53	0.00	0.00
1995	0.00	3.30	0.00	0.07	0.05	0.22	0.00	0.00
3162	0.00	0.00	0.00	0.00	0.00	0.00	0.00	0.00
5012	0.00	0.00	0.00	0.04	0.05	0.00	0.00	0.00
7943	0.00	0.00	0.00	0.00	0.00	0.00	0.02	0.00
ϕ_{Hg1}	6.5	24.1	8.3	30.9	9.7	37.7	12.2	5.9
ϕ_{Hg2}	7.3	24.4	8.4	31.5	9.9	39.5	12.5	6.3
d_{hg}	38.9	142.7	25.8	175.6	24.1	130.3	89.7	29.6
δ_{BD}	2.59	2.01	2.49	1.83	2.38	2.19	2.35	2.33
δ_{SD}	2.79	2.66	2.72	2.68	2.64	3.63	2.69	2.49
A	7.8	18.1	7.6	7.3	12.3	24.0	2.9	9.2
ϕ_s	4.4	6.0	3.4	13.6	6.9	24.5	5.2	2.7
ϕ_{rr}	0.668	0.249	0.413	0.439	0.708	0.649	0.425	0.455
h	191	191	191	38.9	38.9	38.9	38.9	38.9

d_a = Geometric mean pore-sizes for the different pore-size ranges (nm)
d_{hg} = Geometric mean of the entire pore-size distribution (nm)
ϕ_a = Partial porosity (%)
ϕ_{Hg1} = Total porosity measured by mercury porosimetry for pore sizes up to 10 μm (%)
ϕ_{Hg2} = Total porosity measured by mercury porosimetry for pore sizes up to 250 μm (%)
δ_{BD} = Bulk density (g/mL)
δ_{SD} = Skeletal density (g/mL)
A = Surface Area (m^2/g)
ϕ_s = Residual or isolated porosity (%)
ϕ_{rr} = ϕ_s / ϕ_{Hg1}
h = Depth (m) from which the sample was obtained

Specimen preparation for measurement

An irregularly shaped specimen of 2-5 grams was cut from each the six limestone samples, and from two of the kimberlite samples (KLH-5k and KLH-6k). Two specimens of similar shape and size were cut from each of the remaining two kimberlite samples (KLH-2k and KLM-2k). Sample/specimen numbers are listed in Table 1b. Three xenolith specimens were cut from each of the two kimberlite Samples KLH-2k and KLM-2k. Descriptions of these two samples and the locations from which five of the xenolith specimens were extracted are shown in Figure 2.

When the limestone xenolith had prominent alteration rims (KLM-2a and KLM-2e, Table 1b), subspecimens were taken of both the core and rim material. Due to the very limited quantity and to the nature of the rims, it was usually only possible to prepare specimens for mercury porosimetry and thin-section analysis.

At least one irregularly shaped subspecimen of 0.4-2 g was cut from each of the xenolith core specimens for the mercury porosimetry tests. Additional specimens were also cut from the xenolith core for other measurements (e.g. electrical resistivity and immersion porosity) that will be reported separately.

Table 2c. Pore-size distribution data for different pore-size ranges, d_a, obtained by mercury porosimetry for the kimberlite samples from the Kirkland Lake (Ontario).

	KLH-2ak	KLH-2bk	KLH-5ka	KLH-6k	KLM-2ka	KLM-2kb
d_a(nm)	ϕ_a (%)					
3.2	0.19	0.74	0.98	2.50	0.60	1.91
5.0	0.60	1.38	3.54	3.32	1.59	2.47
7.9	0.94	1.59	3.29	1.18	1.27	1.36
12.6	1.80	3.30	1.62	0.57	1.00	0.92
20.0	2.35	3.66	1.11	0.35	0.75	0.62
31.6	1.10	0.74	0.56	0.16	0.52	0.40
50.1	1.25	0.64	0.67	0.24	0.77	0.47
79.4	1.06	0.57	0.58	0.21	0.87	0.45
126	1.01	0.55	0.40	0.09	0.92	0.42
200	0.94	0.47	0.31	0.07	0.95	0.40
316	0.86	0.52	0.42	0.07	1.12	0.42
501	0.70	0.38	0.38	0.02	0.62	0.27
794	1.10	0.57	0.49	0.02	0.57	0.12
1259	1.97	0.38	0.62	0.14	0.90	0.05
1995	0.00	0.17	0.58	0.02	0.00	0.05
3162	0.00	0.19	0.33	0.07	0.00	0.05
5012	0.14	0.14	0.13	0.07	0.05	0.00
7943	0.05	0.02	0.00	0.00	0.00	0.00
ϕ_{Hg1}	16.07	16.00	16.01	9.12	12.50	10.4
ϕ_{Hg2}	16.72	16.96	16.48	9.45	12.88	10.7
d_{hg}	96.9	42.3	31.8	11.3	63.5	19.7
δ_{BD}	2.40	2.37	2.22	2.36	2.49	2.47
δ_{SD}	2.88	2.86	2.67	2.61	2.86	2.77
A	9.57	17.97	26.24	24.74	11.96	19.30
ϕ_s	8.1	7.4	8.9	5.4	7.3	7.1
ϕ_{rr}	0.503	0.461	0.555	0.590	0.585	0.439
h	191	191	124	135	38.9	38.9

d_a = Geometric mean pore-sizes for the different pore-size ranges (nm)
d_{hg} = Geometric mean of the entire pore-size distribution (nm)
ϕ_a = Partial porosity (%)
ϕ_{Hg1} = Total porosity measured by mercury porosimetry for pore sizes up to 10 µm (%)
ϕ_{Hg2} = Total porosity measured by mercury porosimetry for pore sizes up to 250 µm (%)
δ_{BD} = Bulk density (g/mL)
δ_{SD} = Skeletal density (g/mL)
A = Surface Area (m^2/g)
ϕ_s = Storage porosity isolated porosity (%)
ϕ_{rr} = ϕ_s/ϕ_{Hg1}
h = Depth (m) from which the sample was obtained

Mercury porosimetry measurements

Specimens used for mercury intrusion porosimetry were initially oven dried for 24 hours at a temperature of 105°C (220°F), while under vacuum. This was followed by cooling, in a desiccator, prior to the measurement. The pore-size distribution of the samples was determined following the procedures described in previous publications (e.g. Katsube and Walsh, 1987; Katsube and Issler, 1993) using an equilibration time of 45 seconds for each of the high-pressure steps, and 10 seconds for the low-pressure (<0.7 MPa) steps. The measurements were made by using a Micromeritics Autopore 9200 mercury porosimeter with an available pressure range of 0.14-420 MPa and an equivalent pore-size range of 10-0.003 μm. In principle, the mercury porosimeter can generate pressures high enough to force mercury into all accessible pores and measure the volume of mercury taken up by them (Rootare, 1970). Assuming cylindrical pore shapes, the Washburn equation (Washburn, 1921; Rootare, 1970) relates the amount of pressure, p, required to force mercury into pores with pore-size diameter, d, greater than or equal to

$$d = -4\gamma\cos(\theta)/p,$$

Table 3. Pore-size distribution patterns.

Pattern	Pore-size mode (nm)	Type of pores
Type-1	1-10	nano-pores
Type-2	10-100	stress pores
Type-3	100-1000	grain-boundary pores
Type-4	>1000	blind or vuggy pores.

Table 4. Pore-size distribution pattern types in surface limestones.

Category	Samples	Pore-size distribution pattern type
CAT-1	KLD-2, KLD-6	dispersed
CAT-2	KLD-3	Type-1 to Type-2
CAT-3	KLD-4	Type-2
CAT-4	KLD-1, KLD-5	Type-3.

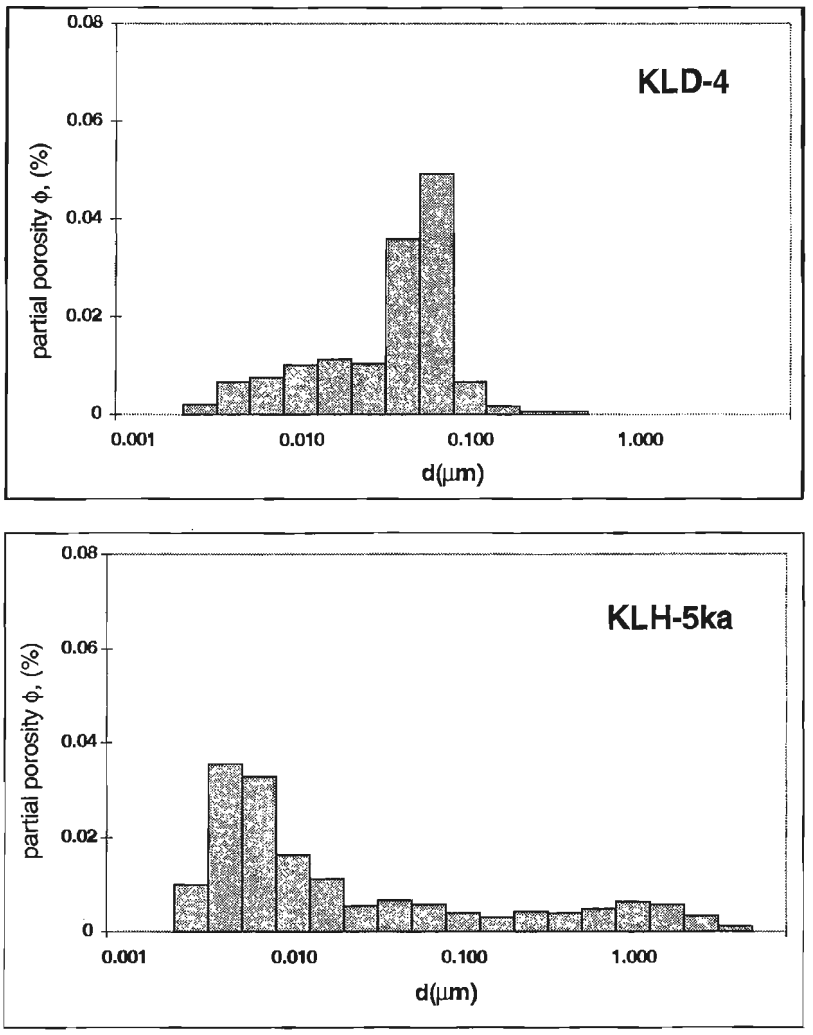

Figure 3.

Typical examples of pore-size distributions for a limestone (KLD-4) sample and a kimberlite (KLH-5ka) sample.

Where γ is the surface tension of mercury, and I is the contact angle. Values of $\theta = 140°$ and $\gamma = 0.48$ N/m were used in this study.

Determination of pore-size distribution

The mercury injection pressure was incrementally increased from 0.14 MPa to 420 MPa in 56 pressure steps, and the volume of mercury intruded for each step measured. The pressure steps, more or less equally divide the entire pressure range on a logarithmic scale. Since each pressure step represents a certain pore-size, the volume of mercury intruded for each step can be converted into the porosity of that pore size (e.g. Katsube and Issler, 1993). The measured pore-size distributions are plotted in a standard format by grouping the data into different size classes (e.g. Katsube and Issler, 1993; Katsube and Williamson, 1994). The standard display format has each decade of the logarithmic pore-size scale (x axis) subdivided into five ranges with equal physical spacing.

Experimental results

Results of the pore-size distribution measurements determined by mercury porosimetry are presented in Tables 2a to 2c. Data for partial porosity, ϕ_a, which is the porosity contributed by each pore-size range, are listed in the rows for each sample. The parameter, d_a (first row), is the geometric mean for each pore-size range (nm). Total porosity, ϕ_{Hgl}, is

Table 5. Pore-size distribution pattern types in limestone-xenolith core material.

Category	Samples	Pore type
CAT-1	KLM-2b, KLH-2b	dispersed
CAT-2	KLH-2a, KLH-2bx	Type-1 to Type-2
CAT-3	KLM-2e	Type-2
CAT-4	KLM-2a	Type-3.

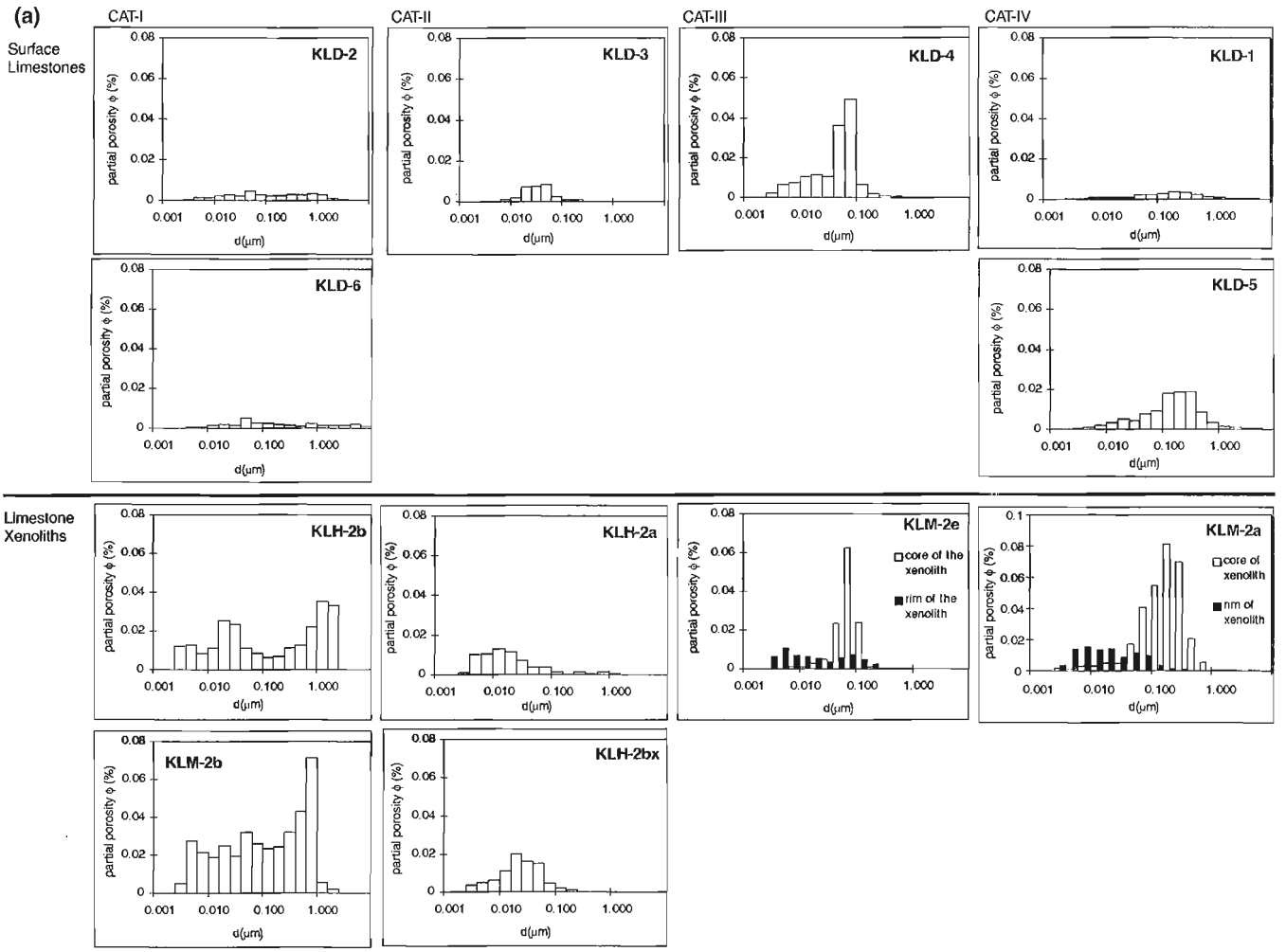

Figure 4a. *The pore-size distributions for six surface limestones and six limestone xenoliths.*

the sum of partial porosity values for pore sizes less than or equal to 10 μm, whereas ϕ_{Hg2} is the sum of the partial porosity values for pore-sizes up to 250 μm. Both ϕ_{Hg1} and ϕ_{Hg2} represent porosities corresponding to the effective porosity ϕ_E, that is the porosity of all interconnected pores in a rock (Katsube et al., 1992). However, ϕ_{Hg1} is more likely to consist of true sample porosity, because ϕ_{Hg2} may include measurement errors such as those originating from the space between the specimen and the sample container. Typical examples of pore-size distributions are displayed in Figure 3 for samples of limestone (KLD-4) and kimberlite (KLH-5ka).

Data for several additional parameters (e.g. δ_{SD}, A and ϕ_s) are also listed in the three tables. However, they are listed here only for the purpose of documentation at this time. The significance of the data and the methods of determination are described in other papers (e.g. Katsube and Issler, 1993; Katsube et al., 1996a, 1996b).

DISCUSSIONS AND CONCLUSIONS

The pore-size distributions for the six surface limestone samples and the six limestone xenoliths are displayed in Figure 4a, and those for the six kimberlite samples are displayed in Figure 4b. As shown in these diagrams, the pore-size distribution patterns vary considerably. However, distinct patterns are observed between the three rock types (limestones, xenoliths, and kimberlites) when their pore-size distributions are compared. Use of the following four types of pore-size distribution patterns are of help when making these comparisons (Table 3).

The relationship between the pore-size modes and the types of pores are empirical only, and are based on studies conducted mainly on granites (Agterberg et al., 1984; Katsube and Hume, 1987) and shales (e.g. Katsube and Williamson, 1994).

The surface limestones display comparatively low porosities, and their pore-size distributions can be divided into the following four categories (CAT-1 to CAT-4), based on their pore-size distribution pattern types (Fig. 4a, Table 4).

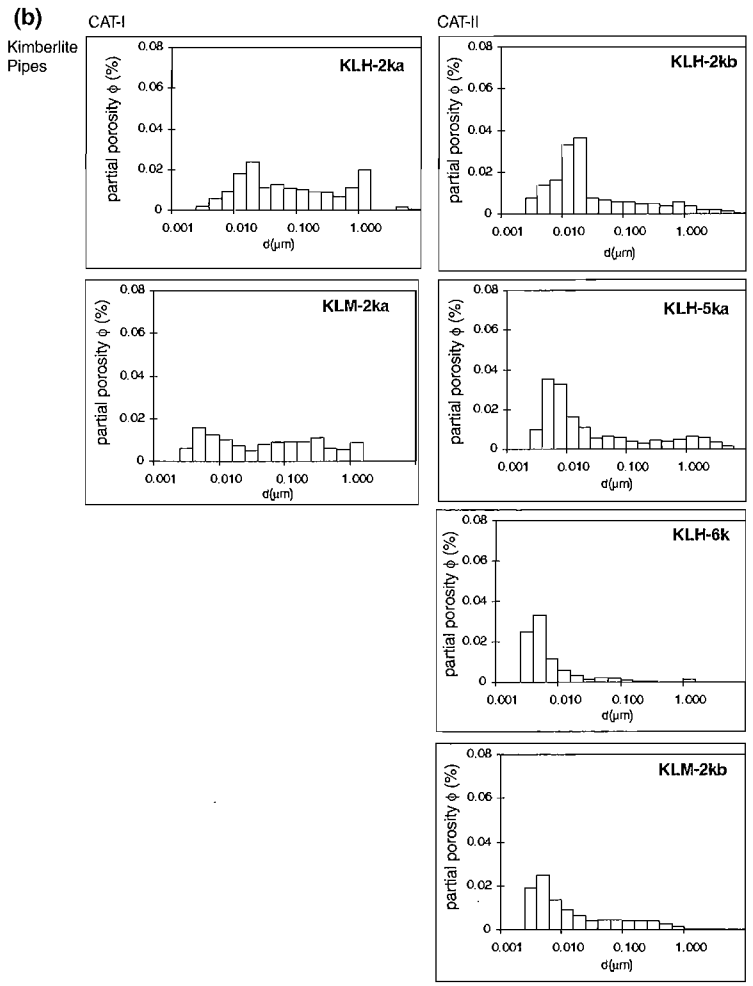

Figure 4b. The pore-size distributions for six kimberlite samples.

Dispersed pore type implies a multimodal pore-size distribution.

The core material of the limestone xenoliths display comparatively high porosities, and their pore-size distributions can also be divided into the following four categories (CAT-1 to CAT-4), similar to those of the surface limestones (Fig. 4a, Table 5).

The pore-size distributions of the rim material for the two xenolith specimens are also displayed in Figure 4a. They both show lower porosities than their core material, and the mode of the pore-size distributions has shifted to the smaller pore-sizes. That is, they have shifted to CAT-2 from CAT-3 and CAT-4.

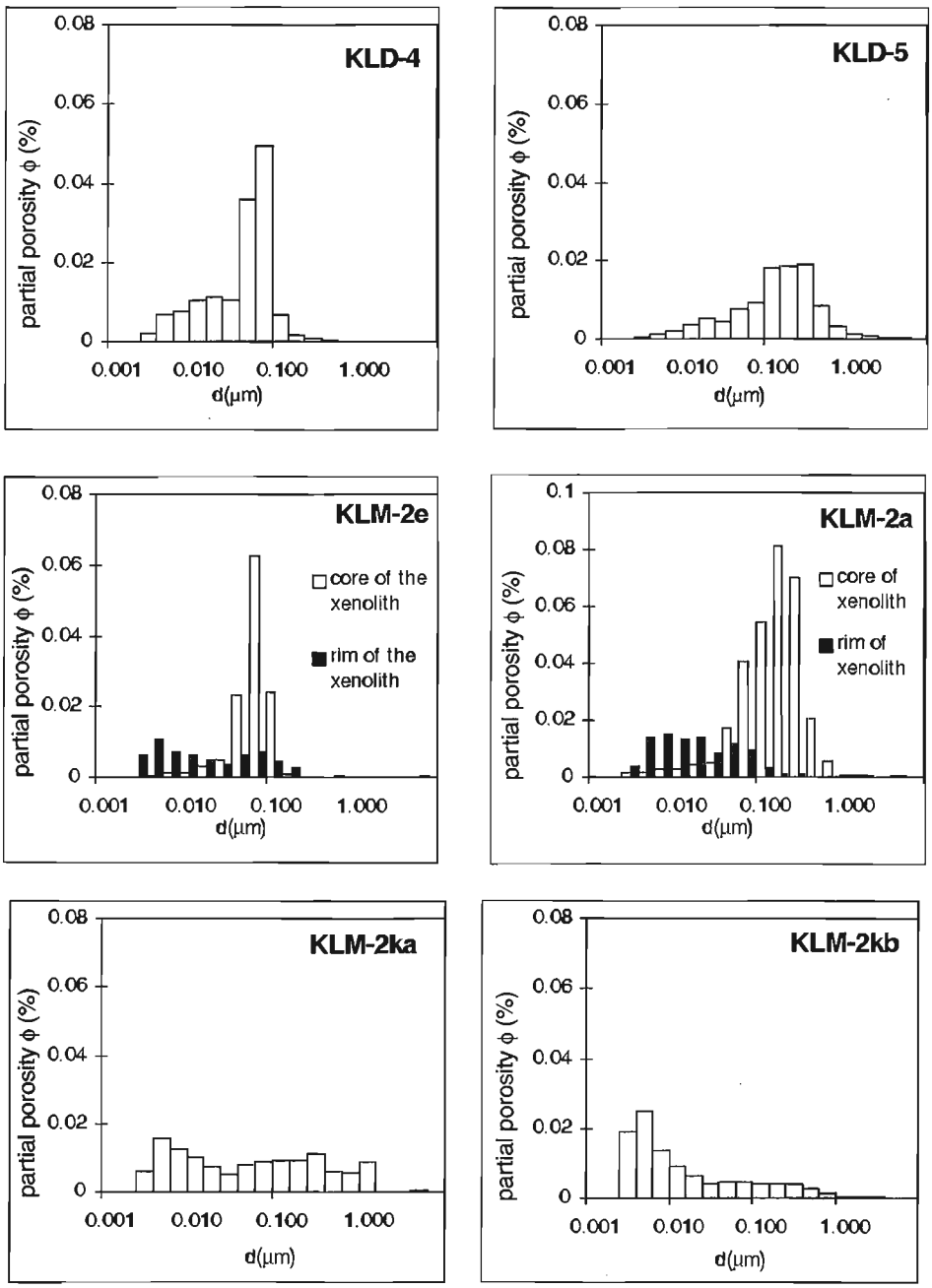

Figure 5. *The pore-size distributions for two surface limestones (KLD-4, KLD-5), two limestone xenoliths (KLM-2e, KLM-2a) and two kimberlite (KLM-2ka, KLM-2kb) samples. Although the core material of the limestone xenoliths shows similarities to the surface limestones, the rim material of these xenoliths shows similarities to that of the kimberlites.*

The six kimberlites generally display comparatively high porosities and can be divided into two of the four categories: CAT-1 (KLH-2ka, KLM-2ka) and CAT-2 (KLH-2b, KLH-5k, KLH-6k, KLM-2b). They are characterized by generally smaller modes. In general, the pore-size distribution pattern of the rim material shows similarities to that of the kimberlite (KLM-2ka, KLM-2kb) that hosted it, as shown in Figure 5.

While the porosities of the core material of the limestone xenoliths are considerably higher than those of the surface limestones, they have pore-size distribution patterns that are similar to those of the surface limestones. The two specimens/subspecimens of rim material from the limestone xenoliths (altered section of the xenoliths) show lower porosities than their corresponding core specimen. It is interesting to note that the rim material displays pore-size distribution patterns unlike their core material, but which are similar to those of the kimberlite sample that hosted them. This most likely reflects the recrystallization of carbonate adjacent to the kimberlite magma. Detailed mineralogical (including scanning electron microscope analysis) and geochemical studies are required to further characterize these reactions.

ACKNOWLEDGMENTS

The authors are grateful to Sudbury Contact Mines Ltd. and Regal Goldfields Ltd. for providing the kimberlite samples and allowing access to their property. The authors acknowledge support for this study from the Canada-Ontario Subsidiary Agreement on Northern Development (1991-95), a part of the Canada-Ontario Economic and Regional Development Agreement. Contributions by D.K. Armstrong were made with permission of the Chief, Sedimentary Geoscience Section, Ontario Geological Survey. The authors are very thankful for the critical review of this paper and for the useful suggestions provided by M. Hannington (GSC, Ottawa).

REFERENCES

Agterberg, F.P., Katsube, T.J., and Lew, S.N.
1984: Statistical analysis of granite pore size distribution data, Lac du Bonnet batholith, Eastern Manitoba; in Current Research, Part A; Geological Survey of Canada, Paper 84-1A, 29-37.

Brummer, J.J., MacFadyen, D.A., and Pegg, C.C.
1992: Discovery of kimberlites in the Kirkland Lake area, Northeastern Ontario, Part II: Kimberlite discoveries, sampling, diamond content, ages and emplacement; Exploration and Mining Geology, v. 1, p. 351-370.

Geological Survey of Canada
1993: Magnetic anomaly map (Residual Total Field), Blake River syncline, Ontario, parts of NTS 42A/1, 42A/8, 32D/4, 32D/5; Geological Survey of Canada, Maps C20369G and C203770G, scale 1:50 000.

Katsube, T.J. and Hume, J.P.
1987: Pore structure characteristics of granitic rock samples from Whiteshell Research Area; in Geotechnical Studies at Whiteshell Research Area (RA-3), CANMET, Report MRL 87-52, p. 111-158.

Katsube, T.J. and Issler, D.R.
1993: Pore-size distribution of shales from the Beaufort-MacKenzie Basin, northern Canada; in Current Research, Part E; Geological Survey of Canada, Paper 93-1E, p. 123-132.

Katsube, T.J. and Scromeda, N.
1994: Physical properties of Canadian kimberlites, Somerset Island and Saskatchewan; in Current Research 1994-B; Geological Survey of Canada, p. 35-42.

Katsube, T.J. and Walsh, J.B.
1987: Effective aperture for fluid flow in microcracks; International Journal of Rock Mechanics and Mining Sciences and Geomechanics Abstracts, v. 24, p. 175-183.

Katsube, T.J. and Williamson, M.A.
1994: Effects of diagenesis on shale nano-pore structure and implications for sealing capacity; Clay Minerals, v. 29, p. 451-461.

Katsube, T.J., Boitnott, G.N., Lindsay, P.J., and Williamson, M.
1996a: Pore structure evolution of compacting muds from the sea floor offshore Nova Scotia; in Current Research 1996-D; Geological Survey of Canada, p. 17-26.

Katsube, T.J., McClenaghan, M.B., and Scromeda, N.
1996b: Petrophysical characteristics of diatreme-facies kimberlites from Kirkland Lake, Ontario; in Current Research 1996-E; Geological Survey of Canada, p. 171-178

Katsube, T.J., Scromeda, N., Bernius, G., and Kjarsgaard, B.A.
1992: Laboratory physical property measurements on kimberlites; in Current Research, Part E; Geological Survey of Canada, Paper 92-1E, p. 357-364.

Keating, P.
1995: A simple technique to identify magnetic anomalies due to kimberlite pipes; Exploration and Mining Geology, v. 4, p. 121-126.

McClenaghan, M.B.
1993: Location of known kimberlite bedrock, float and indicator minerals in drift in the Kirkland Lake area; Geological Survey of Canada, Open File Map 2636, scale 1:100 000.
1996: Kimberlite glacial dispersal studies near Kirkland Lake; in NODA Summary Report 1995-1996, Natural Resources Canada and Ministry of Northern Developement and Mines, p. 50-55.

Ontario Geological Survey
1979: Airborne electromagnetic and total intensity magnetic survey, Kirkland Lake area, Bisley Township, District of Cochrane; Ontario Geological Survey, Maps P.2252, P.2253, P.2258, and P.2259, scale 1:20 000.

Richardson, K.A., Katsube, T.J., Mwenifumbo, C.J., Killeen, P.G., Hunter, J.A.M., Gendzwill, D.J., and Matieshin, S.D.
1995: Geophysical studies of kimberlites in Saskatchewan; in Investigations Completed by the Saskatchewan Geological Survey and the Geological Survey of Canada under the Geoscience Program of the Canada-Saskatchewan Partnership Agreement on Mineral Development (1990-1995),(ed.) D.G. Richardson; Geological Survey of Canada, Open File 3119 (Saskatchewan Geological Survey, Open File Report 95-3), p. 197-205.

Rootare, H.M.
1970: A review of mercury porosimetry; Perspectives of Powder Metallurgy, v. 5, p. 225-252.

Scromeda, N., Katsube, T.J., Bernius, G., and Kjarsgaard, B.A.
1994: Physical properties of Canadian kimberlites from Fort a la Corne, Saskatchewan; in Current Research, 1994-E;, Geological Survey of Canada, p. 171-175.

Washburn, E.W.
1921: Note on a method of determining the distribution of pore sizes in a porous material; in Proceedings of the National Academy of Science, V. 7, p. 115-116.

Geological Survey of Canada Project 870057

APPENDIX

Geological description

Surface limestones

Specimens from these six samples were also prepared for electrical resistivity and immersion porosity measurements, and the results of the tests have been previously reported (Katsube et al., 1996b).

LAKE TIMISKAMING OUTLIER: PALEOZOIC BEDROCK SAMPLES						
Sample #	Location	Formation/ Age	NTS Map	UTME	UTMN	Sample Description
KLD-1 (DKA-94-28B)	Bucke Twp. Quarry	Farr/U. Ordovician	31M/5	600000	5256530	medium- to coarse-grained, bioclastic limestone (grainstone); top 1/3 is tan-grey, bottom 2/3 is blue-grey (with stylolite contact); abundant fossil fragments, mostly crinoidal; some intergranular porosity; one, tan, porous (intergranular), fine-grained, dolomitic zone (burrow or lithoclast?) in blue-grey part.
KLD-2 (DKA-94-32E)	Dymond Twp. Dump	Farr/U. Ordovician	31M/12	596800	5262850	fine- to coarse-grained, fossiliferous, bioclastic limestone (pack-grainstone); grey core with tan weathered rind (most of sample); with tan, porous (intergranular), dolomitic burrows; variety of fossil fragments are silicified; large receptaculitid fossil on top; sub-horizontal, partly open facture, after stylolite(?), with rusty weathering.
KLD-3 (DKA-94-34D)	Loach Quarry	Evanturel Ck (Wabi Gp.)/L. Silurian	31M/12	604360	5269850	light grey-tan, fine-grained, fossiliferous limestone (wackestone and packstone); with rusty argillaceous lithoclasts; abundant shelly fossils (ostracodes, brachiopods, others); small fossil moldic, shelter, and vuggy porosity.
KLD-4 (DKA-94-36H)	Evanturel Creek	Evanturel Ck (Wabi Gp.)/L. Silurian	31M/13	585652	5293875	light grey-green, fine-crystalline, bioturbated, argillaceous dolostone (dolosiltite), with green shale lithoclasts; very fine intercrystalline porosity.
KLD-5 (DKA-94-39B)	Dawson Point	Earlton or Thornloe/M. Silurian	31M/5	606450	5260150	light creamy tan (buff), fine-crystalline, fossiliferous dolostone (wackestone); fossils are partly silicified, and contain secondary calcite; fossils include brachiopods, and thin planar stromatoporoids; some small fossil moldic porosity.
KLD-6 (DKA-94-43A)	Hwy 65, N.of Dawson Point	Thornloe/M. Silurian	31M/12	604575	5265525	light tan, fine-crystalline, fossiliferous dolostone (boundstone and packstone); fossils include tabular stromatoporoids and corals, and pentamerid brachiopods; some fenestral and interskeletal porosity (stromatoporoids and corals) and some fossil moldic porosity (brachiopods); also locally good fracture porosity (small, open, vertical fractures).

Kimberlites

Sample KLH-2: Grey-brown matrix, easily scratched with a penny. Zoning of the limestone xenoliths is weak to absent. Xenolith fragments (subangular to subround) are abundant with sizes of up to 2.5 cm in diameter.

Sample KLM-2: Chloritic blue-green matrix, easily scratched with a penny. Limestone xenolith fragments (subangular to subrounded) with weak to strong zoning of the limestone xenoliths, <2 mm to 5 cm in diameter are abundant.

Sample KLH-5: Greenish-grey, vesicular matrix can be easily scratched with a penny. Phlogopite crystals in the matrix. Serpentine is abundant as an alteration mineral. Limestone xenolith fragments (one partial up to 4.5 cm) vary in composition (likely various stages of alteration) and show strong alteration, represented by prominent zoning. Banding can be seen in some of the xenoliths.

Sample KLM-6: Greenish-grey matrix easily scratched with a penny. Few limestone xenoliths are seen in this sample. Most of the fragments are serpentine. Some zoning of the fragments is apparent. Biotite/phlogopite crystals are also visible in the matrix. There appears to be some fracturing infilled with soft, aphanitic greenish-brown material.

Limestone xenoliths

Specimen KLH-2a: White and cream with visible layering of medium-to fine-grained material (the coarser layers were white). The xenolith is easily scratched with a knife. It also appears to be relatively unaltered. Specimens have also been prepared for thin-section analysis.

Specimen KLH-2b: White and cream, homogenous, and appears to be relatively unaltered. Medium to fine grained and is easily scratched with a knife. A specimen was also sent for thin-section analysis and electrical resistivity measurements.

Specimen KLH-2bx: No information.

Specimen KLM-2a (Core and rim): Displays very prominent alteration rims. The outmost rim (1-4 mm) is purple. The core appears unaltered, homogenous, and very porous. The innermost rim is thin, dark, and translucent. The core is the softest and the thin translucent rim is the hardest, although these differences are small. Mercury porosimetry analysis was done on both core and rim material. A specimen was also prepared for section analysis.

Specimen KLM-2b: Appeared to be unaltered, homogenous, fine grained, and soft. Specimens were also prepared for thin-section analysis and electrical resistivity measurements.

Specimen KLM-2e (Core and rim): White to creamy, fine grained, homogenous, and crumbles easily (abundant fractures). It has a very prominent translucent brown rim (<2 mm) which is very hard (barely scratchable with the knife). Mercury porosimetry analysis was done on both core and rim material. The specimen of rim includes some core material as well, due to difficulty in separating the two. Specimens were also prepared for thin section analysis and electrical resistivity measurements. This xenolith was relatively large (3 x 5 cm), so that both the rim and core material are still available for further testing.

Eastern Canada and National and General Programs

Est du Canada et programmes nationaux et généraux

Field relationships and petrology of Lapeyrère gabbronorite, south-central Grenville Province, Quebec

L. Nadeau and P. Brouillette
GSC Quebec, Sainte-Foy

Nadeau, L. and Brouillette, P., 1997: Field relationships and petrology of Lapeyrère gabbronorite, south-central Grenville Province, Quebec; in Current Research 1997-E; Geological Survey of Canada, p. 61-71.

Abstract: High-grade Grenvillian gneisses and tectonites of the Portneuf-Mauricie region include a number of largely massive, late orogenic gabbroic intrusions. The Lapeyrère gabbronorite is the largest of these bodies, standing out as a prominent positive anomaly on the regional Bouguer gravity map.

The intrusion comprises a variety of rock types defining a suite ranging from 'hornblende-free' gabbronorite to 'pyroxene-free' hornblende-quartz-diorite, with more evolved phases occurring in minor amounts. The rocks commonly exhibit cumulate textures, a weak but pervasive magmatic foliation and local development of compositional layering.

The subtle nature of the layering suggests the establishment of fairly constant physico-chemical conditions during crystallization, and limited convection and thermal erosion during cooling. Internal igneous structural relationships intimate syn- and postsolidification body rotation. This, and the nature of the metamorphic fabric in the wall rocks are consistent with emplacement in the middle crust during regional deformation.

Résumé: Les tectonites et les gneiss grenvilliens à haut rang métamorphique de la région de Portneuf-Mauricie renferment plusieurs intrusions gabbroïques tardi-orogeniques, en grande partie massive. La plus grande de ces intrusions, la Gabbronorite de Lapeyrère, se démarque régionalement par la forte élévation de son anomalie gravimétrique de Bouguer.

L'intrusion comprend plusieurs types de roche qui définissent une suite depuis les gabbronorites 'sans hornblende', aux diorites quartzifères à hornblende 'sans pyroxène', avec des roches plus évoluées en quantités moindres. Ces roches montrent généralement des textures de cumula, une foliation magmatique pénétrante mais peu marquée et, localement, un rubanement compositionnel.

La nature indistincte du rubanement suggère l'établissement de conditions physico-chimiques assez constantes durant la cristallisation, et peu de convection et d'érosion thermique durant le refroidissement. Les relations structurales ignées internes suggèrent des rotations du corps intrusif durant et après sa solidification. Ce dernier point, ainsi que la nature de la fabrique métamorphique des roches des épontes sont compatibles avec une mise en place à un niveau crustal moyen durant la déformation régionale.

INTRODUCTION

This study was undertaken in order to characterize and better understand the petrogenesis and the tectonic setting of a number of late Grenvillian gabbroic intrusions in the Portneuf-Mauricie region, south-central Grenville Province (Fig. 1). Focus is placed here on the field relationships, internal structure, and petrography of the Lapeyrère gabbronorite (Nadeau et al., 1992a; Hébert et Nadeau, 1994), the largest of these bodies. The intrusion is named after a large lake located in the central part of the intrusion. Lakeshore outcrops and a number of quarry test-pits offer excellent exposure.

The Lapeyrère gabbronorite is a tear-shape intrusion of about 160 km^2, and is 10 km wide. It is composed chiefly of gabbronorite with subordinate dioritic rocks. It contains no anorthositic phase and is not spatially associated to an anorthosite body. The intrusion stands out as a strong bull's eye positive Bouguer anomaly, showing in excess of 3 mgal/km on regional Bouguer anomaly vertical gradient maps; there are no other comparable gravity anomalies in the region. The intrusion is largely composed of undeformed, pristine, medium- to coarse-grained rocks with 30 to 50% hypersthene-augite-hornblende, as well as accessory biotite and Fe-Ti opaque oxides. Primary igneous layering and foliation are ubiquitous within the pluton.

AFFILIATION

The Lapeyrère gabbronorite is petrographically similar to and possibly continuous in subsurface with the smaller Édouard gabbronorite located a few tens of kilometeres to the north (Fig. 2; Nadeau and Brouillette, 1994). It also resembles petrographically the Shawinigan norite (Fig. 2; Béland, 1961). In addition, the Lapeyrère intrusion yielded a 1070 ± 3 Ma U/Pb zircon crystallization age (Nadeau et al., 1992b) which is similar within error to the 1077 +10/-2 Ma age obtained for the Shawinigan norite (Corrigan and van Breemen, 1997). These are the youngest gabbroic intrusions in the region. They postdated by over 60 million years the emplacement of the Morin and Lac Saint-Jean complexes and associated mangerite-charnockite-granite suite (AMCG-suite) dated at 1160-1140 Ma (Doig, 1991; Higgins and van Breemen, 1996). The emplacement of the Lapeyrère gabbronorite is about 10 million years older than that of the spatially associated porphyritic granites and monzonites of the Rivière-à-Pierre Suite dated ca. 1058 ± 1 Ma (Nadeau et al., 1992b). It is also significantly older than the ca. 1020 Ma age proposed for the more distant Saint-Urbain Anorthosite complex (Ashwal and Wooden, 1983).

A number of other smaller gabbroic bodies in the area may be genetically linked to the Lapeyrère and Shawinigan intrusions (Fig. 2). The most important ones include: the small (<1 km^2) pristine Wessonneau intrusion which petrographically resembles the rocks at Lac Lapeyrère; a satellite body in the Lejeune plutonic suite composed of compositionally and texturally varied gabbroic rocks which locally intermingle with monzonite and granite; and the Étoile gabbro.

LITHOLOGIES

The intrusion at Lac Lapeyrère includes four mappable units in two main rock groups (Fig. 3a; Table 1):

1. The *gabbronoritic group* consists chiefly of homogeneous i) *gabbronorite* and ii) *hornblende-gabbronorite* in which hornblende is generally more than 6%. Ultramafic rocks are limited to one outcrop of wherlite (sample site 15). Plagioclase-rich (anorthositic) rocks are rare and occur only as centimetre thick lenses in more mafic hosts.
2. The *dioritic group* is made up mainly of diorite and quartz-diorite with hornblende, accessory biotite, and, in places, corroded pyroxenes. Two facies are recognized in the field and petrographically: i) a *homogeneous* facies made up of medium grained, equigranular rocks locally difficult to distinguish in outcrop from the hornblende-gabbronorite, and ii) a subordinate *heterogeneous* facies comprising texturally and compositionnally varied rocks, in part coarse grained to pegmatitic, and locally transitional to monzonite and granodiorite.

The percentage of surface area occupied by each of the lithological types, at the present erosional level, are approximately 59% *gabbronorite*, 19% *hornblende-gabbronorite*, along with 18% *homogeneous* and 4% *heterogeneous diorite and quartz-diorite*. These estimates may be of some significance given the steepness of the magmatic fabric of the body.

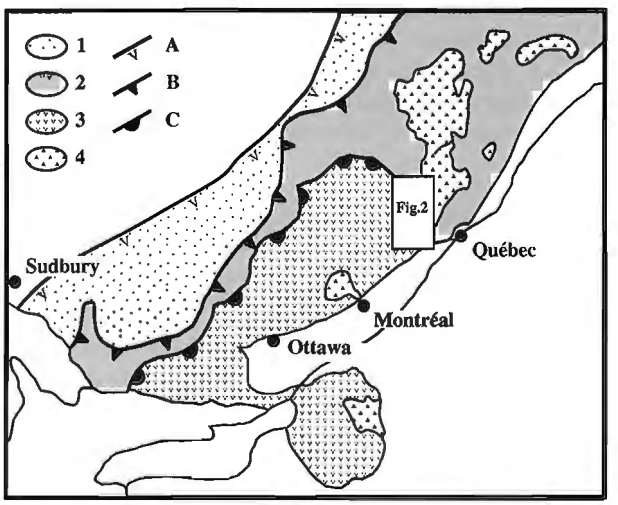

Figure 1. *Location sketch map and tectonic subdivisions of the Grenville Orogen (modified from Rivers et al., 1989). Legend: (1) Parautochthonous Belt; (2) Allochthonous Polycyclic Belt; (3) Allochthonous Monocyclic Belt; (4) Anorthosite-mangerite-charnockite-granite suite; (A) Grenville Front; (B) Allochthon boundary thrust; (C) Monocyclic belt boundary thrust.*

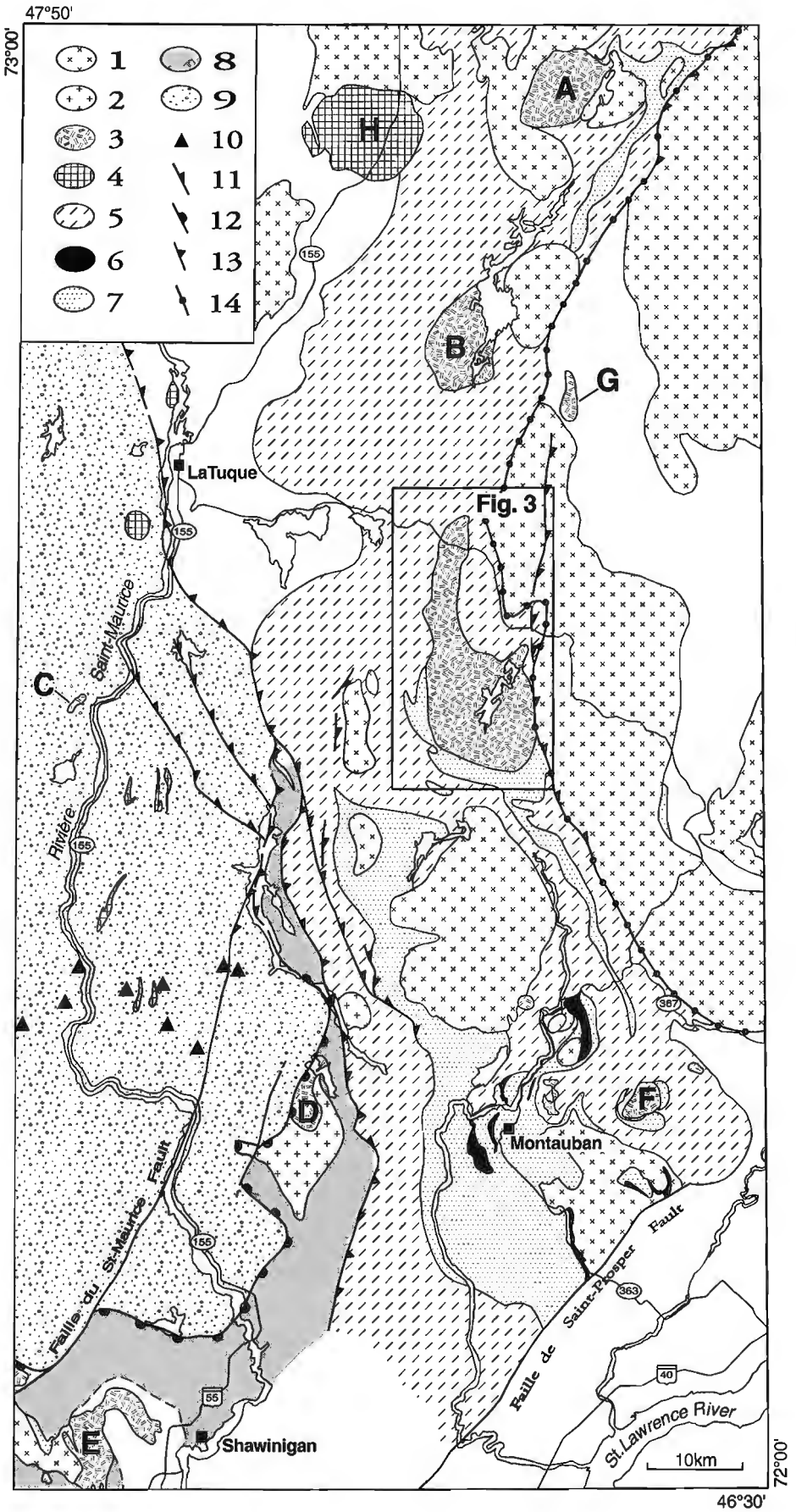

Figure 2.

*Geological sketch map of the Grenville orogen in the Portneuf-Mauricie region (after Nadeau and Brouillette, 1994, 1995). Legend: (1) Granite and monzonite; (2) Lejeune suite; (3) Gabbro-gabbronorite: **A** - Étoile, **B** - Édouard, **C** - Wessonneau, **D** - Lejeune, **E** - Shawinigan, **F** - Montauban, **G** - Sanford; (4) Meta-anorthosite: **H** - Langelier; (5) La Bostonnais complex; Montauban group: (6) Amphibolite; (7) Paragneisses; (8) Morin terrane; (9) Mékinac-Taureau domain; (10) Gabbro; (11) Late-Grenvillian sinistral shear zone; (12) Tectonic boundary beneath Morin terrane; (13) Tectonic boundary beneath Portneuf-Mauricie domain; (14) Boundary of the Parc des Laurentides domains.*

Table 1. Modal compositions of Lapeyrère gabbronorite intrusive suite.

Site	Sample	UTMX	UTMY	Rock name	Qtz	Pl (An)	Kfs	Opx	Cpx	Hbl (B)	Hbl (S)	Bt	Op	Ap	Zrn	Other
2	90NKL-12B	694081	5248286	"chilled" diorite	2	60 (37)	-	15	17	tr	tr	tr	5	tr	-	Spn
3	90NKL-12C	694081	5248286	"chilled" hbl-gabbronorite	tr	55 (53)	-	8	12	6	4	5	10	ac	-	
15	91-SP-304	702725	5236903	metawherlite	-	-	-	4	42	3	-	-	ac	-	-	Ol (50), Spl, Srp
6	91-SP-19	695544	5247966	gabbronorite	tr	76 (55)	-	6	14	3	1	tr	tr	-	-	
9	OUEP-101	694428	5243371	gabbronorite	tr	64 (63)	-	14	16	1	4	ac	ac	-	-	
10	91-SP-2160	694791	5243132	gabbronorite	-	66 (55)	-	4	23	ac	1	tr	5	-	-	
11	90NKS-43	694802	5240936	gabbronorite	ac	66 (61)	-	12	19	2	-	tr	tr	-	-	
24	70235D	702297	5235110	gabbronorite	tr	59 (55)	-	13	18	6	tr	1	3	-	-	
26	90NKL-19734A	697152	5234177	gabbronorite	1	62 (55)	-	9	25	1	2	tr	ac	-	-	Cal
27	90NKL-19734B	697152	5234177	gabbronorite	tr	59	-	17	20	ac	2	ac	ac	-	-	
28	70134C	701717	5234325	gabbronorite	tr	71 (62)	-	14	12	2	tr	tr	1	-	-	
31	OUEP-066	694676	5233663	gabbronorite	2	73 (56)	-	6	10	ac	2	2	4	tr	-	
33	69833	698275	5233719	gabbronorite	2	69 (53)	-	10	12	tr	3	tr	4	-	-	Ep
34	69833A	698363	5233697	gabbronorite	tr	es	-	es	es	ac	-	tr	ac	-	-	
35	69833P	698453	5233675	gabbronorite	-	32 (53)	-	25	30	6	tr	tr	7	-	-	
37	70034N	700724	5234095	gabbronorite	tr	60 (68)	-	14	21	3	tr	tr	2	-	-	
38	69833D	698646	5233401	gabbronorite	-	71	-	8	14	2	1	1	3	-	-	
39	69833E	698624	5233266	gabbronorite	tr	78 (55)	-	8	11	1	tr	tr	2	-	-	
40	70033K	700682	5233578	gabbronorite	-	61 (66)	-	11	16	8	tr	tr	4	tr	-	
42	90NKL-19733A	697422	5233102	gabbronorite	-	71 (53)	-	11	12	tr	2	tr	4	-	-	
43	90NKL-19633A	696752	5232850	gabbronorite	-	67 (53)	-	14	16	ac	ac	ac	ac	-	-	
44	90NKL-19633B	696752	5232850	gabbronorite	-	25 (55)	-	16	54	3	-	tr	ac	tr	-	
45	69933B	699548	5233139	gabbronorite	-	es (53)	-	es	es	tr	-	tr	mi	ac	-	
46	70033N	700193	5233082	gabbronorite	-	63 (68)	-	16	17	3	tr	tr	1	-	-	
50	OUEP-072	697710	5232338	gabbronorite	ac	65 (65)	-	14	16	1	3	ac	ac	-	-	
58	90NKS-19730	697700	5230450	gabbronorite	tr	80 (65)	-	5	8	tr	6	ac	ac	tr	-	
59	70030B	700218	5230153	gabbronorite	-	63 (53)	-	15	12	6	tr	tr	4	-	-	
60	70130L	701918	5230324	gabbronorite	tr	es (56)	-	es	es	tr	-	ac	ac	-	-	
61	70129A	701315	5229944	gabbronorite	tr	64 (40)	-	13	19	tr	tr	tr	4	tr	-	
63	90NKS-19729	697909	5229654	gabbronorite	-	52 (57)	-	17	27	tr	2	tr	2	-	-	
67	90NKS-39728	697815	5228931	gabbronorite	tr	80 (58)	-	10	10	tr	tr	-	tr	-	-	
68	70028A	700031	5228957	gabbronorite	tr	69 (53)	-	19	6	3	tr	tr	3	-	-	
70	69828B	698785	5228585	gabbronorite	tr	75	-	11	9	tr	2	1	2	-	-	
74	90NKS-19628	696856	5228077	gabbronorite	-	58	-	10	21	2	4	ac	5	tr	-	
75	90NKS-19928B	699450	5228150	gabbronorite	tr	65 (58)	-	13	20	ac	ac	ac	ac	-	-	
76	90NKD-10028	700299	5228015	gabbronorite	-	76	-	8	14	tr	ac	ac	1	tr	-	
80	90NKL-10027A	700150	5227700	gabbronorite	tr	67	-	11	15	tr	1	tr	5	tr	tr	
81	70127A	701150	5227800	gabbronorite	1	53 (60)	-	8	25	3	tr	3	7	tr	-	
90	90NKD-10125	701580	5225835	quartz-gabbronorite	3	69	-	8	8	3	ac	6	3	ac	tr	
16	OUEP-088	702452	5236734	quartz-gabbronorite	2	60 (58)	-	12	20	ac	3	2	tr	tr	-	
48	90RG-49331	692972	5231919	quartz-gabbronorite	11	52	-	1	7	10	8	7	4	ac	-	
49	OUEP-062	694431	5231695	quartz-gabbronorite	4	70 (68)	-	10	14	tr	-	1	ac	-	-	
65	70229E	702339	5229270	quartz-gabbronorite	2	73 (53)	-	8	10	2	1	1	3	tr	tr	
4	91-MD-1030	694676	5248091	hbl gabbronorite	tr	62 (55)	-	9	18	3	7	tr	tr	-	-	Cal
5	90NKL-10&3	695426	5248127	hbl gabbronorite	ac	72 (55)	-	8	12	7	-	tr	ac	-	-	
7	90NKL-10B	696461	5247334	hbl gabbronorite	tr	60 (55)	-	11	13	2	10	1	3	ac	-	Cal
8	OUEP-099	694310	5244494	hbl gabbronorite	1	54 (55)	-	14	16	ac	13	1	ac	-	-	
12	OUEP-110	695903	5237837	hbl gabbronorite	tr	72 (63)	-	4	6	3	11	1	3	tr	tr	
19	90NKL-19635	696826	5235326	hbl gabbronorite	tr	66 (55)	-	10	13	2	5	1	2	tr	tr	Ol

METAMORPHISM AND DEFORMATION

Unexpectedly, most of the rocks of the Lapeyrère intrusion are undeformed and exhibit original plutonic textures. A tectonic foliation is present only locally, namely in narrow shear zones and along the margin of the body. The deformation has taken place under lower amphibolite facies conditions, as indicated by the assemblage plagioclase-quartz-hornblende-biotite±epidote typical of the foliated rocks, and lack of chlorite.

The country rocks have been regionally metamorphosed to uppermost amphibolite facies and contain granitic mobilizate in variable amounts (Hébert et Nadeau, 1994). Peak regional metamorphic pressure and temperature estimates of 680°C and 5.7 kbar have been measured from fabric-forming mineral assemblages in pelitic gneisses adjacent to the body (Lévesque, 1995).

In contrast to the pristine nature of the Lapeyrère gabbronoritic and dioritic rocks, nearby metadiorites of La Bostonnais complex range in outcrop from massive to well foliated and gneissic or migmatitic, with igneous pyroxenes extensively or completely replaced by metamorphic hornblende. Such differences in deformation and metamorphic overprint in otherwise comparable lithologies clearly indicate that the Lapeyrère intrusion is late Grenvillian, after peak metamorphism but prior the end of deformation.

FIELD RELATIONSHIPS

Contacts and wall rocks

Along its southeast flank, the main mass of the body is shear-bounded, via a sinistral strike-slip ductile fault zone, against younger ca. 1058 ± 2 Ma (Nadeau et al., 1992b) massive to

Table 1 (cont.)

Site	Sample	UTMX	UTMY	Rock name	Qtz	Pl (An)	Kfs	Opx	Cpx	Hbl (B)	Hbl (S)	Bt	Op	Ap	Zrn	Other
20	70035F	700848	5235256	hbl gabbronorite	-	60 (53)	-	12	13	9	3	tr	3	-	-	
36	69833R	698736	5233714	hbl gabbronorite	1	57 (52)	-	8	15	1	12	tr	6	-	-	
55	90NKP-20031A	700346	5231384	hbl gabbronorite	tr	43	-	15	14	22	4	-	2	-	-	
62	90RG-39329	693695	5229744	hbl gabbronorite	tr	es (53)	-	mi	es	ma	mi	tr	tr	tr	-	
96	90NKL-40025	700950	5225330	hbl gabbronorite	2	84 (53)	-	7	8	1	13	2	3	tr	-	
1	90NKL-1282A	693797	5248708	hbl gabbronorite	4	32	-	2	6	7	49	ac	ac	-	-	Spn
52	69832E	698990	5232250	px-diorite	tr	33 (45)	-	27	34	3	-	tr	4	tr	-	
91	70125F	701824	5225853	px-diorite	tr	70 (45)	-	10	10	4	tr	tr	6	tr	tr	
78	90NKP-39527A	695850	5227500	px-hbl diorite	2	68	-	8	8	ac	9	tr	5	-	-	
89	90CH-19925	699691	5225961	px-hbl-bt diorite	4	31 (38)	-	15	25	8	-	16	tr	ac	tr	
77	90NKP-19427A	694600	5227650	px-hbl quartz-diorite	14	58 (45)	-	2	3	1	15	5	2	tr	tr	
64	69329A	693805	5229187	px-hbl quartz-diorite	7	70 (45)	-	6	tr	12	tr	3	2	tr	-	
95	70025A	700889	5225303	px-hbl quartz-diorite	4	73 (55)	-	9	tr	7	2	2	3	tr	-	
32	OUEP-144	695301	5233695	px-bt quartz-diorite	13	65 (38)	-	4	7	2	tr	8	1	tr	tr	
14	91-SP-306	701627	5236956	hbl diorite	tr	51 (46)	-	-	tr	41	8	tr	tr	tr	-	
56	69931A	699653	5231085	hbl diorite	tr	es (42)	-	-	-	es	es	tr	mi	tr	-	Spn
79	90NKP-39527B	695850	5227500	hbl diorite	tr	45	-	1	2	ac	44	1	6	-	-	
13	91-SP-313A	702031	5237122	hbl-bt diorite	6	65 (37)	-	ac	ac	13	6	8	1	tr	tr	Spn
25	70235A	702814	5235248	hbl-bt diorite	3	52 (48)	-	-	-	2	41	1	1	tr	-	Ttn
87	70326C	703479	5226937	hbl-bt diorite	8	63 (40)	-	tr	tr	19	4	4	2	tr	-	
72	70128B	701959	5228424	quartz-diorite	ma	es (28)	-	-	-	es	-	mi	tr	tr	tr	
82	70227A	702074	5227547	quartz-diorite	11	72	-	-	-	5	-	7	3	-	-	
29	90NKD-20334A	703750	5234550	hbl-bt quartz-diorite	3	64 (40)	-	tr	tr	1	22	7	2	ac	tr	Spn
41	70333B	703707	5233492	hbl-bt quartz-diorite	ma	es	-	tr	tr	es	ma	mi	ac	tr	tr	
69	69428C	694125	5228484	hbl-bt quartz-diorite	7	68 (37)	-	7	tr	12	1	2	2	tr	-	
83	90NKD-30227A	702788	5227294	hbl-bt quartz-diorite	8	56 (36)	-	-	-	25	-	9	3	ac	ac	
88	70326A	703576	5226731	hbl-bt quartz-diorite	6	70 (42)	-	9	tr	3	4	7	1	tr	tr	
30	90NKD-30333	703810	5233983	tonalite	20	47	-	-	-	21	ac	10	2	tr	-	
17	90RG-19335	693846	5235377	opx granodiorite	33	49	12	4	-	tr	-	ac	1	-	-	
86	90NKP-29527A	695400	5227200	hbl-bt granodiorite	20	70 (48)	3	-	-	2	3	1	1	tr	tr	Grt, Ep, Ser
73	OUEP-030	704113	5228411	granodiorite	17	31 (30)	9	-	tr	3	30	2	2	-	tr	Chl (6)
51	69832C	698990	5232480	quartz-monzodiorite	17	47	9	-	-	1	22	4	tr	-	-	Ser, Chl
47	90RG-19332	692939	5232388	quartz-monzodiorite	30	25	40	-	-	tr	-	5	tr	tr	-	Chl, Spn
66	OUEP-031	703460	5229289	quartz-monzodiorite	31	20	38	ac	ac	ac	ac	7	2	-	tr	
84	90NKD-30227B	702768	5227294	quartz-syenite	20	10	65	-	-	-	-	2	2	tr	-	
21	70035B	700823	5235136	"hydrated" gabbronorite	mi	es (58)	-	-	-	es	es	mi	tr	-	-	Spn
22	70134J	701458	5234757	"hydrated" gabbronorite	1	60 (52)	-	-	-	39	tr	tr	tr	-	-	
23	70134P	701619	5234923	"hydrated" gabbronorite	-	es (50)	-	tr	tr	ma	es	tr	tr	-	-	
57	90NKP-30030A	700482	5230728	metadiorite	18	50	-	-	ac	30	-	-	-	-	-	Ep (2), Chl
93	70225H	702547	5225987	metadiorite	5	65	-	-	-	8	3	17	2	-	tr	Ep

Note: Modal percentages were obtained by points counts on regular size thin sections. Samples are fine- to medium-grained. Between 800 and 1000 points were counted on each thin section. Visual estimates are reported as follow: es (essential) >15%; ma (major) 5-15%; mi (minor) 1-5%; ac (accessory) 0.3-1.0%; and tr (trace) <0.3%. Hornblende habits: (B) blocky; (S) symplectic. For mineral abbreviations, refer to Kretz (1983).

weakly deformed porphyritic granites and quartz-monzonites of the Rivière-à-Pierre suite (Fig. 3a). An intense deformation fabric is limited to a zone a few hundred metres thick on either side of the fault. There is no evidence of a large lateral offset along the fault. This and the absence of gabbroic bodies east of the fault suggest that faulting has not dismembered the intrusion itself, and that the localization of the fault has been partly controlled by the initial intrusive contact between the two large plutonic masses. The latter is consistent with the presence of a few aplite and granite dykes in dioritic rocks adjacent to the faulted contact.

Elsewhere, the body is enveloped by the older, 1.45-1.38 Ga (Nadeau et al., 1992b), highly deformed and interleafed, supracrustal rocks of the Montauban group and orthogneisses of the La Bostonnais complex (Fig. 3a; Hébert and Nadeau, 1994). At map-scale the gneissosity in the country rocks is conformable to the outline of the intrusion and no lithological or structural cut-off is observed adjacent to the contact. In addition, the absence in the immediate wall rocks of crosscutting dykes, intrusive breccia, or apophyses emanating from the intrusion suggest that the emplacement of the body did not involve brittle fracturing and stoping. Likewise, wall rock enclaves are scarce, small, and rounded, and appear to be limited to the 'heterogeneous' dioritic facies.

The abrupt positive gravity gradient at the contact of the body and the steepness of the gneissosity in the wall rocks suggest that the intrusion is deeply rooted. The overall structural concordance and the absence of brittle intrusive structures further intimate that the transport and intrusion of the magma were permitted by ductile shouldering of the country rock at intermediate or lower crustal levels. Alternately, these relationships may be attributed to postcrystallization sinking of the rock body, ripping off and leaving its initial intrusive envelope behind; such displacement of the rock body may have been driven by an inversion in buoyancy due to crystallization (Glazner, 1994).

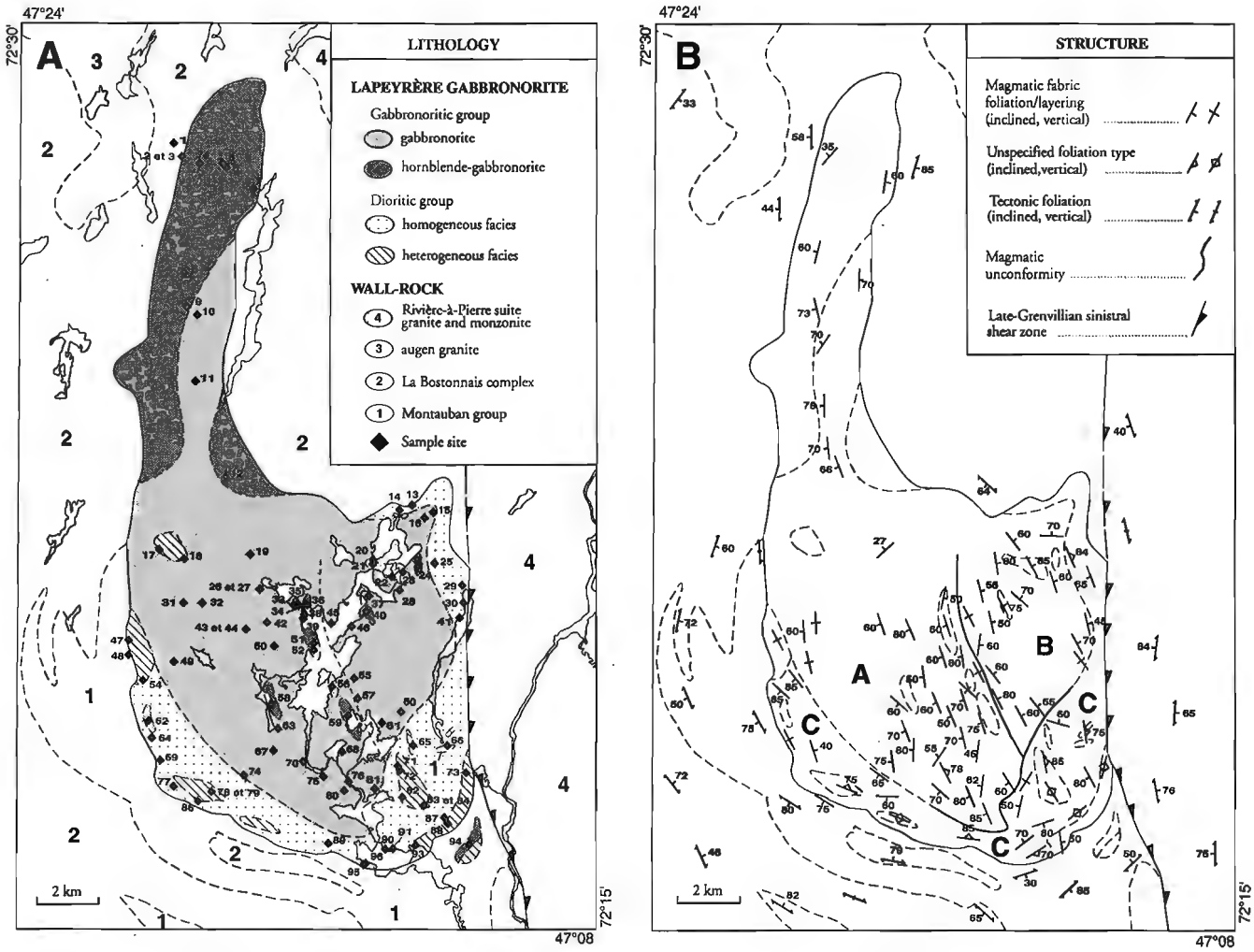

Figure 3. *Geological sketch map of the Lapeyrère gabbronorite* ***A****) lithology,* ***B****) structure.*

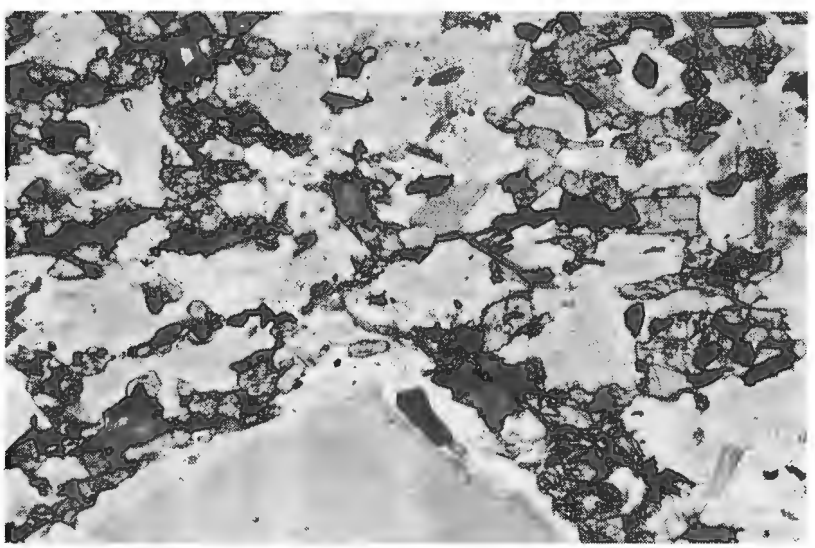

Figure 4.

Diabasic texture in plagioclase porphyritic chilled diorite (field = 0.8 mm).

Chilled margin and contact aureole

The contact of the body has not been directly observed. Fine grained, plagioclase porphyritic hornblende-gabbronorites with diabasic textures outcrop at least at one locality (sample site 3) immediately at the contact, therefore intimating the presence of a thin chilled margin (Fig. 4). In addition, these chilled rocks are associated in outcrop with fine grained homogeneous hypersthene-augite diorites (sample 2), further suggesting that rocks of this group may also occur discontinuously all along the margin of the intrusion.

Within a few tens of metres of the contact, gneisses of the envelope show no distinctive mesoscopic contact metamorphic effects. Sillimanite, biotite, garnet, and cordierite in paragneisses appear to be synkinematic since they mark or are enveloped by the well developed foliation and lineation of the rock. In addition, postkinematic porphyroblastic and decussate textures typical of contact aureoles have not been recognized in the field or in thin section.

The apparent absence of field evidence for a thermal aureole is peculiar given the size of the intrusion, its depth of emplacement, and the solidus temperature of gabbroic magma. This point will be further examined in the discussion.

INTERNAL STRUCTURE

Magmatic foliation

The rocks appear largely massive and monotonous in outcrop. In more detail, however, they exhibit a weak but pervasive mineral foliation and local development of compositional layering. The foliation is caused by the preferred orientation of prismatic plagioclase and pyroxene crystals (Fig. 5). It is considered of magmatic origin because, where present, the foliation and the compositional layering are invariably conformable. In addition, foliated samples collected away from the contact show pristine igneous textures with no plagioclase microstructure indicative of ductile deformation or recrystallization. This is otherwise consistent with the ubiquitous development of cumulate textures.

Compositional layering

Where present, layering is subtle and recognized by the presence of sharp interfaces between facies with contrasting mafic contents. Away from the interface, the mafic mineral content grades progressively to a value typical of the rest of the outcrop. Layers are typically decimetre thick and laterally continuous for no more than a few tens of metres. Mesoscale magmatic features such as crosslamination, channel scour, block structure, and cognate xenoliths have not been recognized.

The layering described here is not comparable to the well defined and repeated, decimetre to metre thick, compositional and size-graded layering of the type commonly present in massif-type anorthosites and layered intrusions (e.g. Emslie, 1980; Irvine, 1987). The subtle nature of the layering here, as observed on large outcrops and quarry test-pits appears to be an intrinsic property of the Lac Lapeyrère intrusion. The subtle layering characteristic of the gabbronoritic rocks suggests the establishment of fairly constant physico-chemical conditions during crystallization, and limited convection and thermal erosion during cooling. The pervasive magmatic foliation and the sporadic layering are indicative of crystal settling.

Igneous structural subunits

The magmatic fabric, defined by the foliation and the compositional layering, is generally moderate to steeply dipping, persistent in attitude over large areas, and defines a simple map pattern (Fig. 3b). This pattern does not strictly conform to that of a concentrically zoned body. Truncation of the internal magmatic fabric is suggested by the inversion in the dip directions between the western (structural subunit A) and the

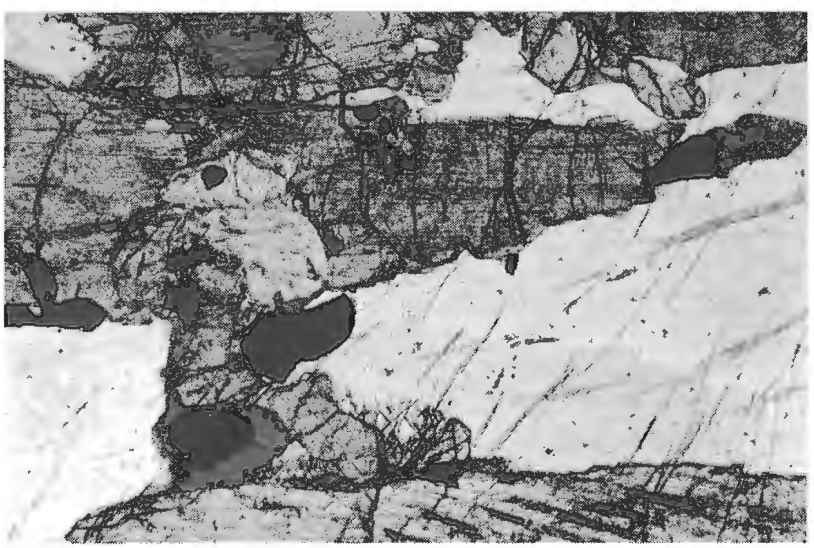

Figure 5.

Alignment of pyroxene and plagioclase crystals giving a magmatic foliation in gabbronorite. Plagioclase and pyroxenes are the cumulus phases, with interstitial hornblende and opaque oxyde (field = 2.5 mm).

eastern (subunit B) halves of the body and by the abrupt changes in strike direction observed in the southern part of the intrusion (subunit C).

While faulting may not be ruled out in the case of the dip inversion from subunit A to B, the structural break documented in the southern part of the body cannot be attributed to external deformation as it is comprised within the body and is not related to a fault. Moreover, structural subunit C also appears to correspond closely to the main outcrop area of the dioritic rocks. The inference drawn from these observations are that the rocks of structural subunit C resulted from a separate magma pulse, or that the partially solidified magma chamber was tilted. These interpretations can be extended to structural subunits A and B, even in the apparent absence of clear-cut crosscutting relationship within gabbronoritic rocks; internal igneous unconformities may have remained undetected due to unfavourable exposures and the subtle nature of the lithological variations.

PETROGRAPHY

Deformation and metamorphic recrystallization have occurred only locally, along narrow shear zones and the margin of the body. Away from these zones, deformation effects are limited to undulose extinction and rare mechanical twins in plagioclase; recrystallization structures and granoblastic textures are absent. In addition, some large framework plagioclase prisms in dioritic rocks feature primary concentric zoning.

Accordingly it is apparent that the mineral assemblages and textures are essentially of magmatic origin, including the complex exsolution structures in pyroxenes and their hornblende-quartz coronitic overgrowths. This is otherwise consistent with the scarcity of garnet, epidote, and chlorite typical of metamorphosed mafic rocks.

Gabbronorite group

Gabbronoritic rocks form more than 80% of the outcrop area of the intrusion. They are generally fine- to medium-grained, equigranular, and dark brown on fresh and weathered surfaces. These rocks are fairly homogeneous in outcrop appearance and commonly exhibit a distinct magmatic foliation.

Modal compositions are given in Table 1. As a group the gabbronoritic rocks present wide ranges in modal composition. Most samples, however, are fairly tightly grouped. The average sample consists of 63% labradorite (An 57), 26% pyroxenes with a hypersthene/augite ratio of 0.6, and 4% hornblende as the main varietal mineral. Plagioclase is unzoned, nonperthitic, but typically dusted with minute opaque oxide inclusions. Trace amounts of myrmekite commonly occurs as thin films and bulbs along plagioclase grain-boundaries. Pyroxenes generally exhibit complex exsolution structures. Interstitial quartz is commonly present from trace amounts up to 2%. Serpentinized olivine has been found only in one outcrop where it occurs as cumulate in a wherlite (sample 15). Opaque Fe-Ti oxides are constant accessories, rarely over 4%. Reddish-brown biotite and apatite are widespread in trace amounts. Zircon is rare or absent.

Two varieties of hornblende are optically recognized: i) light 'apple' green hornblende and quartz forms delicate postcumulus symplectic corona on pyroxenes, while ii) dark 'olive' green hornblende occurs in thick and discontinuous rims on pyroxenes and as stubby matrix crystals. An increase in hornblende content generally corresponds with major textural changes. It is therefore appropriate to distinguish two subgroups i.e. 'normal' *gabbronorite*, from *hornblende-gabbronorite*, in which hornblende makes up more than 6% of the rock. It is emphasized that these two subgroups are transitional texturally and in modal composition.

Gabbronoritic rocks exhibit a variety of cumulate textures with plagioclase, orthopyroxene, and clinopyroxene as the essential cumulus minerals (Fig. 6). Hornblende, biotite, and other accessories occur as intercumulus-intergranular phases. Accordingly, the textural type is directly related to the

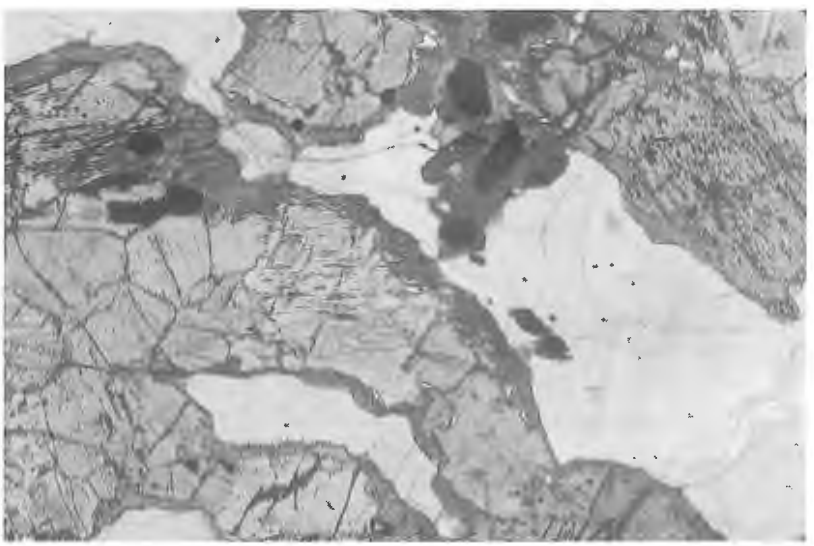

Figure 6.

Postcumulus and intergranular-interstitial hornblende in hornblende-gabbronorite (field = 2.5 mm).

amount of accessory minerals. Gabbronorite samples with very few accessory minerals including hornblende, exhibit adcumulate to mesocumulate textures. In contrast, textures in accessory-enriched hornblende-gabbronorite range from orthocumulus to granular. Ophitic texture is absent.

Diorite group

Rocks of the dioritic group occur preferentially as a carapace along the margin of the intrusion, between the gabbronoritic core and paragneisses in the wall rocks (Fig. 3a). Rocks of the homogeneous and heterogeneous facies outcrop over approximately 18% and 4% respectively of the total surface area of the intrusion.

The homogeneous facies is chiefly composed of medium grained hornblende-diorite and hornblende quartz-diorite which are fairly uniform in texture, grain size, and modal compositions. These rocks are difficult to distinguish in the field from the hornblende-gabbronorite. They can usually be recognized in hand sample by the abundance of hornblende, biotite, and quartz; the absence or limited content in pyroxenes; and by the milky-white colour of plagioclase giving the rocks a medium to dark grey salt-and-pepper colour on fresh and weathered surfaces.

The subordinate heterogeneous facies includes texturally and compositionally varied rocks, in parts coarse grained to pegmatitic, chiefly quartz-dioritic to granodioritic, but locally associated and possibly grading into minor K-feldspar porphyritic monzonitic and granodioritic phases (Table 1). In addition, these rocks locally contain partly digested rounded paragneiss enclaves and schlierens which adds to the disorder and indicate local wall rock assimilation. Rocks of this facies typically occur as decimetre- to subkilometre-scale stringers, pods, and screens in more homogeneous rocks.

Because of their large grain size and variability, the rocks of the heterogeneous facies are improper for detailed petrographic examination. Hence, the following description emphasizes the characteristics of their more homogeneous and finer grained counterpart.

Modal compositions of diorite and quartz-diorite are given in Table 1. In spite of overall widely variable modal contents, most samples fall within much closer compositional brackets. The average sample consists of approximately 5% intergranular quartz, 57% andesine (An 42), and 35% ferromagnesian minerals, including 17% hornblende and 5% biotite. Corroded ortho- and clinopyroxene are widespread, commonly in accessory amounts rarely exceeding 10%. Opaque Fe-Ti oxides are constant accessories, averaging 2.5% but locally up to 6%. Apatite and zircon are ubiquitous.

Plagioclase is generally clear, lacking the minute opaque inclusions and the myrmekitic intergrowth typical of plagioclase in gabbronorite. Hornblende is the main mafic mineral, varying in amounts from a few per cent up to 50%. It occurs in two varieties as described above in "Gabbronorite group" (Fig. 7).

Homogeneous dioritic rocks are texturally more diverse than gabbronorites. Subhedral to anhedral framework crystals are generally medium grained with sporadic xenocrystic plagioclase prisms up to 1 cm, and a markedly finer grained matrix. Textures range from subhedral plagioclase±pyroxenes orthocumulus to anhedral granular (Fig. 8). Large plagioclase framework crystals and xenocrysts are commonly zoned and generally markedly more calcic than matrix crystals. There is no evidence for adcumulus growth on plagioclase and pyroxenes. To the contrary, the widespread development of hornblende-quartz symplectites, in places pseudomorphic after pyroxenes, is an obvious manifestation of disequilibrium between the framework crystals and intergranular melt (Fig. 7).

As pointed out above, homogeneous dioritic rocks are difficult to distinguish in the field from hornblende-gabbronorite. Petrographic variations in textures and modal compositions suggest that they can be transitional into one another; such a relationship, however, remains to be demonstrated in outcrop.

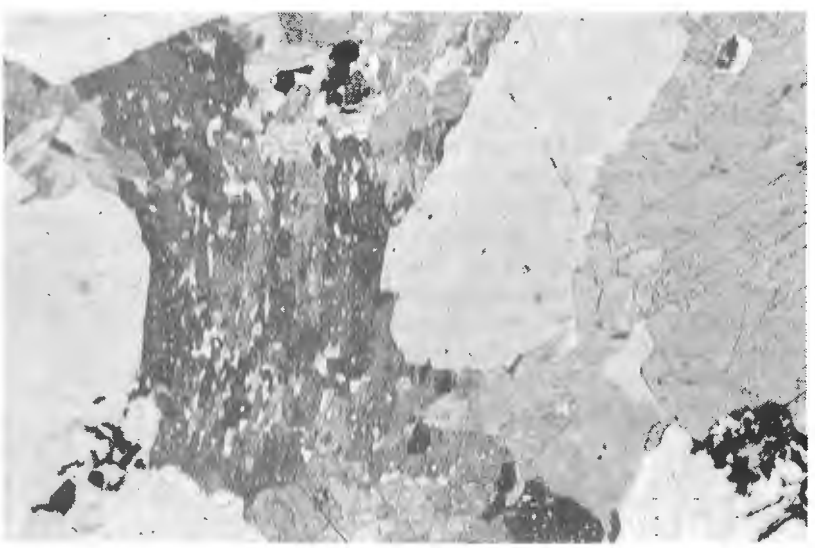

Figure 7.

Contrasting hornblende habits in diorite, blocky versus hornblende-quartz symplectite (field = 2.5 mm).

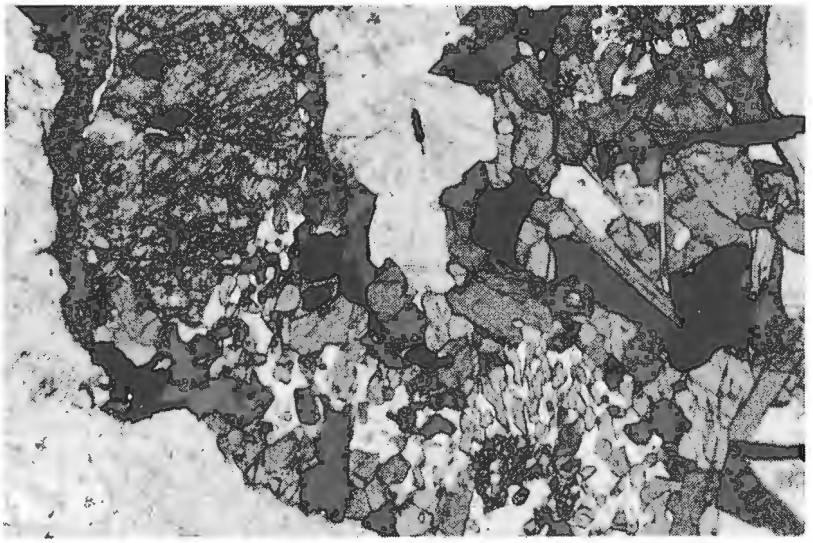

Figure 8.

Orthocumulus texture in pyroxene-hornblende quartz-diorite (field = 2.5 mm).

DISCUSSION

Magmatic evolution

Field and petrographic relationship suggest a continuous textural and compositional transition from 'dry' hornblende-free gabbronorite to 'hydrous' pyroxene-free hornblende-quartz-diorite. Hornblende-gabbronorite and hornblende-diorite represent intermediate members in the suite. This sequential transition is accompanied by associated increases in the amounts of accessory quartz, Fe-Ti opaque oxides, biotite, apatite, and zircon. Moreover, the widespread occurrence of cumulus textures, namely in gabbronoritic rocks, is an obvious manifestation of the importance played by crystal settling and fractional crystallization in the diversification of the suite. In addition, the spatial association noticed between the dioritic rocks and the paragneisses in the wall rock raises the possibility of further diversification of the original magma by assimilation.

Magmatic polarity and body rotation

The nature of the rock suite suggests magmatic differentiation from a single parent magma. In addition, an overall top to the south polarity can be proposed for the intrusion by assuming that the dioritic rocks crystallized at the top of the magma chamber where residual magma was concentrated following gravitational crystal settling. This is also consistent with the magmatic fabric being initially near subhorizontal. These, and the recognition of two igneous unconformities within the intrusion suggest either that the intrusion resulted from a number of magma pulses extracted from a deeper and fractionated magma chamber, or that the intrusion was emplaced as a single magma pulse and tilted at later stages of its solidification and fractionation. The high dihedral angles of the igneous unconformities require significant body rotation.

Relationship to regional metamorphism and cooling

The apparent absence of a thermal aureole is significant in assessing models of intrusion and the cooling history of the body and its country rocks. It is emphasised that the gneissosity in the country rocks is conformable to the outline of the intrusion, and that metamorphic minerals in the immediate wall rock are synkinematic. In addition, metamorphic assemblages in sheared rocks from the intrusion independently suggest that postemplacement tectonic deformation has taken place at minimum wall rock temperatures and depths consistent with the epidote-amphibolite facies, i.e. at temperatures in excess of 450°C.

These observations are consistent with syntectonic emplacement in the middle crust, where wall rocks are already hot so that the thermal gradient set by the intrusion is considerably reduced. Hence, the shouldering and the heat from the intrusion added to the tectonic thermal regime, producing a concordant wall rock and regional metamorphic fabrics.

A U-Pb monazite age of 1388 ± 1 Ma has been obtained for paragneisses located less than 2 km from the Lapeyrère intrusion (Corrigan, 1995). This age has been interpreted as the age of cooling through the 725°C isotherm after regional metamorphism. This interpretation is not easily reconciled with emplacement of the Lapeyrère intrusion ca. 1070 ± 3 Ma (Nadeau et al., 1992b). Indeed, first order thermal considerations for gabbroic bodies of comparable size emplaced in the middle crust suggest that temperatures in excess of 750°C can be reached several kilometres away from the intrusion and maintained for a geologically significant time (Jaeger, 1957, 1959, 1964; Turner, 1981). Such thermal regime is inconsistent with the monazite cooling age. However upper amphibolite temperatures (650-725°C) may nonetheless have been maintained in the host rock during pluton emplacement. A tentative model which can account for the occurrence of an older cooling age in the present wall rock is that the body sank after solidification, leaving its initial intrusive envelope behind (Glazner, 1994). Such a model is otherwise consistent with postcrystallization body rotation, and late Grenvillian syntectonic emplacement.

ACKNOWLEDGMENTS

Susie Nantel, Claude Hébert, and Serge Perreault from the Ministère des Richesses naturelle du Québec are gratefully acknowledged for kindly providing field data and a large collection of samples and thin sections used in this study. Greg Lynch is thanked for reviewing the manuscript.

REFERENCES

Ashwal, L.D. and Wooden, J.L.
1983: Sr and Nd isotope geochronology, geologic history, and origin of the Adirondack anorthosite; Geochimical Cosmochimical Acta, v. 47, p. 1875-1885.

Béland, J.
1961: Rapport géologique 97, Région de Shawinigan; ministère des Richesses naturelles du Québec, Rapport géologique 97, 59 p., carte 1327, échelle 1:63 360.

Corrigan, D.
1995: Mesoproterozoic evolution of the south-central Grenville orogen: structural, metamorphic, and geochronologic constraints from the Mauricie transect; Ph.D. thesis, Carleton University, Ottawa, Ontario, 216 p.

Corrigan, D. and van Breemen, O.
1997: U-Pb age constraints for lithotectonic evolution of the Grenville Province along the Mauricie transect, Quebec; Canadian Journal of Earth Sciences, v. 34, p. 299-316.

Doig, R.
1991: U-Pb zircon dates of Morin anorthosite suite rocks, Grenville Province, Quebec; Journal of Geology, v. 99: p. 729-738.

Emslie, R.F.
1980: Geology and petrology of the Harp Lake complex, Central Labrador: an example of Elsonian magmatism; Geological Survey of Canada, Bulletin 293, 136 p.

Glazner, A.F.
1994: Foundering of mafic pluton and density stratification of continental crust; Geology, v. 22, p. 435-438.

Hébert, C. et Nadeau, L.
1994: Géologie de la région de Talbot (31 P/01); ministère des Ressources naturelles du Québec, carte 2213 ET 95-01, échelle 1/50 000.

Higgins, M.D. and van Breemen, O.
1996: Three generations of anorthosite-mangerite-charnockite-granite (AMCG) magmatism, contact metamorphism and tectonism in the Saguenay-Lac-Saint-Jean region of the Grenville Province, Canada; Precambrian Research, v. 79, p. 327-346.

Irvine, T.N.
1987: Layering and related structures in the Duke Island and Skaergaard intrusions: similarities, differences, and origins; in Origins of Igneous Layering, (ed.) I. Parsons; NATO Advanced Science Institutes Series C: Mathematical and Physical Sciences, v. 196, p. 185-245.

Jaeger, J.C.
1957: The temperature in the neighbourhood of a cooling intrusive sheet; American Journal of Science, v. 255, p. 306-318.
1959: Temperature outside a cooling intrusive sheet; American Journal of Science, v. 257, p. 44-54.
1964: Thermal effects of intrusions; Reviews of Geophysics and Space Physics, v. 2, p. 443-466.

Kretz, R.
1983: Symbols for rock-forming minerals; American Mineralogist, v. 68, p. 277-279.

Lévesque, S.
1995: Zonation métamorphique et évolution thermique de la région Portneuf-Mauricie, orogène de Grenville; thèse de maîtrise, Université Laval, Québec, 150 p.

Nadeau, L. and Brouillette, P.
1994: Structural map of the La Tuque area (NTS 31P), Grenville Province, Quebec; Geological Survey of Canada, Open File 2938, scale 1:250 000.
1995: Structural map of the Shawinigan area (NTS 31I), Grenville Province, Quebec; Geological Survey of Canada, Open File 3012, scale 1:250 000.

Nadeau, L., Brouillette, P., and Hébert, C.
1992a: Geology and structural relationships along the east margin of the St. Maurice tectonic zone, north of Montauban, Grenville Orogen, Quebec; in Current Research 1992-C; Geological Survey of Canada, Paper 92-1C, p. 139-146.

Nadeau, L., van Breemen, O., and Hébert, C.
1992b: Géologie, âge et extension géographique du groupe de Montauban et du complexe de La Bostonnais; Résumé de conférences, ministère de l'Énergie et des Resources du Québec, DV 92-03, p. 35-39.

Rivers, T., Martignole, J., Gower, C.F., and Davidson, A.
1989: New tectonic divisions of the Grenville Province, southeast Canadian Shield; Tectonics, v. 8, p. 63-84.

Turner, F.J.
1981: Metamorphic Petrology: Mineralogical, Field and Tectonic Aspects; 2nd edition, McGraw-Hill, New York, 524 p.

Geological Survey of Canada Project 92002QN

L'utilisation du géoradar et des méthodes électriques pour la cartographie des formations aquifères du piémont laurentien, Québec

Y. Michaud, R. Fortier[1], M. Parent et J. Pilon[2]
Centre géoscientifique de Québec, Sainte-Foy

Michaud, Y., Fortier, R., Parent, M. et Pilon, J., 1997 : L'utilisation du géoradar et des méthodes électriques pour la cartographie des formations aquifères du piémont laurentien, Québec; dans Recherches en cours 1997-E; Commission géologique du Canada, p. 73-82.

Résumé : Une campagne de levés géophysiques de surface a été entreprise afin de compléter l'information stratigraphique sur les séquences quaternaires du piémont laurentien et d'évaluer le potentiel et les limites de certaines méthodes géophysiques pour la délimitation de formations aquifères dans les dépôts meubles. Le géoradar, la résistivité électrique et la polarisation provoquée ont été utilisés dans les unités aquifères du delta de la rivière Sainte-Anne, du delta de la rivière Jacques-Cartier et au voisinage de la Moraine de Saint-Narcisse. Les résultats montrent que ces méthodes géophysiques sont complémentaires et permettent d'identifier les différentes unités stratigraphiques, d'établir leur étendue latérale et de visualiser leur agencement. De plus, ces méthodes géophysiques permettent de déterminer la profondeur de la nappe phréatique.

Abstract: Geophysical investigations are being conducted to complement stratigraphic data on Quaternary sequences of the Laurentian piedmont and to evaluate the potential and limitations of selected geophysical methods for the delineation of aquifers in surficial deposits. Ground penetrating radar (GPR), electrical resistivity, and induced polarization have been used on surface aquifers in Sainte-Anne River delta in the Jacques-Cartier River delta, and in the vicinity of the Saint-Narcisse Moraine. Results show that these geophysical methods are complementary and that they can be used to identify different stratigraphic units and to determine their lateral extent and their organization. They can also be used to determine the depth of the water table.

[1] Département de géologie, Université Laval, Sainte-Foy, Québec G1K 7P4
[2] Division de la science des terrains, Ottawa

INTRODUCTION

La compilation de cartes hydrogéologiques nécessite une connaissance approfondie du terrain autant au niveau de l'information de surface que de l'information en profondeur. Ainsi, la carte des formations superficielles constitue une source indispensable d'information qui doit être complétée par des levés stratigraphiques, afin de connaître l'étendue et la géométrie des unités quaternaires. La recherche d'information en profondeur s'effectue principalement de trois façons : (1) levés des coupes stratigraphiques accessibles en bordure des rivières ou dans les sablières de la région, (2) compilation des descriptions de forages disponibles dans l'annuaire des puisatiers et dans les banques de données de divers ministères et organismes, et (3) exécution de levés géophysiques de surface.

Dans le cadre du projet de cartographie des aquifères du piémont laurentien, une campagne de levés géophysiques a été entreprise afin (1) d'augmenter la densité de l'information stratigraphique dans certains secteurs, (2) d'évaluer la continuité des contacts stratigraphiques entre les unités quaternaires, et (3) d'évaluer le potentiel et les limites de certaines méthodes géophysiques pour la délimitation de formations aquifères dans les séquences quaternaires.

Une méthode électromagnétique (géoradar) et deux méthodes électriques (résistivité électrique et polarisation provoquée) ont été choisies pour atteindre ces objectifs. Puisque l'épaisseur des sédiments dans la région de Portneuf atteint communément de 30 à 40 m, ces méthodes géophysiques présentent un potentiel intéressant en exploration hydrogéologique pour caractériser les secteurs où l'information est manquante.

Jusqu'à maintenant, une dizaine de sites ont fait l'objet de levés géophysiques et de forages. Trois cas types sont présentés ci-dessous à titre d'exemples.

CONTEXTE HYDROGÉOLOGIQUE DE LA MRC DE PORTNEUF

La Municipalité régionale de comté (MRC) de Portneuf est située sur la rive nord du fleuve Saint-Laurent, à mi-chemin entre Québec et Trois-Rivières (fig. 1). Elle chevauche les unités physiographiques des basses terres du Saint-Laurent et des Laurentides. Les eaux souterraines circulent dans trois types d'unités géologiques : (1) des sables et graviers quaternaires mis en place dans la Mer de Champlain (principaux aquifères exploités par les municipalités); (2) des roches sédimentaires paléozoïques (calcaires et shales); et (3) des roches métamorphiques et intrusives du socle précambrien (gneiss granitiques et tonalitiques).

Emplacement des sites d'étude

Pour des fins d'hydrogéologie, la région peut être subdivisée en trois grand types de terrain : (1) les grandes unités aquifères, telles que les deltas des rivières Sainte-Anne et Jacques-Cartier; (2) la Moraine de Saint-Narcisse; et (3) les bassins argileux, secteurs susceptibles de contenir des aquifères captifs. Les trois cas types étudiés se trouvent respectivement dans le delta de la rivière Sainte-Anne, un peu au nord de Saint-Raymond (site 2), dans le delta de la rivière Jacques-Cartier, au nord-est de Pont-Rouge (site 3), et au

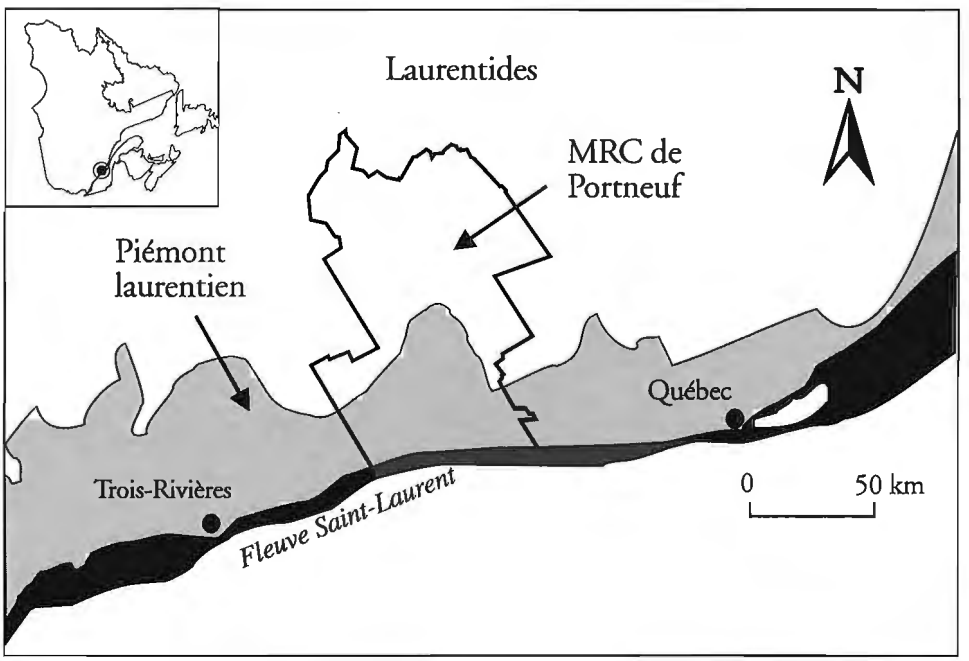

Figure 1. Localisation du piémont Laurentien et de la MRC de Portneuf.

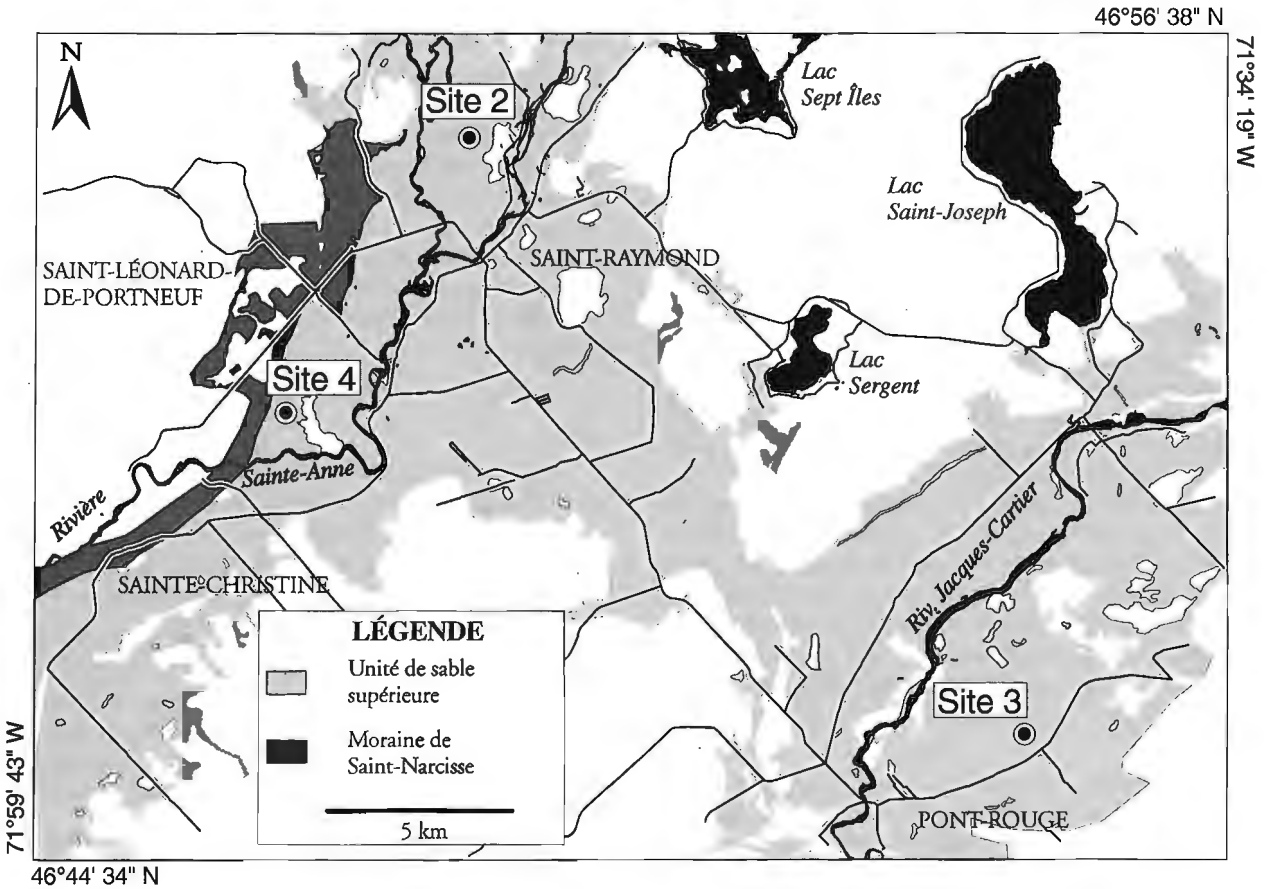

Figure 2. *Emplacement des sites étudiés et des sondages géophysiques.*

voisinage de la Moraine de Saint-Narcisse, au sud de Saint-Léonard-de-Portneuf (site 4) (fig. 2). Le tableau 1 présente la nature des travaux effectuées à chacun des sites.

MÉTHODOLOGIE

Le géoradar et les méthodes électriques comme la résistivité électrique et la polarisation provoquée sont fréquemment employés en hydrogéologie pour reconnaître les aquifères et les unités stratigraphiques. Ce sont des méthodes d'investigation nondestructives qui fournissent des informations ponctuelles (sondages de résistivité électrique) ou bidimensionnelles (géoradar et polarisation provoquée) sur l'épaisseur, l'étendue latérale, la continuité, la géométrie et la structure interne des unités stratigraphiques.

Ces méthodes géophysiques font appel à la propagation d'ondes électromagnétiques ou à la circulation d'un courant électrique dans le sol pour étudier la variation spatiale des propriétés électriques des matériaux (constante diélectrique et conductivité électrique). La nature et la structure interne des unités stratigraphiques du sol peuvent être déduites indirectement à partir de ces variations spatiales. Il faut caler les levés géophysiques et les forages réalisés aux sites d'étude afin d'étalonner les levés et de raffiner leur interprétation. À

Tableau 1. Nature des travaux réalisées aux trois sites étudiés

Site 2	**Saint-Raymond nord**	
	Forages	Pion-1, Pion-2, cptu-6
	Géophysique	Pneuf-2 (ligne géoradar)
Site 3	**Pont-Rouge**	
	Forages	Fr-96-0003, Pion-3
	Géophysique	Pneuf-3 (ligne géoradar)
	Installations	piézomètre, capteur de pression et câble thermistance (Therm-1)
Site 4	**Saint-Léonard-de-Portneuf**	
	Forages	Fr-96-0004A, Fr-96-0005
	Géophysique	Pneuf-1, SP-1, morai-1, chen-1 (lignes géoradar) Gph-96-05-PP (polarisation provoquée) Gph-96-05-RS (résistivité électrique) Gph-96-06-RS (résistivité électrique)
	Installations	piézomètre, capteur de pression

chacun des trois sites choisis, au moins un forage a été réalisé pour identifier les unités stratigraphiques et mesurer le niveau de la nappe phréatique. Les forages ont été réalisés au moyen d'une tarière à tige creuse et d'une foreuse à percussion de marque Pionjär munie d'un carottier de type *«Flow-through»* de 20 cm de longueur et de 1,3 cm de diamètre intérieur.

Levés de géoradar

Les levés de géoradar ont été réalisés à l'aide d'un appareil PulseEKKO 100 fabriqué par Sensors and Software Inc. Le géoradar est un outil d'investigation géophysique de haute résolution capable de fournir des profils détaillés sur une profondeur maximale d'une trentaine de mètres. Il fonctionne sur le principe de la propagation dans le sol d'une onde électromagnétique à haute fréquence et de la réflexion de cette onde au contact de matériaux de constantes diélectriques différentes (Davis et Annan, 1992), comme les contacts stratigraphiques et le niveau de la nappe phréatique. Plusieurs types d'antennes dont les fréquences varient de 12,5 à 900 MHz sont employés selon la profondeur et la résolution souhaitées. Règle générale, la profondeur maximale d'investigation diminue et la résolution des unités stratigraphiques augmente lorsque la fréquence d'émission des ondes électromagnétiques augmente.

Les sondages effectués dans la région de Portneuf ont été réalisés à l'aide d'un émetteur de 400 volts et d'antennes de 50 MHz. Les ondes électromagnétiques ont été émises à un intervalle régulier de 1 m, avec un espacement constant de 2 m entre les antennes émettrice et réceptrice. Dans les sols sableux, cette configuration permet d'atteindre des réflecteurs situés jusqu'à une trentaine de mètres de profondeur, tout en conservant une résolution de l'ordre de 40 cm d'épaisseur (Jol, 1995). Les structures dont l'épaisseur est inférieure à la résolution ne sont pas repérées. Les profils de géoradar comportent généralement une série de traces verticales. Chaque trace représente l'émission d'une onde à un endroit particulier le long du levé. Les réflecteurs associés aux variations de constante diélectrique apparaissent sur les profils comme des échos continus subhorizontaux. La position de ces réflecteurs sur les profils est identifiée en fonction de la distance parcourue le long du levé et du temps de propagation de l'onde électromagnétique depuis l'antenne émettrice jusqu'au réflecteur et depuis le réflecteur jusqu'à l'antenne réceptrice, qui varie selon la profondeur. Il est donc nécessaire d'estimer la vitesse de propagation des ondes électromagnétiques en effectuant des levés de type point commun (CMP: common mid point). Pour un sable sec, la vitesse de propagation est de 0,15 m/ns tandis que pour un sable saturé, elle est de 0,06 m/ns (Davis et Annan, 1992).

Chacun des profils a subi un traitement informatique minimal. On n'a pas eu recourt à la migration du signal ou à l'élimination par filtrage des basses et hautes fréquences. On a procédé à une faible amplification du signal (gain) et à l'application d'un filtre temporel le long des traces et entre plusieurs traces, afin d'éliminer les petits réflecteurs et d'améliorer la continuité des réflecteurs linéaires.

Sondages de résistivité électrique

Les sondages de résistivité électrique nécessitent la circulation d'un courant électrique dans le sol entre deux électrodes métalliques plantées à la surface (les électrodes A et B) et la mesure des différences de potentiel induit entre deux autres électrodes (les électrodes M et N). La résistivité électrique ρ d'un conducteur est définite comme la mesure de la difficulté d'un courant électrique à circuler à travers ce conducteur. C'est une des caractéristiques électriques du matériau dont est constitué le conducteur. Elle est calculée selon la formule suivante :

$$\rho = kR$$

où

ρ	est la résistivité électrique (ohm-m),
$R = \Delta V/I$	est la résistance (ohm),
ΔV	est la différence de potentiel induit (volt),
I	est le courant électrique (ampère) et
k	est une constante géométrique (m).

La résistance (R) du conducteur est le rapport entre le courant (I) qui circule dans le conducteur et la différence de potentiel induit (ΔV) dans ce conducteur. La constante géométrique (k) de proportionnalité entre ρ et R dépend de la configuration des électrodes utilisée et de la séparation entre les électrodes du dipôle de courant et du dipôle de potentiel.

Pour un sédiment non consolidé à la température ambiante, la résistivité électrique varie habituellement entre 10 et 10^3 ohm-m. En général, la conductivité électrique d'un sol est de nature électrolytique et due à l'eau interstitielle. La résistivité électrique d'un sol dépend donc de la concentration des minéraux dissous dans l'eau interstitielle, de la porosité du sol, de sa teneur en eau et de la présence d'argile.

Un résistivimètre Terrameter SAS300 d'Atlas Copco a été utilisé pour réaliser tous les sondages de résistivité électrique, selon la configuration dite de Schlumberger. La profondeur d'investigation z pour cette configuration est donnée par la formule suivante (Barker, 1989) :

$$z = 0{,}38L$$

où

z	est la profondeur d'investigation (m) et
$L = AB/2$	est la moitié de la distance séparant les électrodes du dipôle de courant.

La variation de la résistivité électrique apparente en fonction de la distance AB/2 pour un sondage est portée sur un graphique bi-logarithmique. Le sondage peut être interprété qualitativement, semi-quantitativement, par abaques ou quantitativement à l'aide d'un programme d'interprétation (Zohdy, 1989).

Profils de polarisation provoquée

Pour obtenir des profils de polarisation provoquée, tout comme dans les sondages de résistivité électrique, il faut faire circuler un courant électrique dans le sol et mesurer les différences de potentiel induit. L'effet de polarisation provoquée se produit lorsqu'on coupe le courant électrique brusquement. Le voltage mesuré aux électrodes du dipôle de potentiel ne devient pas nul instantanément, mais décroît plus ou moins lentement après une diminution initiale importante. Le temps de décroissance, de l'ordre de quelques secondes, représente un retour à un état initial avant la perturbation créée par la circulation du courant électrique dans le sol.

De l'énergie électrique sous forme d'énergie chimique est emmagasinée dans le sol lorsqu'un courant électrique y circule. Cette énergie chimique emmagasinée est ensuite dissipée lorsque le courant est coupé brusquement de sorte que le sol retrouve son équilibre électrique initial. Les variations de la mobilité des ions en solution dans l'eau interstitielle du sol permettent l'accumulation de cette énergie. Cet effet est connu sous le nom de «polarisation de membrane». La polarisation du milieu est caractérisée par la chargeabilité, qui est la décroissance du voltage dans le temps après l'interruption de la circulation du courant.

Pour les profils de polarisation provoquée on a utilisé, la configuration dite «dipôle-dipôle», dans laquelle les dipôles de courant et de potentiel sont colinéaires et séparés l'un de l'autre par une distance variable que l'on augmente à intervalles réguliers. La séparation des électrodes de chacun des dipôles est constante. La profondeur d'investigation z pour la configuration dipôle-dipôle est donnée par la formule suivante (Barker, 1989) :

$$z=0{,}25L$$

où

L = (n+2) a est la longueur totale de la configuration et

a est la séparation entre les électrodes de chacun des dipôles (m).

L'instrument utilisé pour mesurer simultanément la résistivité et la chargeabilité est un appareil de polarisation provoquée dans le domaine des temps modèle SYSCAL R2E du BRGM. Un cycle complet de mesure dure 8 s. La séparation choisie entre les électrodes de chacun des dipôles est de 10 m et le facteur n varie entre 1 et 8.

RÉSULTATS

Delta de la rivière Sainte-Anne

Le site d'étude est situé presque à mi-chemin entre le Bras-du-nord-de-la-rivière-Sainte-Anne et la rivière Sainte-Anne. Il s'agit d'une épaisse séquence de matériaux sableux découpés en terrasses par les deux rivières. Un levé de géoradar d'une longueur de 2,3 km a été réalisé entre les deux rivières sur trois niveaux de terrasses, soit à 190 m, à 170 m et à 145 m d'altitude.

Le profil de géoradar effectué sur la terrasse supérieure (fig. 3) montre (1) la présence d'un grand réflecteur subhorizontal plongeant de 12 à 20 m de profondeur et (2) une série de réflecteurs avec un pendage apparent vers le nord-ouest d'environ 20°. De plus, de petits réflecteurs un peu moins structurés sont identifiés dans l'unité sous-jacente. Les résultats du forage à percussion (Pion-1) indiquent la présence d'un sable moyen dans l'unité supérieure et d'un sable fin à partir de 13 m de profondeur. Ainsi, le réflecteur principal peut être interprété comme un contact stratigraphique entre deux unités sableuses d'origine deltaïque, avec des lits frontaux dans l'unité supérieure et une unité plus homogène à la base (prodeltaïque). Le niveau de la nappe phréatique ne peut être reconnu sur ce profil.

Delta de la rivière Jacques-Cartier

Le site du delta de la rivière Jacques-Cartier (site 3) se trouve à environ 3,5 km au nord-est de Pont-Rouge le long de la route 358, sur la rive sud de la rivière Jacques-Cartier. Il s'agit d'une grande terrasse relativement plane située à une altitude de 130 m.

Le site a fait l'objet de sept petits levés de géoradar, chacun d'environ 300 m de longueur, étalés sur une distance de 3,8 km. Le profil de géoradar d'un de ces segments (fig. 4) indique la présence de trois réflecteurs parallèles à la surface, soit un réflecteur (1) latéralement continu à environ 5 m de profondeur, un deuxième réflecteur (2) à environ 12 m de profondeur, et un troisième réflecteur (3) dont la profondeur varie entre 20 à 24 m. Une série de réflecteurs (4) ont un pendage apparent de 10° à 15° vers le sud-est. Le forage Pion-3 a rencontré la nappe phréatique à une profondeur de 5,50 m. La présence d'un contact stratigraphique entre un sable moyen et un sable silteux à près de 12 m de profondeur mène à l'interprétation suivante du profil de géoradar. Les réflecteurs parallèles à la surface représentent respectivement le niveau de la nappe phréatique (1), le contact stratigraphique d'une unité de sable deltaïque en surface et d'une couche de sédiments marins fins (2) et, finalement, le contact avec le substratum rocheux variant de 20 à 24 m de profondeur (3). Les réflecteurs obliques (4) seraient des plans de stratification présents dans l'unité de sable supérieure (lits frontaux) et permettent d'identifier ce faciès sédimentaire.

Moraine de Saint-Narcisse

Le segment étudié de la Moraine de Saint-Narcisse (site 4) est situé dans la partie sud de la municipalité de Saint-Léonard-de-Portneuf, entre le rang Saint-Jacques et la rivière Sainte-Anne. Plusieurs forages et levés géophysiques ont été réalisés aux abords de la crête morainique, étant donné l'intérêt sédimentologique et hydrogéologique que présente le site (tableau 1).

Au site 4, la Moraine de Saint-Narcisse se présente comme une longue crête de till d'environ 100 m de largeur et de 3 à 5 m de hauteur bordée de part et d'autre de sédiments sableux en surface. Le forage Fr-96-0004, sur le versant amont de la moraine, a permis de reconnaître la présence d'une mince couche de sable en surface (1,5 m d'épaisseur), suivie en

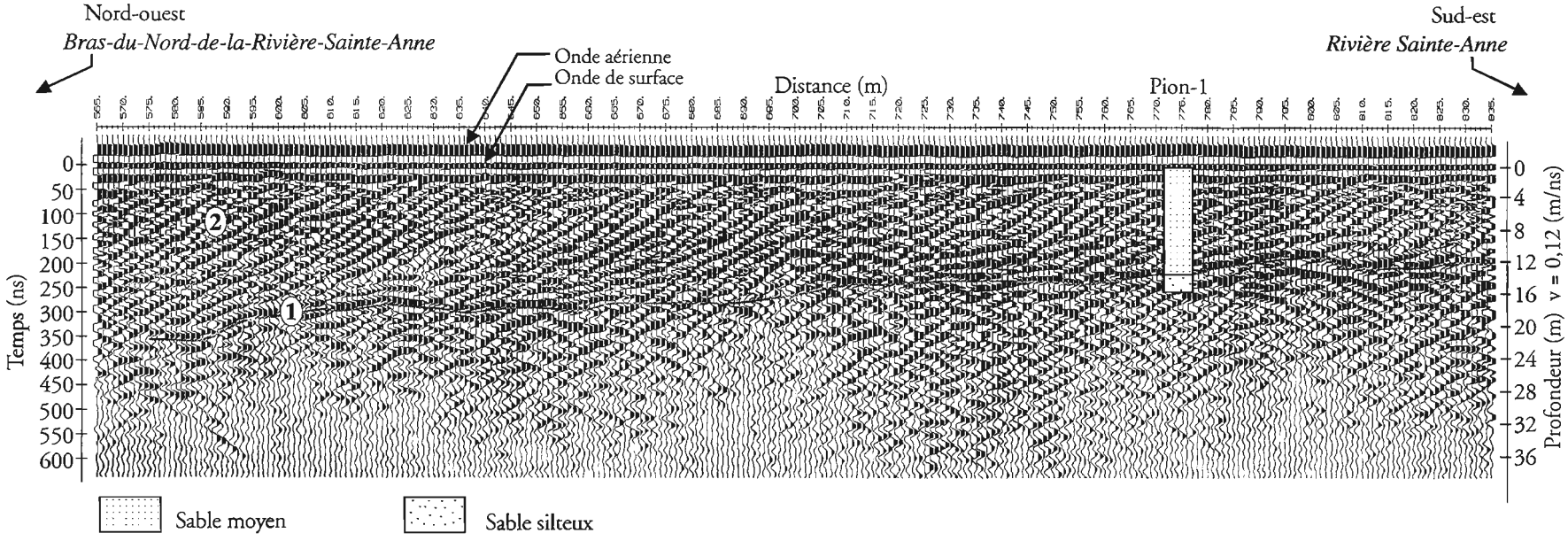

Figure 3. *Profil de géoradar et emplacement du forage Pion-1 sur la terrasse de 190 m d'altitude, le long du delta perché de la rivière Sainte-Anne, à Saint-Raymond.*

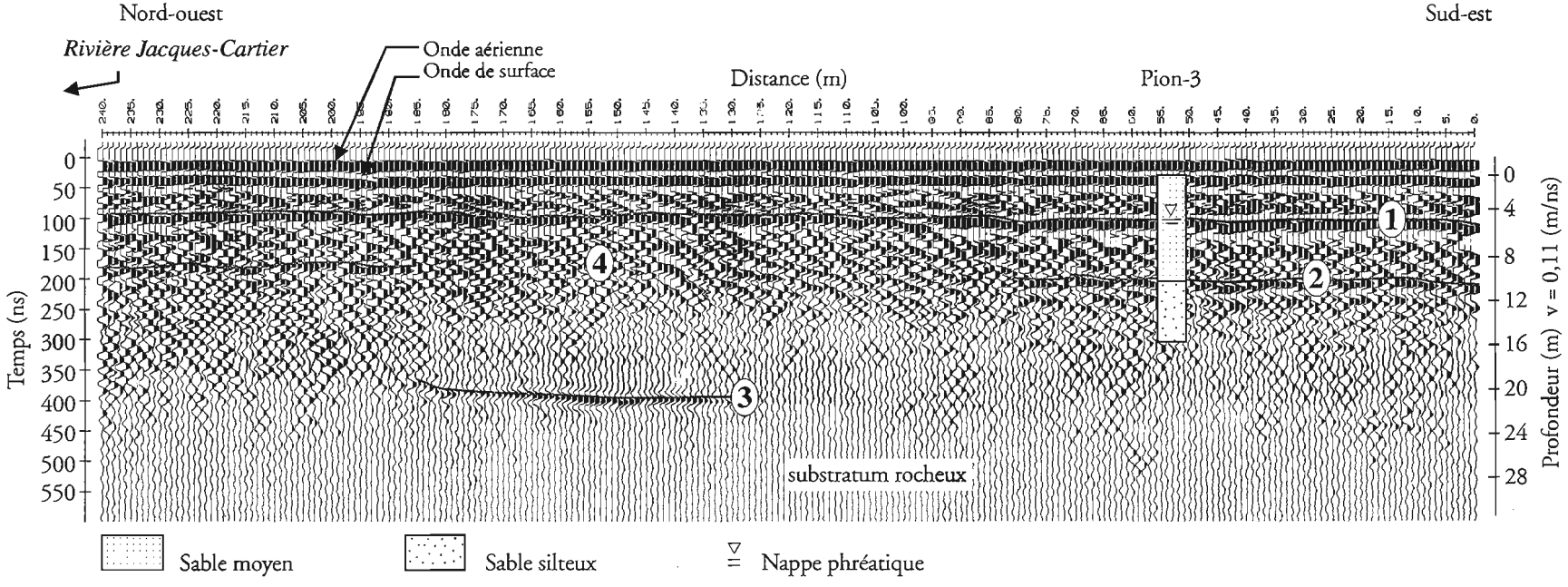

Figure 4. *Profil de géoradar et emplacement du forage Pion-3 le long du delta perché de la rivière Jacques-Cartier, à Pont-Rouge.*

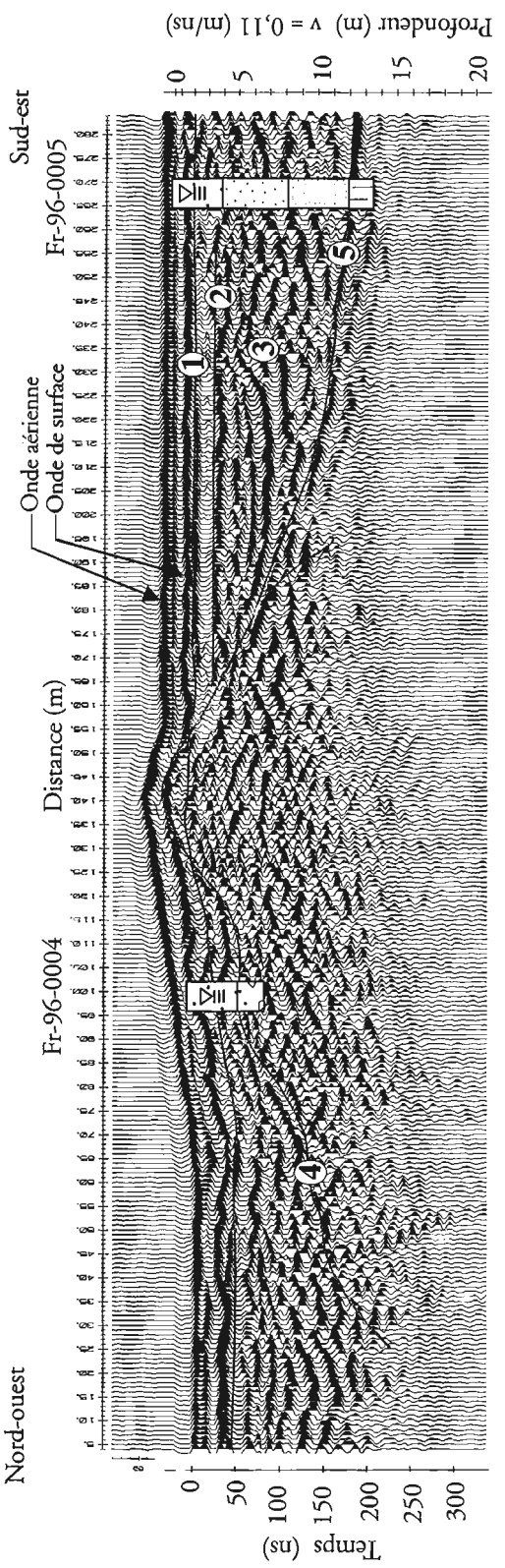

Figure 5. Profil de géoradar perpendiculaire à la Moraine de Saint-Narcisse et emplacement des forages Fr-96-0004 et Fr-96-0005 dans le secteur de Saint-Léonard-de-Portneuf.

profondeur de matériaux hétérométriques variant des silts argileux jusqu'aux blocs. Le forage Fr-96-0005, à quelques 130 m en aval de la moraine, a permis d'identifier la présence d'une couche de sable moyen à grossier sur les trois premiers mètres, suivie de couches de sable moyen à fin jusqu'à 7,5 m de profondeur et enfin d'alternances de couches silteuses et argileuses jusqu'à une profondeur d'au moins 12 m, profondeur à laquelle le forage s'est arrêté. Dans les deux cas, le niveau de la nappe phréatique a été établi à une profondeur de 2,1 m.

Les résultats des levés géophysiques concordent très bien avec la description des matériaux prélevés lors des forages. Le profil de géoradar morai-1 (fig. 5), qui traverse perpendiculairement la crête morainique, révèle la présence de cinq réflecteurs importants et de quelques réflecteurs secondaires situés près de la surface, sur le versant amont de la crête, et indiquant la présence de matériaux remaniés (sables littoraux). Le réflecteur 1, qui est continu d'un bout à l'autre du profil, représente le niveau de la nappe phréatique. Les réflecteurs 2, 3 et 4 sont interprétés comme étant le contact entre des sables littoraux et des sables deltaïques (réflecteur 2), la structure en chenaux des sables deltaïques (réflecteur 3) et le contact supérieur de l'unité de till constituant la Moraine de Saint-Narcisse (réflecteur 4). Le réflecteur 5 est le contact stratigraphique des silts argileux de la Mer de Champlain, qui sont situés sous les sables deltaïques à partir de la position de 200 m. En raison de l'atténuation du signal dans le till, il est difficile d'identifier le matériel sous la crête morainique.

Le profil de polarisation provoquée obtenu sur la Moraine de Saint-Narcisse (fig. 6) coïncide avec le profil de géoradar. Il présente une valeur de résistivité apparente supérieure à 3 000 ohm-m à l'endroit de la moraine (entre les positions de 35 et de 85 m, jusqu'à une profondeur de 7,5 m), et supérieure à 1 000 ohm-m pour le versant amont de la moraine. Le versant aval de la moraine est caractérisé par des couches sableuses subhorizontales reconnues en sondage. L'isoligne de résistivité apparente de 500 ohm-m de ce versant correspond au réflecteur 3 du levé de géoradar. Toujours pour ce versant, les valeurs de résistivité inférieures à 250 ohm-m entre des profondeurs de 10 et 20 m coïncident avec la couche de silt et argile identifiée lors du forage. La moraine recouvre vraisemblablement un sable, puisque les valeurs de résistivité sont supérieures à 500 ohm-m et comparables à celles mesurées pour les couches sableuses de la surface. Le contact entre ces sables, sous la moraine et le dépôt de silt et argile du versant aval, est clairement identifié par un fort contraste de chargeabilité totale près de la position de 95 m (allant de +30 ms dans les sables sous la moraine à -30 ms dans le dépôt de silt et argile). La nappe phréatique ne peut pas être identifiée sur ces pseudo-sections, car la profondeur d'investigation minimale de ces profils est de l'ordre de 5 m en raison de la distance entre les électrodes.

L'interprétation du premier sondage de résistivité électrique (fig. 7), près du lieu du forage Fr-96-0005, permet d'identifier les contacts entre, d'une part, le dépôt de sable en surface (résistivité vraie de 4 000 ohm-m) et la couche de silt et argile (250 ohm-m) à une profondeur de 6 m et, d'autre part, la couche de silt et argile et une couche de till (700 ohm-m) à

une profondeur de 25 m. Le niveau de la nappe phréatique ne peut être déterminé avec exactitude pour ce sondage, car on confond la diminution de la résistivité normalement associée à la nappe et la diminution due au passage de la couche de sable en surface à la couche de silt et argile. Ce sondage n'a pas atteint le substratum rocheux. Pour le deuxième sondage (fig. 7), à environ 1 km plus au sud de la Moraine de Saint-Narcisse, tout près d'un banc d'emprunt de sable d'une hauteur de 6 m, le contact entre la couche de sable (2 000 ohm-m) et la couche de silt et argile (200 ohm-m) est clairement délimité par un très fort contraste de résistivité à une profondeur de 10 m. Le niveau de la nappe phréatique est difficile à identifier sur le sondage et se trouve à une profondeur d'environ 1,50 m. Ce sondage, dont la profondeur d'investigation est de l'ordre de 35 m n'a pas atteint le till ou le substratum rocheux. Le dépôt de sable et la couche de silt et argile s'épaississent donc vers le sud en s'éloignant de la moraine, ce que laissait d'ailleurs présager l'interprétation géomorphologique du site.

DISCUSSION ET CONCLUSION

Les résultats obtenus par les trois méthodes géophysiques choisies et l'interprétation des levés réalisés permettent d'identifier les différentes unités stratigraphiques et de déterminer leur profondeur, leur étendue latérale et leur continuité. Par contre, ces levés géophysiques de surface nécessitent un calage avec une source directe d'information telle les forages pour étalonner les méthodes et confirmer l'interprétation. Ces méthodes géophysiques permettent non seulement d'obtenir des informations importantes sur l'épaisseur et le type des sédiments, la profondeur des contacts stratigraphiques et le niveau de la nappe phréatique, mais aussi de suivre les contacts entre les unités et de mieux saisir l'agencement de ces unités stratigraphiques.

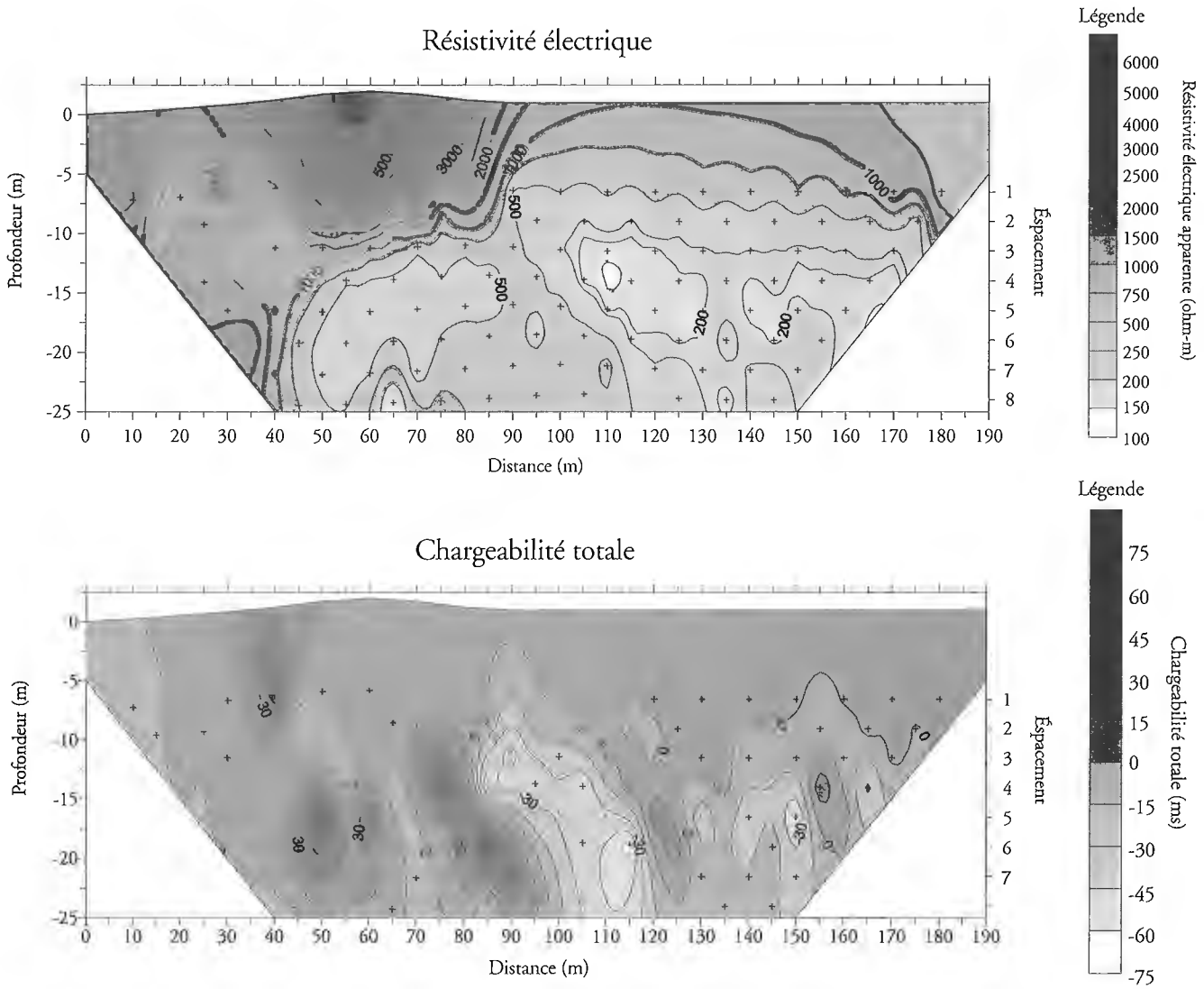

Figure 6. *Profil de polarisation provoquée (résistivité et chargeabilité) selon la configuration dipôle-dipôle sur la Moraine de Saint-Narcisse, Saint-Léonard-de-Portneuf.*

Bien que les levés de géoradar fournissent des profils détaillés des contacts entre les différentes unités stratigraphiques du terrain étudié, ils ne donnent pas une idée exacte des propriétés physiques des matériaux de ces unités. La vitesse de propagation des ondes électromagnétiques dans ces matériaux, évaluée à l'aide des levés du type point milieu commun (CMP), peut donner des indications sur les propriétés physiques des matériaux, mais celles-ci demeurent imprécises. Par contre, ces propriétés physiques peuvent être déduites des valeurs de résistivité électrique et de chargeabilité obtenues par des méthodes électriques. Il est alors possible de distinguer une couche de sable et une couche de silt et argile en fonction des valeurs de résistivité et de chargeabilité obtenues. Les contacts entre les unités stratigraphiques ne sont pas aussi nettes sur les profils obtenus par des méthodes électriques que sur les profils de géoradar, mais on peut mieux différencier les unités stratigraphiques.

Le géoradar est un outil géophysique particulièrement efficace dans les dépôts sableux, où se trouvent les formations aquifères. Il est particulièrement utile pour identifier

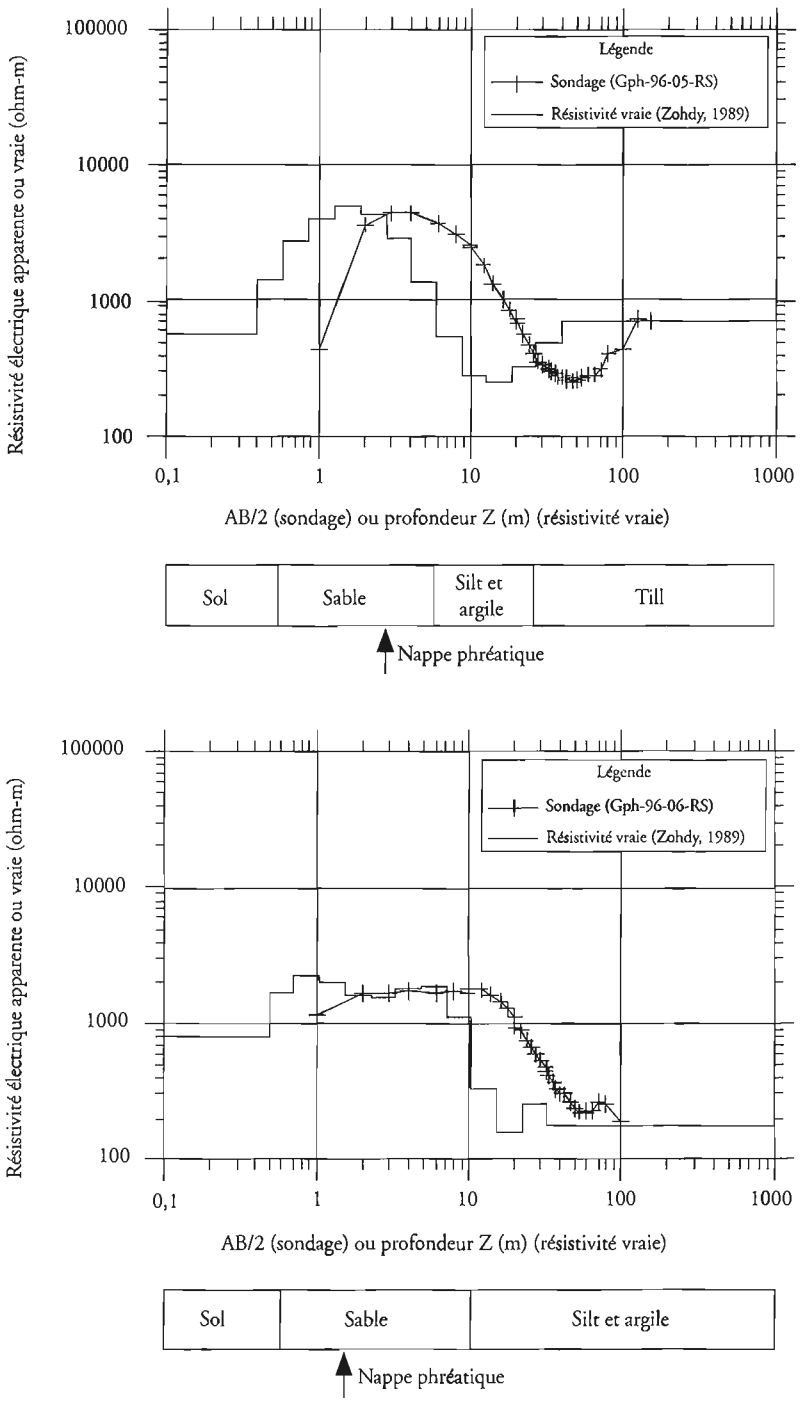

Figure 7.

Sondages de résistivité électrique près de la Moraine de Saint-Narcisse, Saint-Léonard-de-Portneuf.

plusieurs faciès sédimentaires. Par contre, la très faible pénétration des ondes électromagnétiques dans les sédiments marins fins attribuée à la forte atténuation des ondes radar dans un milieu conducteur tel que des argiles salines (Davis et Annan, 1992) est un désavantage certain. De plus, la profondeur d'investigation maximale du géoradar est limitée à une trentaine de mètres avec des antennes de 50 Mhz. Il existe des antennes de 25 Mhz et de 12,5 Mhz permettant d'atteindre une plus grande profondeur, mais elles sont difficiles à manipuler en raison de leur grande dimension (>2 m). Pour des dépôts dont l'épaisseur est supérieure à une trentaine de mètres, il faut faire appel à d'autres méthodes géophysiques, telles les méthodes électriques, dont la profondeur d'investigation est limitée seulement par la puissance d'émission du courant, la difficulté de manipuler de très longs fils électriques sur le terrain et la continuité de l'étendue latérale des formations.

L'interprétation des sondages de résistivité électrique et des profils de polarisation est complexe, puisque le calcul de l'inverse du potentiel est non univoque. En effet, on peut adapter plusieurs modèles en couches de la résistivité vraie en fonction de la profondeur aux valeurs observées des sondages et profilages. La seule façon d'établir un modèle unique par un découpage adéquat en un nombre fini de couches est le calage du modèle avec l'information obtenue par forage. Dans une région donnée où la succession stratigraphique varie latéralement, quelques sondages et profilages peuvent suffire pour obtenir un bon étalonnage. Par la suite, des levés peuvent être réalisés dans cette région même aux endroits pour lesquels il n'y a pas eu de forages. Pour les profils de polarisation provoquée, seule une interprétation qualitative a été réalisée.

Les levés de géoradar, les sondages de résistivité électrique et les profils de polarisation provoquée sont des méthodes géophysiques complémentaires. Bien que les levés de géoradar donnent de nombreux détails sur la structure des unités stratigraphiques du terrain étudié, les méthodes électriques fournissent des informations complémentaires sur les propriétés électriques des matériaux. En étalonnant ces propriétés et les résultats des forages, il est possible de déterminer le type de dépôt et la profondeur de la nappe phréatique.

REMERCIEMENTS

Cette contribution fait partie du projet-pilote de cartographie hydrogéologique régionale de la CGC-Québec, entrepris en collaboration avec le MEF et la MRC de Portneuf. Les auteurs aimeraient remercier Éric Boisvert pour la réalisation de certaines figures et la gestion de la base de données, Philippe-Antoine Hamel, Caroline Belland-Pelletier, Daniel Paradis et Allison Shaw pour leur aide sur le terrain et Normand Tassé pour ses commentaires à la suite de la lecture critique du manuscrit. De plus, les auteurs aimeraient souligner la grande collaboration de la population de la MRC de Portneuf et l'intérêt qu'elle a manifesté pour cette étude.

RÉFÉRENCES

Barker, R.D.
1989: Depth of investigation of colinear symmetrical four-electrode arrays; Geophysics, v. 54, no. 8, p. 1031-1037.

Davis, J.L. and Annan, A.P.
1992: Application of ground penetrating radar to mining, groundwater and geotechnical projects: selected case histories, *in* Ground penetrating radar, (ed.) J.A. Pilon, Geological Survey of Canada, Paper 90-4, p.49-55.

Jol, H.M.
1995: Ground penetrating radar antennae frequencies and transmitter powers compared for penetration depth, resolution and reflection continuity; Geophysical Prospecting, v. 43, p. 693-709.

Zohdy, A.A.R.
1989: A new method for the automatic interpretation of Schlumberger and Wenner sounding curves; Geophysics, v. 54, no. 2, p. 245-253.

Projet 960001HD de la Commission géologique du Canada

Analyse hydrologique pour l'évaluation de la recharge en eau souterraine dans le bassin versant de la rivière Portneuf sur le piémont laurentien, Québec

D. Paradis [1], R. Lefebvre [1] et Y. Michaud
Centre géoscientifique de Québec, Sainte-Foy

Paradis, D., Lefebvre, R. et Michaud, Y., 1997: Analyse hydrologique pour l'évaluation de la recharge en eau souterraine dans le bassin versant de la rivière Portneuf sur le piémont laurentien, Québec; dans Recherches en cours 1997-E; Commission géologique du Canada, p. 83-88.

Résumé : Une évaluation de la recharge des eaux souterraines est faite pour la municipalité régionale de comté (MRC) de Portneuf, dans le cadre d'un projet de cartographie hydrogéologique régionale. Cette évaluation est basée sur la compilation des données météorologiques et hydrométriques pour la période allant de 1973 à 1992. Ces données sont interprétées par modélisation hydrologique. Le modèle matriciel à bilan hydrologique CEQUEAU est appliqué au bassin versant de la rivière Portneuf. La recharge moyenne des eaux souterraines calculée pour l'ensemble du bassin versant est de 299 mm/an pour des précipitations moyennes de 1 174 mm/an.

Abstract: An assessment of groundwater recharge is performed for the Portneuf Regional County Municipality, as part of a regional hydrogeological mapping project. This assessment is based on the compilation of meteorological and hydrometric data for the period from 1973 to 1992. These data are interpreted by hydrological modelling. The CEQUEAU hydrological balance matrix model is applied to the Portneuf River drainage basin. The average groundwater recharge calculated for the entire drainage basin is 299 mm/year for average precipitation of 1174 mm/year.

[1] INRS-Géoressources, 2535, boul. Laurier, Sainte-Foy, Québec G1V 4C7

INTRODUCTION

Les eaux souterraines représentent une ressource renouvelable de première importance. Au Québec, environ 17 % de la population comptent sur les eaux souterraines pour leur approvisionnement en eau potable. En milieu rural, cette proportion est de l'ordre de 90 %. Les eaux souterraines sont utilisées comme source d'eau potable, et également à des fins agricoles et industrielles.

Un projet de cartographie hydrogéologique a été entrepris en 1995 par le Centre géoscientifique de Québec (CGC-Québec et INRS-Géoressources) en partenariat avec le ministère de l'Environnement et de la Faune (MEF) dans le cadre de l'établissement d'une politique de conservation et de protection des eaux souterraines par le MEF. Ce projet-pilote a pour objectif de définir l'approche à suivre pour la délimitation des aquifères et la caractérisation des ressources en eaux souterraines. On compte ainsi fournir des outils de connaissance permettant aux MRC d'intégrer la protection de leurs ressources en eaux souterraines dans leurs plans d'aménagement du territoire. La région choisie pour le projet-pilote est la MRC de Portneuf. Cette région offre de bons exemples d'aquifères du piémont laurentien et est représentative des besoins en eaux souterraines et des conditions rencontrées généralement sur la rive nord du Saint-Laurent, de l'Outaouais jusqu'à Charlevoix.

La MRC de Portneuf est située sur la rive nord du Saint-Laurent, à mi-chemin entre Québec et Trois-Rivières (fig. 1). Elle chevauche les unités physiographiques des basses-terres du Saint-Laurent et des Laurentides. Les eaux souterraines circulent dans trois types d'unités géologiques : 1) des sédiments quaternaires non-consolidés mis en place principalement par la Mer de Champlain ; 2) des roches sédimentaires paléozoïques (calcaires et shales); 3) des roches cristallines du socle précambrien de la Province du Grenville.

La connaissance de la recharge des eaux souterraines est essentielle pour toute étude hydrogéologique. Plusieurs méthodes ont été proposées pour évaluer la recharge (Simmers, 1988), mais ce paramètre reste souvent difficile à préciser. L'objectif de notre étude est de faire l'évaluation de la recharge de l'eau souterraine pour le bassin versant de la rivière Portneuf. Le bassin versant de la rivière Portneuf a été retenu comme région d'étude parce qu'il est représentatif des conditions rencontrées dans la MRC de Portneuf. L'évaluation de la recharge a été faite à l'aide du programme de modélisation hydrologique CEQUEAU (Morin et Paquet, 1995).

PROFILS PHYSIQUE ET HYDROLOGIQUE DU BASSIN VERSANT DE LA RIVIÈRE PORTNEUF

Le bassin versant de la rivière Portneuf couvre un territoire de 363 km^2. Il occupe la partie centre sud de la MRC de Portneuf et est entouré par le bassin versant de la rivière Sainte-Anne à l'ouest et celui de la rivière Jacques-Cartier à l'est (fig. 2). L'ensemble du bassin versant est dominé par la forêt (73,6 %) et par des terres agricoles (23 %). Les lacs et les rivières couvrent 3,25 % du territoire et les milieux urbains, moins de 1 %.

Le bassin de la rivière Portneuf se situe presque entièrement dans la zone physiographique des basses-terres du Saint-Laurent. La partie nord de la rivière coule principalement sur

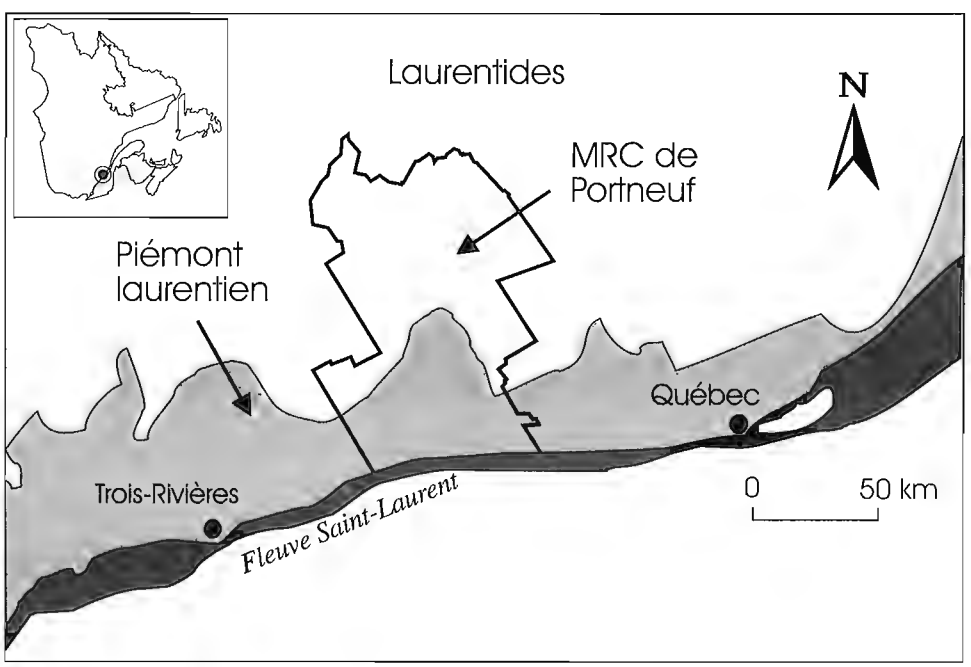

Figure 1. *Emplacement de la MRC de Portneuf.*

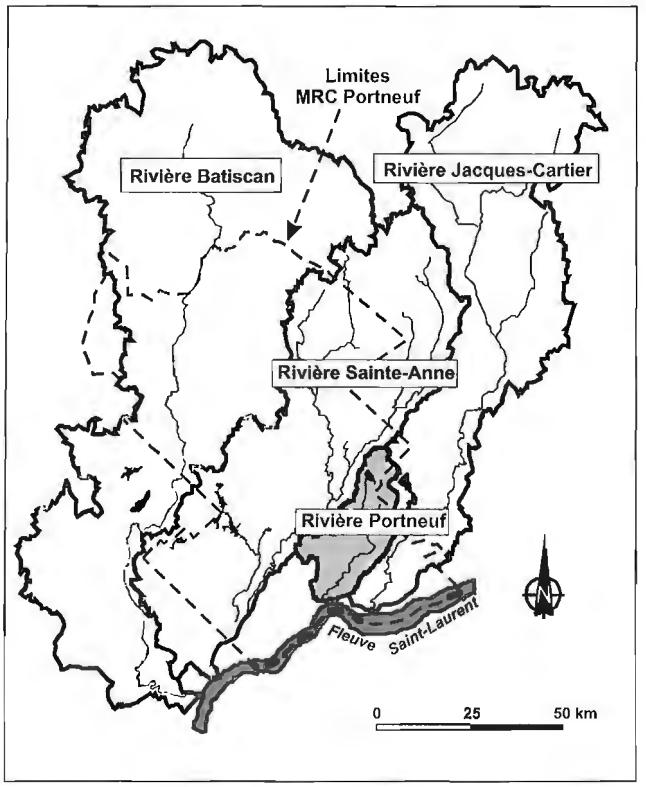

Figure 2. Bassins versants de la MRC de Portneuf.

des argiles marines déposées lors de l'épisode de la Mer de Champlain, tandis que la partie la plus au sud coule sur des sables d'origine fluviatile.

Les lacs Sept-Îles et Sergent, situés à des altitudes moyennes respectives de 204 m et de 149 m, se déversent dans la rivière Portneuf qui a une longueur maximale d'environ 35 km entre son embouchure et le lac Sept Îles. À la confluence de la rivière Portneuf et du fleuve Saint-Laurent, le débit annuel moyen de la rivière était de 8,6 m^3/s pour la période de 1973 à 1992. Au cours de cette période le débit mensuel moyen a atteint un maximum de 40,5 m^3/s en avril et un minimum de 3,0 m^3/s en août en période d'étiage.

Les températures moyennes mensuelles sont de l'ordre de -13,3 °C pour le mois de janvier et de 18,6 °C pour le mois de juillet. Les précipitations moyennes annuelles sont de l'ordre de 1 174 mm d'équivalent en eau. Le tableau 1 présente les moyennes mensuelles des précipitations totales et des températures calculées à partir des mesures enregistrées aux huit stations météorologiques présentes sur le territoire. (fig. 3).

MÉTHODOLOGIE

La première étape de la détermination de la recharge des eaux souterraines consiste à compiler des données hydrométriques et météorologiques pour la période de 1973 à 1992. Le choix de la période d'étude a été fait afin de pouvoir considérer l'équilibre des composantes du cycle hydrologique tout en tenant compte de la disponibilité des données. En tout, six stations météorologiques et une station hydrométrique ont été utilisées (fig. 3).

Tableau 1. Moyennes mensuelles des précipitations totales et de la température pour l'ensemble du bassin versant de la rivière Portneuf.

	Précipitation	Température
	mm	°C
Janvier	81,3	-13,3
Février	63,2	-11
Mars	77,5	-4,7
Avril	81,2	3,5
Mai	108,4	11,1
Juin	113,2	16
Juillet	123	18,6
Août	113,1	17,5
Septembre	123,5	12
Octobre	105,7	5,8
Novembre	92,4	-0,7
Décembre	91,5	-9,5
Total	1 174	

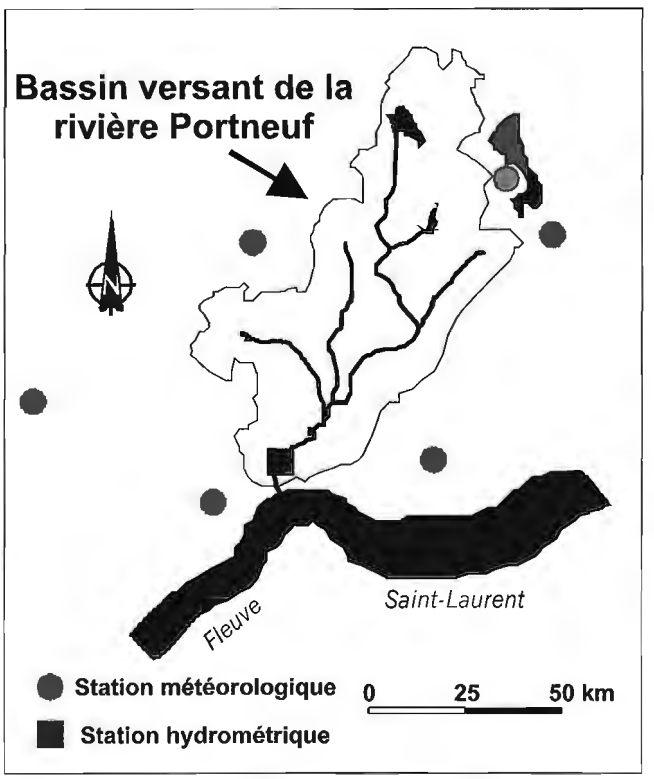

Figure 3. Station hydrométrique et stations météorologiques.

Le modèle hydrologique CEQUEAU (Morin et Paquet, 1995) a été utilisé pour interpréter les données. Le modèle CEQUEAU est un modèle déterministe matriciel qui permet de simuler la quantité d'eau en rivière sur une base journalière. C'est un modèle à bilan qui tient compte des caractéristiques physiques du bassin versant et de leur variations dans le temps et dans l'espace. L'avantage du modèle CEQUEAU, comparativement aux méthodes de bilan d'eau basées sur des mesures du niveau de la nappe (Stoertz et Bradbury, 1989) ou aux méthodes de bilan hydrologique conventionnelles (Ilamas, 1985), est qu'il permet de valider les composantes du bilan hydrologique par la reproduction d'hydrogrammes de cours d'eau qui peuvent être comparés aux hydrogrammes établis directement en rivière.

L'application du modèle CEQUEAU à un bassin versant nécessite l'ajustement de paramètres pour que le modèle reproduise le mieux possible les débits observés. Ces paramètres peuvent être de trois types : 1) les constantes déterminées à l'aide des caractéristiques hydrologiques et physiographiques (temps de concentration du bassin, pourcentage de surface imperméable); 2) les paramètres déterminés selon la physique du phénomène (taux de fonte en forêt, exposant de la formule de Thorntwaite); et 3) les paramètres déterminés par tâtonnement (seuil d'infiltration vers la nappe, coefficient de vidange du sol). La vérification de l'ajustement du modèle se fait par l'analyse des résultats numériques et graphiques.

Pour l'analyse numérique, afin de quantifier la précision des résultats, le modèle calcule deux critères d'ajustement : le coefficient de corrélation et le coefficient de NASH. Le coefficient de corrélation varie entre 0 et 1 et indique surtout la covariance entre les valeurs calculées et observées. Il est sensible aux déphasages. Le coefficient de NASH représente le rapport de la variance résiduelle en fonction de la variance des débits observés et peut varier entre -1 et 1. La valeur 1 est obtenue lorsque les débits simulés sont identiques aux débits observés et la valeur -1 est obtenue dans le cas contraire.

Afin d'assurer le bon ajustement des paramètres pour les conditions du bassin versant de la rivière Portneuf, la période d'étude a été divisée en deux : 1) la période 1973-1982 pour un premier ajustement des paramètres du modèle et 2) la période 1983-1992 pour l'étalonnage.

RÉSULTATS

Le programme CEQUEAU produit des fichiers de résultats numériques qui doivent être vérifiés afin de valider la simulation. Les résultats à vérifier sont : 1) les lames annuelles des débits observés et calculés; 2) le coefficient de corrélation; et 3) le critère de NASH. Les tableaux 2 et 3 présentent les résultats obtenus pour les périodes d'ajustement et d'étalonnage.

Pour l'analyse graphique, on utilise une représentation temporelle des débits à la station hydrométrique. Les débits représentés peuvent être journaliers, mensuels, maximum mensuels ou minimum mensuels. Les figures 4 et 5 montrent les moyennes interannuelles des débits journaliers (hydrogrammes) observés et calculés pour la période d'ajustement et pour la période d'étalonnage.

Ce type de graphique nous renseigne sur toutes les composantes de l'hydrogramme et il permet de déterminer les paramètres à modifier lors du calage du modèle. Entre autres, on peut y déterminer la précision de la simulation des étiages, des crues et de la fonte des neiges.

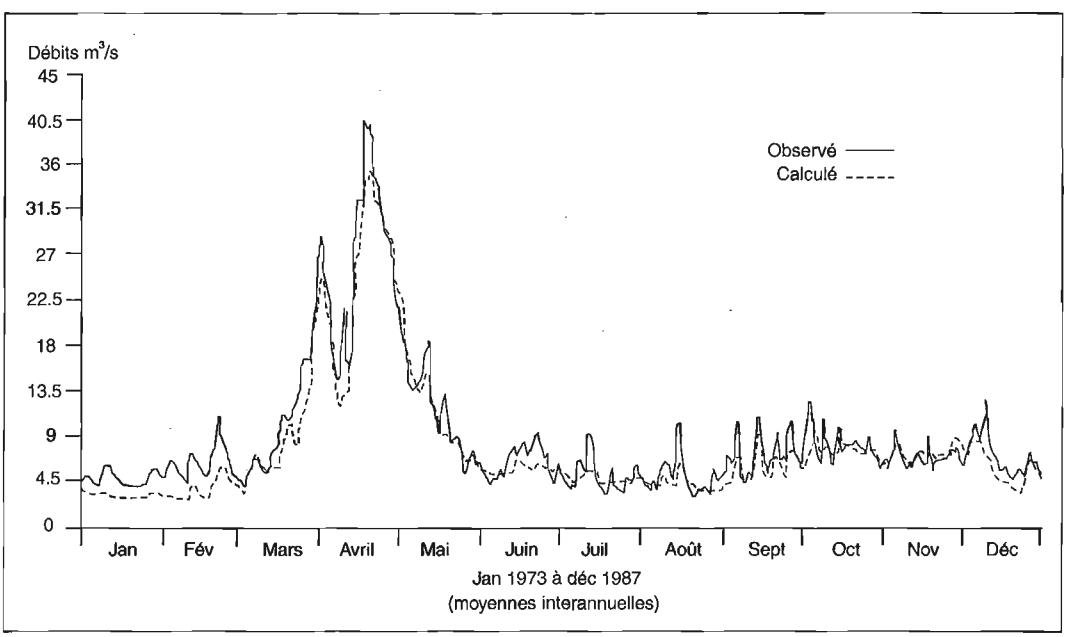

Figure 4. *Hydrogrammes des moyennes interannuelles pour la période d'ajustement.*

Tableau 2. Résultats numériques pour la période d'ajustement.

Année	Lame annuelle observée	Lame annuelle calculée	Coefficient de corrélation	Critère NASH
1973	942,9	709,2	0,76	0,50
1974	855,19	768	0,89	0,78
1975	599,96	605,4	0,92	0,83
1976	1 010,8	871,2	0,79	0,54
1977	642,31	564	0,94	0,86
1978	590,64	574,7	0,91	0,82
1979	778,81	715,3	0,91	0,82
1980	623,08	551,1	0,90	0,79
1981	858,8	733.2	0,85	0,68
1982	657,5	625,2	0,95	0,90
Moyenne	755,9	671,7		

Tableau 3. Résultats numériques pour la période d'étalonnage.

Année	Lame annuelle observé	Lame annuelle calculée	Coefficient de corrélation	Critère NASH
1983	891,7	860,2	0,89	0,76
1984	648,8	655,1	0,92	0,85
1985	580,4	615,7	0,97	0,93
1986	876,8	923,8	0,93	0,85
1987	627,6	649,5	0,90	0,79
1988	636,5	655,6	0,96	0,92
1989	672,1	709,7	0,95	0,90
1990	887,9	855,3	0,91	0,80
1991	654,8	671,3	0,95	0,89
1992	812,9	726,1	0,86	0,73
Moyenne	728,9	732,2		

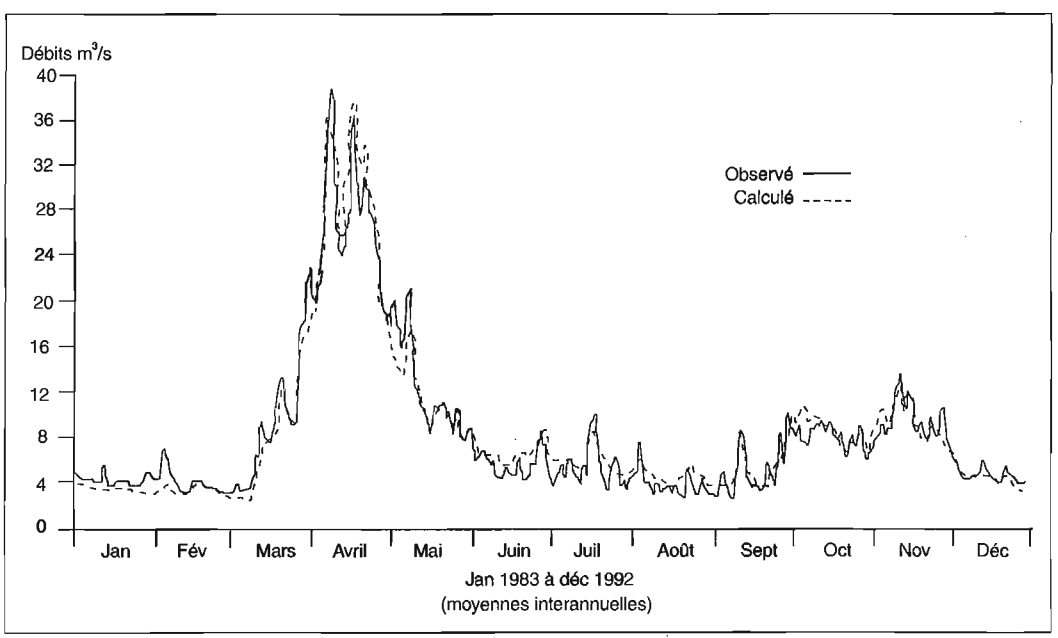

Figure 5. Hydrogrammes des moyennes interannuelles pour la période d'étalonnage.

Une fois tous les paramètres du modèle convenablement ajustés et étalonnés, les valeurs de recharge sont extraites des fichiers d'écriture du programme. La valeur moyenne de la recharge calculée sur l'ensemble du bassin versant de la rivière Portneuf est de 299 mm/an pour toute la période d'étude. Cette valeur de recharge correspond à 25 % des 1 174 mm de précipitation tombant en moyenne chaque année sur la région.

DISCUSSION

Les résultats obtenus pour la période d'étalonnage sont comparables à ceux qui ont été obtenus pour la période d'ajustement. En effet, pour les moyennes interannuelles, le coefficient de NASH est de 0,92 pour la période d'ajustement et de 0,96 pour la période d'étalonnage. De plus, la différence entre les lames d'eaux interannuelles observées et calculées pour les deux périodes sont respectivement de 11,1 % et de 0,4 %.

Compte tenu des coefficients de corrélation obtenus, on peut conclure que les simulations des débits calculés correspondent bien aux débits observés. En effet, les coefficients oscillent autour de 90 %, exception faite de l'année 1973 (tableau 2). Aussi, les valeurs des critères de NASH obtenus indiquent une bonne simulation de la variance des débits calculés par rapport aux débits observés (tableau 3), car la majorité des coefficients sont au dessus de 80 %.

De façon générale, les débits observés et calculés sont en phase (fig. 3 et 4). En effet, la fonte des neiges et les oscillations du débit automnal sont bien simulées pour les deux périodes. Par contre, la simulation des étiages hivernaux et estivaux est moins précise.

CONCLUSION

De façon générale, les résultats des simulations obtenus dans cette recherche sont satisfaisants. Tout de même, il serait possible d'améliorer le synchronisme des hydrogrammes en définissant des coefficients d'infiltrations pour chacune des parties du bassin versant au lieu d'utiliser un coefficient homogène d'infiltration pour l'ensemble du bassin. Cela permettrait de tenir compte du fait que la partie nord de la rivière coule sur de l'argile et la partie sud, sur du sable.

Bien qu'il soit possible d'obtenir un bon ajustement des paramètres du modèle CEQUEAU, il n'en reste pas moins que la solution n'est pas unique. En effet, pour un ensemble de paramètres différents, il est possible d'obtenir un ajustement tout aussi acceptable des hydrogrammes observés et calculés. Pour faciliter le choix du bon ensemble de paramètres, le modèle devrait être étalonné directement avec des mesures de recharge prises sur le terrain.

À ce jour, quatre piézomètres ont été installés dans les principales zones de recharge des différents bassins versants de la MRC de Portneuf afin d'enregistrer les variations du niveau de la nappe phréatique. Après une année de prise de données, il sera possible de comparer ces valeurs et les valeurs calculées au moyen du programme CEQUEAU et, par le fait même, d'apporter les corrections nécessaires au modèle.

REMERCIEMENTS

Cette contribution fait partie du projet de cartographie des aquifères du piemont laurentien de la CGC-Québec. Les auteurs aimeraient remercier G. Morin de l'INRS-Eau, qui nous a fourni le programme CEQUEAU nécessaire à la réalisation de ce travail, et Normand Bergeron pour la lecture critique du manuscrit.

RÉFÉRENCES

Llamas, J.
1985 : Hydrologie générale : principes et applications; Chicoutimi, Gaëtan Morin Éditeur, 460 p.

Morin, G. et Paquet, P.
1995 : Le modèle de simulation de quantité et de qualité CEQUEAU; Manuel de référence, INRS-Eau, rapport de recherche no. 433, 318 p.

Simmers, J.
1988 : Estimation of Natural Groundwater Recharge, NATO ASI Series C, 222, D. Reidel Publishing Company, 510 p.

Stoertz, M.W. and Bradbury, K.R.
1989 : Mapping recharge areas using a ground-water flow model - a case study; Ground Water v. 27, no. 2, p. 220-229.

Projet 960001HD de la Commission géologique du Canada

Premiers résultats de la caractérisation isotopique des aquifères de la région de Portneuf, Québec

F. Vitali, M.M. Savard et É. Bourque
Centre géoscientifique de Québec, Sainte-Foy

Vitali, F., Savard, M.M. Et Bourque, É, 1997: Premiers résultats de la caractérisation isotopique des aquifères de la région de Portneuf, Québec; dans Recherches en cours 1997-E; Commission géologique du Canada, p. 89-95.

Résumé : La caractérisation isotopique de l'eau souterraine est en cours dans la municipalité régionale de comté (MRC) de Portneuf. L'étude préliminaire de la composition isotopique ($\delta^{13}C$) du carbone inorganique dissous et les mesures de l'oxygène dissous indiquent l'existence d'aquifères variés dans cette région. Des nappes libres ont été reconnues dans les dépôts meubles le long de la rivière Sainte-Anne, et au niveau de la rivière Jacques Cartier. La présence de nappes à recharge lente a été envisagée, notamment dans les municipalités de Grondines et de Portneuf. L'étude révèle également l'existence à Saint-Thuribe d'une «nappe fossile» composée d'eau de mer qui n'a probablement pas été réalimentée depuis sa formation pendant la transgression de la Mer de Champlain.

Abstract: The isotopic characterization of groundwater in the "municipalité régionale de comté" (MRC) of Portneuf is ongoing. The preliminary study of $\delta^{13}C$ of dissolved inorganic carbon (DIC) and dissolved oxygen indicates the existence of various types of aquifers in the area. Unconfined aquifers have been identified in surficial materials along the Sainte-Anne River, and near the Jacques Cartier River. Slowly recharging aquifers may exist near the towns of Grondines and Portneuf. There is also a "fossil aquifer" composed of seawater, that has likely not been recharged since its formation during the Champlain Sea transgression.

INTRODUCTION

La municipalité régionale de comté (MRC) de Portneuf, au Québec (fig. 1), fait actuellement l'objet d'un projet pilote de cartographie hydrogéologique régionale et de détermination de la vulnérabilité des aquifères. La région possède des zones urbaines, des zones industrielles, des zones agricoles et des zones forestières ainsi que de beaux exemples d'aquifères du piémont laurentien. Ces aquifères représentent la source d'approvisionnement en eaux souterraines la plus importante de la rive nord du Saint-Laurent, depuis l'Outaouais jusqu'à Québec (Bourque et al., 1996). Dans la MRC de Portneuf, les eaux souterraines circulent dans trois types d'unités géologiques : 1) des sédiments non consolidés mis en place dans la Mer de Champlain; 2) des roches sédimentaires paléozoïques (calcaires et shales); et 3) des roches précambriennes (gneiss granitiques et tonalitiques).

La caractérisation isotopique des aquifères de la partie sud de la MRC, qui est limitée au nord par Rivière-à-Pierre et Lac-Sergent et au sud par le fleuve Saint-Laurent (fig. 2), est en cours. L'étude des isotopes stables (C, H, O, N) fournira des résultats fondamentaux qui permettront de comprendre les processus contrôlant l'alimentation et le temps de séjour des eaux souterraines de ces aquifères et de déterminer les éventuels contaminants nitrés. Les premières mesures isotopiques obtenues sont présentées dans cet article et portent sur le $\delta^{13}C$ du carbone inorganique dissous (CID) dans les eaux souterraines prélevées dans les différentes unités géologiques de la région lors de campagnes d'échantillonnage entreprises en automne 1995 et en été 1996. Ces résultats, couplés aux mesures de l'oxygène dissous dans l'eau, donnent une indication sur les types d'aquifères trouvés dans la partie sud de la MRC de Portneuf.

MÉTHODOLOGIE

L'échantillonnage a été réalisé durant l'automne de 1995 et l'été de 1996. Les sites choisis étaient représentatifs du territoire et des principaux aquifères. Afin de minimiser la contamination lors de l'échantillonnage, dans la mesure du possible on a rempli les bouteilles directement à partir de robinets. Dans ce cas, on fait couler l'eau des robinets jusqu'à ce que sa température devienne stable, afin d'assurer que l'eau n'avait pas résidé dans les tuyaux. On a également utilisé des tubes en Téflon^{MD} stériles pour prélever les échantillons dans les réservoirs ou les puits de surface, et des contenants stériles pour prélever les échantillons dans les bassins de rétention.

$\delta^{13}C_{CID}$

Les mesures des isotopes du carbone inorganique dissous (CID) ont toujours été effectuées le lendemain de l'échantillonnage. Le carbone inorganique dissous a été extrait des échantillons d'eau par acidification en utilisant de l'acide phosphorique à 100 %, et purifié en utilisant une ligne permettant de piéger l'eau et de chasser les gaz incondensables. Le CO_2 extrait a par la suite été analysé à l'aide de deux spectromètres de masse, l'un de type Sira 12 utilisé en 1995 (Université d'Ottawa) et l'autre de type Prism III utilisé en 1996 (CGC-Q, laboratoire Delta). Les valeurs de $\delta^{13}C$ ont une précision supérieure à 0,2 ‰.

Oxygène dissous

Des sondes à électrodes CIBA-CORNING et YSI (modèle 600) ont été utilisées pour mesurer l'oxygène dissous. Elles permettent de déterminer la quantité d'oxygène dissous ayant traversé une membrane perméable, en mesurant le courant responsable de la réduction de l'oxygène. Ce courant est

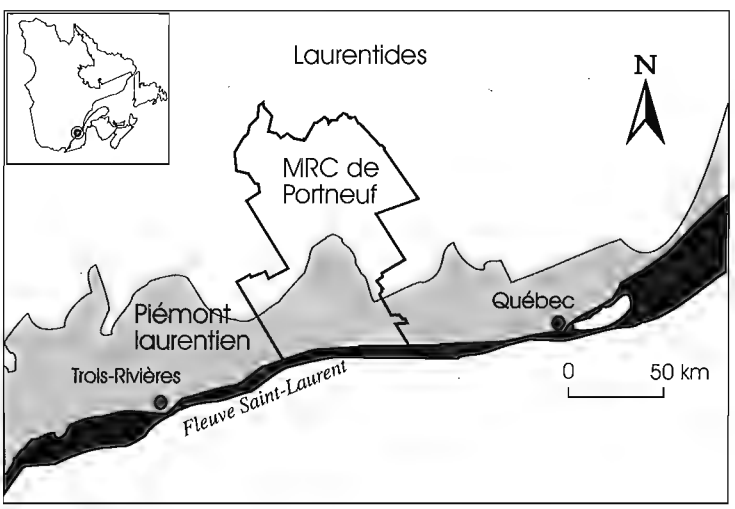

Figure 1.

Emplacement de la MRC de Portneuf.

proportionnel à la pression partielle d'oxygène. Ces appareils permettent d'apporter des corrections pour tenir compte des changements de température. Afin de pouvoir mieux visualiser les variations entre les différents puits, les résultats sont présentés sous forme de pourcentage de la pression partielle d'oxygène.

RÉSULTATS

La composition isotopique ($\delta^{13}C_{CID}$) des eaux souterraines dans le sud de la MRC a été mesurée dans 36 échantillons prélevés lors de la campagne d'automne et dans 30 échantillons prélevés lors de la campagne d'été. Elle présente de fortes variations allant de -25 ‰ à -7,6 ‰, pour les échantillons prélevés l'automne, et de -23,1 ‰ à -1,7 ‰, pour les échantillons prélevés l'été.

Puisque la composition isotopique du carbone inorganique dissous des eaux souterraines peut varier selon la saison (Rightmire, 1978; Reardon et al., 1979; Pawellek et Veizer, 1994), les résultats obtenus lors de chacune des campagnes d'échantillonnage sont présentés sur des graphiques différents. De plus, afin de permettre de bien visualiser les variations de $\delta^{13}C_{CID}$, les résultats ont été groupés en cinq classes de valeurs et ces classes sont indiquées pour les puits échantillonnés (fig. 3a, b). Les puits échantillonnés sont codés selon la municipalité dans laquelle ils se trouvent (tableau 1). La répartition en cinq classes tient compte des divers mécanismes pouvant influer sur la composition isotopique ($\delta^{13}C_{CID}$) des eaux souterraines, à savoir la diffusion du CO_2 atmosphérique, la respiration des plantes, la décomposition des plantes, la dissolution des carbonates et l'altération des silicates (Klopmann et al., 1994; Love et al., 1994; Pawellek et Veizer, 1994, Probst et al., 1994; Rose et al., 1996). La limite entre deux classes est arbitraire, car plusieurs mécanismes peuvent jouer en même temps. Les échantillons appartenant à deux classes successives peuvent avoir la même origine, ce qui sera beaucoup moins probable pour des échantillons appartenant à des classes non successives.

Il est également utile de connaître la quantité d'oxygène dissous dans les différents puits pour déterminer les différents types d'aquifères. La quantité d'oxygène dissous est représentée graphiquement (fig. 4a, b). Les intervalles de valeurs obtenus vont de 17 % à 100 %, pour les échantillons prélevés en automne 1995, et de 0 % à 100 %, pour les échantillons prélevés en été 1996. On constate que l'oxygène dissous est fréquemment plus abondant dans les puits creusés dans des sédiments meubles que dans les puits forés dans des roches sédimentaires ou métamorphiques (fig. 4a, b).

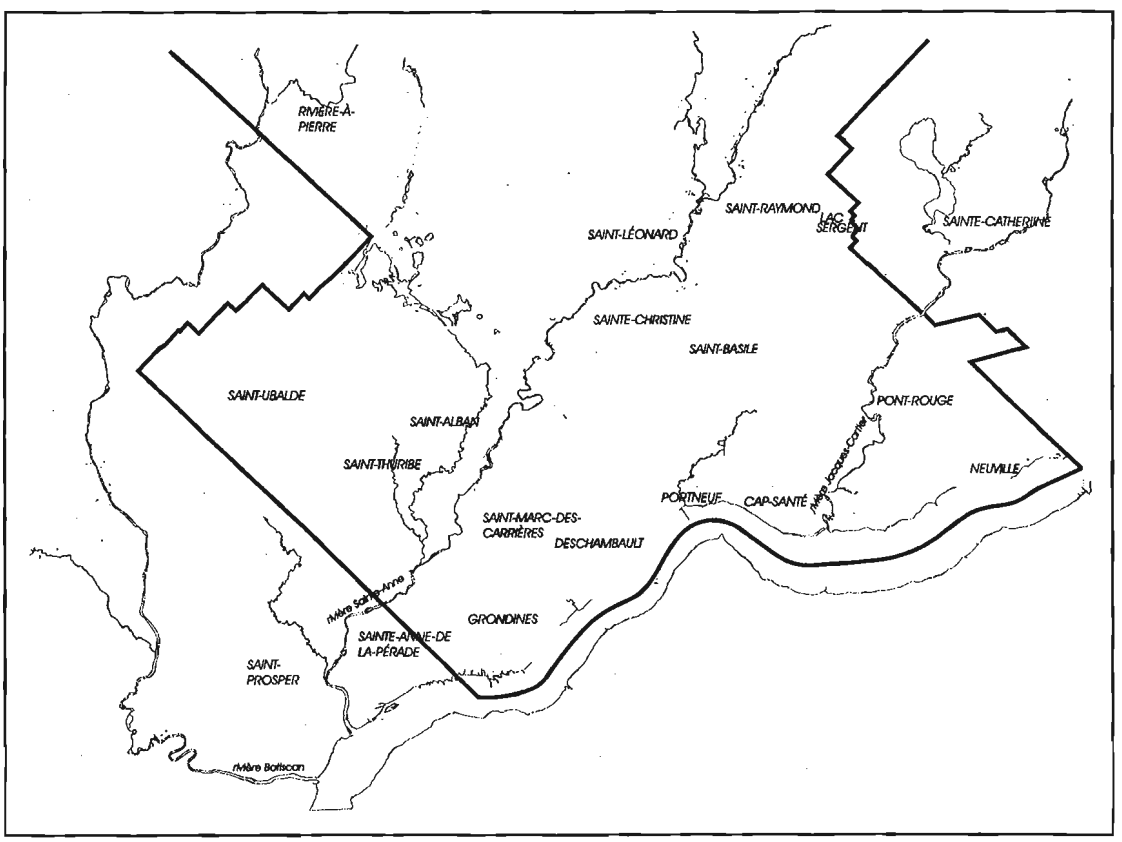

Figure 2. *Municipalités visées par l'étude isotopique.*

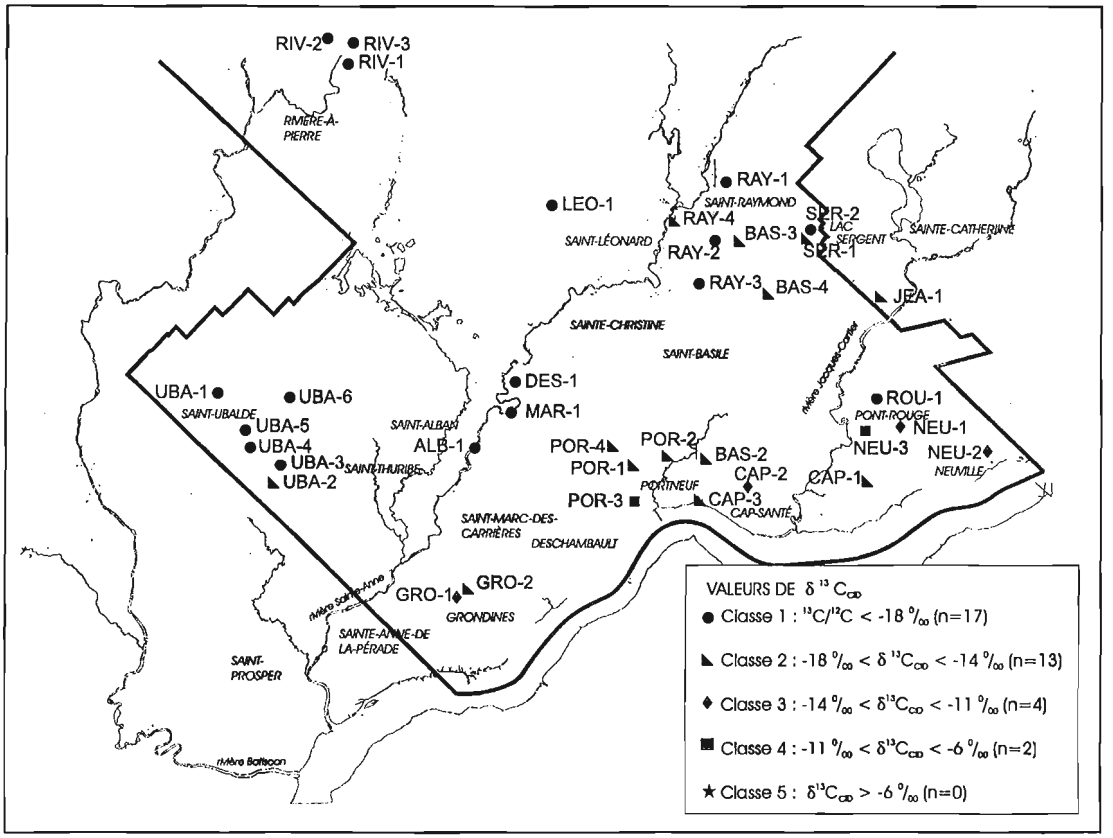

Figure 3a. $\delta^{13}C_{CID}$ *des eaux souterraines échantillonnées à l'automne 1995.*

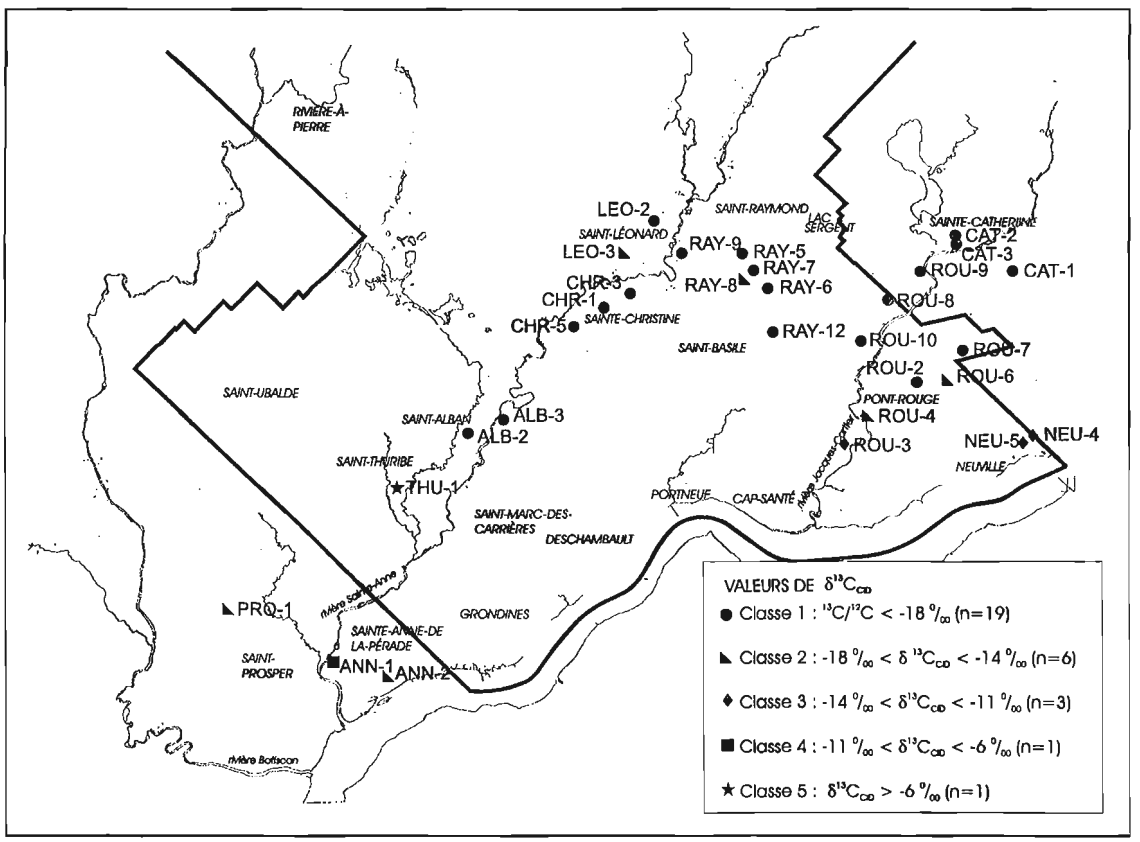

Figure 3b. $\delta^{13}C_{CID}$ *des eaux souterraines échantillonnées à l'été 1996.*

Tableau 1. Municipalités étudiées et abréviations utilisées.

Localités	Abréviations	Localités	Abréviations
Saint-Alban	ALB	Saint-Marc	MAR
Sainte-Anne-de-la-Pérade	ANN	Neuville	NEU
Saint-Basile	BAS	Portneuf	POR
Cap-Santé	CAP	Saint-Prosper	PRO
Sainte-Catherine	CAT	Saint-Raymond	RAY
Sainte-Christine	CHR	Rivière-à-Pierre	RIV
Deschambault	DES	Pont-Rouge	ROU
Grondines	GRO	Lac Sergent	SER
Sainte-Jeanne	JEA	Saint-Thuribe	THU
Saint-Léonard	LEO	Saint-Ubalde	UBA

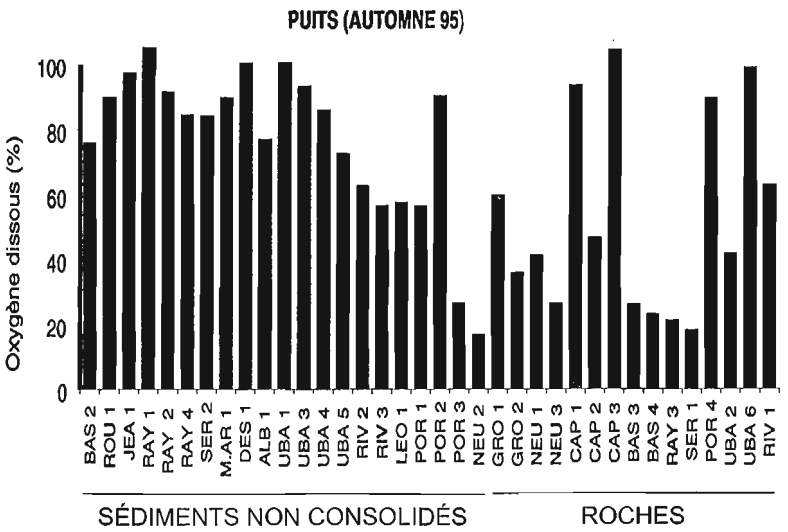

Figure 4a.

Oxygène dissous dans les eaux souterraines échantillonnées à l'automne 1995.

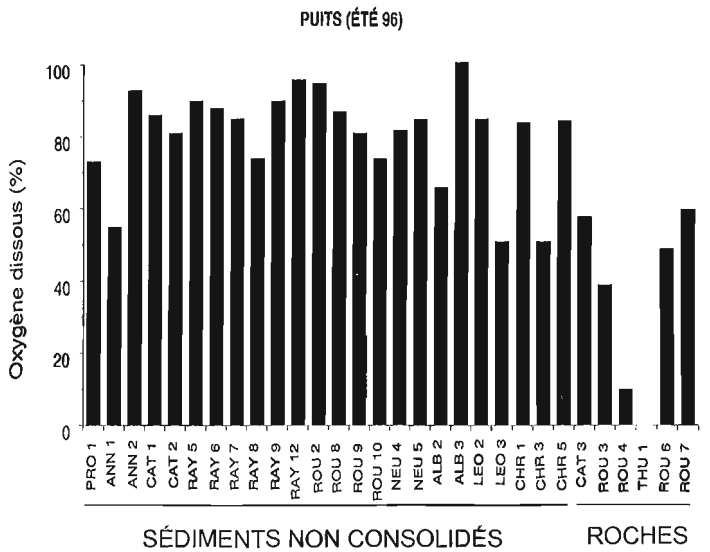

Figure 4b.

Oxygène dissous dans les eaux souterraines échantillonnées à l'été 1996.

DISCUSSION

Nappes libres

Le rapport $^{13}C/^{12}C$ du carbone inorganique dissous (CID) des eaux souterraines permet de déterminer les zones principales de recharge et d'émergence des aquifères (Leaney et Herczeg, 1995). Dans les régions tempérées, une valeur de $\delta^{13}C_{CID}$ très négative est fréquemment une indication de nappes à temps de séjour court (Landmeyer et Stone, 1995; Sukhija et al., 1996). Ces nappes contiennent également un taux élevé d'oxygène dissous. Par contre, une valeur de $\delta^{13}C_{CID}$ élevée, se rapprochant de celle des carbonates, indique un aquifère à temps de séjour plus long (Tenu et al., 1985; Edmunds et al., 1987; Tellam, 1994; Le Gal La Salle et al., 1996). Les teneurs en oxygène dissous sont alors plus faibles. Les géologues du Centre géoscientifique de Québec (CGC-Q) font actuellement la cartographie détaillée des unités géologiques de la partie sud de la MRC de Portneuf. Une connaissance précise de ces unités permettra d'identifier les principaux pôles de mélange susceptibles d'influer sur la composition isotopique ($\delta^{13}C_{CID}$) des eaux souterraines.

Il est déjà possible de constater que les eaux souterraines à faible valeur de $\delta^{13}C_{CID}$ (classe 1 et éventuellement classe 2) se trouvent essentiellement le long de la rivière Sainte-Anne (de Saint-Alban à Saint-Raymond) et de la rivière Jacques Cartier (de Sainte-Catherine à Pont Rouge). Les puits correspondants sont forés dans des unités meubles (Bourque et al., 1996), et leurs eaux présentent des pourcentages élevés en oxygène dissous. Ces puits semblent être situés dans des zones d'émergence d'eaux souterraines qui ont eu peu d'interaction avec la roche encaissante.

Recharge lente des aquifères de Portneuf et de Grondines

Des indications de l'absence de recharge récente ont été décelées dans les aquifères des municipalités de Portneuf et de Grondines. En effet, en ce qui concerne la municipalité de Portneuf, aucun des puits étudiés n'appartient à la classe 1 et un d'entre eux (POR 3), foré dans des dépôts meubles, appartient à la classe 4. La lithologie de ces puits étant variée, il faudra obtenir des informations géologiques détaillées avant de pouvoir interpréter les variations de $\delta^{13}C_{CID}$ dans les eaux de ces puits.

Les eaux des puits de la région de Grondines (classes 2 et 3), qui circulent dans du calcaire, semblent avoir subi un contact prolongé avec la roche encaissante, sans réalimentation récente. Les faibles pourcentages d'oxygène dissous dans les eaux de ces puits (fig. 4a, b) renforcent cette hypothèse. Une analyse isotopique de l'oxygène et de l'hydrogène des eaux permettra de vérifier cela. Si les études ultérieures confirment la faiblesse de la recharge des nappes de Portneuf et de Grondines, on pourra conclure que ces aquifères sont bien protégés contre les polluants anthropiques éventuels.

Nappe fossile de Saint Thuribe

Le puits Thu 1 dans la municipalité de Saint-Thuribe mérite une attention particulière. En effet, la valeur de $\delta^{13}C_{CID}$ y est élevée, soit de -1,7 ‰, et la quantité d'oxygène dissous y est nulle. Ces deux résultats témoignent d'une très longue interaction entre la roche encaissante et la nappe souterraine, sans recharge de l'aquifère. Il s'agit d'une véritable «nappe fossile». De plus, les analyses chimiques des eaux de ce puits ont révélé des concentrations en éléments majeurs équivalentes à celles de l'eau de mer. Il s'agirait donc d'une lentille d'eau salée remontant probablement à l'époque de la Mer de Champlain.

CONCLUSIONS

Les valeurs préliminaires obtenues pour la composition isotopique ($\delta^{13}C_{CID}$), couplées aux données sur l'oxygène dissous dans les eaux souterraines, ont permis de mettre en évidence la variabilité des aquifères de la région de Portneuf, ainsi que la présence possible d'aquifères à recharge assez lente à Grondines et à Portneuf. La présente étude révèle également l'existence, dans la municipalité de Saint-Thuribe, d'une «nappe fossile» composée d'eau de mer qui n'a probablement pas été réalimentée depuis sa formation pendant la transgression de la Mer de Champlain. Une connaissance plus détaillée des roches encaissant les puits forés dans des roches sédimentaires et métamorphiques permettra d'identifier avec plus de précision les phénomènes d'interaction entre l'eau et la roche encaissante et les variations isotopiques ($\delta^{13}C_{CID}$) qui en résultent. De plus, les analyses isotopiques de l'oxygène et de l'hydrogène des eaux souterraines permettront de déterminer les mécanismes qui influent sur les aquifères et la durée de recharge de ces aquifères, de savoir si les eaux circulent d'un aquifère à un autre.

REMERCIEMENTS

Les analyses isotopiques ont été réalisées au laboratoire Delta (CGC-Q) et à l'Université d'Ottawa. Les auteurs tiennent à remercier M. Luzincourt et G. Saint-Jean pour l'aide technique qu'ils ont fournie, Y. Michaud pour sa participation à la coordination du projet et R. Lefebvre pour ses commentaires constructifs sur le manuscrit.

RÉFÉRENCES

Bourque, E., Laflèche, M.R., Lefebvre, R. et Michaud, Y.
1996: Résultats initiaux de la caractérisation géochimique des aquifères du piémont laurentien dans la municipalité régionale de comtés de Portneuf (Québec); dans Recherches en cours, 1996-E; Commission géologique du Canada, p. 225-232.

Edmunds, W.M., Cook, J.M., Darling, W.G., Kinniburgh, D.G., Miles, D.L., Bath, A.H., Morgan-jones, M., and Andrews, J.N.
1987: Baseline geochemical conditions in the Chalk aquifer, Berkhire, U.K.: a basis for groundwater quality management; Applied Geochemistry, v. 2, no. 3, p. 251-274.

Klopmann, W., Dever, L., and Edmunds, M.
1994: Isotopic and geochemical investigations of Chalk Groundwater of the Champagne Region, France; Z. dt. geo. Ges. no. 145, p. 143-152.

Landmeyer, J.E. and Stone, P.A.
1995: Radiocarbon and $\delta^{13}C$ values related to ground-water recharge and mixing; Ground Water, v. 33, no. 2, p. 227-234.

Leaney, F.W. and Herczeg, A.L.
1995: Regional recharge to a karst aquifer estimated from chemical and isotopic composition of diffuse and localised recharge, South Australia; Journal of Hydrology, v. 164, p. 363-387.

Le Gal La Salle, C., Marlin, C., Savoye, S., and Fontes, J. Ch.
1996: Geochemistry and ^{14}C dating of groundwaters from Jurassic aquifers of North Aquitaine Basin (France); Applied Geochemistry, v. 11, p. 433-445.

Love, A.J., Herczeg, A.L., Leaney, F.W., Stadter, M.F., Dighton, J.C., and Armstrong, D.
1994: Groundwater residence time and palaeohydrology in the Otway Basin, South Australia: ^{2}H, ^{18}O, and ^{14}C data; Journal of Hydrology, v. 157-187.

Pawellek, F. and Veizer J.
1994: Carbon cycle in the upper Danube and its tributaries: $\delta^{13}C_{DIC}$ constraint; Israel Journal of Earth Science, v. 43, p. 187-194.

Probst, J.L., Mortatti, J., and Tardy, Y.
1994: Carbon rivers fluxes and weathering CO_2 consumption in the Congo and Amazon River Basin; Applied Geochemistry, v. 9, p. 9-13.

Reardon, E.J., Allison, G.B., and Fritz, P.
1979: Seasonal chemical and isotopic variations of soil CO_2 at Trout Creek, Ontario; Journal of Hydrology, v. 43, p. 355-371.

Rightmire, C.T.
1978: Seasonal variation in pCO_2 and ^{13}C content of soil atmosphere; Water Ressource Research, v. 14, p. 691-692.

Rose, T.P., Davisson, M.L., and Criss, R.E.
1996: Isotope hydrology of voluminous cold springs in fractured rock from an active volcanic region, northeastern California; Journal of Hydrology, v. 179, p. 207-236.

Sukhija, B.S., Reddy, D.V. , Nagabhushanam, P., Hussain, S., Giri, V.Y., and Patil, D.J.
1996: Environmental and injected tracers methodology to estimate direct precipitation recharge to a confined aquifer; Journal of Hydrology, v. 177, p. 77-97.

Tellam, J.H.
1994: The groundwater chemistry of the Lower Mersey Basin Permo-Triasic Sandstone Aquifer System, UK, 1980 and pre-industrialisation-urbanisation; Journal of Hydrology, v. 161, p. 287-325.

Tenu, A., Davidescu, F.D. et Slavescu A.
1985: Recherches isotopiques sur les eaux souterraines des formations calcaires dans la Dobroudja méridionale (Roumanie); dans Isotope Hydrology 1984, International Atomic Energy Agency, IAEA-SM 299/43, p. 439-453.

Projet 960001HD de la Commission géologique du Canada

Electrical characteristics of mineralized and nonmineralized rocks at the Brunswick No. 12 deposit, Bathurst mining camp, New Brunswick[1]

T.J. Katsube, N. Scromeda, M.E. Best[2], and W.D. Goodfellow
Mineral Resources Division, Ottawa

Katsube, T.J., Scromeda, N., Best, M.E., and Goodfellow, W.D., 1997: Electrical characteristics of mineralized and nonmineralized rocks at the Brunswick No. 12 deposit, Bathurst mining camp, New Brunswick; in Current Research 1997-E; Geological Survey of Canada, p. 97-107.

Abstract: Electrical characteristics of mineralized and nonmineralized rock samples from the Brunswick No. 12 massive sulphide deposit have been studied to determine the electrical connectivity of the mineralization and hence its relationship to mineral deposits. The objective is to obtain information to assist in the interpretation of airborne, ground, and borehole electromagnetic surveys.

Laboratory results indicate that electrical resistivities (ρ_r) for mineralized rocks and nonmineralized host rocks (hanging and footwall sediments, iron-formation, chloritized iron-formation, and basement rocks) are in the ranges of <10 Ω-m and 7000 to >10 000 Ω-m, respectively. However, different types of mineralogical and microstructural interferences cause an increase in the measured range of ρ_r values (2 to 20 000 Ω-m). These include thin quartz veins that raise ρ_r by at least 13 000 Ω-m, and thin veins containing fine- to medium-sized sulphide grains that reduce ρ_r to 5-50 Ω-m. Furthermore, interbedded sulphide and silicate layers can produce electrical anisotropies as high as 1000:1 or larger.

Résumé : Les chercheurs ont étudié les caractéristiques électriques d'échantillons de roches minéralisées et non minéralisées prélevés dans le gisement de sulfures massifs Brunswick No. 12, afin de déterminer la connectivité électrique de la minéralisation et, partant, son lien avec les gîtes minéraux. L'objectif visé consiste à obtenir des informations pour améliorer l'interprétation des levés électromagnétiques aériens, terrestres et diagraphiques.

Les résultats de laboratoire indiquent que les résistivités électriques (ρ_r) des roches minéralisées et des roches encaissantes non minéralisées (roches sédimentaires d'éponte supérieure et d'éponte inférieure, formation de fer, formation de fer chloritisée et roches du socle) s'inscrivent respectivement dans les intervalles <10 Ω-m et 7 000 à >10 000 Ω-m. Toutefois, divers types d'interférences d'origine minéralogique et microstructurale entraînent un élargissement de l'intervalle des valeurs mesurées de ρ_r (de 2 à 20 000 Ω-m). C'est le cas notamment des veinules de quartz, qui accroissent ρ_r d'au moins 13 000 Ω-m, et des filonnets contenant des grains de sulfures de taille petite à moyenne, qui réduisent ρ_r à 5-50 Ω-m. Des couches interstratifiées de sulfures et de silicates peuvent en outre induire des anisotropies électriques atteignant ou dépassant 1 000:1.

[1] Contribution to the 1994-1999 Bathurst Mining Camp, Canada-New Brunswick Exploration Science and Technology (EXTECH II) Initiative
[2] Bemex Consulting International, 5288 Cordova Bay Road, Victoria, British Columbia V8Y 2L4

INTRODUCTION

The electrical characteristics of mineralized and nonmineralized rock samples from the Brunswick No. 12 massive sulphide deposit have been studied in order to determine the electrical connectivity of the sulphide mineralization and its relationship to mineral deposits and tectonic fabrics. The objective of this study is to provide information to assist in the interpretation of airborne, ground, and borehole EM surveys. The Brunswick No. 12 deposit is one of five chosen for this type of study in the Bathurst mining camp. These deposits were chosen because of variations in their EM responses, their sulphide mineral grain-sizes, and their tectonic features.

The electromagnetic responses from massive sulphide ore bodies in the Bathurst mining camp are quite variable. Factors such as grain size, mineralization, fractures, and crosscutting veins all affect the EM response of massive sulphides. Previous work (Katsube et al., 1996c) suggests that electrical anisotropy may also be an important factor which can affect the magnitude of the EM responses. Therefore, this study includes laboratory electrical measurements made in three-directions whenever possible. Some of these results have been previously reported (Katsube et al., 1996a, b, c). The purpose of this paper is to document the geological information on the samples, to describe the investigation methods and to present the results that were obtained thus far.

METHOD OF INVESTIGATION

Samples and sample preparation

Ten core samples (sample numbers X-12-1 to X-12-10) were obtained from hole no. 5175 of the Brunswick No. 12 deposit. Information on their depth and geological units are listed in Table 1 and shown in Figure 1.

At least two specimens were cut from each sample: one being used to determine bulk density, δ_B, and electrical resistivity, ρ_r; and one for the determination of effective porosity, ϕ_E. Some samples were cut into several rectangular or disk-shaped specimens (e.g. a, b, c, and d) so that different components of the inhomogeneities and anisotropy of the sample could be characterized by the ρ_r measurements, as shown in Figure 2. Specimens prepared for anisotropic studies were of rectangular shapes (Table 2a) to allow three directional electrical resistivity measurements. The three directions are identified by α, β, and γ. Those prepared for ϕ_E measurements were either partial-disc or irregular in shape. The δ_B and ρ_r measurements were performed on 19 specimens prepared from 10 samples. The measurement of ϕ_E was made on specimens from only 8 of these samples containing no, or the least amount of, visible sulphides. The geometric characteristics of the specimens used for ρ_r and δ_B measurements are listed in Table 2a and 2b. Preparations are in progress for petrographic thin section analysis and scanning electron microscope analysis of selected samples/specimens.

Table 1. Sample identification for samples from Brunswick number 12 hole 5175 – from Thomas (1995), based on drill core logs provided by Noranda Exploration Ltd.

Sample no.	Depth (m)	Geological unit
X-12-1	27.36	Hanging wall sediments
X-12-2	38.71	Iron-formation
X-12-3	44.35	Chloritic iron-formation
X-12-4	53.95	Massive sulphides
X-12-5	68.58	Iron Formation
X-12-6	76.20	Chloritic iron-formation
X-12-7	82.60	Semimassive sulphides
X-12-8	90.37	Footwall sediments
X-12-9	97.23	Crystal tuff
X-12-10	111.86	Quartz eye schist

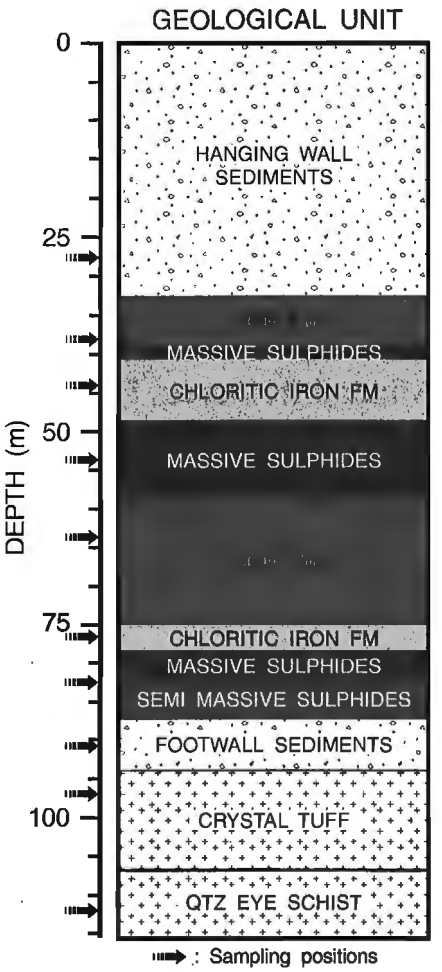

Figure 1. *Geological log of Brunswick No. 12 hole 5175 (modified from Thomas, 1995). The "arrow" signs in the figure indicate the positions of the samples that were used in this study.*

Bulk density and effective porosity measurements

The caliper method (API, 1960) has been used to determine the bulk density (δ_B) of the samples, by measuring the dimensions and weight of the rectangular and disc specimens. These

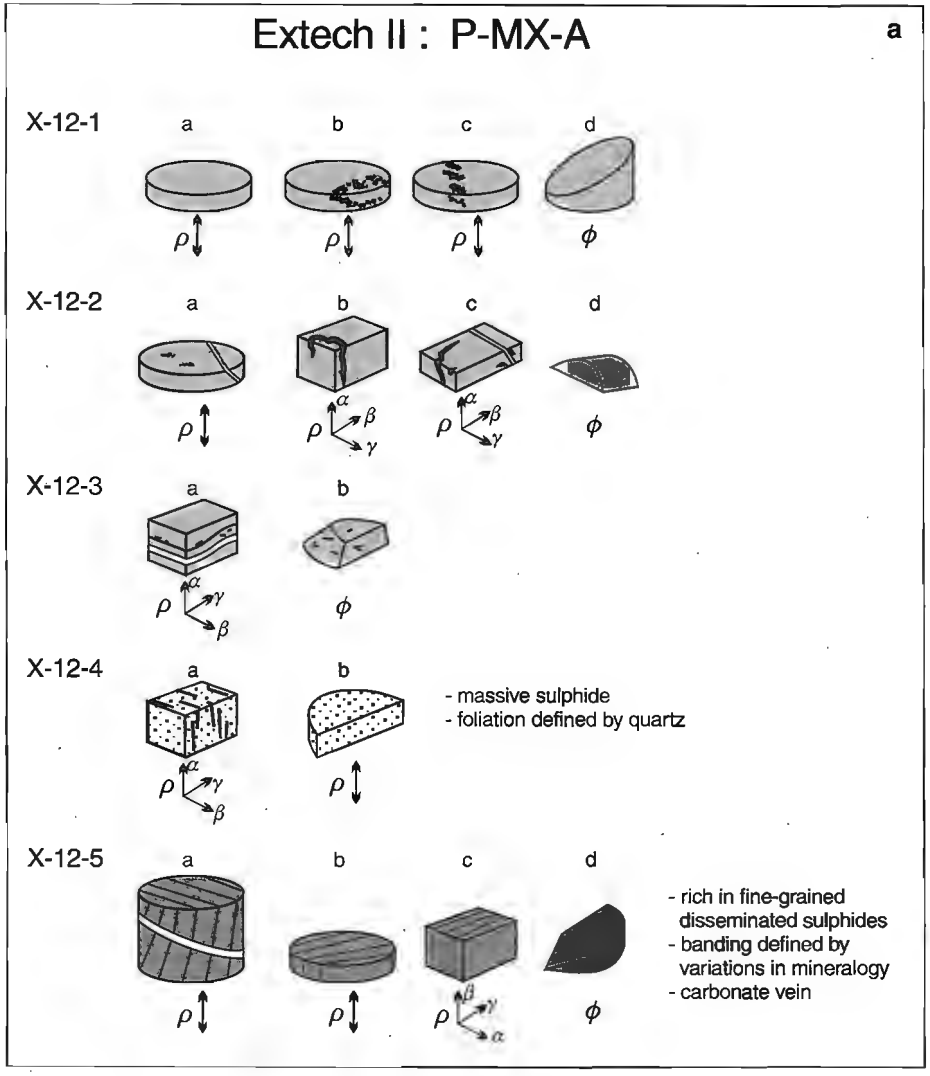

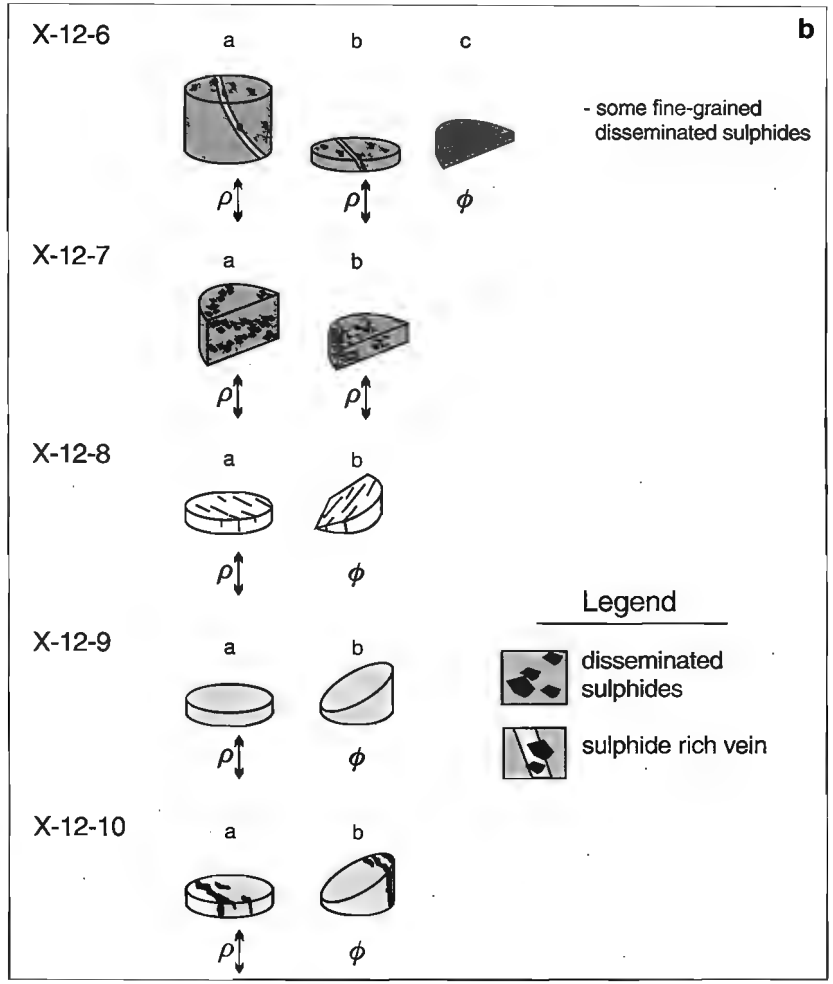

Figure 2. Block diagrams of specimens from the ten samples used for electrical resistivity and porosity measurements in this study ***a****) for samples X-12-1 to X-12-5, and* ***b****) for samples X-12-6 to X-12-10.*

measurements are also used in the procedure to determine porosity. Effective porosity (ϕ_E), in principle, represents the pore volume of all interconnected pores. In this study, it is determined from the difference in weight between the oven-dried and water-saturated rock specimen. Another parameter derived on a routine basis is the irreducible water saturation, S_{ir}, which represents the pore space occupied by the bound or adsorbed water on the pore surfaces, at room temperature (23°C) and atmospheric pressure (Scromeda and Katsube, 1994; Katsube and Scromeda, 1995).

The "API Recommended Practice for Core-Analysis Procedures" (API, 1960) has generally been followed in these measurements. Details of the standard procedures routinely used in our measurements are described in the literature (Katsube and Salisbury, 1991; Katsube et al., 1992; Scromeda and Katsube, 1994; Katsube and Scromeda, 1995).

Table 2a. Dimensions of rectangular specimens cut out from the samples for electrical measurements.

Sample/ Specimen	a_1 (cm)	a_2 (cm)	ℓ (cm)	W (g)	V (cm^3)	K_G (10^{-2}m)	δ_B (g/mL)
X-12-2bα	1.117	1.287	1.318	6.7209	1.89	1.09	3.55
X-12-2bβ	1.117	1.318	1.287	6.7209	1.89	1.14	3.55
X-12-2bγ	1.287	1.318	1.117	6.7209	1.89	1.52	3.55
X-12-2cα	1.217	1.358	0.506	3.0592	0.84	3.27	3.66
X-12-2cβ	0.506	1.217	1.358	3.0592	0.84	0.45	3.66
X-12-2cγ	0.506	1.358	1.217	3.0592	0.84	0.57	3.66
X-12-3aα	1.037	1.240	0.817	3.5075	1.05	1.57	3.34
X-12-3aβ	0.817	1.240	1.037	3.5075	1.05	0.98	3.34
X-12-3aγ	0.817	1.037	1.240	3.5075	1.05	0.68	3.34
X-12-4aα	0.930	1.152	0.976	4.8418	1.05	1.10	4.63
X-12-4aβ	0.976	1.152	0.930	4.8418	1.05	1.21	4.63
X-12-4aγ	0.930	0.976	1.152	4.8418	1.05	0.79	4.63
X-12-5cα	0.782	1.206	0.739	2.5448	0.70	1.28	3.65
X-12-5cβ	0.739	1.206	0.782	2.5448	0.70	1.14	3.65
X-12-5cγ	0.739	0.782	1.206	2.5448	0.70	0.48	3.65

α, β, γ = Three directions of measurement
a_1, a_2 = Length of the two sides of the rectangular specimen
ℓ = Thickness of specimen
W = Weight of specimen under room dry conditions
V = Volume of specimen
K_G = Geometric factor (equation 1)
δ_B = Bulk density

Table 2b. Dimensions of disk-shaped specimens cut out from the samples.

Sample/ Specimen	r_D (cm)	ℓ (cm)	W (g)	V (cm^3)	K_G (m)	δ_B (g/mL)
X-12-1a	2.270	0.529	6.1106	2.14	7.65	2.85
X-12-1b	2.274	0.498	5.7574	2.02	8.16	2.85
X-12-1c	2.272	0.489	5.6455	1.98	8.29	2.85
X-12-2a	2.272	0.535	7.7005	2.17	7.58	3.55
X-12-4b	2.260	0.555	4.5349	1.00	3.33	4.42
X-12-5a	2.278	1.864	25.6879	7.60	2.19	3.38
X-12-5b	2.274	0.487	7.1444	1.98	8.34	3.61
X-12-6a	2.267	1.106	14.4721	4.46	3.65	3.24
X-12-6b	2.272	0.642	8.0064	2.60	6.31	3.08
X-12-7a	2.210	2.131	11.3933	2.90	0.63	3.97
X-12-7b	2.220	0.808	4.6003	1.30	1.93	3.65
X-12-8a	2.223	0.545	6.2567	2.12	7.12	2.96
X-12-9a	2.227	0.558	6.4762	2.17	6.98	2.98
X-12-10a	2.262	0.490	5.9777	1.97	8.20	3.04

r_D = Diameter
ℓ = Thickness of specimen
W = Weight of specimen under room dry conditions
V = Volume of specimen
K_G = Geometric factor (equation 1)
δ_B = Bulk density

Bulk electrical resistivity measurements

The bulk electrical resistivity (ρ_r) is determined from measurements of complex electrical resistivity, ρ^*, procedures for which are described in recent publications (e.g. Katsube et al., 1991, 1992, 1996a, c; Katsube and Salisbury, 1991; Katsube and Scromeda, 1994;). Complex electrical resistivity (ρ^*) consists of two components: real resistivity, ρ_R, and imaginary resistivity, ρ_I (e.g. Katsube, 1975; Katsube and Walsh, 1987; Katsube and Salisbury, 1991). These measurements were made on specimens saturated in distilled water for 24-48 hours (Katsube and Salisbury, 1991). The parameters, ρ^*, ρ_R, and ρ_I are measured over a frequency range of 1-10^6 Hz, and ρ_r usually represents a bulk electrical resistivity at frequencies of about 10^2-10^3 Hz. It (ρ_r) is a function of the pore structure and pore fluid resistivity, and is understood to exclude any other effects, such as pore surface, dielectric polarization, or any other polarizations (Katsube, 1975; Katsube and Walsh, 1987).

The geometric factor, K_G (with the units 10^{-2} m), required for derivation of ρ^* from the actual electrical measurements, is defined as

$$K_G = A/\ell, \qquad (1)$$

where A (cm^2) is the cross-section area and ℓ (cm) is the thickness. This parameter was determined for all specimens prior to the electrical measurements, using the specimen dimensional data in Tables 2a and 2b.

EXPERIMENTAL RESULTS

The results of the bulk density (δ_E) determinations are listed in Tables 2a and 2b. They are in the range of 2.85-4.63 g/mL, and likely represent samples with various degrees of sulphide mineralization. Some specimens show slightly different δ_B values although they do represent the same sample (e.g. sample X-12-7, Table 2b), likely due to the variation in sulphide mineral content within a sample, or due to other inhomogeneities (e.g. sample X-12-5, Table 2a, b). The effective porosities (ϕ_E) are listed in Table 3 for specimens visibly barren of sulphide minerals and display values that range from 0.39 to 2.3%. The smaller values are typical of crystalline rocks (Katsube and Mareschal, 1993; Katsube and Scromeda, 1995) and the larger ones resemble those of tight sedimentary rock (Daly et al., 1966). However, the δ_B values used in the ϕ_E determination procedure are for specimens used in the

Table 3. Results of the effective porosity measurements for specimens representing the section of a sample that are void or contain the least amount of visible sulphides.

Sample/ Specimen	δ_B (g/mL)	δ_B-S	W_W (g)	W_D (g)	S_{ir} (%)	ϕ_E (%)
X-12-1d	2.85	X-12-1a	7.2762	7.2648	32.5	0.45
X-12-2d	3.55	X-12-2c	1.2358	1.2342	12.5	0.46*
X-12-3b	3.34	X-12-3a	2.7527	2.7416	10.8	1.35*
X-12-5d	3.18	X-12-5a	7.4630	7.4168	85.9	2.11
X-12-6c	3.08	X-12-6b	4.9792	4.9725	64.2	0.42
X-12-8b	2.96	X-12-8a	5.0352	5.0244	15.7	0.64
X-12-9b	2.98	X-12-9a	3.9301	3.9250	37.3	0.39*
X-12-10b	3.04	X-12-10a	7.9000	7.8852	40.5	0.57*

δ_B = Bulk density
δ_B-S = Specimen used for δ_B determination
W_w = Wet weight
W_D = Dry weight
S_{ir} = Irreducible water saturation
ϕ_E = Effective porosity
* = Values suspected of reduced accuracy

Table 4. Results of electrical resistivity measurements.

Sample/ Specimen	ρ_r (10^3 Ω-m)		
	Mes. #1	Mes. #2	Mean
X-12-1a	3.26	2.74	3.00
X-12-1b	2.09	2.63	2.36
X-12-1c	3.53	3.87	3.70
X-12-2a	0.13	0.079**	0.11**
X-12-2α	0.50	1.03	0.77
X-12-2β	0.57*	1.08	0.83*
X-12-2γ	1.74	2.89	2.32
X-12-2α	0.10	0.27	0.19
X-12-2β	0.11	0.95	0.53
X-12-2γ	1.10	1.73	1.42
X-12-3α	13.33	12.71	13.02
X-12-3β	0.0070**	0.0093**	0.0082**
X-12-3γ	0.024**	0.0005**	0.0015**
X-12-4α	0.0003**	0.0003**	0.0003**
X-12-4β	0.0004**	0.0003**	0.0004**
X-12-4γ	0.0004**	0.0004**	0.0004**
X-12-4b	0.0018**	0.0016**	0.0017**
X-12-5a	21.81*	22.23*	22.02*
X-12-5b	10.18	7.61	8.90
X-12-5α	0.14	0.16	0.15
X-12-5β	8.24	6.63	7.44
X-12-5γ	5.33*	5.29*	5.31*
X-12-6a	0.012**	0.0048**	0.0084**
X-12-6b	0.013**	0.092	0.053**
X-12-7a	0.0017**	0.0028	0.0069**
X-12-7b	0.0068**	0.0029**	0.0049**
X-12-8a	0.59	0.69	0.64
X-12-9a	1.31	1.94	1.63
X-12-10a	0.0072**	0.0076**	0.0074**

α, β, γ = Three directions of measurement
ρ_r = Bulk electrical resistivity
Mes. (#1) = Measurement after 24 hours of saturation
Mes. (#2) = Measurement after 48 hours of saturation
* = ρ_r value smaller than the true ones
** = ρ_r value with possible error ranges larger than ±100%.

electrical measurements, and not for those used for the ϕ_E determination. Since the sulphide mineral content can differ between the two specimens, these δ_B values do not necessarily represent the true values of the specimen used for the ϕ_E determination. Therefore, although the δ_B values of the specimens with the least degree of sulphides has been selected, the ϕ_E values could contain some errors. Those suspected of such errors are marked by astericks in Table 3. The δ_B measurements are not performed on the same specimens as those for the ϕ_E determination, because the ϕ_E specimens are, usually, irregular in shape. The caliper method for δ_B determination can not be used on such specimens.

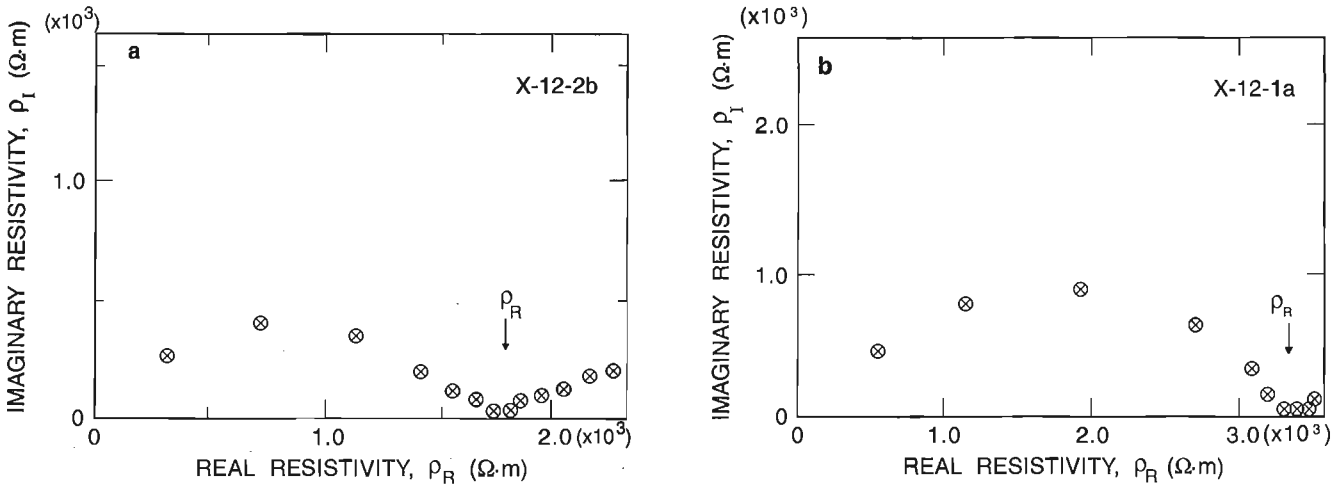

Figure 3. *Typical examples of complex resistivity (ρ^*) plots used to determine bulk electrical resistivity (ρ_r), where ρ_R and ρ_I are the real and imaginary resistivities (Katsube, 1975; Katsube and Walsh, 1987; Katsube and Salisbury, 1991). **a)** Imaginary resistivity (ρ_I) as function of real resistivity (ρ_R), for sample/specimen X-12-2bγ (24 hour saturation) displaying two suppressed arcs; one (left-hand side) representing the electrical characteristics of the rock sample, and the other (right-hand side) representing electrode polarization (EP). The EP is probably due to the combined effect of the current electrode of the measuring system and the sulphide minerals. Such patterns are normally seen in intermediate resistivity rocks. **b)** ρ_I as function of ρ_R, for sample/specimen X-12-1a (24 hour saturation) displaying a suppressed arc representing the electrical characteristics of the rock sample, a pattern usually seen in highly resistive rocks.*

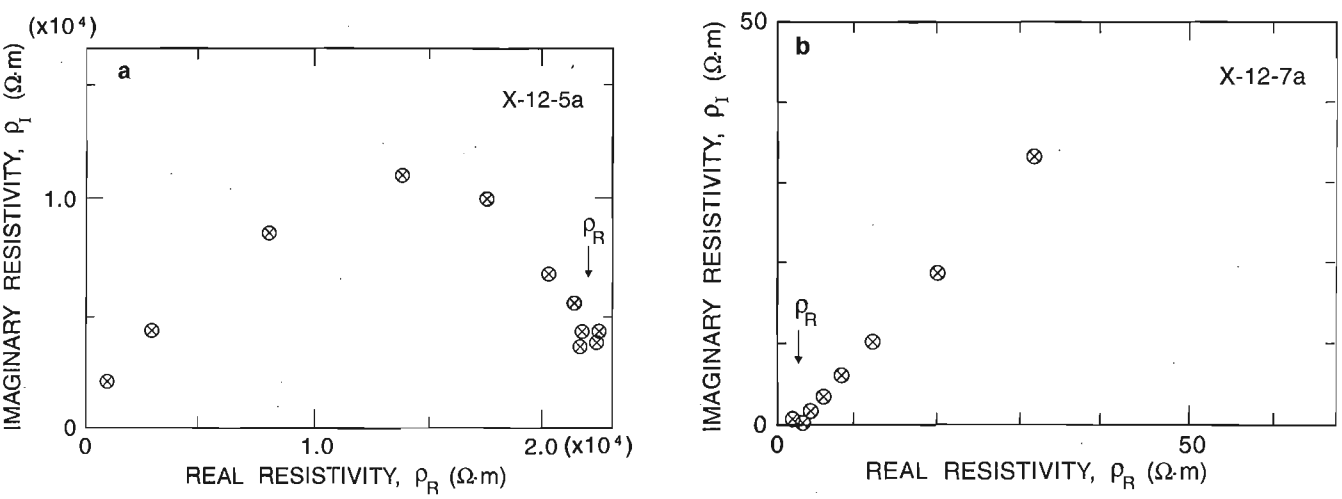

Figure 4. *Typical examples of complex resistivity (ρ^*) plots, for cases where difficulty is experienced in determining ρ_r; **a)** ρ_I as function of ρ_R, for sample/specimen X-12-5a (24 hour saturation) displaying a slightly distorted arc representing the electrical characteristics of the rock sample, a pattern commonly seen in extremely highly resistive rocks (Katsube et al., 1992). **b)** ρ_I as function of ρ_R for sample/specimen X-12-7a (48 hour saturation), displaying extensively suppressed arc (left-hand side) representing the electrical characteristics of the rock sample and a strong EP effect (right-hand side), a typical case where difficulty was experienced in determining ρ_r (Katsube et al., 1996c).*

The results of the electrical resistivity (ρ_r) measurements are listed in Table 4. Determinations have been made at 24 and 48 hours after water saturation, to check the stability of the ρ_r values with time. Under this state, it is expected that the distilled water has chemically equilibrated with the rock, and represents the in situ condition. Normally, differences up to ±20% of their mean are considered to be within measurement error and represent stable conditions. In the present study, many of the low resistivity values exceed that value (e.g. sample X-12-2, X-12-6), probably because they were below the measurement resolution. Twenty-nine determinations (including three-directional measurements) were made for 17 specimens, representing the 10 samples. Some examples of the complex resistivity plots used to determine the low to high values of ρ_r are shown in Figure 3 and 4. Details of this analytical procedure are described elsewhere (e.g. Katsube and Scromeda, 1994; Katsube et al., 1996c). Figure 3 displays typical examples of complex resistivity plots where no difficulties were experienced in determining ρ_r (specimens X-12-2b, X-12-1a). The error range of ρ_r for these cases are considered to be less than ±20%. Figure 4 displays typical examples of complex resistivity plots where difficulties were experienced in determining ρ_r (specimens X-12-5a, X-12-7a). Figure 4a displays a distorted arc, a pattern commonly seen in very highly resistive rocks (Katsube et al., 1992), which implies that the true ρ_r value is larger than that listed in Table 4. Figure 4b represents a case typical of low resistivity rocks where the electrode polarization (EP) effect is dominant, and considerable difficulty is experienced in determining ρ_r (Katsube et al., 1996c). The error ranges of ρ_r for such cases are considered to be more than ±100%.

The ρ_r values are in the range of $0.3\text{-}2\text{x}10^4$ Ω-m for these samples, the lower values resembling those of rocks containing relatively large amounts of sulphides (Keller, 1982), and the higher values being typical of crystalline rocks (Katsube and Hume, 1987, 1989; Katsube and Mareschal, 1993).

DISCUSSION

The two samples (X-12-4 and X-12-7) representing massive or semimassive sulphides display bulk electrical resistivity values (ρ_r) of less than 10 Ω-m (Table 4). No electrical anisotropy has been identified in these samples, probably due to the lack of resolution of the electrical measuring system at these low resistivities. The error range for ρ_r values less than 10 Ω-m is significant for the present electrical measuring system, thus the reduced resolution. The rest of the samples have inhomogeneities and anisotropies that can be reliably identified by this measuring system. The samples have been cut in ways and shapes to allow different electrical components (e.g. host rock, sulphide and nonsulphide veins, bedding; Fig. 2) of a sample to be characterized. The host rock component is considered to represent basic rock properties, and the other components are considered to be interferences in this study.

Sample X-12-5 (iron-formation) displays considerable electrical inhomogeneity, ranging from 150 Ω-m to 22 000 Ω-m (Table 4). The electrical resistivity (ρ_r) characteristics of this sample are represented by three specimens, X-12-5a, X-12-5b, and X-12-5c (Fig. 2a, Table 4). The ρ_r value for specimen X-12-5a (22 000 Ω-m, Table 4) represents the electrical resistivity of the iron-formation sample in the direction parallel to the foliation, but interrupted by a thin quartz vein (1 mm thick, Fig. 2a). Specimen X-12-5b is essentially a section of specimen X-12-5a without the interruption of the quartz vein, thus its ρ_r value (8900 Ω-m) represents the true electrical resistivity, in the direction of the bedding, of that sample. The ρ_r values for specimen X-12-5c represent the electrical resistivities of the same sample in all three directions (α=150, β=7400 and γ=5300 Ω-m). However, unlike most cases, the direction across the foliation or bedding (α-direction) shows the lowest electrical resistivity, for reasons not currently understood. It is therefore concluded that this sample is characterized by electrical resistivities of

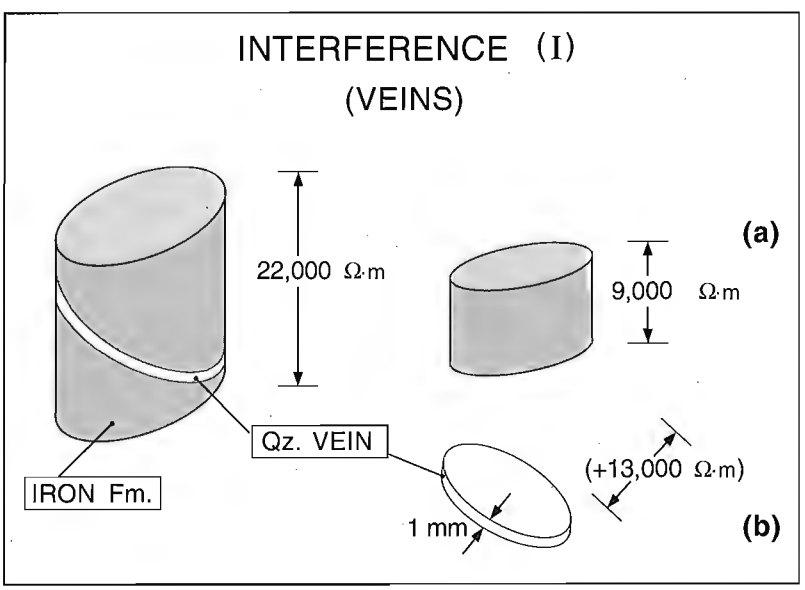

Figure 5.

*Block diagram presenting a simplified explanation for type I interference. A quartz vein (1 mm thick) cuts across an iron-formation sample, raising the electrical resistivity from 9000 Ω-m to 22 000 Ω-m: **a**)iron-formation without vein is 9000 Ω-m, and **b**) vein increased iron-formation resistivity by +13 000 Ω-m.*

150-8900 Ω-m, and that the thin quartz vein raises the electrical resistivity of the host rock by about 13 000 Ω-m. This is referred to as type I interference, and is diagrammatically explained in Figure 5. This implies that if this vein cuts across a conductive body (e.g. sulphide ore body) it could raise its resistivity from <5 Ω-m, as an example, to >10 000 Ω-m. Sample X-12-2, is also an iron-formation sample, which shows some electrical anisotropic characteristics (Tables 5, 6). However, no relationship to its geological characteristics are observed. Further thin section and scanning electron microscope (SEM) analysis is required to study the reason for the anisotropy.

Samples X-12-6 and X-12-7 are typical of rocks with thin veins which contain very fine- to medium-sized grains of sulphides (Fig. 2b). For example, sample X-12-6 has thin siliceous veins containing very fine sulphide grains. These two samples yield ρ_r values in the order of 5-50 Ω-m. The host

Table 5. Measured and interpreted electrical resistivity (ρ_r) ranges for rocks identified in the Brunswick number 12 hole 5175.

Rock types	Samples (X-12-)	TI	ρ_r (Ω-m)	
			Measured	Interpreted
Sulphides	4		0.3 - 7	<10 (0.3 - 2)
Hanging and footwall sediments	1, 8	II	600 - 4000	>10 000
Iron-formations	(2), 5	I, II, III	100 - 20 000	ρ_{rH} = 100 - 5000 ρ_{rV} = 7000 - 9000
Chloritized iron-formations	3, (6)	III	2 - 13 000	ρ_{rH} < 10 ρ_{rV} =12 000 - 13 000
Basement rocks	9, 10	II	600 - 2000	>10 000
Veinlets quartz sulphides	5 6, 7			+ 13 000

ρ_r = Bulk electrical resistivity
ρ_{rH} = Bulk electrical resistivity values taken in the direction parallel to the foliation or bedding
ρ_{rV} = Bulk electrical resistivity values taken perpendicular to the foliation or bedding
() = Samples that play minor role in the interpretation, due to significant interferences (type I, II, and III)
TI = Type of interferences, I, II, or III, observed

Table 6. Electrical resistivity anisotropy characteristics of iron-formation and chloritized iron-formation samples.

Sample No.	Specimen No.	ρ_{rH} (minimum)	ρ_{rV} (maximum)	λ
Iron-formation				
X-12-2	b	770	2300	3:1
	c	190	1400	7.5:1
X-12-5	c	150	7400	50:1
Chloritized iron-formation X-12-3	a	<10	13 000	1300:1

ρ_{rH} = Bulk electrical resistivity values taken in the direction parallel to the foliation or bedding
ρ_{rV} = Bulk electrical resistivity values taken perpendicular to the foliation or bedding
λ = Electrical resistivity anisotropy

rock of these two samples consists mostly of silicate material which is most likely derived from the chloritic iron-formation. Visual inspection suggests that the host rock may contain up to 1-5% of sulphides which are disconnected and are unlikely to have any effect of significance on the ρ_r values. From the previous (sample X-12-5, interference type I) and the next two studies (X-12-3, interference type III) the host rock is interpreted to have ρ_r values in the range of >10 000 Ω-m. Such resistivity values are typical for crystalline rocks of igneous or metamorphic origin (Katsube and Hume, 1989; Katsube and Mareschal, 1993). That is, these veins are reducing the ρ_r values to 1-50 Ω-m from >10 000 Ω-m. These effects are referred to as the type II interference. This model is explained diagrammatically in Figure 6. These low values (8-50 Ω-m), due to the veins, appear to depend more on the continuity of the sulphide mineral grains within the vein, rather than the number or thickness of the veinlets.

Sample/specimen X-12-3, from the chloritized iron-formation (Table 1, Fig. 2a), consists of interbedded, alternating sulphide-rich and silicate (barren of sulphides) layers. It displays a significant electrical anisotropy: 1-8 Ω-m in the directions parallel to the bedding and 12 000-13 000 Ω-m in the direction perpendicular to the bedding. It is interpreted that the sulphide-rich layers are the cause of the low resistivity, and the silicate layers the cause of the high resistivity. This type of arrangement of high and low resistivity layers is referred as the type III interference, and is diagrammatically

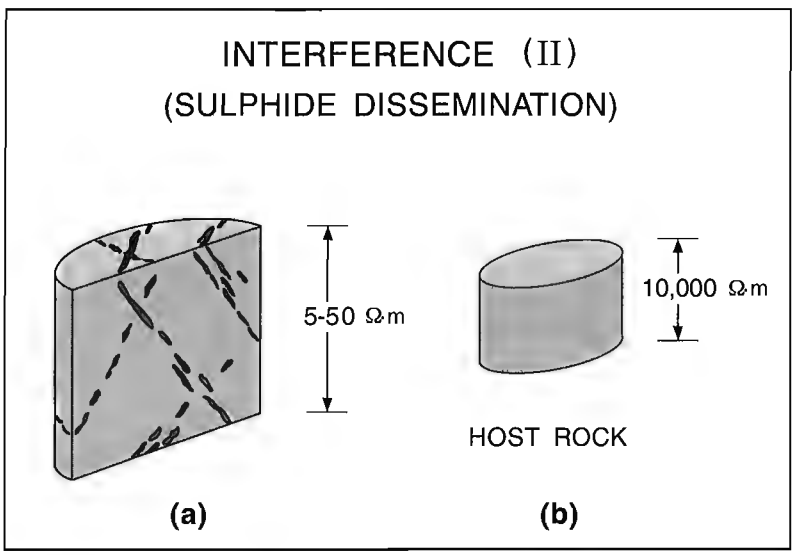

Figure 6.

Block diagram explaining type II interference. In this case, a number of thin veins (<1 mm thick) containing sulphides cut across metamorphosed footwall iron-formation rocks, reducing the ρ_r values from >10 000 Ω-m (estimated) to 5-50 Ω-m. These lower values (5-50 Ω-m) appear to depend more on the continuity of the sulphide mineral grains within the vein, rather than the number or thickness of the veins ***a****) host rock with sulphide veins: 5-50 Ω-m;* ***b****)host rock resistivity: 10 000 Ω-m.*

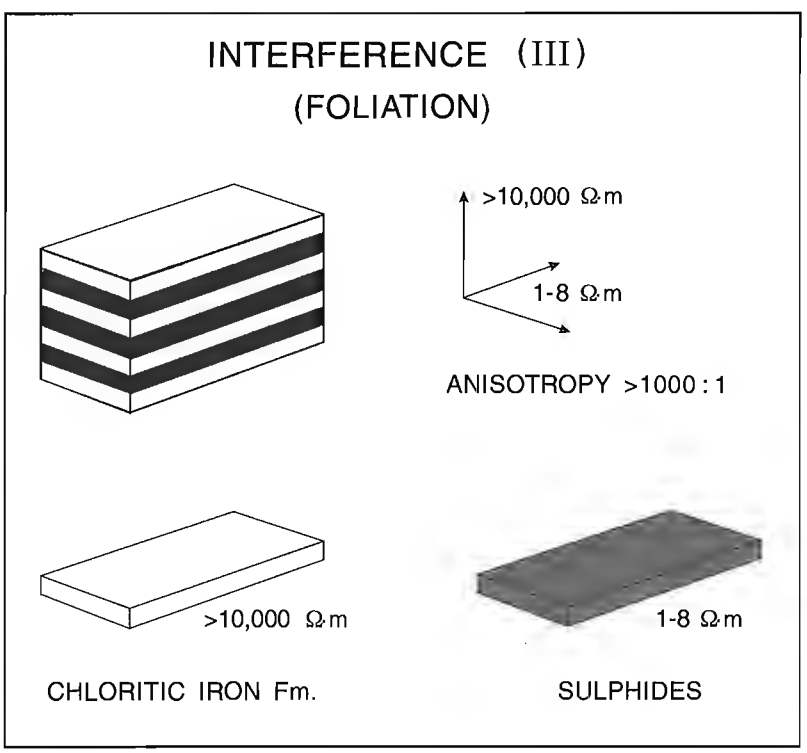

Figure 7.

Block diagram explaining the type III interference. This represents a case where strong directional effects are seen in the electrical resistivity distribution of a chloritized iron-formation sample. This sample/specimen consists of an interlayering of sulphide-rich material (1-8 Ω-m) and nonsulphide material (>10 000 Ω-m), resulting in electrical resistivities of 1-8 Ω-m in directions parallel to the foliation, and of >10 000 Ω-m in the direction vertical to the foliation.

portrayed in Figure 7. This implies an electrical anisotropy of greater than 1000:1, one of the largest reported to date (Katsube et al., 1996a, b, c).

The results of the interpretation of the electrical characteristics of these rocks, using the reported information on the electrical properties of crystalline rocks (Katsube and Hume, 1989; Katsube and Mareschal, 1993) and the three types of interferences observed in this study, are listed in Table 5. The first column lists the four rock types represented by the 10 samples investigated, and some of the electrical structural components of the rock (e.g., quartz and sulphide veins). The actual measured and the interpreted ranges of ρ_r values are listed in columns 4 and 5, respectively. The ρ_r values are interpreted to be <10 Ω-m for the sulphides, mainly based on the data for sample X-12-4 (Table 4). The ρ_r values for the hanging and footwall sediments and the basement rocks are both interpreted to be >10 000 Ω-m, considerably larger than the actually measured values (600-4000 and 600-2000 Ω-m, respectively). This is due to the significant effects of interference type II (sulphide veins), which has reduced ρ_r. Such values (>10 000 Ω-m) are very common for crystalline and metamorphic rocks of the types that our samples represent (Katsube and Hume, 1989; Katsube and Mareschal, 1993). The range of measured ρ_r values (100-20 000 Ω-m) is larger than those of the interpreted ρ_{rH} and ρ_{rV} values (100-9000 Ω-m) for the iron-formation, due to the elimination of the interference type I which had raised the resistivity considerably. The ρ_{rH} and ρ_{rV} represent bulk electrical resistivities taken in the directions parallel and perpendicular to the foliation or bedding.

The electrical resistivity anisotropy (λ) has been determined for samples that show such characteristics (iron-formation and chloritized iron-formation), and the results are listed in Table 6. The parameter λ is determined by dividing the largest ρ_r value by the smallest one. For example

$$\lambda = 7440/150{:}1 \approx 50{:}1,$$

for sample/specimen X-12-5c (Tables 4, 6). The massive sulphide sample (X-12-4) also displays anisotropic characteristics (Table 4). However, since the values for all directions are less than 10 Ω-m, below the resolution of the measuring system, it has not been included in the λ calculations. The results indicate that λ is 3:1 to 50:1 for the iron-formation, and 1300:1 for the chloritized iron-formation. The latter is one of the largest reported to date (Katsube et al., 1996a, b, c).

CONCLUSIONS

The results of this study indicate that the electrical resistivities (ρ_r) for mineralized rocks and nonmineralized host rocks (hanging and footwall sediments, iron-formation, chloritized iron-formation, and basement rocks) are in the ranges of 0.3-10 Ω-m and 7000 to >10 000 Ω-m, respectively. However, the range of values for the host rocks can be influenced by three types of interferences: type I, type II, and type III, resulting in the actual measured range of ρ_r values being larger (2-20 000 Ω-m, Table 5). Interference type I signifies the presence of thin (about 1 mm) quartz veins, a single one of which could raise the ρ_r by 13 000 Ω-m. In type II interference, the thin veins (e.g. quartz) contain fine- to medium-sized sulphide grains, which can reduce the ρ_r values to 5-50 Ω-m from host rock ρ_r values of >10 000 Ω-m. Type III interference is characterized by electrical anisotropy effects that can be as high as 1000:1 or larger. A maximum ρ_r of 12 000 to 13 000 Ω-m and a minimum ρ_r of <10 Ω-m have been measured.

These results contribute to progress in our understanding of the quantitative effects of electrical structural components of a rock, such as quartz veins, sulphide veins, and anisotropy. Studies using petrographic thin section and scanning electron microscope analyses are necessary to understand the relationship between electrical, mineralogical, and textural characteristics.

ACKNOWLEDGMENTS

The authors thank S. Connell (GSC) for assisting the geological examination of the samples used in this study. The authors are grateful for the critical review of this paper and for the very useful suggestions by M.D. Thomas (GSC).

REFERENCES

API (American Petroleum Institute)
1960: Recommended practices for core-analysis procedure: API Recommended Practice 40 (RP 40) First Edition, American Petroleum Institute, Washington, D.C., p. 55.

Daly, R.A., Manger, E.G., and Clark, S.P., Jr.
1966: Density of rocks; Section 4 in Handbook of Physical Constants; The Geological Society of America, Inc., Memoir 97, p. 19-26.

Katsube, T.J.
1975: The electrical polarization mechanism model for moist rocks; in Report of Activities, Part C; Geological Survey of Canada, Paper 75-1C, p. 353-360.

Katsube, T.J. and Hume, J.P.
1987: Electrical properties of granitic rocks in Lac du Bonnet batholith; in Geotechnical Studies at Whiteshell Research Area (RA-3), CANMET, Report MRL 87-52, p. 205-220.
1989: Electrical resistivity of rocks from Chalk River; in Workshop Proceedings on "Geophysical and Related Geoscientific Research at Chalk River, Ontario", Atomic Energy of Canada Limited Report AECL-9085, p. 105-114.

Katsube, T.J. and Mareschal, M.
1993: Petrophysical model of deep electrical conductors; graphite lining as a source and its disconnection due to uplift; Journal of Geophysical Research, v. 98, no. B5, p. 8019-8030.

Katsube, T.J. and Salisbury, M.
1991: Petrophysical characteristics of surface core samples from the Sudbury structure; in Current Research, Part E; Geological Survey of Canada, Paper 91-1E, p. 265-271.

Katsube, T.J. and Scromeda, N.
1994: Physical properties of Canadian kimberlites, Somerset Island, Northwest Territories and Saskatchewan; in Current Research 1994-B; Geological Survey of Canada, p. 35-42.
1995: Accuracy of low porosity measurements in granite; in Current Research 1995-C; Geological Survey of Canada, p. 265-270.

Katsube, T.J. and Walsh, J.B.
1987: Effective aperture for fluid flow in microcracks; International Journal of Rock Mechanics and Mining Sciences and Geomechanics Abstracts, v. 24, p. 175-183.

Katsube, T.J., Best, M.E., and Mudford, B.S.
1991: Petrophysical characteristics of shales from the Scotian shelf; Geophysics, v. 56, p. 1681-1689.

Katsube, T.J., Scromeda, N., Mareschal, M., and Bailey, R.C.
1992: Electrical resistivity and porosity of crystalline rock samples from the Kapuskasing Structural Zone, Ontario; in Current Research, Part E; Geological Survey of Canada, Paper 92-1E, p. 225-236.

Katsube, T.J., Best, M., and Jones, A.G.
1996a: Electrical anisotropy of mineralized and non mineralized rocks; in Society of Exploration Geophysicists Expanded Abstracts with Authors' Biographies, Technical Program, 66th Annual Meeting and International Exhibition (Denver, November 10-15, 1996), Volume II, p. 1279-1281.

Katsube, T.J., Jones, A.G., Scromeda, N., and Schwann, P.
1996b: Electrical characteristics of rock samples from the La Ronge Domain of the Trans-Hudson Orogen, northern Saskatchewan; in Current Research 1996-E; Geological Survey of Canada, p. 159-169.

Katsube, T.J., Palacky, G.J., Sangster, D.F., Galley, A.G., and Scromeda, N.
1996c: Electrical properties of disseminated sulphide ore samples from Snow Lake; in EXTECH I: A Multidisciplinary Approach to Massive Sulphide Research in Rusty Lake-Snow Lake Greenstone Belts, Manitoba, (ed.) G.F. Bonham-Carter, A.G. Galley, and G.E.M. Hall; Geological Survey of Canada, Bulletin 426, p. 319-329.

Keller, G.V.
1982: Electrical properties of rocks and minerals: in Handbook of Physical Properties of Rocks, Volume I (ed.) R.S. Carmichael; CRC Press, Inc., Florida, p. 217-293.

Scromeda, N. and Katsube, T.J.
1994: Effect of temperature on drying procedures used in porosity measurements of tight rocks; in Current Research 1994-E; Geological Survey of Canada, p. 283-289.

Thomas, M.D.
1995: Rock property measurements in support of Extech-II gravity and magnetic studies, Bathurst Mining Camp in Geoscience Research 1994, (comp., ed.) J.P. Langton, New Brunswick Department of Natural Resources and Energy, Minerals and Energy Division, Miscellaneous Report 15, p. 70-77.

Geological Survey of Canada Project 870057

Predicted permafrost distribution in Canada under a climate warming scenario

I.M. Kettles, C. Tarnocai[1], and S.D. Bauke[2]
Terrain Sciences Division, Ottawa

Kettles, I.M., Tarnocai, C., and Bauke, S.D., 1997: Predicted permafrost distribution in Canada under a climate warming scenario; in Current Research 1997-E; Geological Survey of Canada, p. 109-115.

Abstract: Information on present-day permafrost distribution in Canada and on its expected distribution after climate warming was needed to produce the peatland component of a climate change atlas presently being compiled at the Geological Survey of Canada. For this purpose, maps of Canada showing present and predicted distribution of permafrost in four zones – continuous, widespread, sporadic, and localized – were generated, based on existing compilations made by other scientists. Using GIS techniques, the maps of present and predicted distribution were overlaid to produce a derivative map showing predicted changes in permafrost conditions. Calculations based on the derivative map show that the extent of land underlain directly by permafrost is presently estimated at 4 065 200 km^2 or 42% of the total surface area of Canada, and with climate warming it is expected to be reduced to 2 333 800 km^2 or 24%. This represents an expected change of 43% in the proportion of surface area underlain directly by permafrost.

Résumé : On a recueilli des données sur la répartition actuelle du pergélisol au Canada et sur sa répartition prévue compte tenu du réchauffement climatique, afin de produire la section sur les tourbières d'un atlas des changements climatiques auquel la Commission géologique du Canada travaille actuellement. À partir des données déjà compilées par d'autres chercheurs, on a dressé des cartes du Canada qui représentent la répartition actuelle et prévue du pergélisol selon une division en quatre zones : pergélisol continu, pergélisol étendu, pergélisol sporadique et pergélisol localisé. Au moyen de systèmes d'information géographique, les chercheurs ont superposé les cartes de répartition actuelle et de répartition prévue pour obtenir une représentation des variations prévues de l'état du pergélisol. Les calculs effectués à partir de cette carte dérivée indiquent que la superficie des terres reposant directement sur du pergélisol est actuellement estimée à 4 065 200 km^2, soit 42 % de la superficie totale du Canada, et que, sous l'effet du réchauffement climatique, elle baisserait à 2 333 800 km^2, soit 24 % de la superficie totale. La variation prévue de la proportion de la superficie reposant directement sur du pergélisol se chiffre donc à 43 %

[1] Agriculture and Agri-Food Canada Research Branch, K.W. Neatby Bldg., 960 Carling Ave., Ottawa, Ontario K1A 0C6
[2] 3310 Southgate Rd., Ottawa, Ontario K1V 8X4

INTRODUCTION

The Geological Survey of Canada is currently preparing an atlas showing the probable impact of climate warming on major depositional processes affecting the Canadian landmass. Peatlands were identified as an important component of the atlas because they cover 12% of Canada's land area. Peatland distribution was examined and estimates were made concerning peatland sensitivity to the effects of the climate change predicted to result from doubling of atmospheric CO_2 levels.

Peatlands occur in all permafrost areas. In fact, along the southern boundary of the permafrost region, the first occurrence of permafrost is in the peatlands. Permafrost is thus a very important factor affecting peatland processes in the permafrost region, and any changes in permafrost conditions will affect these peat deposits (Zoltai, 1988). Climate warming will severely alter peatland processes, especially in perennially frozen peatlands. Some areas that now fix carbon will begin to emit carbon in the form of greenhouse gases as peat materials thaw and decompose.

The interrelationships between permafrost and peatlands made it necessary to examine the permafrost changes resulting from climate warming predicted by various researchers (Woo et al., 1992; Zoltai, 1995; Anisimov and Nelson, 1996). Because the permafrost distribution maps produced by these researchers differed in some areas and, in some cases, were inadequate when applied to peatlands, it was necessary to develop a modified $2xCO_2$ permafrost distribution map for this study. In this paper, the following subjects are addressed: 1) existing data about the present and predicted permafrost distribution are examined; 2) modified maps of present and predicted permafrost distribution in Canada are generated, based on existing maps compiled by other scientists; 3) the modified present and predicted permafrost distribution maps were overlaid in a GIS environment to produce a new derivative map showing expected changes in permafrost conditions; and 4) using GIS methods, the present areal distribution of permafrost in Canada is estimated and the expected area of permafrost resulting from climate warming is predicted.

PERMAFROST IN CANADA

Permafrost is defined as a state of the ground where ground temperatures in soil or rock remain at, or below, a temperature of 0°C for at least two years (National Research Council, 1988). In Canada, however, most permafrost has existed for a long time. In the permafrost region, the upper part of the ground which thaws each summer is called the active layer. It ranges in thickness from more than 1.5 m in some subarctic and continental regions, to 15-30 cm in arctic regions (French, 1989). The position of the base of permafrost is controlled by the balance between heat from the Earth's interior and cold air conditions at the ground surface (Heginbottom et al., 1995). Permafrost ranges in thicknesses from 0.5 m or less in subarctic and continental regions, to occurrences of hundreds of metres in the high arctic.

At present in Canada, there is a latitudinal zonation in the occurrence and thickness of permafrost; permafrost becomes thicker and more continuous with increasing latitude (Brown, 1967, 1970; Zoltai, 1995). This suggests that climate is the most important control on distribution (Brown, 1967; Zoltai, 1995) but distribution is also affected by local climate, topography, geology, and vegetation (Heginbottom et al., 1995). Zoltai (1995) recognized four permafrost zones, which he described with respect to permafrost development in peatlands:

1. Localized permafrost zone (LPZ) – permafrost occurs as small isolated lenses in peat that reach into the mineral substrate only under palsas. (Palsas and other peat landforms are described in Zoltai (1988)).
2. Sporadic permafrost zone (SPZ) – permafrost occurs more frequently in bogs or as isolated occurrences in minerotrophic fens. In this zone, however, more peatlands are unfrozen than frozen. Permafrost reaches the mineral soil beneath palsas and peat plateaus.
3. Widespread permafrost zone (WPZ) – most peatlands are permanently frozen, but there are unfrozen fens and shallow lakes are free of permafrost.
4. Continuous permafrost zone (CPZ) – all land surfaces and even shallow ponds or lakes are underlain by permafrost.

Similar zones are portrayed in the National Atlas map of present permafrost distribution (Heginbottom et al., 1995) although they are named differently. In that atlas, there are estimates of the proportion of land area affected by permafrost within each of the four zones – LPZ: 0-10%; SPZ:10-50%; WPZ: 50-90%; and CPZ: 90-100%.

PRESENT-DAY PERMAFROST DISTRIBUTION

There are two recent compilations of present-day permafrost distribution. The National Atlas compilation (Heginbottom et al., 1995), was based on a framework of physiographic units described by Bostock (1970), with pertinent and available information related to permafrost being considered for each unit. In compiling this map, it was assumed that the variability in all geological conditions within a physiographic unit was less than the variability between adjacent units (Heginbottom and Dubreuil, 1993). Zoltai (1995, Fig. 1) generated a present-day permafrost distribution map for the western Canada based on drill core and other field data collected by himself and others.

The boundaries of the different permafrost zones for the two compilations are mostly similar for the Northwest Territories and Yukon. Further south, however, Zoltai's compilation is more detailed for northern Alberta and differs from the National Atlas compilation (Heginbottom et al., 1995) for some parts of northern Saskatchewan and northern Manitoba, in areas where Zoltai's compilation is based on data from numerous boreholes. In the compilation showing present-day permafrost distribution in this report (Fig. 1), Zoltai's map was used to generate permafrost zone boundaries for areas of

western Canada and boundaries for the remaining areas were based on the National Atlas compilation (Heginbottom et al., 1995).

PREDICTED PERMAFROST DISTRIBUTION WITH A DOUBLING OF ATMOSPHERIC CO_2 LEVELS

Some estimates of changes in permafrost distribution resulting from warmer climatic conditions have been deduced using empirical reconstructions based on proxy data (Zoltai, 1995) and by manipulating $2xCO_2$ global circulation models (GCMs) (Woo et al., 1992; Anisimov and Nelson, 1996). Zoltai (1995, Fig. 3) produced a tentative map of permafrost distribution in peatlands in western Canada 6000 years ago, during the period of warmer climate which followed the disappearance of glacial ice from North America. His reconstruction is based on data from macrofossil analysis and radiocarbon dating of peat cores, which indicate whether permafrost was present or absent at the time of peat formation. He also indicated that some cautious paleoclimate implications might be drawn from the reconstructed permafrost distribution for 6000 years ago. Based on the positions of present and past boundaries of the permafrost zones, and the present mean annual temperatures for the region, he suggested that the mean annual temperatures were about 5°C warmer than at present. This temperature increase is close to the one predicted to occur in the same region as a result of the doubling of atmospheric CO_2 levels (Houghton et al., 1996, p. 42-43).

Woo et al. (1992) generated a diagram showing projected shifts in the boundaries of discontinuous and continuous permafrost resulting from a surface temperature change of 4-5°C. In their analysis, they assumed that the predicted temperature change will cause a spatially uniform increase in surface temperature of the same magnitude, and have superimposed this increase on current ground temperatures to

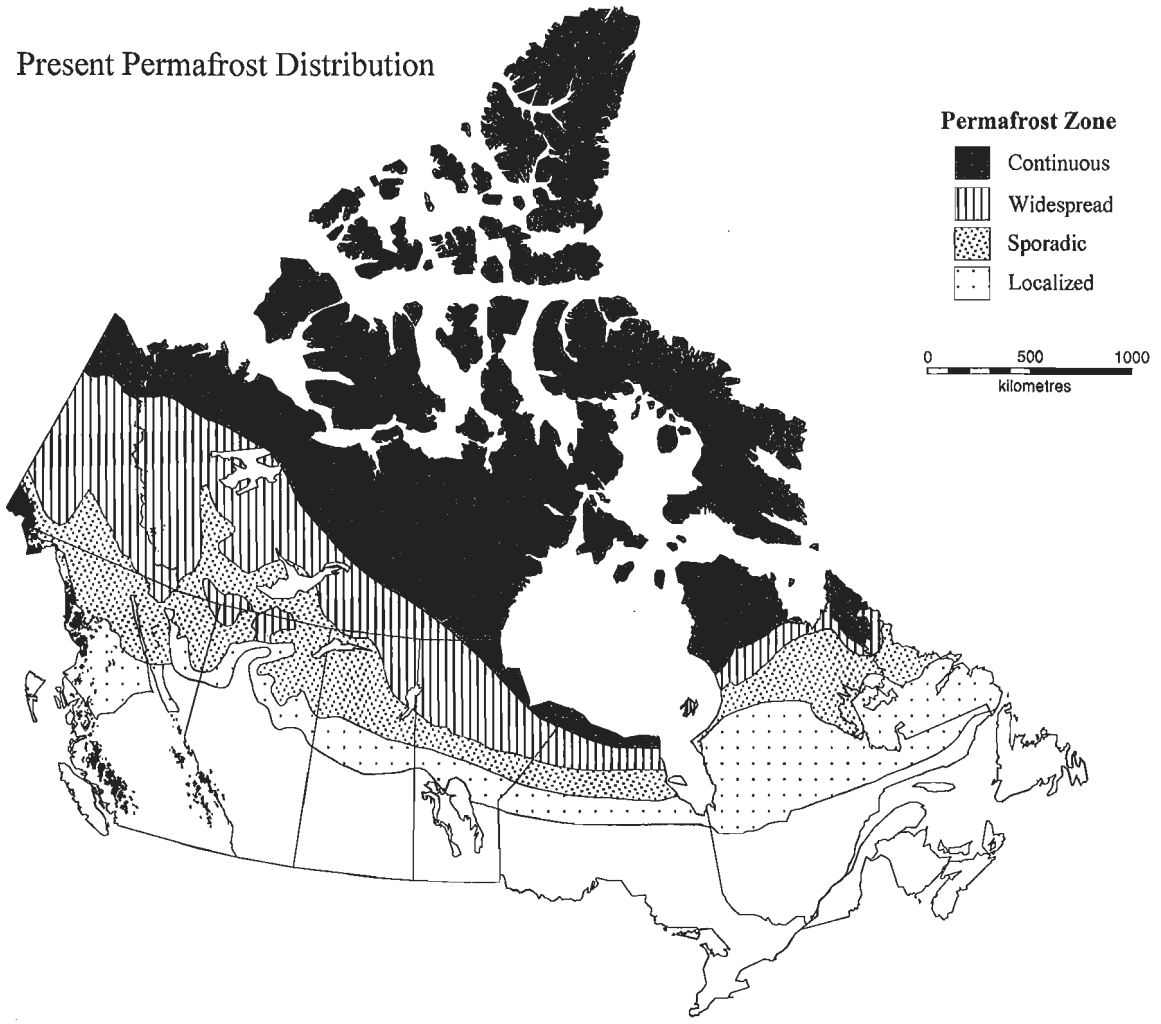

Figure 1. Map showing present distribution of permafrost, based on Heginbottom et al. (1995) and Zoltai (1995, Fig. 2). Glacier cover is shown in black.

produce their map. As a result, their new boundaries are equilibrium positions where it is assumed that there is no change in other climatic factors or vegetation.

More recently, another analysis was undertaken by Anisimov and Nelson (1996) to predict permafrost distribution in northern circumpolar regions, based on a 2°C global warming. In their study, they manipulated three GCMs and an empirical paleoreconstruction, based on paleobotanical and paleogeological data, and produced maps showing the new positions of permafrost boundaries. Four permafrost zones were identified which are similar to the CPZ, WPZ, SPZ, and LPZ. In their maps showing predicted permafrost distributions, the positions of specific permafrost zones, based on the three GCM scenarios, appear to correspond in most areas. When compared to Zoltai's projections (1995), the positions of the CPZ and WPZ boundaries seem similar in many areas, but there is less correspondence between the predicted southern limits of the SPZ and LPZ. The southern limits of the SPZ and LPZ appear to lie more than 150 km further south in the projections of Anisimov and Nelson (1996).

The map showing predicted permafrost distribution in this report (Fig. 2) is based on the reconstructions of Zoltai (1995) for Northwest Territories, Alberta, Saskatchewan, and Manitoba, and on the predictions of Anisimov and Nelson (1996) elsewhere in Canada. Some modifications were made to Anisimov's and Nelson's projections in small areas in northern Quebec, Baffin Island, and northern British Columbia, based on altitude and local geology. In addition, the southern limit of the LPZ in northwestern Ontario reflects Zoltai's compilation rather than the predictions of Anisimov and Nelson because Zoltai's LPZ boundary is based on data for numerous boreholes in adjacent areas of northeastern Manitoba.

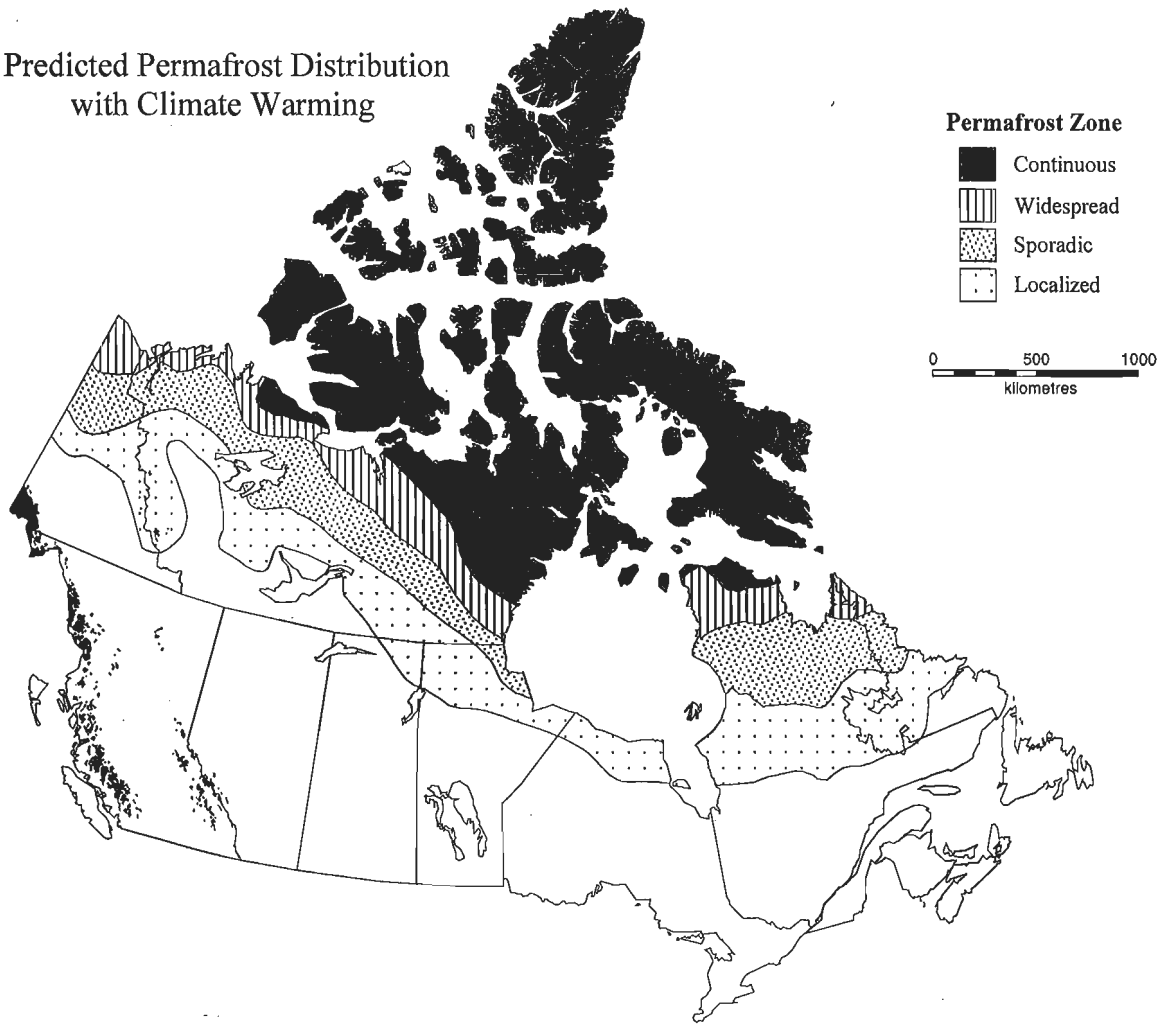

Figure 2. *Map showing the predicted distribution of permafrost resulting from climate warming, based on Zoltai (1995) and Anisimov and Nelson (1996). Glacier cover is shown in black.*

PREDICTED CHANGE IN PERMAFROST DISTRIBUTION

The predicted shifts in the distribution of permafrost within the four zones are shown in Figure 3. The most pronounced changes are expected to occur in the northern areas of the western provinces and the southern Northwest Territories and southern Yukon. The southern limits of discontinuous and continuous permafrost are expected to migrate more than 300 km northward in many areas.

In order to better assess the magnitude of the expected change, some calculations were made (Table 1), based on the compilations generated for this report (Fig. 1 to 3). As previously mentioned, the actual areal extent of land underlain by permafrost within zones varies from zone to zone, ranging from 0-10% in LPZ to 90-100% in CPZ (Heginbottom et al., 1995). For calculation purposes we have assumed the following:

1. Glaciers were considered as nonpermafrost areas and their distribution is assumed to be unchanged after climate warming. Although the alpine glaciers are expected to shrink in some areas, there are many uncertainties in predicting the effects of climate warming on their distribution (Warwick et al., 1996). In addition, the changes in glacier distribution are expected to have a very minor effect on peatland distribution and processes.
2. The percentage of land underlain by permafrost within the LPZ is 5%, the SPZ is 30%, the WPZ is 70%, and the CPZ is 100%. The first three figures represent the midpoint of the range of percentages suggested by Heginbottom et al. (1995) for the proportion of the land surface underlain by permafrost in each of the four zones.

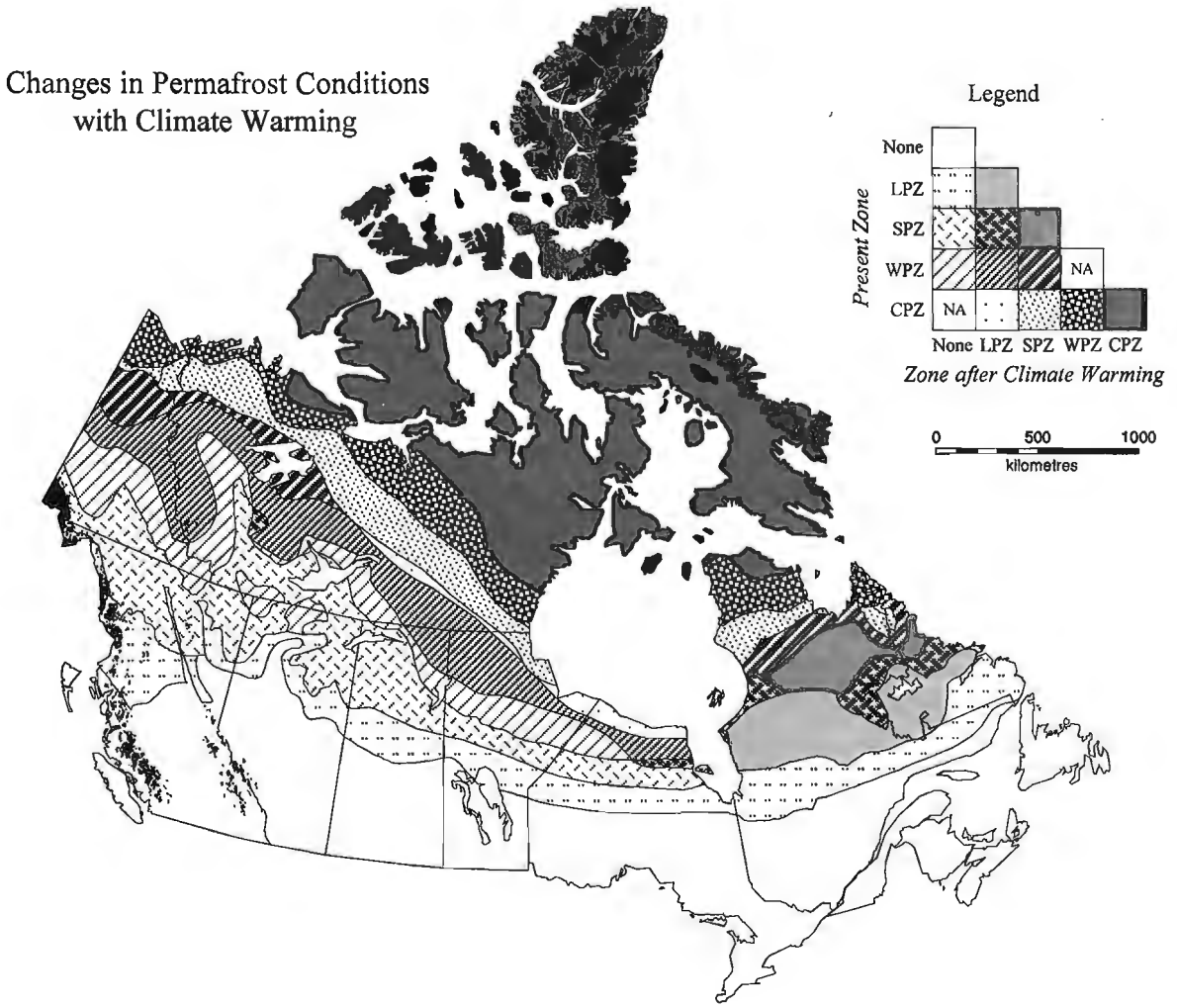

Figure 3. *Map showing the predicted shifts in permafrost zones, based on compilations in Figures 1 and 2. For example, the part of the present SPZ portrayed in a solid grey colour remains unchanged (SPZ), while the portion shown with a heavy crosshatch pattern changes to LPZ and the part with light crosshatching becomes permafrost-free. Glacier cover is shown in black.*

Results show that the extent of land underlain directly by permafrost is presently estimated at 4 065 200 km^2 or at 42% of the total landmass and with climate warming it is expected to be reduced to 2 333 800 km^2 or 24%. This represents an expected loss in surface area underlain by permafrost of 43%. On this basis, the discontinuous permafrost zones seem to be most affected by the expected warming. The surface area of land underlain by permafrost is expected to decrease by 90% in the WPZ, 84% in the SPZ, and 71% in the LPZ (Table 1). Continuously frozen areas (CPZ) are expected to become 19% less extensive.

SUMMARY

Several existing compilations of permafrost distribution based on fieldwork, proxy data, and global circulation models were utilized to produce new compilations showing present-day permafrost distribution, predicted permafrost distribution resulting from climate warming, and the predicted changes in permafrost conditions. The new compilations were analyzed, using GIS methods, to give an estimate the magnitude of the change expected in Canada's permafrost region resulting from the expected climate warming. Results

Table 1. Areas of present and predicted permafrost distribution with predicted climate warming, (based on Fig. 3).

Present Pf or other zone	Total surface area covered by present zone[1] (km^2)	Expected change in present Pf zone	Total surface area of subzone[3] (km^2)	Surface area of lakes[4]	Surface area adjusted for lake cover (km^2)	Present surface area underlain by Pf[5] (km^2)	Predicted surface area underlain by Pf after climate warming[5] (km^2)	Loss of surface area underlain by Pf (%)
CPZ	2 937 600							
		CPZ to CPZ	1 756 400	37 700	1 718 700	1 718 700	1 718 700	0
		CPZ to WPZ	455 000	14 100	440 900	440 900	308 600	30
		CPZ to SPZ	467 400	28 200	439 200	439 200	131 800	70
		CPZ to LPZ	88 200	3 000	85 200	85 200	4 300	95
		Glaciers in CPZ[2]	170 600					
		Total	2 937 600			2 684 000	2 163 400	19
WPZ	1 504 400							
		WPZ to SPZ	255 700	30 600	225 100	157 600	67 500	57
		WPZ to LPZ	691 900	36 400	655 500	458 900	32 800	93
		WPZ to Pf-free	556 300	24 200	532 100	372 500	0	100
		Glaciers in WPZ	500					
		Total	1 504 400			989 000	100 300	90
SPZ	1 205 600							
		SPZ to SPZ	161 400	5 800	155 600	46 700	46 700	0
		SPZ to LPZ	132 200	4 800	127 400	38 200	6 400	83
		SPZ to Pf-free	895 100	63 000	832 100	249 600	0	100
		Glaciers in SPZ	16 900					
		Total for SPZ	1 205 600			334 500	53 100	84
LPZ	1 244 700							
		LPZ to LPZ	367 000	27 000	340 000	17 000	17 000	0
		LPZ to Pf-free	860 500	46 100	814 400	40 700	0	100
		Glaciers in LPZ	17 200					
		Total	1 244 700			57 700	17 000	71
Pf-free	2 879 200							
		Pf-free to Pf-free	2 860 200	181 100	2 679 100	0	0	0
		Glaciers in Pf-free	19 000					
		Total	2 879 200		2 679 100			
To tal	9 771 500		9 771 500	502 000	9 269 500	4 065 200	2 333 800	43
Proportion of total area of Canada underlain directly by permafrost							42 %	
Proportion of total area of Canada expected to be underlain directly by permafrost after climate warming							24 %	
Predicted change in proportion of surface area underlain directly by permafrost							43 %	

For calculation purposes:

[1] Area including lakes and glaciers

[2] Glaciers are not considered permafrost areas and their distribution is assumed to be unchanged after climate warming

[3] Area of permafrost zones includes lakes

[4] Area adjusted, based on National Atlas of Canada digital base (1: 7 500 000)

[5] Actual areal extent of permfrost within permafrost zones: CPZ – 100%; WPZ – 70%; SPZ – 30%; and LPZ – 5%.

Abbreviations: Pf – permafrost
Permafrost Zones: CPZ – continuous; WPZ – widespread; SPZ – sporadic; and LPZ – localized

show that 43% of the estimated 4 065 200 km^2 of surface area presently underlain by permafrost is expected to become permafrost-free. Areas of discontinuous permafrost are expected to be most severely affected. Permafrost may disappear from 90%, 84%, and 71% of the surface area presently affected in the widespread, sporadic, and localized permafrost zones, respectively.

ACKNOWLEDGMENTS

The authors wish to thank J.A. Heginbottom for reviewing this manuscript; F. Nelson for providing a permafrost map at a larger scale; and R. Fulton and L. Halsey for some helpful advice.

REFERENCES

Anisimov, O.A. and Nelson, F.E.
1996: Permafrost distribution in the northern hemisphere under scenarios of climatic change; Global and Planetary Change, v. 14, p. 59-72.

Bostock, H.S.
1970: Physiographic regions of Canada; Geological Survey of Canada, Map 1254A; scale 1:5 000 000.

Brown, R.J.E.
1967: Permafrost in Canada; University of Toronto Press, Toronto, 234 p.
1970: Permafrost in Canada; National Research Council Publication 9769 and Geological Survey of Canada Map 1246A, scale 1:7 603 200.

French, H.M.
1989: Cold climate processes; in Chapter 9 of Quaternary Geology of Canada and Greenland, (ed.) R.J. Fulton ; Geological Survey of Canada, no. 1, (also Geological Society of America, The Geology of North America, v. K-1), p. 604-615.

Heginbottom, J.A. and Dubreuil, M-A.
1993: A new permafrost and ground ice map for the National Atlas of Canada; in Permafrost: Proceedings of the 6th International Conference, Beijing; p. 255-260.

Heginbottom, J.A., Dubreuil, M-A, and Harker, P.A. (comp.)
1995: Canada - Permafrost; National Atlas of Canada, Natural Resources of Canada, Ottawa (MCR 4177).

Houghton, J.T., Meira Filho, L.G., Callandar, B.A., Harris, N., Kattenberg, A., and Maskell, K. (ed.)
1996: Technical summary; in Climate Change 1995, Contribution of WGI to the Second Assessment Report of the Intergovernmental Panel on Climate Change; Cambridge University Press, Great Britain, 572 p.

National Research Council, Canada, Permafrost Subcommittee
1988: Glossary of permafrost and related ground ice terms; Technical Memorandum No. 142, National Research Council Canada, Ottawa, 156 p.

Warwick, R.A., LeProvost, C., Meier, M.F, J. Oerlemans, and Woodworth, P.L.
1996: Changes in sea level; in Chapter 7 in Climate Change 1995, (ed.) J.T. Houghton, L.G. Meira Filho, B.A. Callandar, N. Harris, A. Kattenberg, and K. Maskell; Cambridge University Press, Great Britain, p. 359-406.

Woo, M., Lewkowicz, A.G., and Rouse, W.R.
1992: Response of the Canadian permafrost environment to climatic change; Physical Geography, v. 13, p. 287-317.

Zoltai, S.C.
1988: Wetland environments and classification; in Wetlands of Canada, (ed.) National Wetlands Working Group, Canada Committee on Ecological Land Classification; Environment Canada, Ecological Land Classification Series, No. 24, 454 p.
1995: Permafrost distribution in peatlands of west-central Canada during the Holocene warm period 6000 years BP; Geographie physique et Quaternarie, v. 49, p. 45-54.

Geological Survey of Canada Project 930040

Pore surface area characteristics of the Nolichucky Shale within the Oak Ridge Reservation (Tennessee, U.S.A.): implication for fluid expulsion efficiency

T.J. Katsube, J. Dorsch[1], and S. Connell
Mineral Resources Division, Ottawa

Katsube, T.J., Dorsch, J., and Connell, S., 1997: Pore surface area characteristics of the Nolichucky Shale within the Oak Ridge Reservation (Tennessee, U.S.A.): implication for fluid expulsion efficiency; in Current Research 1997-E; Geological Survey of Canada, p. 117-124.

Abstract: Pore-surface area characteristics, represented by the relationship between residual porosity ratio and pore-surface area (ϕ_{rr}-A), have been determined for mudrock samples from the Nolichucky Shale on the Oak Ridge Reservation (Tennessee, U.S.A.) and for samples of mudrock-saprolite developed from these shales. The purpose is to obtain important petrophysical information, required for petroleum exploration and assessment of barrier quality to contaminant migration.

Results indicate that the ϕ_{rr}-A relationship for fresh mudrock and mudrock fragments from the saprolite is positive, implying that these Cambrian shales are likely mature and have undergone considerable diagenesis. The mudrock saprolite groundmass samples display a ϕ_{rr}-A relationship which is zero to slightly negative, suggesting likely most pore cement has been dissolved to the extent that the original grains have lost most of their cement coating, effectively displaying characteristics of an immature sedimentary rock.

Résumé : Les caractéristiques de la surface des pores, représentées par la relation entre l'indice de porosité résiduelle et la surface des pores (ϕ_{rr} - A), ont été déterminées pour des échantillons de mudrock prélevés dans le Shale de Nolichucky, dans l'Oak Ridge Reservation (Tennessee, États-Unis), et pour des échantillons de saprolite à mudrock dérivé de ces shales. L'objectif visé consiste à obtenir des renseignements pétrophysiques importants qui sont nécessaires à l'exploration pétrolière et à l'évaluation des propriétés des roches aptes à confiner la migration des contaminants.

Les résultats indiquent que la relation ϕ_{rr} - A pour les mudrocks non altérés et pour les fragments de mudrock provenant du saprolite est positive, ce qui implique que ces shales cambriens sont probablement matures et ont subi une diagenèse poussée. Les échantillons de matrice du saprolite à mudrock présentent une relation ϕ_{rr} - A variant de nulle à légèrement négative, ce qui suggère que la plus grande partie du ciment interstitiel a très probablement été dissoute à tel point que les grains d'origine ont perdu l'essentiel de leur enduit de ciment, propriété caractéristique d'une roche sédimentaire immature.

[1] Oak Ridge National Laboratory, P.O. Box 2008, Oak Ridge, Tennessee, U.S.A. 37831-6400

INTRODUCTION

Pore-surface area characteristics have been determined for a set of samples of mudrock from the Nolichucky Shale of the Bear Creek Valley on the Oak Ridge Reservation (ORR, Tennessee, U.S.A.) and for samples of mudrock-saprolite developed from these shales. These characteristics are represented by the relationship between the storage/effective porosity ratio (ϕ_{rr}) and the pore-surface area (A). This data provides information on fluid expulsion characteristics of shales (Katsube and Williamson, 1995, in press), required in petroleum exploration, and on the evolution of shale pore-structure due to weathering. The purpose of this paper is to provide petrophysical information on Upper Cambrian shales to the data bank on shale pore-surface characteristics.

Pore-size distribution has been previously determined (Dorsch, et al., 1996; Dorsch and Katsube, 1996), by the mercury porosimetry method, for samples of fresh mudrock from the Nolichucky Shale of the Bear Creek Valley on the Oak Ridge Reservation (ORR, Tennessee, U.S.A.) and of mudrock saprolite developed from these shales. This saprolite material is composed of saprolite groundmass and less weathered mudrock fragments. The pore-size distribution has been determined for all three types of material: fresh mudrock from the bedrock (BR), mudrock fragments (FR) from within the saprolite groundmass and saprolite groundmass (SP). These measurements were made as part of a study conducted to gather quantitative data on porosity and pore-structure in order to model matrix diffusion which is an important transport mechanism of chemical species within the saprolite mantle on the Oak Ridge Reservation (Dorsch, et al., 1996; Dorsch and Katsube, 1996). This pore-size distribution data contains information that can be used to determine the pore-surface area characteristics of these mudrocks. The methods used to determine the pore-surface area (A) characteristics are described in this paper.

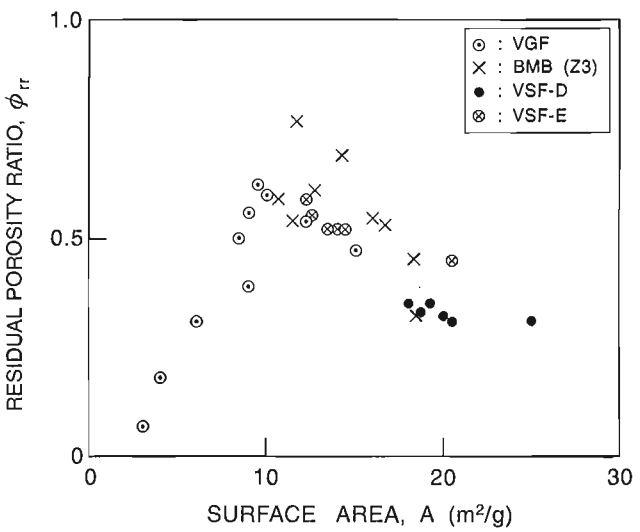

Figure 1. *Residual porosity ratio (ϕ_{rr}) as a function of surface area (A) for shale samples from the Venture Gas Field (VGF) and Beaufort-Mackenzie Basin (BMB), and experimentally compacted muds (VSF-D and VSF-E) from the Venture Gas Field (after Katsube and Williamson, in press).*

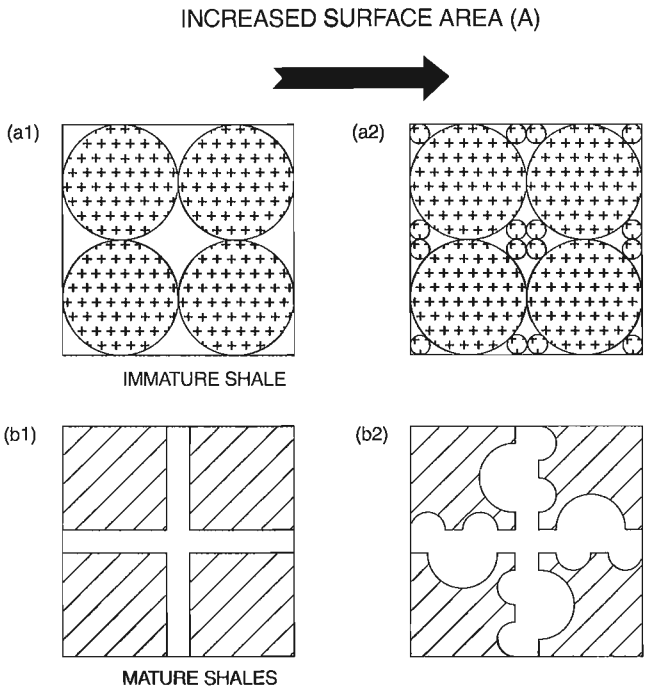

Figure 2. *A simplified shale texture model for explanation of the positive and negative ϕ_{rr}-A relationships shown in Figure 1, suggesting that an increase in A implies a ϕ_E reduction for diagenetically immature shales, and a ϕ_E increase for mature shales (after Katsube and Williamson, in press).*

It has been suggested (Katsube and Williamson, in press) that the ϕ_{rr}-A relationship is positive for diagenetically mature shales, and negative for immature shales (Fig. 1). A simplified model offered for explanation of this relationship is shown in Figure 2. This model suggests that an increase in A implies a ϕ_E reduction for diagenetically immature shales, and a ϕ_E increase for mature shales. Figure 2a1 represents a well sorted immature shale and Figure 2a2 represents a poorly sorted immature shale with an associated increase in A. Figure 2b1 represents a mature (cemented) shale and Figure 2b2 represents a mature shale containing dissolution pores with an associated increase in A.

The Conasauga Group represent the fill of a Late to Middle Cambrian intrashelf basin that developed on the Laurentian passive continental margin, bordering the evolving Iapetus ocean. The basin fill constitutes an alternation of mudrock- and carbonate-dominated stratigraphic units (e.g. Read, 1989; Srinivasan and Walker, 1993). The Conasauga Group is contained within stacked thrust sheets of the Appalachian foreland fold-and-thrust belt. The present retrieval depths of our mudrock samples are less than 400 m.

Mudrock of the Conasauga Group, however, was buried under a considerable thickness of rock and apparently experienced significant chemical diagenesis which led to thorough lithification. The estimated burial depth gives a minimum of 4 km (Foreman, 1991) for East Tennessee. A larger burial depth, however, is more likely based on the regional structural geology. Equivalent strata in Virginia are believed to have been buried to between 6 and 8.5 km (Montanez, 1994).

Data on the diagenetic history of Conasauga Group mudrock is sparse. Lee et al. (1991) report a general paucity of cement. However, the occurrence of pore-filling organic matter, calcite cement, authigenic quartz, kaolinite, barite, and framboidal and authigenic pyrite was observed by others (Lee et al., 1991; Baxter, 1988). Other diagenetic events detected were feldspar dissolution, glauconite formation and alteration, illitization and chloritization of kaolinite, and chloritization of biotite (Baxter, 1989).

METHOD OF INVESTIGATION

Samples and petrophysical data

The set of samples used in this analytical study consists of 10 fresh mudrock (BR) samples from the bedrock, 5 mudrock-fragment (FR) samples from within the saprolite groundmass, and 5 saprolite (SP) samples from the saprolite groundmass. Sample identification numbers and rock type are listed in Table 1. The sample sizes are in the order of 1-2 cm^3, so that complete intrusion of mercury is ensured for measurement of the tight low-permeability material. Existing petrophysical data, including shale pore-size distribution data, for these 20 samples was collected from previous publications (Dorsch, et al., 1996; Dorsch and Katsube, 1996), and is compiled in Table 1.

Table 1. Petrophysical data of Nolichucky shale samples from within the Oak Ridge Reservation (based on Dorsch et al., 1996; Dorsch and Katsube, 1996).

Sample No., ID		Fm	h (m)	δ_{Ghe}	δ_{BD}	δ_{SD}	ϕ_{He}	ϕ_{Hg1} (%)	ϕ_{Hg2} (%)	A	ϕ_s	ϕ_{rr}
KS-3	A16		44.5	2.73	2.69	2.77	9.9	2.7	3.1	4.0	0.6	0.23
KS-4	A17		58.3	2.78	2.70	2.81	12.2	3.4	3.9	4.9	1.7	0.50
KS-5	A18		80.3	2.79	2.71	2.83	3.2	3.8	4.2	5.8	1.2	0.31
KS-6	A19		99.8	2.79	2.69	2.83	2.9	4.3	5.0	6.6	2.2	0.51
KS-7	A20	BR	109.5	2.76	2.77	2.93	4.9	4.3	5.2	6.6	1.8	0.43
KS-8	A21		151.6	2.79	2.70	2.83	3.9	4.0	4.7	5.6	1.7	0.43
KS-9	A22		158.3	2.70	2.68	2.83	4.7	5.1	6.1	7.7	2.1	0.42
KS-10	A23		171.9	2.79	3.21	3.39	14.7	4.6	5.4	6.9	1.4	0.31
KT-1	A24		181.1	2.77	2.69	2.80	4.1	3.7	4.1	6.9	0.4	0.10
KT-2	A25		201.2	2.80	2.67	2.78	10.4	3.2	3.9	5.0	1.4	0.44
KSP-2	GW-822-12		6.3	2.81	2.50	2.75	16.7	8.8	9.2	14.3	5.4	0.61
KSP-3	GW-822-15		7.2	2.81	2.53	2.85	13.5	10.7	11.2	12.6	6.6	0.62
KSP-4	GW-823-6	FR	3.8	2.78	2.36	2.75	18.1	13.7	14.0	14.5	9.9	0.72
KSP-5	GW-823-7		4.3	2.78	2.39	2.75	15.1	12.2	12.8	17.2	8.9	0.73
KSP-6	GW-823-8		5.8	2.80	2.40	2.67	17.3	9.5	10.1	15.3	12.5	0.70
KSP11	GW-822-2		1.40	2.90	1.81	2.37	38.9	22.0	23.7	1.44	18.7	0.85
KSP12	GW-822-3		1.98	2.87	1.92	2.71	33.6	28.5	29.3	18.8	17.1	0.60
KSP13	GW-823-1	SP	0.46	2.76	1.48	2.36	51.6	29.5	37.5	2.67	24.5	0.83
KSP14	GW-823-4		2.55	2.70	1.64	2.66	39.3	26.7	38.2	11.2	23.5	0.88
KSP15	GW-823-5		3.22	2.72	1.91	3.20	31.7	27.2	40.0	16.0	22.6	0.83

Fm = Formation
BR = Fresh mudrock from the bedrock
FR = Mudrock fragments (from within the saprolite groundmass)
SP = Saprolite groundmass
ϕ_{He} = Total porosity measured by helium porosimetry
ϕ_{Hg1} = Total porosity measured by mercury porosimetry for pore sizes up to 10 μm (%)
ϕ_{Hg2} = Total porosity measured by mercury porosimetry for pore sizes up to 250 μm (%)
ϕ = Immersion porosity
δ_{Ghe} = Grain density (g/mL)
δ_{BD} = Bulk density (g/mL)
δ_{SD} = Skeletal density (g/mL)
A = Surface area (m^2/g)
ϕ_s = Storage porosity
ϕ_{rr} = Residual porosity ratio
h = Depth (m) from which the sample was obtained

Shale pore-structure models

Several pore-structure models are commonly used to explain the inter-relationship between the different shale petrophysical characteristics or between the shale texture and petrophysical characteristics (Katsube and Williamson, 1994). Two of them, the "storage-connecting pore model" (Fig. 3a) and the "pore-size distribution model", consisting of a bundle of tubular pores with different diameters (Fig. 3b), are required to explain the ϕ_{rr}-A relationship.

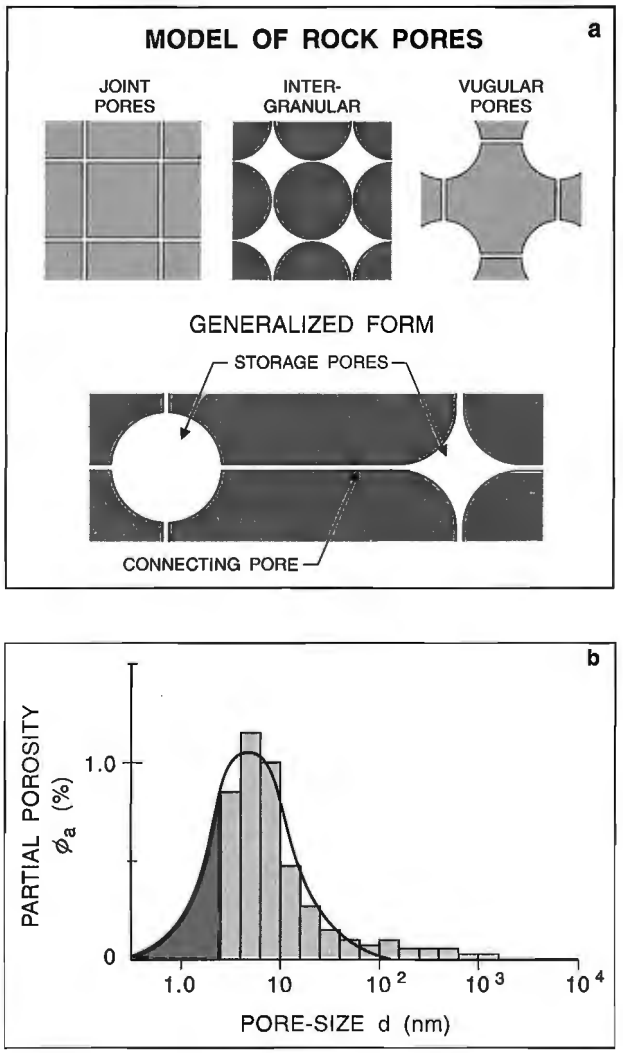

*Figure 3. Some of the pore-structure models used for characterizing shales (Katsube and Williamson, 1994): **a)** storage-connecting pore model (Katsube and Collett, 1975), and **b)** pore-size distribution model (Katsube, 1992). The ϕ_a is partial porosity, and d is the general expression for pore-sizes.*

Pore-surface area (A) determination

The display format used for the pore-size, d, distribution (Fig. 3b), has each decade of the logarithmic pore-size scale (x-axis) subdivided into 5 ranges with equal physical spacing (Katsube and Issler, 1993). The porosity contained in each pore-size range is represented by the partial porosity, ϕ_a. In principle, the sum of ϕ_a for all pore-sizes is equal to ϕ_E. Pore surface area (A), in this case, is the sum of the pore surface area of all pore-sizes represented by cylindrical tubes of varied diameters and length, and can be expressed by

$$A = \Sigma[4\phi_{ai}/(d_{ai}\delta_{BD})], \quad (1)$$

where ϕ_{ai} and d_{ai} are the partial porosity and geometric mean pore-size for the different pore-size ranges, and δ_{BD} is the bulk density of the sample. The derivations of Equation (1) are described in the Appendix.

Storage/effective porosity ratio (ϕ_{rr})

The effective porosity, ϕ_E, represents the pore space in all interconnected pores (Katsube and Williamson, 1994; in press), and is expressed by

$$\phi_E = \phi_s + \phi_c \quad (2)$$

where ϕ_s and ϕ_c are the porosities of the storage and connecting pores (Fig. 3), respectively. The residual porosity ratio (ϕ_{rr}) is represented by

$$\phi_{rr} = \phi_s/\phi_E. \quad (3)$$

The ϕ_{rr} is determined by taking the ratio of the total mercury residual volume over the total intrusion volume, using mercury porosimetry. This is based on the assumption that mercury is trapped in the storage pores on depressurization.

ANALYTICAL RESULTS

The pore-surface area (A) values determined using equations (AX5) and (AX6) in the appendix, or equation (1) are listed in Tables 1 and 2. Examples of equation (AX5) used to determine the surface area for the different pore-size ranges and the final pore-surface area (A) values determined by use of equation (1) or (AX5) are listed in Table 2 for three samples (A16, 823-6 and 822-3). The results of the storage/effective porosity ratio (ϕ_{rr}) values determined, by taking the ratio of the total mercury residual volume over the total intrusion volume of mercury porosimetry measurements, are listed in Table 1. Total intrusion volume, in this case, implies the volume of mercury that has intruded the pore-sizes of 2.5 nm to 10 μm. Essentially, ϕ_{Hgl} in Table 1 is being used to represent ϕ_E in equation (3).

Table 2. Some examples of pore-size distribution and surface area (A) data for different pore-size ranges, d_a, obtained by mercury porosimetry for three Nolichucky shale samples (based on Dorsch et al., 1996; Dorsch and Katsube, 1996).

	A16		823-6		822-3	
d_a(nm)	δ_a (%)	A_a (m^2/g)	ϕ_a (%)	A_a (m^2/g)	ϕ_a (%)	A_a (m^2/g)
3.2	0.34	1.02	0.45	2.38	0.61	3.97
5.0	0.92	1.93	1.27	4.31	1.65	6.88
7.9	0.58	0.72	1.39	2.98	1.11	2.93
12.6	0.50	0.41	1.96	2.64	1.25	2.07
20.0	0.37	0.24	2.64	2.24	1.40	1.46
31.6	0.26	0.09	1.65	0.89	1.09	0.72
50.1	0.29	0.09	2.10	0.71	1.80	0.75
79.4	0.26	0.02	1.13	0.24	2.07	0.54
126	0.08	0.00	0.45	0.06	1.96	0.32
200	0.11	0.00	0.21	0.02	2.15	0.22
316	0.03	0.00	0.12	0.01	2.45	0.16
501	0.00	0.00	0.07	0.00	2.42	0.20
794	0.00	0.00	0.14	0.00	2.84	0.07
1259	0.00	0.00	0.02	0.00	3.18	0.05
1995	0.00	0.00	0.02	0.00	1.36	0.01
3162	0.00	0.00	0.05	0.00	0.63	0.00
5012	0.00	0.00	0.02	0.00	0.38	0.00
7943	0.00	0.00	0.00	0.00	0.17	0.00
ϕ_{Hg1} (%)	3.75		13.7		28.5	
ϕ_{Hg2} (%)	4.17		14.0		29.3	
d_{hg} (nm)	30.5		27		182	
δ_{BD} (g/mL)	2.64		2.36		1.92	
A (m^2/g)		4.53		14.5		20.3
h (m)	41.1		3.79		1.98	

d_a = Geometric mean pore-sizes for the different pore-size ranges (nm)
d_{hg} = Geometric mean of the entire pore-size distribution (nm)
ϕ_a = Partial porosity (%)
ϕ_{Hg1} = Total porosity measured by mercury porosimetry for pore sizes up to 10 μm (%)
ϕ_{Hg2} = Total porosity measured by mercury porosimetry for pore sizes up to 250 μm (%)
δ_{BD} = Bulk density (g/mL)
h = Depth (m) from which the sample was obtained

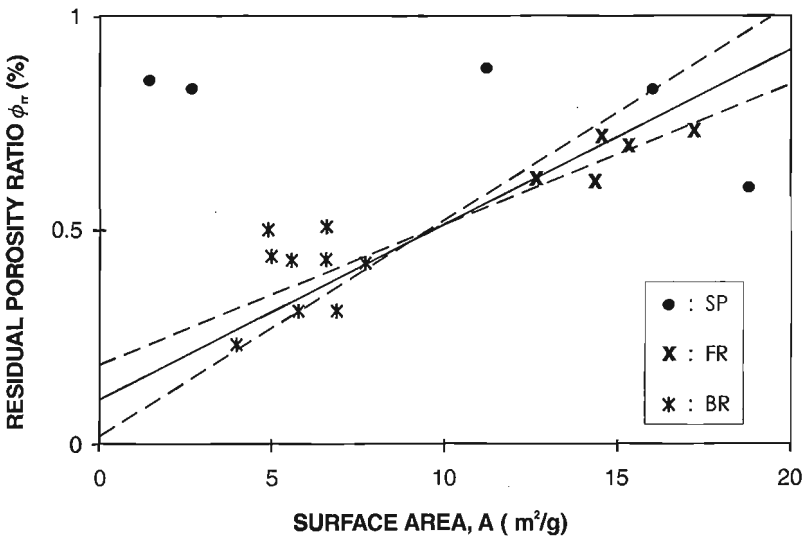

Figure 4.

Residual porosity ratio as a function of surface area (ϕ_{rr}-A) for the Nolichucky Shale samples from within the Oak Ridge Reservation. Data for fresh mudrock (BR), mudrock fragments (FR) from the saprolite and mudrock saprolite groundmass (SP) are displayed here. The solid line represents the reduced major axis (RMA: Davis, 1986; Katsube and Agterberg, 1990), and the broken lines represent the two normal regression lines (NRLs).

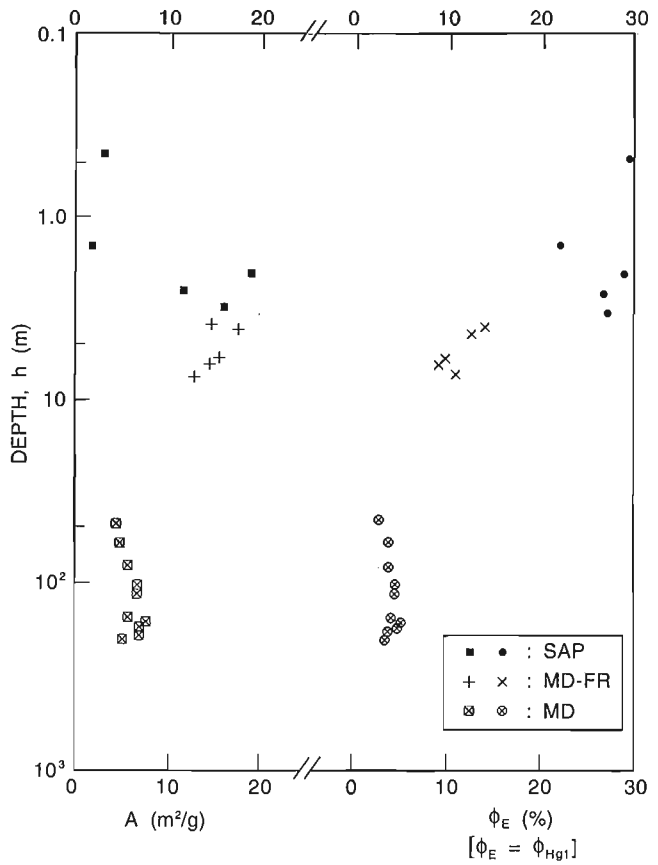

Figure 5. *Effective porosity (ϕ_E) and surface area (A) as a function of depth for the Nolichucky Shale samples from within the Oak Ridge Reservation. In this case $\phi_E = \phi_{Hg1}$. (h_w = depth of weathering, SAP = mudrock saprolite groundmass (SP in text), MD-FR = mudrock fragments (FR in text), MD = fresh mudrock (BD in text).*

The A values are in the range of 1.5-19 m²/g for these samples, a range similar to those previously obtained for shales (Katsube and Williamson, in press). The ϕ_{rr} values are in the range of 0.1-0.9, values also similar to those previously obtained. The A values for the fresh mudrock samples (samples A16 to A25) are in the range of 4.0-7.7 m²/g, a range resembling those of diagenetically mature shales (Katsube and Williamson, in press).

The ϕ_{rr}-A relationship for these mudrock samples is shown in Figure 4. If the fresh mudrock (BR) and mudrock fragments (FR) are considered to belong to the same group, they show a positive ϕ_{rr}-A relationship, similar to that of mature shales (Katsube and Williamson, in press). The mudrock saprolites groundmass (SP) display a ϕ_{rr}-A relationship that has a slope that is close to zero or slightly negative, suggesting a relationship that is somewhat between a mature and immature shale.

DISCUSSION AND CONCLUSIONS

It is not surprising that the ϕ_{rr}-A relationship of the set of fresh mudrock (BR) and mudrock fragments (FR) within the saprolite groundmass is positive, since these samples are from Cambrian shales which are most likely mature and have undergone considerable diagenesis. The reason for the low A and ϕ_{rr} values of the BR-samples (Fig. 4) can be explained by the model in Figure 2b1, and the larger A and ϕ_{rr} values of the FR-samples can be explained by the model in Figure 2b2. This implies that the pore-surface area has increased due to dissolving of the cement.

It is interesting that the mudrock saprolite groundmass (SP) samples display rather large ϕ_{rr} values and show a ϕ_{rr}-A relationship that has a slope of zero or tends to be slightly negative. The large ϕ_{rr} values indicate that the storage porosity is considerably larger than the connecting porosity, which is likely a result of most of the pore cement being dissolved, to the extent that the original grains have lost most of their cement coating, and are effectively displaying characteristics of an immature sedimentary rock (Fig. 2a1). The fact that the ϕ_{rr}-A relationship is not positive, and has a slope of zero or tends to be slightly negative, supports this explanation. The fact that the slope of the ϕ_{rr}-A relationship is not clearly negative may imply that there are still remnants of the cement coating around the grains. The low A values displayed by some of these SP samples may suggest that they have a significant course grain content.

The effective porosity versus depth (ϕ_E-h) and surface area versus depth (A-h) relationships are shown in Figure 5. Although there is a data gap between the depths (h) of 10-40 m, the trends of the ϕ_E-h relationship suggest that the ϕ_E values decrease with h to about 10-20 m, at which point they stabilize with depth at 3-5 %, as previously indicated (Dorsch and Katsube, 1996). This depth, probably, indicates the depth to which weathering has penetrated. Therefore, this point is referred to as the depth of weathering (h_w). The surface area (A) is more or less constant with decreasing depth, at about 4-8 m²/g, until h_w from which point A increases with decreasing h. However, it is interesting that A decreases with decreasing h, from about 2-3 m. This decreased A may suggest that most of the cement coating the coarse grain material of the original sediments have been dissolved by the weathering process, an explanation that is consistent with that offered above. Most of the fine grain material contained in the original shale may also have been dissolved.

ACKNOWLEDGMENTS

The authors acknowledge the support from the Y-12 HSE&A-Division, the X-10 ER Groundwater Division, and the ORRHAGS of the Oak Ridge National Laboratory. The authors are grateful to M.A. Williamson (GSC Atlantic) for critically reviewing this paper.

REFERENCES

Baxter, P.M.
1989: Clay Mineral Diagenesis in the Pumpkin Valley Shale, Oak Ridge, Tennessee: M.Sc. thesis, Louisiana State University, Baton Rouge, 197 p.

Davis, J.C.
1986: Statistics and Data Analysis in Geology; John Wiley & Sons, New York, p. 200-204.

Dorsch, J. and Katsube, T.J.
1996: Effective porosity and pore-throat sizes of mudrock saprolite from the Nolichucky shale within Bear Creek Valley on the Oak Ridge Reservation: implication for contaminant transport and retardation through matrix diffusion; Oak Ridge National Laboratory (U.S. Department of Energy), ORNL/GWPO-025, p. 72.

Dorsch, J., Katsube, T.J., Sanford, W.E., Dugan, B.E., and Tourkow, L.M.
1996: Effective porosity and pore-throat sizes of Conasauga group mudrock: application, test and evaluation of petrophysical techniques; Oak Ridge National Laboratory (U.S. Department of Energy), ORNL/GWPO-021, p. 113.

Foreman, J.L.
1991: Petrologic and geochemical evidence for water-rock Interaction in the mixed carbonate-siliciclastic Nolichucky Shale (Upper Cambrian) in East Tennessee; Ph.D. Dissertation, University of Tennessee, Knoxville, TN, 228 p.

Katsube, T.J.
1992: Statistical analysis of pore-size distribution data of tight shales from the Scotian Shelf; in Current Research, Part E; Geological Survey of Canada, Paper 92-1E, p. 365-372.

Katsube, T.J. and Agterberg, F.P.
1990: Use of statistical methods to extract significant information from scattered data in petrophysics; in Statistical Applications in the Earth Sciences, (ed.) F.P. Agterberg and G.F. Bonham-Carter; Geological Survey of Canada, Paper 89-9, p. 263-270.

Katsube, T.J. and Collett, L.S.
1975: Electromagnetic propagation characteristics of rocks; in The Physics and Chemistry of Rocks and Minerals, (ed.) R.G.J. Strens; John Wiley & Sons Ltd., Toronto, p. 279-295.

Katsube, T.J. and Issler, D.R.
1993: Pore-size distribution of shales from the Beaufort-MacKenzie Basin, northern Canada; in Current Research, Part E; Geological Survey of Canada, Paper 93-1E, p. 123-132.

Katsube, T.J. and Williamson, M.A.
1994: Effects of diagenesis on shale nano-pore structure and implications for sealing capacity; Clay Minerals, v. 29, p. 451-461.
1995: Critical depth of burial of subsiding shales and its effect on abnormal pressure development; in Proceedings of the Oil and Gas Forum' 95 ("Energy from Sediments"); Geological Survey of Canada, Open File 3058, p. 283-286.
in press: Shale petrophysical characteristics; permeability history of subsiding shales: Submitted for publication in the Proceedings of "GSA Annual Meeting - New Orleans", Louisiana, November 6-9, 1995.

Lee, S.Y., Hyder, L.K., and Alley, P.D.
1991: Microstructural and mineralogical characterization of selected shales in support of nuclear waste repository studies; in Microstructures of Fine-grained Sediments, (ed.) R.H. Bennett, W.R. Bryant, and M.H. Hulbert; Springer-Verlag, Heidelberg, p. 545-560.

Montanez, I.P.
1994: Late diagenetic dolomitization of Lower Ordovician, Upper Knox Carbonates: a record of the hydrodynamic evolution of the Southern Appalachian basin; American Association of Petroleum Geologists Bulletin, v. 78, p. 1210-1239.

Read, J.F.
1989: Controls on evolution of Cambrian-Ordovician passive margin, U.S. Appalachians; in Controls on Carbonate Platform and Basin Development, (ed.) P.D. Crevello, J.L. Wilson, J.F. Sarg, and J.F. Read; Society of Economic Paleontologists and Mineralogists, Special Publication 44, p. 147-165.

Srinivasan, K. and Walker, K.R.
1993: Sequence stratigraphy of an intrashelf basin carbonate ramp to rimmed platform transition: Maryville Limestone (Middle Cambrian), southern Appalachians; Bulletin of the Geological Society of America, v. 105, p. 883-896.

Geological Survey of Canada Project 870057

APPENDIX

Let us define the partial porosity (ϕ_{ai}) for the i-th pore-size range by

$$\phi_{ai} = V_{pi}/V, \tag{AX1}$$

where V_{pi} and V are the pore volume for the i-th pore-size range and V is the volume of the sample, respectively. Since the "pore-size distribution model" (Fig. 3b) consists of a bundle of tubular pores with different diameters, V_{pi} and A_i are considered to be the volume and surface area of the i-th tubular pore with a diameter of d_{ai} and a length of ℓ_{ai}:

$$V_{pi} = \pi d_{ai}^2 \ell_{ai}/4, \tag{AX2}$$

and

$$A_i = \pi d_{ai} \ell_{ai}. \tag{AX3}$$

From equations (AX1) and (AX2) we obtain

$$\ell_{ai} = 4\phi_{ai} V/(\pi d_{ai}^2). \tag{AX4}$$

Therefore, from equations (AX3) and (AX4) we obtain

$$A_i = 4V\phi_{ai}/d_{ai}.$$

Since surface area is usually normalized to the weight, $V\delta_{BD}$, of the sample, where δ_{BD} is the bulk density, A_i is generally expressed by

$$A_i = 4\phi_{ai}/(d_{ai}\delta_{BD}). \tag{AX5}$$

Therefore, the surface area (A) for all pore-sizes in that sample is expressed by

$$A = \Sigma[4\phi_{ai}/(d_{ai}\delta_{BD})]. \tag{AX6}$$

AUTHOR INDEX

Geological Survey of Canada Current Research, is released twice a year, in January and July. The four parts published in January 1997 (Current Research 1997-A to D) are listed below and can be purchased separately.

Recherches en cours, une publication de la Commission géologique du Canada, est publiée deux fois par année, en janvier et en juillet. Les quatre parties publiées en janvier 1997 (Recherches en cours 1997-A à D) sont énumérées ci-dessous et sont vendues séparément.

Part A:	Cordillera and Pacific Margin
Partie A :	Cordillère et marge du Pacifique
Part B:	Interior Plains and Arctic Canada
Partie B :	Plaines intérieures et région arctique du Canada
Part C:	Canadian Shield
Partie C :	Bouclier canadien
Part D:	Eastern Canada and national and general programs
Partie D :	Est du Canada et programmes nationaux et généraux
Part E:	this volume
Partie E :	ce volume